Amélioration des performances des radars HF à ondes de surface par étude d'antenne compacte et filtrage adaptatif appliqué à la réduction du fouillis de mer

Emilie Bronner

THÈSE DE DOCTORAT DE L'UNIVERSITÉ PARIS 6

Spécialité

Électronique et Sciences de l'Univers

présentée par

Mlle Emilie BRONNER

Pour obtenir le grade de

DOCTEUR DE L'UNIVERSITÉ PARIS 6

Amélioration des performances des radars HF à ondes de surface par étude d'antenne compacte et filtrage adaptatif appliqué à la réduction du fouillis de mer

soutenue le 9 novembre 2005

devant le jury composé de:

M. Alain BOURDILLON, professeur à l'Université de Rennes 1, Rapporteur
M. Jacques DAVID, professeur à l'Université de Toulouse, Rapporteur
M. Walid TABBARA, professeur à l'Université Paris 6 (UPMC), Examinateur
M. Ronan MOULINET, ingénieur DGA, Examinateur
M. Marc HÉLIER, directeur de thèse, professeur à l'UPMC, Examinateur
M. Jean-Philippe MOLINIÉ, ingénieur DEMR-RHF, ONERA, Examinateur
M. Philippe BOURBON, membre de l'Institut Français de Navigation, Invité
M. Stéphane SAILLANT, ingénieur DEMR-RHF, ONERA, Invité

French extended summary - Résumé français étendu

Introduction

Dans le cadre d'un programme de recherche commun conduit par l'ONERA (Office National d'Etudes et de Recherches Aérospatiales) en France et par la DSTA (Defence Science and Technology Agency) de Singapour, une thèse a été proposée dans le but d'améliorer les performances des radars HF à ondes de surface. Co-financée par l'ONERA et la DSTA, l'étude a été réalisée au sein de l'équipe "Radars Basses Fréquences" de l'ONERA en collaboration avec la DSTA pour les expérimentations et les discussions techniques. La thèse s'est déroulée sur 3 ans et a été supervisée par Marc HELIER, professeur à l'Université de Paris 6 et par Stéphane SAILLANT, ingénieur à l'ONERA. Les deux pays impliqués dans ce sujet sont très intéressés par les radars HF à ondes de surface car ils offrent de nouvelles possibilités par rapport aux radars classiques. Ces pays souhaitent en fait collaborer dans le but de développer un démonstrateur efficace de ce type de radars. Or ils sont récents et ne sont pas encore opérationnels dans de nombreux pays. L'objectif de cette thèse est d'apporter des améliorations, concernant le matériel et le traitement radar utilisés, en vue d'accroître les performances des radars HF à ondes de surface.

L'utilité des radars en navigation maritime est depuis longtemps une évidence. Embarqués sur bateaux ou installés sur les côtes, ils constituent aujourd'hui des équipements essentiels pour garantir la sûreté de navigation des navires, quelles que soient les conditions météorologiques. Il s'agit en général d'équipements fonctionnant dans le domaine des micro-ondes, c'est-à-dire avec des fréquences de l'ordre de quelques gigahertz, soit des longueurs d'onde associées de l'ordre du centimètre. Si de tels systèmes apportent aux navigateurs des informations de grande qualité, en particulier lorsqu'ils sont couplés à des logiciels informatiques, de cartographie ou d'anti-collision par exemple, ils sont néanmoins limités par les propriétés physiques de la propagation des ondes de très haute fréquence. En effet, celle-ci s'effectue en ligne droite, ce qui limite la portée des radars micro-ondes à l'horizon. Ainsi, pour un radar installé sur une tour à terre, en bordure côtière, a 150 m de hauteur, la limite de détection d'un navire, ayant des superstructures de 20 m de hauteur, serait d'une trentaine de milles, soit environ 55 kilomètres.

La convention des Nations Unies sur le droit de la mer de Montego Bay a défini, en 1982, la zone économique exclusive (ZEE) comme la zone maritime comprenant la mer territoriale et s'étendant jusqu'à 200 milles (soit 370 kilomètres) des lignes de base des côtes. Dans cette zone, les états riverains exercent des droits, en particulier en matière d'exploration et d'exploitation des ressources naturelles vivantes ou non vivantes, des eaux surjacentes, du lit marin et du sous-sol. Ces droits s'accompagnent aussi d'obligations en ce qui concerne la protection et la préservation du milieu marin. Une surveillance de la zone économique exclusive apparaît donc comme indispensable avec la possibilité de dénombrer et suivre les navires qui la traversent.

Or, d'après notre précédent calcul de portée, on constate que les radars fonctionnant dans le domaine micro-onde sont loin de couvrir l'étendue des 200 milles de la zone économique exclusive. Certes, il est toujours possible d'avoir recours à une surveillance aérienne ou navale de cette zone, mais elle est coûteuse et nécessairement limitée dans le temps et l'espace. Il en est de même pour les satellites actuels qui n'ont ni la résolution spatiale, ni la résolution temporelle nécessaire pour fournir une surveillance efficace en temps réel. Néanmoins, on peut aujourd'hui compléter cette surveillance partielle par la mise en oeuvre d'un autre type de radar, tel que le radar HF à ondes de surface qui est mieux adapté à la couverture de grandes étendues maritimes.

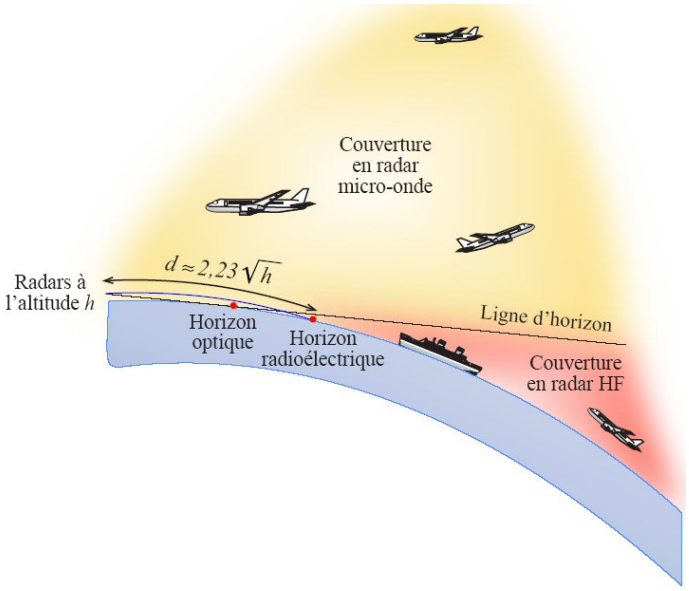

Figure 1: Couvertures d'un radar HF à ondes de surface et d'un radar micro-onde

En effet, le radar à ondes de surface utilise des ondes de hautes fréquences comprises entre 3 et 30 MHz qui ont la particularité de se propager à la surface de la mer au-delà de la limite de l'horizon, c'est-à-dire jusqu'à quelques centaines de kilomètres. Ce type de radar peut ainsi recevoir des échos de cibles sur des distances beaucoup plus grandes que les radars usuels dont le rayon d'action est défini par la portée optique ou par l'horizon (voir illustration des couvertures radar sur la figure 1 ci-dessus).

Ainsi, les radars HF à ondes de surface sont employés dans les domaines de la surveillance maritime, l'océanographie et la détection de cibles. En effet, ils trouvent tout d'abord de nombreuses applications dans le domaine civil. Instruments utiles pour la surveillance maritime à grande distance, ils permettent de détecter ou traquer d'éventuelles activités illégales telles que les trafics de drogue, les activités de contrebande et de piraterie ou encore l'immigration clandestine. D'autres applications sont la protection de l'environnement et des ressources naturelles contre par exemple la pêche excessive ou la pollution. Enfin, ces radars peuvent fournir des informations sur le vent et l'état de la mer, données utiles aux océanographes et scientifiques. Les applications dans le domaine militaire sont essentiellement la détection de cibles telles que les navires, les avions volant à basse altitude ou encore les missiles.

Au niveau national et international, les radars HF à ondes de surface sont relativement récents et ne sont pas encore totalement opérationnels et performants pour le moment. En effet, ils sont encore au stade d'étude ou de développement dans de nombreux pays car certains points restent à être améliorés comme par exemple la résolution angulaire et distance des radars, les problèmes liés aux fréquences HF utilisées (encombrement du spectre HF, tailles d'antennes très importantes, etc), les perturbations de signal causés par le fouillis ionosphériques et le fouillis de mer, etc.

Chapitre 1: Les radars HF à ondes de surface

Le premier chapitre de ce document est une introduction au radar HF à ondes de surface, contexte et base de cette étude. Il donne une vue globale du système radar à travers un historique de son évolution et il dresse un bilan de la situation de son développement de nos jours, sur le plan national et international. Puis, les particularités et le principe de fonctionnement de ces radars sont détaillés. Ce chapitre est en fait une introduction essentielle pour que le lecteur se familiarise avec le vocabulaire du domaine radar et comprenne le fonctionnement de ce système complet mais complexe qui combine différentes technologies pour générer, transmettre, collecter et traiter des signaux. Par exemple, l'étape de traitement radar qui permet l'extraction des données utiles à partir des mesures brutes est une phase qu'il s'agit de bien comprendre car elle concentre beaucoup de notions qui seront utilisées tout au long du document. À la fin de cette partie, que l'on qualifiera de bibliographique, les principaux inconvénients dont souffre le radar HF à ondes de surface à l'heure actuelle sont présentés. Nombre de ces problèmes restent à résoudre dans le but de rendre ces radars plus opérationels et efficaces qu'ils ne le sont aujourd'hui. La problématique de cette thèse est d'améliorer les performances des radars HF à ondes de surface et parmi ces quelques désavantages, deux d'entre eux seront choisis comme sujets d'étude.

Le premier problème à résoudre et traité dans la première partie de cette thèse **(chapitres 2 et 3)** concerne la taille trop importante des antennes HF. En effet, le radar HF à ondes de surface utilise en général une antenne d'émission et des antennes de réception regroupées en réseau phasé, le tout étant situé à proximité du bord de mer. Les éléments courament utilisés pour émettre et recevoir les ondes HF sont dimensionnés au quart de la longueur d'onde. Or en HF, les longueurs d'ondes étant comprises entre 10 et 100 m, les antennes

résultantes peuvent donc mesurer de 2.5 à 25 m de hauteur. Des antennes HF performantes de plus petite dimension n'existent pas sur le marché aujourd'hui. De plus, la plupart des études sur les petites antennes concernent le domaine micro-onde. Les antennes réprésentant un poste important du système radar, il y a un véritable challenge à compacter leur taille pour plusieurs raisons. Tout d'abord, il s'agit de limiter l'encombrement physique de l'antenne pour des raisons pratiques (déploiement facile, transport, coût, etc) et un gain de compacité permettrait également de gagner en discrétion et furtivité. De plus, des petits éléments seraient bénéfiques pour limiter les effets de couplage au sein du réseau phasé de réception. Et enfin, une réduction de taille est vraiment incontournable pour permettre des configurations radar embarquées sur bateaux. Toutes les améliorations possibles resultant d'un effort de compacité ont pour but final d'améliorer la détection des cibles et la disponibilité des radars HF à ondes de surface.

Le second point à améliorer concerne la réduction du fouillis de mer. En effet, les radars HF à ondes de surface illuminent la surface de la mer avec une onde HF pour atteindre des grandes portées de détection. Or ces fréquences HF de longueurs d'ondes décamétriques vont interférer avec les vagues qui ont elles aussi des longueurs d'ondes décamétriques. Il en résulte une diffusion des ondes électromagnétiques sur la surface de la mer, connue sous le nom de diffusion de Bragg. L'analyse spectrale du signal radar retour met en évidence les échos provenant de la mer car ils sont caractérisés par deux pics dominants entourés d'un continuum de second ordre. Ces échos marins, que l'on qualifiera de fouillis de mer, se situent dans la partie spectrale utile dans laquelle les échos de cibles à détecter sont attendus. Ainsi, les échos de cibles sont parfois délicats à repérer dans le cas où les échos marins ont un niveau élevé et cela déteriore les capacités de détection des radars HF à ondes de surface. Pour rémédier à ce problème, il est nécessaire de réduire le fouillis de mer et une méthode de traitement de signal sera étudiée et développée dans la deuxième partie de la thèse **(chapitres 4 et 5)**.

Chapitre 2: Choix et simulation d'une antenne HF compacte pour radar HF à ondes de surface

La démarche mise en oeuvre dans cette thèse pour résoudre les problèmes posés par une taille trop importante des antennes HF est de concevoir un nouvel élément HF ayant des dimensions compactes. Dans un premier temps, il s'agit de trouver une façon de compacter la taille des antennes HF habituelles et de concevoir un modèle qui sera simulé avec un code électromagnétique pour avoir un étalonnage de ses performances initiales. Puis, cette antenne de base sera modifiée et optimisée pour que ses caractéristiques finales correspondent au cahier des charges permettant son fonctionnement dans un radar HF à ondes de surface. Enfin, un prototype de l'élément final sera fabriqué puis testé en configuration radar réelle pour valider les simulations.

Le chapitre 2 présente donc tout d'abord un éventail de quelques antennes couramment utilisées par les radar HF à ondes de surface pour mettre en évidence l'encombrement de ces éléments et ainsi justifier la problématique de cette partie. Puis, l'élément à imaginer devant répondre à un cahier des charges précis imposé par les besoins des radars HF à

ondes de surface, il est nécessaire de recenser les différentes caractéristiques auxquelles il devra répondre. La compacité étant le premier point à améliorer, une taille maximale de 1 m serait déjà un progrès tout en restant bien inférieure à la hauteur des éléments usuels pouvant mesurer de 2.5 à 25 m, suivant la fréquence.

Les autres caractéristiques de l'antenne ne doivent pas être dégradées par des dimensions réduites et elles doivent être compétitives avec les perfomances des antennes usuelles utilisées pour les radars HF à ondes de surface. Un objectif délicat à atteindre est la réalisation d'une antenne pouvant fonctionner à plusieurs fréquences, typiquement à une fréquence basse autour de 5 MHz et à une fréquence haute autour de 15 MHz, avec dans chaque cas une bande de quelques kHz. Une impédance de 50 Ohms est souhaitée pour une bonne adaptation entre l'antenne et le reste de l'équipement. Une polarisation verticale est également requise pour permettre une propagation optimale des ondes de surface. Puis, une antenne passive serait préférée à une active afin d'éviter les problèmes de phase que l'on ne maîtrise pas toujours très bien dans les dispositifs actifs et afin d'envisager une utilisation de l'antenne en émission et en réception. Concernant le diagramme de rayonnement de l'antenne, un gain maximum dans la direction de la mer est essentiel pour permettre de propager et recevoir efficacement les ondes de surface.

Enfin, dans le but d'associer les éléments compacts en réseau phasé, il est recommandé d'éviter des antennes avec des structures trop complexes pour permettre une reproduction en série facile. Un contrôle précis de la phase entre éléments étant la base du fonctionnement des réseaux phasés, ce point est important. De plus, en imaginant un design simple composé de matériaux courants, l'antenne peut être fabriquée à bas coûts ou du moins à coûts modérés.

Pour répondre à toutes les spécifications précédentes, la démarche a été dans un premier temps de trouver une faon de compacter la taille des antennes HF habituelles. Parmi la littérature et les différentes études disponibles dans le domaine des communications sans fil, un premier choix a été fait pour réduire la taille des antennes usuelles en courbant des fils de cuivre comparativement à ce qui est fait dans la technologie des antennes à méandres. Ce choix était très important car toutes les évolutions de design suivantes se sont basées sur ce concept simple qui consiste à replier de la longueur dans un volume réduit. L'utilisation de méandres a donc été choisie car cela permet d'atteindre des performances record dans un petit volume donné.

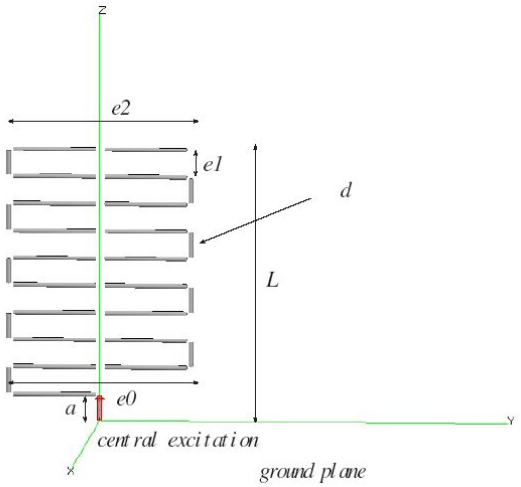

Figure 2: Paramètres géométriques définissant l'antenne générique

- Hauteur totale = L = 1 m
- Largeur (haut et bas) = e0 = e2 = 0.7 m
- Excitation centrale
- Diamètre des fils = d = 0.005 m
- Matériau : cuivre
- Distance au sol et entre les branches horizontales = a = e1 = 0.1 m

Ainsi, par analogie avec les modèles existants et en les simplifiant au maximum, une première antenne compacte appelée "antenne générique" a été imaginée. Cette antenne est une structure filaire à méandres représentée sur la figure 2.7. Ses dimensions concordent avec les spécifications de taille imposées et sa longueur déployée est d'environ 7.5 m.

Le fonctionnement de cette antenne à méandres est semblable à celui d'un monopole. En effet, les courants traversant la structure sont en phase d'une partie verticale à une autre tandis qu'ils sont opposés dans les branches horizontales. Aux légères différences de phase près, les effets des segments horizontaux se compensent deux à deux et ne contribuent donc pas au rayonnement de l'antenne. Comme seules les parties verticales rayonnent efficacement, la polarisation de ce type d'antenne est rectiligne et verticale, ce qui est parfait pour les ondes de surface. L'impédance de l'antenne est composée d'une partie active et réactive. Pour l'antenne générique, la part active est créée par la somme des puissances rayonnées par chaque dipôle vertical. La part réactive est quant à elle liée à la longueur totale de la structure. Cela signifie donc que la petite taille de l'antenne sera prise en compte dans le rayonnement impliquant des performances radiatives assez faibles. Mais pour des questions d'adaptation, la longueur totale déployée est prise en compte pour déterminer les fréquences de résonance. Ainsi, plus l'antenne sera longue, plus les fréquences de résonance

seront basses. Le but ici est donc d'essayer d'obtenir une longueur d'antenne déployée comparable à la taille des antennes usuelles tout en conservant un volume minimal.

L'antenne générique est considérée comme une antenne électriquement petite et il en découle que son gain, son efficacité, son impédance, etc. peuvent être calculés de manière théorique grâce à des formules issues de la théorie des petites antennes. Pour déterminer ses caractéristiques précises et confirmer la théorie, l'antenne a été simulée sous NEC-2, qui est un code electromagnétique mondialement reconnu comme performant pour la simulation des éléments filaires. Les caractéristiques de cette antenne ont également été simulées grâce à un code électromagnétique privé chez France Télécom, pour avoir confirmation des résultats de NEC-2. Les deux codes donnent des résultats approchants mais les caractéristiques de l'antenne ne correspondent pas aux spécifications attendues, surtout en ce qui concerne l'impédance de l'antenne et les bandes de fréquence opérationnelles qui se situent autour des 17 MHz. Cela implique une continuation des recherches pour trouver une géométrie optimale répondant aux spécifications.

Chapitre 3: Optimisation, réalisation et validation d'un prototype d'antenne HF compacte

Le troisième chapitre de cette thèse a un objectif simple: trouver la plus petite antenne possible ayant les performances des antennes HF classiques de grande taille. Pour atteindre cet objectif, la première étape a été de rechercher les paramètres géométriques de l'antenne générique qui influencent positivement ses performances. Après de nombreuses séries de tests, il est apparu que le facteur géométrique le plus influent était tout simplement la taille de l'antenne. Ainsi les recherches suivantes ont été orientées vers l'augmentation de la taille de l'antenne tout en conservant un volume entrant dans les spécifications requises. Pour combiner compacité et performance, l'idée a été d'augmenter la longueur totale déployée de l'antenne en ajoutant une seconde structure à méandres en parallèle et reliée à la première, comme présenté sur la figure 3.

La hauteur de l'ensemble ne change pas mais la longueur totale est ainsi doublée. Ce nouveau design a également été simulé sous NEC-2 et son impédance a été nettement améliorée grâce au doublement de structure. La possible bande opérationnelle se situe par contre autour des 18 MHz, ce qui est encore trop élevé comparé aux fréquences recherchées. Pour vérifier les résultats de simulations de NEC-2, un prototype de cette double antenne compacte a été réalisé (voir partie droite de la figure 3) et testé. Les mesures confirment bien les simulations mais des efforts doivent donc être faits pour permettre un fonctionnement de l'antenne dans les parties basses de la bande HF.

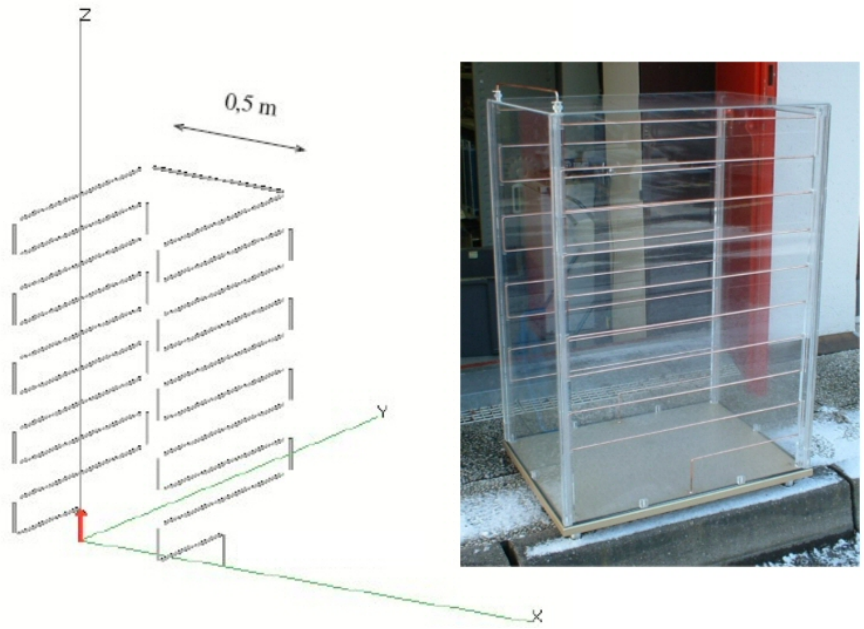

Figure 3: Modèle d'antenne compacte double (à gauche) et son prototype (à droite)

Au lieu de doubler la structure, une autre idée a été d'ajouter des sinusoïdes sur les parties horizontales de l'antenne générique, celles qui ne contribuent pas au rayonnement, pour accroître sa longueur totale tout en conservant un seul panneau. Les résultats de ce nouveau design on été améliorés et un prototype d'antenne sinusoidale réalisé comme le montre la figure 4.

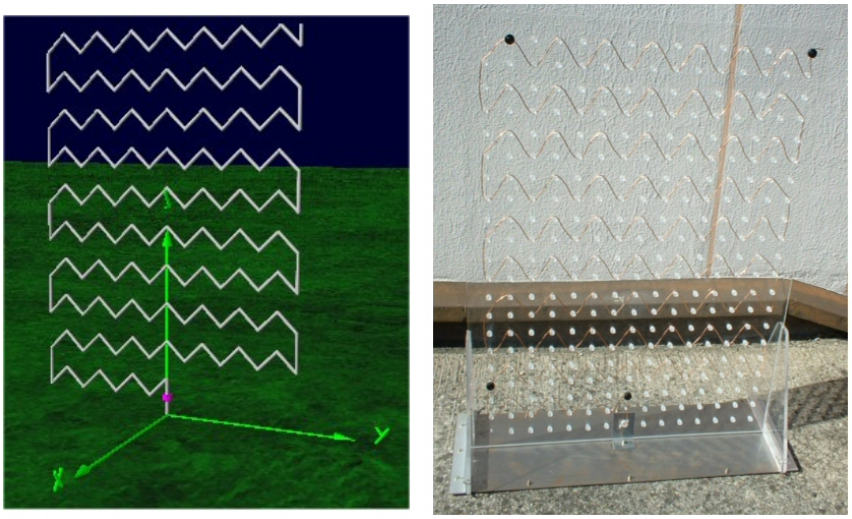

Figure 4: Modèle d'antenne sinusoïdale simulée sous NEC-2 (à gauche) et son prototype (à droite)

Cette fois, les résultats de simulation différaient des mesures réelles où l'antenne présente une résonance autour des 13 MHz avec une bande de quelques kHz. Avec des techniques

utilisant des stubs[1], il est possible, et cela a été vérifié, d'adapter l'antenne à n'importe quelle fréquence de la bande HF ou à plusieurs fréquences simultanément.

À ce stade de l'étude, l'antenne sinusoïdale présentait des caractéristiques satisfaisantes mais sa fragilité et son manque de stabilité dûs à sa composition sur un seul panneau a été un point critique car le prototype s'est souvent cassé pendant les séances d'expérimentations par vent fort ou de transport. Il a donc été décidé de continuer les recherches et des tester une solution intermédiaire combinant une structure doublée avec des sinusoides. En effet, l'antenne finale imaginée est une structure mixte entre les deux concepts précédents, stable et mesurant 50 cm de haut, 85 cm de largeur et 50 cm de profondeur comme le montre la figure 3.25.

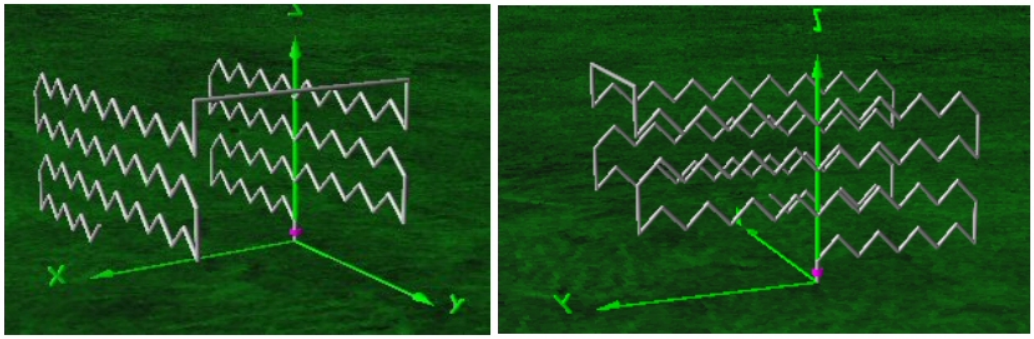

Figure 5: Vue sous deux angles du design final simulé sous NEC-2

À cause des problèmes rencontrés par les codes de simulations pour modéliser les sinusoïdes et établir des prévisions proches de la réalité, beaucoup d'essais ont été nécessaires avant d'aboutir au design final de l'antenne HF compacte et à la réalisation de son prototype (voir figure 3.26).

Figure 6: Prototype final de l'antenne HF compacte

[1]Un stub est un morceau de câble se terminant par un court-circuit ou par un circuit ouvert. Ce câble a une longueur bien précise et il est connecté en parallèle à la ligne principale à une distance précise de l'antenne permettant ainsi son adaptation à une fréquence.

Conclusion sur la partie antenne HF compacte

L'antenne HF compacte à été réalisée (voir prototype en figure 3.26) et le prototype a été testé en configuration radar côtier et embarqué. D'un côté, les résultats d'expérimentations prouvent que l'antenne a les mêmes capacités de détection que des antennes HF de grande taille (dans les expériences, le prototype a été comparé à une antenne biconique de taille 16 fois supérieure). Mais d'un autre côté, comme cela était prévisible, sa petite taille globale est très pénalisante pour être utilisée en émission car son gain est trop faible. Cette antenne peut être adaptée à toutes les fréquences HF de 5 à 30 MHz à l'aide de stubs. La structure rayonnante est composée de brins de cuivre, le plan de masse est en aluminium et le radome entourant et protégeant l'antenne est en fibre de verre. Elle a une polarisation verticale et son diagramme de rayonnement, comparable à celui d'un monopole, présente un gain maximum dans la direction de la mer, ce qui est idéal pour propager les ondes de surface. Ce design final d'antenne HF compacte répond donc à toutes les spécifications du cahier des charges initial et cela est une très bonne conclusion pour cette partie de l'étude. Ainsi avec une petite antenne passive compacte, le radar HF à ondes de surface embarqué peut maintenant être facilement envisageable et l'aspect encombrant des antennes ne sera plus non plus un problème sur les côtes où plusieurs éléments, associés en réseau phasé, restent discrets et furtifs. De plus, un élément compact est un avantage au sein du réseau phasé pour limiter les effets de couplage entre antennes qui peuvent perturber les signaux radar. L'objectif de départ est donc atteint et cette antenne peut intéresser plusieurs pays impliqués dans les radars HF.

Au sujet de cette première partie, l'essentiel à retenir est la démarche intellectuelle qui a mené au design final de l'antenne HF compacte ainsi que les problèmes causés par les codes de simulations. En effet, cette antenne compacte est très difficile à simuler correctement, principalement à cause de la présence des sinusoïdes. Les différents codes électromagnétiques utilisés ont des limitations et il se trouve que l'antenne HF compacte est hors de leur domaine de validité. Les longueurs des segments utilisés pour modéliser les parties sinusoïdales étaient très petites devant les longueurs d'onde décamétriques. A cause de cette minuscule longueur, les conditions de maillage requises par NEC-2 pour un calcul optimal n'étaient pas respectées. Cela signifie que des hypothèses de calcul ne sont alors plus valables, ce qui expliquerait les différences trouvées entre les résultats de simulations et les mesures réelles. De plus, le code électromagnétique NEC-2 n'est pas dédié aux très basses fréquences comme celles de la bande HF. Le code source original ne prend pas en compte certains termes qui deviennent très importants en basses fréquences et qui ne peuvent plus alors être négligés. D'autres codes comme ceux de France Télécom (SR3D) ou celui de l'ONERA (Elsem 3D) ont été utilisés pour essayer de mieux refléter la réalité pour l'antenne HF compacte mais là aussi sans succès. Cela veut dire que cette étude a été complexe sans codes électromagnétiques performants. Ainsi, l'essentiel de l'étape d'optimisation de l'antenne a nécessité la réalisation de nombreux prototypes, sans quoi cela aurait été impossible. De plus, au sein du cahier des charges initial, certaines spécifications étaient difficiles à atteindre (comme le fonctionnement en très basses fréquences) alors que d'autres étaient simples à respecter. Pour les satisfaire toutes, de nombreux compromis ont du être trouvés. Malgré de nombreuses simulations de différentes formes et géométries, inspirées du repli en méandres, et dû au manque de codes efficaces, une grande partie de cette thèse

a donc été expérimentale. Durant ce projet, des centaines heures ont été consacrées aux expérimentations par tous les temps, sur tous les sites en France et à Singapour, avec de nombreux prototypes et elles ont été très utiles pour bien comprendre le problème complexe du design d'antenne en HF et des procédures à respecter pour avoir des mesures exploitables.

Dans le futur, une modification du code source original de NEC-2 devrait être envisagée, mais dans ce cas, tous les nouveaux outils pratiques de visualisation des résultats ne seraient plus utilisables et l'exploitation des résultats du code modifié serait alors longue et laborieuse. Il serait également intéressant de découvrir et tester d'autres codes électromagnétiques mais ils sont généralement chers et cela représentent un lourd investissement.

Au sujet de l'antenne HF compacte elle-même, beaucoup d'idées devraient être testées dans le futur. Par exemple, pour une configuration embarquée, il faudrait réfléchir à des structures hybrides utilisant des méandres et des boucles magnétiques dans le but de réduire les effets néfastes des plaques métalliques verticales qui perturbent le rayonnement. Autre idée, un dielectrique pourrait être ajouté dans l'espace libre situé entre les deux structures de l'antenne. Il est aussi possible d'envisager de plonger les fils de cuivre dans un dielectrique qui aurait pour effet "d'allonger" virtuellement leur longueur et permettre ainsi d'obtenir des fréquences de résonance naturelles encore plus basses. Enfin, il est aussi possible d'utiliser la superdirectivité pour créer un réseau ayant un gain supérieur à un réseau phasé classique en réduisant intelligement l'espace entre antennes et en leur appliquant un jeu de phase spécial. Ces réseaux superdirectifs sont très difficiles à mettre en place à cause du contrôle très précis de la phase qui est nécessaire et à la difficulté d'adapter les antennes.

Chapitre 4: Création d'une base de données d'échos de mer simulés

Un autre inconvénient majeur des radars HF à ondes de surface concerne le rôle perturbant des échos provenant de la mer dans la détection des cibles. En effet, les antennes des radars à ondes de surface illuminent la surface de la mer avec une onde HF qui interagit avec les vagues. Cette interaction est due à leurs longueurs d'ondes décamétriques voisines et elle est connue sous le nom de diffusion résonante de Bragg. En effet, quand la longueur d'onde des vagues correspond à la moitié de la longueur d'onde radar émise, le phénomène de résonance de Bragg apparaît et ces vagues renvoient alors vers le radar un fort écho. Spectralement, ces échos renvoyés apparaissent avec des décalages Doppler bien précis appelés fréquences de Bragg f_b (f_b (en Hz) $= \pm 0,102\sqrt{f_0}$ avec f_0: fréquence émise par le radar en MHz).

En observant le spectre d'un écho de mer (voir figure 7 ci-dessous), on remarque donc clairement deux pics distincts aux fréquences de Bragg représentant le fort retour des vagues de longueur d'onde $\lambda_0/2$, qui se déplacent vers le radar et dans le sens opposé. Ce sont les pics de premier ordre du phénomène de Bragg, appelées aussi raies de Bragg. Mais comme la surface de la mer est composée d'une multitude de vagues d'amplitude, de vitesse et de direction différentes, les interactions entre ces vagues produisent un continuum de second ordre dont la forme et le niveau dépendent de l'état de la mer (calme, agitée, etc). Pour la détection, le signal utile est constitué par les échos de cibles. Les échos provenant de la mer

sont donc inutiles voire gênants et on emploit souvent le terme de "fouillis de mer" pour les caractériser.

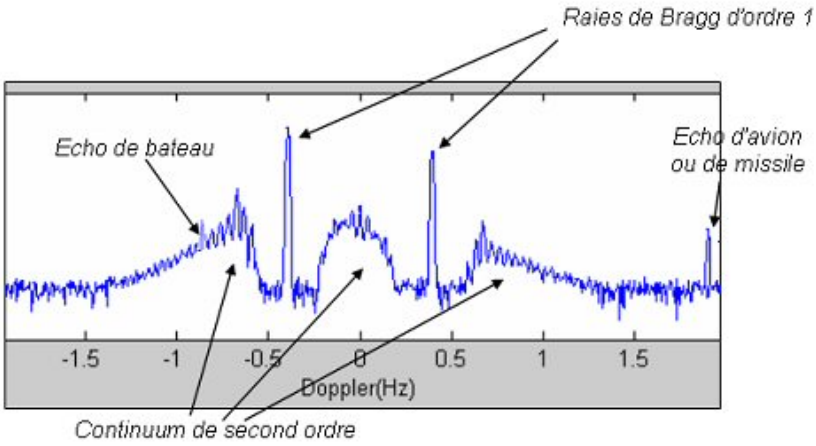

Figure 7: Modèle de spectre d'échos de mer

Or, il se trouve que les échos provenant de la mer sont situés dans le spectre utile où les échos de cibles sont généralement détectés. Si le niveau des signaux marins est élevé, ils peuvent parfois empêcher la détection des cibles et de ce fait déteriorer les performances des radars. La seconde partie de cette thèse a donc pour but de réduire l'influence du fouillis de mer dans le but d'améliorer les capacités de détection des radars HF à ondes de surface. Lors de séances expérimentales permettant la validation du prototype d'antenne HF compacte, des signaux ont été acquis et traités, et la présence de fouillis de mer est très visible sur les images résultantes. Pour réduire l'influence du fouillis marin, il est tout d'abord essentiel d'avoir une bonne connaissance des caractéristiques des échos de mer. En fait, le chapitre 4 propose une partie détaillée sur le phénomène de Bragg et sur les caractéristiques spectrales des échos marins dans le but de se familiariser avec les spectres de mer. On trouve dans la littérature des modèles de spectres de mer (exemple de spectre en figure 7) pour toutes conditions (fréquences radar, vitesses de vent, états de mer, etc) et grâce à eux il est alors possible de mettre en évidence les conditions qui causent plus ou moins de fouillis marin gênant.

Pour comparer ces modèles de spectres de mer à des mesures réelles, l'idée a été de créer une base de données d'échos de mer simulés présentés sous forme d'images Doppler distance, qui sont des images où les échos rétrodiffusés apparaissent en fonction de leur distance au radar et de leur vitesse radiale. Pour ce faire, un algorithme a été développé (voir figure 8) et optimisé dans le but de créer des données simulées proches de la réalité prenant en compte par exemple les pertes de propagation différentes en fonction de la distance, le bruit externe, les paramètres radar (puissance émise, nombre d'antennes utilisées, etc). L'algorithme permet également de simuler la présence d'une ou plusieurs cibles fictives ayant des caractéristiques précises (distance au radar, vitesse radiale et section équivalente radar).

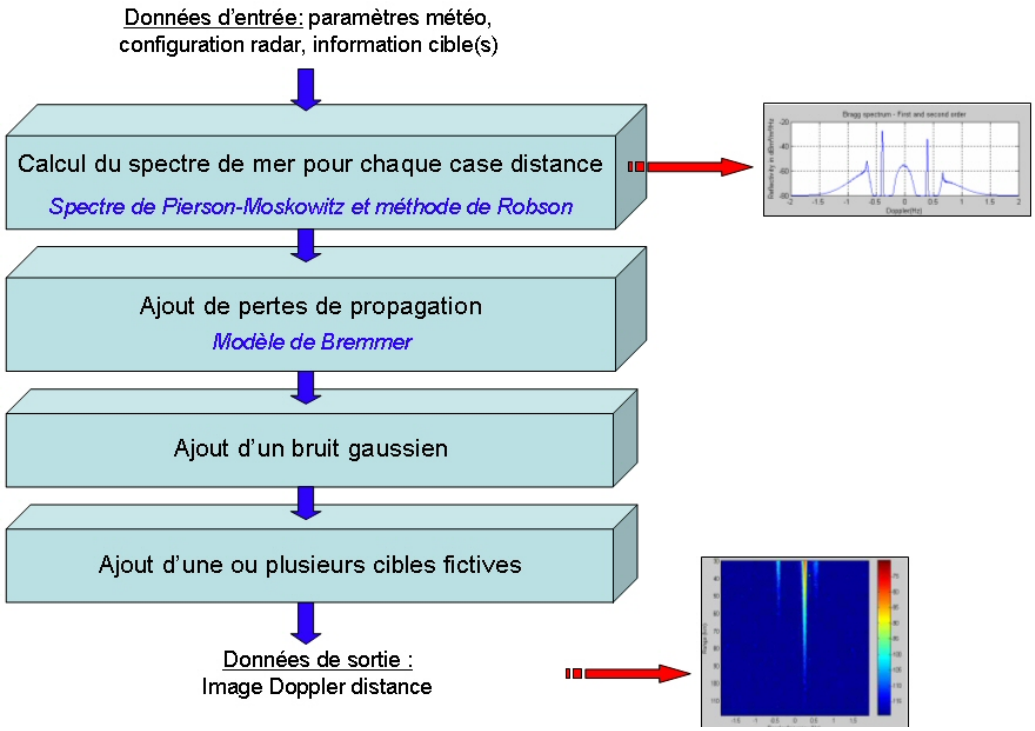

Figure 8: Algorithme permettant la simulation d'image Doppler distance avec des échos marins

Au final, de nombreux exemples de données simulées ont été comparées avec des images provenant de mesures réelles de radars à ondes de surface et ils sont très ressemblants, les modèles utilisés rendent donc bien compte de la réalité comme le montre la figure 4.29. Sur l'image de droite apparaît en plus des raies de Bragg, une raie centrale (à 0 Hz) correspondant aux échos du sol ou des objets fixes.

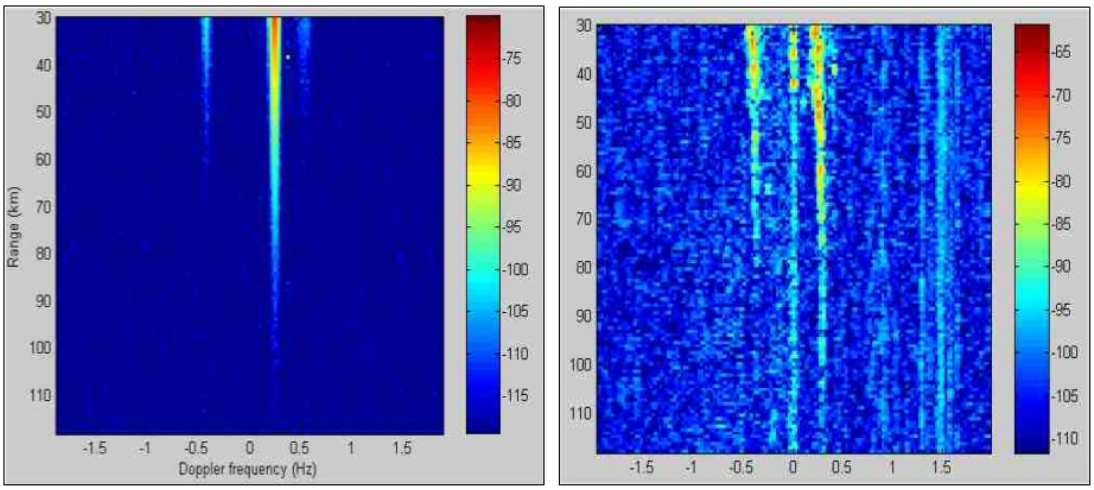

Figure 9: Comparaison entre une image Doppler distance simulée (à gauche) et une image obtenue à partir de mesures réelles (à droite), avec les mêmes paramètres radar

Les données des radars à ondes de surface sont encore très rares et la base de données simulées semble être une intéressante solution intermédiaire sur laquelle les algorithmes de filtrage d'échos de mer vont pouvoir être testés dans tous les cas de figures (toutes conditions météorologiques, tous paramètres radar, etc).

Chapitre 5: Développement et validation d'un algorithme de filtrage réduisant le fouillis de mer

Pour abaisser le niveau du fouillis de mer, une manière simple est de réduire les dimensions de la surface de mer éclairée par le radar. Cela peut se faire en augmentant la largeur de bande du radar ou la longueur du réseau phasé de réception ou alors en travaillant à hautes fréquences. Par ce biais, le niveau du fouillis peut être réduit mais pas suffisamment pour améliorer la détection des cibles. De plus, ces modifications radar sont souvent difficiles à mettre en oeuvre à cause d'un manque de place, d'un encombrement du spectre HF et des trop fortes pertes de propagation à hautes fréquences. C'est pourquoi pour un nettoyage des données optimum, une méthode de traitement de signal semble être une meilleure solution. Le chapitre 5 a donc pour objet le développement et la validation d'un algorithme de traitement de signal permettant de réduire le fouillis de mer.

L'étude des échos de mer grâce à la base de données simulées nous a permis de mieux maîtriser les interactions entre les ondes HF et vagues. En fait, le phénomène de diffusion de Bragg est fortement basé sur le principe de cohérence car il apparaît seulement quand les ondes radar interagissent avec un jeu de vagues sélectionnées. L'importante contribution du fouillis de mer est due au fait qu'un grand nombre de vagues respectent la condition de résonance au même instant, leur crêtes étant en phase. Cela signifie qu'il y a une régularité spatiale dans les trains de vagues et cette affirmation se vérifie souvent dans la réalité quand on regarde la mer et qu'on apercoit des séries de vagues bien régulières.

Pour cette raison, nous avons décidé d'utiliser les propriétés physiques des vagues, en l'occurence leur cohérence spatiale, pour élaborer une méthode efficace de réduction de fouillis. Simplement, on suppose l'hypothèse que si le fouillis apparait à cause d'un principe de cohérence, il doit être possible de le réduire en utilisant la même propriété. Ainsi, nous avons envisagé l'utilisation de méthodes d'atténuation de bruit pour réduire l'infuence des échos de mer. Ces techniques détectent et filtrent des signaux gênants cohérents. Pour traiter notre cas précis, le choix a été orienté vers une méthode de filtrage adaptatif. Une grande partie de ce chapitre est dédié à la présentation du principe de filtrage adaptatif. Puis, une étape incontournable est l'étude de la cohérence des échos de mer réels car cette cohérence est la base de la méthode de filtrage. Un premier algorithme assez simple a été imaginé pour adapter la théorie à la réduction des échos de mer et il a été testé avec succès sur des données simulées issues de notre base de données. En effet, des échos de cible fictives cachés dans des raies de Bragg ont pu être détectés après filtrage adaptatif car le niveau du fouillis de mer fût considérablement réduit.

Malheureusement, en appliquant directement cet algorithme sur des données réelles, les effets furent tout à fait différents et le filtrage pas très efficace. C'est pourquoi, un algorithme plus compliqué (voir description en figure 10) a été développé dans le but de prendre en compte nombreux aspects des données réelles.

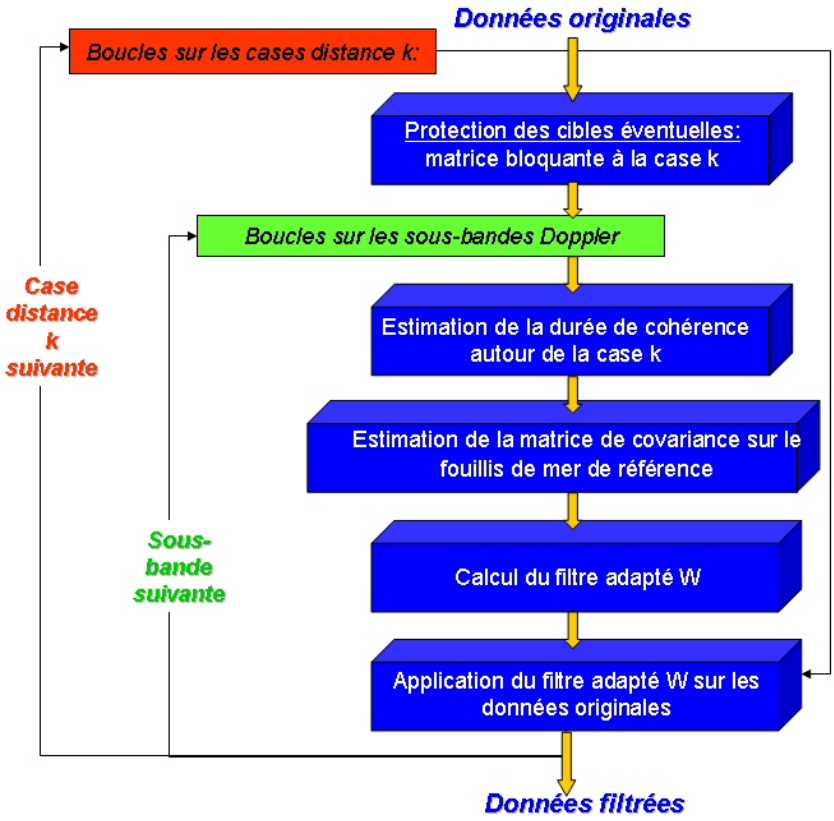

Figure 10: Algorithme de filtrage du fouillis de mer réel

Par exemple, dans la nouvelle version de l'algorithme présenté ci-dessus, les données à traiter doivent être séparées en sous-bandes pour un filtrage optimal et chaque partie doit être filtrée avec les propriétés de cohérence correspondant à sa propre sous-bande. De plus, les cibles éventuelles doivent être protégées avant filtrage pour éviter qu'elles ne soient prise en compte dans l'estimation de la matrice de covariance qui va nous servir pour calculer le filtre adapté. Ainsi, une matrice bloquante a été implémentée pour réduire l'influence d'une cible éventuelle ainsi que de ses lobes de corrélation. Une autre amélioration de l'algorithme concerne le calcul du filtre adapté qui est différent selon si la matrice de covariance est correctement estimée ou non. Si la matrice est bien estimée, le filtre adapté sera simplement calculé grâce à l'inversion de cette dernière. Et si elle est mal estimée, une décomposition en valeurs propres et vecteurs propres sera nécessaire. Ensuite, une recherche du nombre de signaux cohérents présents dans la matrice de covariance sera effectuée à l'aide d'un critère appelé MDL (Minimum Description Length) et le filtre adapté sera ainsi calculé grâce aux vecteurs propres correspondant aux signaux cohérents détectés. En conclusion, l'algorithme final adopté est beaucoup plus compliqué que la première version, il a été optimisé mais le filtrage n'est pour le moment pas très performant sur données réelles. Dans certains cas, les raies de Bragg et la raie centrale sont réduites mais dans d'autres cas le filtrage empire la situation. Ces résultats sont décevants pour l'instant car l'efficacité n'est pas assurée dans tous les cas.

Les deux figures 5.65 et 5.66 présentent un image Doppler distance avant et après filtrage adaptatif. Sur cet exemple, la raie centrale a été efficacement réduite. Les raies de Bragg

ont également été filtrées mais on se demande si des cibles n'auraient pas été affectées par le filtrage car il ne reste plus d'échos de cibles potentielles après filtrage dans la zone traitée. De plus, le traitement des données en 3 sous-bandes reste trop visible au moment de la reconstitution de l'image finale.

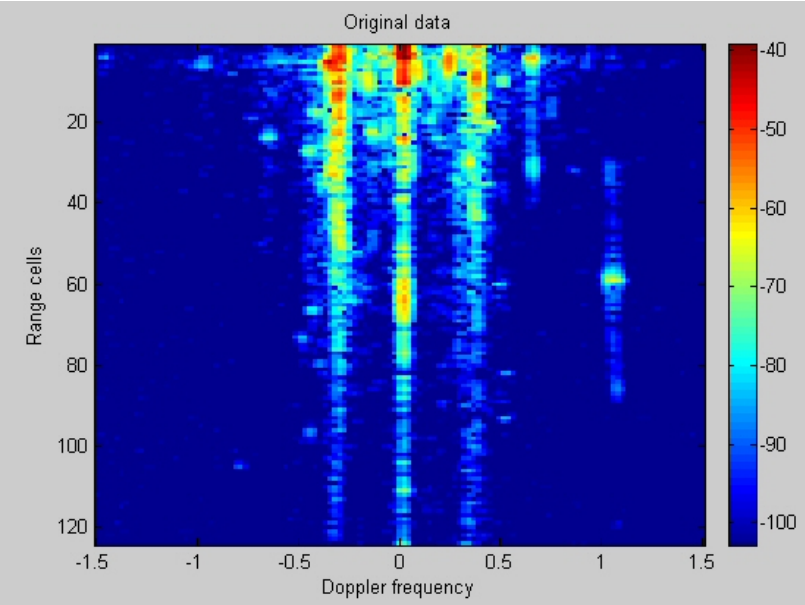

Figure 11: Données réelles originales avant filtrage adaptatif optimisé

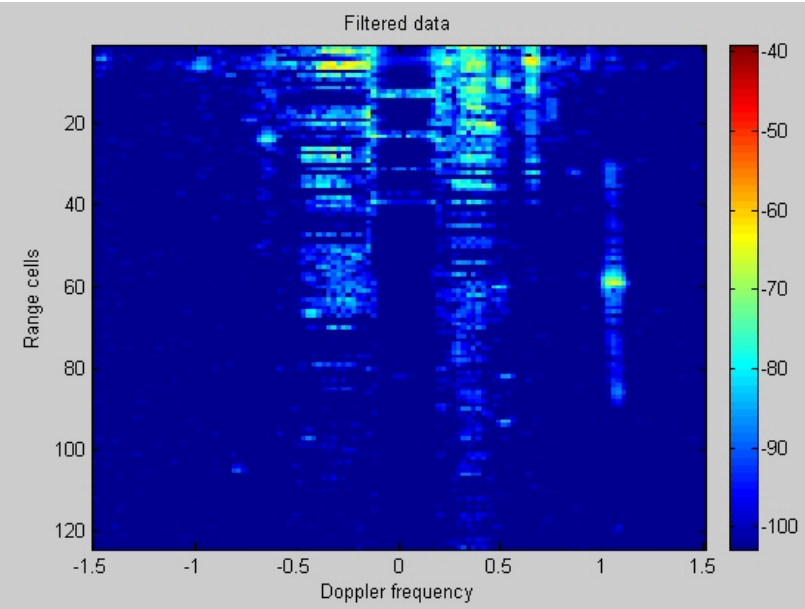

Figure 12: Résultats après filtrage adaptatif optimisé

Conclusion sur la partie réduction du fouillis de mer

Dans la seconde partie de cette thèse, le développement d'une méthode de filtrage efficace du fouillis de mer a été très difficile pour plusieurs raisons. Tout d'abord, le très petit nombre d'échantillons de données réelles donne seulement des indications à propos de la cohérence du fouillis de mer mais nous ne pouvons pas vraiment conclure avec certitude sur ce point. Par exemple, la cohérence du continuum de Bragg du second ordre est délicate à affirmer car il n'est pas très visible sur les données réelles dont nous disposons. En fait, pour cette étude, le radar utilisé pour obtenir des données réelles étant un radar de recherche, développé en collaboration avec Singapour, il n'est pas encore opérationnel ce qui signifie que l'acquisition des données n'est pas automatique, il faut planifier des missions, etc. Ainsi, nous avons seulement quelques fichiers de données réelles qui ont été acquis avec la même bande (400 kHz), à 3 fréquences différentes (5.255 MHz, 10.750 MHz and 16.050 MHz) mais l'état de mer n'est pas précisé, de même que la présence ou le type de cibles au moment des acquisitions sont inconnus, les réglages des paramètres radar sont également vagues. Avec ces informations floues et peu nombreuses, il est impossible de faire des statistiques sur la cohérence des données réelles ou de vérifier que le niveau des échos détectés correspond bien à des cibles avec le bon niveau attendu. Des statistiques doivent être établies avec des mesures précises des paramètres météorologiques (vitesse du vent, du courant, orientations, etc). Des expériences avec des cibles coopératives sont obligatoires pour avoir des cibles étalons connues et tester ainsi la méthode de filtrage.

Un autre point qui a impliqué les principaux problèmes de filtrage concerne le critère MDL qui détermine le nombre de signaux cohérents (que l'on suppose être du fouillis de mer). Ce critère est très puissant sur des données simulées mais ne marche qu'à moitié quand on l'applique sur données réelles. Ceci est certainement à la qualité des signaux réels, si les données sont pondérées ou non, etc. Le principe de base du critère MDL est qu'il détecte une rupture dans la courbe des valeurs propres de la matrice de covariance qui indique une séparation entre les signaux cohérents et les autres. Dans les données réelles, les courbes de valeurs propres sont assez plates et monotones et le critère MDL détecte difficilement la rupture. Ainsi quand les conditions sont optimales, le critère donne un nombre de signaux cohérents tout à fait possible (ce nombre ne peut être vérifié avec les données réelles mais il est plausible) et le résultat final du filtrage adaptatif est satifaisant. Mais quand le critère est faux (cela arrive souvent), le filtrage fournit un résultat très décevant, généralement pire que les données originales.

De plus, les problèmes peuvent venir des phases de génération et réception qui sont faites en grande partie numériquement et qui causent des distorsions et modifications des signaux. En fait, la fonction permettant l'étude de la cohérence des échos de mer devrait être ajustée avec les signaux émis et reçus avant le filtrage des données.

Enfin, cette seconde partie de thèse a seulement été étudiée pendant un an et demi, le reste du temps étant consacré à la partie antenne, et cela n'est pas suffisant pour entrer dans le sujet du radar HF à ondes de surface, maîtriser le filtrage adaptatif et pour résoudre tous les problèmes rencontrés dans cette partie. Le manque de temps peut expliquer le résultat modéré présenté à la fin de cette thèse. Cependant, je suis optimiste quant au succès de cette méthode de réduction de fouillis de mer à cause de plusieurs résultats enourageants qui démontrent la faisabilité de la méthode mais son efficacité dans tous les cas reste à être approfondie. Mon travail sur ce sujet est en quelque sorte une pré-étude pour la réduction

du fouillis de mer par filtrage adaptatif et beaucoup de points ont déjà été éclaircis.

Pour toutes ces raisons, il est impossible de conclure réellement cette étude car beaucoup de points restent à être étudiés avant de proposer une méthode efficace de filtrage.

D'autres idées peuvent être approfondies dans le futur. Après quelques discussions avec des collègues (Michel Menelle et Marc Lesturgie), d'autres méthodes de réduction du fouillis ont pu être envisagées. Par exemple, une méthode utilisant un filtre temporel tel qu'un filtre LPC (Linear Predictive Coefficient) devrait être en mesure de "prédire" la continuité temporelle de divers signaux cohérents contenus dans le signal radar reu. Ainsi, les signaux provenant de la mer devraient différer des autres signaux temporels et on devrait pouvoir les réduire sans pour autant réduire les signaux provenant des cibles éventuelles. Néanmoins, ce ne sont que des suppositions et cette méthode doit être implémentée et vérifiée pour tirer des conclusions sur sa faisabilité. Une autre idée serait d'étudier la phase des signaux provenant de la mer, au cours des cases distance par exemple. Si la phase des signaux est stable d'une case distance à une autre, il est peut être possible de la réinjecter déphasée de 180 ° dans le but d'annuler ou réduire l'influence des échos de mer.

Conclusion

Pour conclure ce rapport, j'aimerais ajouter quelques points. Tout d'abord, cette thèse fut une très bonne expérience au vu de la variété des sujets abordés. D'un côté, cette étude a nécessité une bonne compréhension de l'ensemble du système radar, de l'antenne, au traitement des données, en passant par le matériel, l'électronique, etc et cela rend le sujet très intéressant car très complet. Mais d'un autre côté, on ressent une certaine frustration parce que le sujet est si vaste que l'on a parfois seulement un survol de certains points. Dû au manque de temps, tous ne peuvent être étudiés, c'est pourquoi nous avons décidé de choisir deux inconvénients du radar HF à ondes de surface à approfondir dans cette étude. Néanmoins, nous étions souvent confrontés aux autres inconvénients mentionnés dans le rapport (spectre HF encombré, compatibilité électromagnétique, fouillis ionosphérique) surtout pendant les expérimentations terrain. Enfin, les deux parties de cette thèse étant totalement différentes et il était parfois délicat de passer d'un sujet à l'autre.

De nombreux pays ont lancé des programmes de recherche sur le radar HF à ondes de surface mais la communication entre eux est encore rare c'est pourquoi il n'y a pas beaucoup de bibliographie sur le sujet alors que tout le monde rencontre les mêmes problèmes et cela est regrettable. J'espère que ce document, rédigé en anglais pour une meilleure diffusion, pourra servir de point de départ à d'autres personnes.

D'un point de vue personnel enfin, cette période de thèse fut très instructive. De plus, j'ai recontré des personnes brillantes et une collaboration internationale était également très intéressante à vivre. L'écriture de la thèse en anglais était également nécessaire pour que les équipes singapouriennes puissent comprendre les résultats.

Ph D. THESIS OF THE UNIVERSITY OF PARIS 6

Specialty

Electronics and Universe Science

presented by

Emilie BRONNER

In order to obtain the degree

DOCTOR OF THE UNIVERSITY OF PARIS 6

Improvements of HF Surface Wave Radars Perfomance by Compact Antenna Study and Adaptive Filtering used to Reduce Sea Clutter

defended on the 9th of November 2005

in front of the jury composed of :

Mr Alain BOURDILLON, professor at the University of Rennes 1, Reporter
Mr Jacques DAVID, professor at the University of Toulouse, Reporter
Mr Walid TABBARA, professor at the University of Paris 6 (UPMC), Examiner
Mr Ronan MOULINET, engineer in DGA, Examiner
Mr Marc HELIER, thesis director, professor at UPMC, Examiner
Mr Jean-Philippe MOLINIE, engineer in DEMR-RBF, ONERA, Examiner
Mr Philippe BOURBON, member of the French Institute of Navigation, Invited member
Mr Stephane SAILLANT, engineer in DEMR-RBF, ONERA, Invited member

Acknowledgments

At the end of this thesis, I would like to thank many persons for their help, technical or moral, all along this project. First, I would like to thank Gilbert Auffray for his welcome in his research team in ONERA. I have learnt at lot with him and I have appreciated his availability, his support and his advice.

Then, I thank Stéphane Saillant, my ONERA supervisor, for his continuous help and his comforting support, mainly in the last period of the thesis.

Thanks to Jean-Philippe Molinié, my private teacher in signal processing, for his interesting teaching and his patience when my mind had difficulties to understand.

Thanks also to my thesis director, Professor Marc Hélier, for letting me proceed my own way until I needed some guidance, and for being there when asked, with many advice and moral support to achieve this project.

Thanks also to all my ONERA colleagues of the "Radar Basses Frequences" team (Véronique, Juanito, Philippe, Valérie, Michel, Bruno D., Florent, Bruno U., Patrick, Gérard) for their friendship and energy expended in everyday life or external activities, for their encouragement and the permanent warm atmosphere. They have been my second family for three years and I will not forget them. I also thank the numerous students (Patrick, Ping, Victorien, Marc, Philippe), members of the team for a few months, who helped me and whom I was pleased to meet.

I would also like to thank the Singaporian team of DSTA, especially Hian Lim Chan and Xin Sui Goh, and NTU (Radar Lab) for their warm welcome on their island and for their technical discussions.

A warm thankyou to all my friends and especially to Nicolas, Alexandre and Sébastien for their support and faithfulness with the passing years. I also thank Mr Bourbon for his good advice about this report.

Last but not least, many thanks and love to my parents and my family who have been a great source of strength all through this work.

I dedicate this thesis to Blandine.

General summary

HF Surface Wave Radars (HFSWR) find applications in various fields such as maritime surveillance, oceanography or target detection. They use electromagnetic waves, with frequencies comprised between 3 and 30 MHz, that propagate over the sea surface beyond the horizon limit, reaching a few hundreds of kilometers. Thus, these radars can provide a greater detection range than those possible with horizon-limited microwave radars. Nevertheless, they are still recent and not totally operational for the moment all over the world because of several drawbacks. The objective of this thesis is to try to solve two of these drawbacks in order to improve performance of HF Surface Wave Radars.

First, one of the major constraints that is studied in this thesis concerns the size of HF antennas that is too important. For practical reasons and to envisage a shipboard radar configuration, it is necessary to reduce the size of the HF elements by designing a new compact HF antenna responding specifications of HFSWR. The first part of this document presents problematics, design requirements and then all the intellectual process that leads to the realization of a final compact HF prototype.

Then, another way of improving performance of HF Surface Wave Radars, and mainly detection capability, is to reduce disturbing impact of sea echoes on radar signals. Actually, when the sea surface is illuminated by a high frequency wave, it backscatters a portion of the incident energy to the source because of a special interaction between HF waves and sea waves. On that account, echoes of potential targets are sometimes hidden by echoes coming from sea surface and then the second objective of this thesis is to reduce the impact of disturbing sea echoes. A signal processing method such as adaptative filtering is studied and implemented to achieve this objective in the second part of this report.

Key words : HF Surface Wave Radar, small antenna, meander line antenna, electromagnetics codes, Bragg scattering, sea spectrum, coherence, adaptive filtering, MDL criterium.

Introduction

In the frame of a joint research program conducted by ONERA (Office National d'Etudes et de Recherches Aerospatiales) from France and DSTA (Defence Science and Technology Agency) from Singapore, a thesis has been proposed in order to improve performance of High Frequency Surface Wave Radars. Co-financed by ONERA and DSTA, the study has been conducted in ONERA within the "Rabar Basses Frequences" team with the collaboration of DSTA for experiments and technical decisions. This thesis was three-year project supervised by Marc HELIER, professor at the University of Paris 6, as a thesis director and by Stephane Saillant, engineer in ONERA. Both of the countries involved in this project are interested in High Frequency Surface Wave Radars because of their numerous advantages compared to usual radars.

In fact, the use of radars in maritime navigation is an obviousness for a long time. On board or on coasts, they represent today essential elements to guarantee safety in ship navigation whatever the weather. In general, they are microwave radars, meaning frequencies in the order of a few gigahertz and wavelengths about the centimeter. Such systems provide great quality information for navigators, in particular when they are associated to cartographic software for example. Nevertheless they are limited by physical properties of propagation of the very high frequency waves. In fact, propagation occurs in straight line and that limits radar range to the horizon, typically to 30 nautical miles or 55 kilometers.

Therefore, in 1982, the United Nations Convention of Montego Bay about sea rights extended sovereignty of coastal states up to 200 nautical miles (around 370 kilometers) from their coasts, defining the Exclusive Economic Zone (EEZ). These conditions give new rights to states, particularly in terms of exploration and exploitation of natural resources, they are also related to obligations concerning protection and preservation of marine environment (excessive fishing, pollution, illegal activities). It means that for more than twenty years, a surveillance of the EEZ has been essential with the possibility of counting and tracking ships sailing in this zone.

The problem is that microwave radars cannot cover the 200 nautical miles of the EEZ because they are limited by the horizon. It is always possible to have recourse to aerial or naval surveillance of the zone, but it is expensive and necessarily limited in time and space. Today, it is feasible to complete microwave radars with High Frequency Surface Wave Radars that have better detection capabilities. The first difference between a surface wave radar and a microwave radar is the carrier frequency which is comprised between 3 and 30 MHz. This corresponds to the "HF" or "High Frequencies" domain. The second

difference concerns the electromagnetic field propagation mode : while in the microwave domain, the propagation occurs in free space in a quasi-optic manner, meaning in straight line, in HF, this is the sea surface itself that guides electromagnetic waves, such qualified as surface waves. These waves propagate in vertical polarization above sea surface. Ships or other low flying objects send back through the radar a portion of the incident surface wave as a backscattered surface wave which can be detected by the radar system up to ranges about hundreds of nautical miles, which is compatible with the extent of the Exclusive Economic Zone.

High Frequency radars are sometimes referred to over-the-horizon (OTH) radars because of their capacity to receive targets echoes over much long distances than microwave radars. Two types of HF radars exist : sky wave and surface wave radars. Sky wave radars are the most common types of HF radars. They receive backscattered echoes thanks to reflection of HF waves on the ionosphere. They normally cover the range interval between about 500 and 3,500 km. Both of these radars can measure the range, azimuth, signal amplitude and Doppler characteristics of observed objects. The HF surface wave radars can be coastal or shipboard and they have a lot of applications in the civil domain. First, these are useful instruments for the maritime long ranges surveillance such as the coverage of the EEZ extent. The surveillance far from coasts allows detection and tracking of potential illegal activities such as drug trafficking, contraband or pirate activities and clandestine immigration. Other applications are the environment and natural resources protection such as excessive fishing or pollution. Finally, these radars can provide information about wind and sea state that are useful data for oceanographers and scientists. Military applications of HFSWR include the detection of ocean vessels (ranging from large ships to small boats), low-altitude cruise missiles or low-flying aircrafts.

Both of the countries involved in this project, France and Singapore, are interested in HF surface wave radars and they would like to collaborate in order to develop an efficient demonstrator. The **(chapter 1)** of this document is an introduction to the HF Surface Wave Radars, context and basis of this project. It gives a general overview of the radar system through an historic of its evolution and explains its situation nowadays at an international and national level. These kind of radars are still recent and they are not totally operational for the moment. Then, particularities and precise principle of the radar are detailed to allow the reader to better understand the sensitivity of certain points. Especially the important radar processing step that allows extraction of useful information from measured data. This part concentrates many important aspects that will be very useful all along the document. It is an essential introduction to the vocabulary of radar terms and it is a summary of the functioning of this complete and complex system that combines many different technologies to generate, transmit, collect and process data. This is a kind of bibliographical part that ends with the main drawbacks that still remain to solve in order to provide HF Surface Wave Radars more operational and efficient than they are today. Their principal constraints are the important size of the HF antennas, the electromagnetics problems that can occur mainly in case of a shipboard radar configuration, a low resolution for detection, a disturbing effect of echoes coming from sea surface or ionosphere. Among all these drawbacks, two of them are chosen to be dealt with in this study in order to improve radar performance.

One of the major constraints that will be studied in this thesis concerns the size of the

HF antennas. HF surface wave radars consist in general in a transmitting antenna and in receiving antennas arranged in phased array, located close to the water edge. In fact, the current elements used to transmit and receive the HF waves are generally sized to a quarter wavelength. HF wavelengths being comprised between 10 and 100 m that results in important antenna size, from 2.5 to 25 m of height. Smaller efficient elements do not exist on the market today. Moreover, most of the studies about small antennas concern microwave domain. The antennas being an important part of the radar system, there is a real challenge to compact their size for several reasons. First, in order to limit overall dimensions of antennas and gain in discretion. Then, to limit coupling effects between antennas within the phased array. Finally, a size reduction is really necessary to allow a shipboard radar configuration. All these possible improvements implied by compactness would have for final effect to improve targets detection.

The intellectual process to solve the problem caused by important HF antennas size is to design a new HF antenna with compact dimensions. The element to imagine has to respond specifications required by HF surface wave radars. Compactness is the major point to improve and a maximum size of 1 m for the height of the new antenna would be a great progress. Other parameters must not be degraded by the size reduction and they have to provide the same characteristics than usual HF antennas used in HF surface wave radars. An impedance of 50 ohms and a vertical polarization are recommanded. Then, a passive antenna would be better than an active one to avoid phase shifting of active device and to allow the use of the antenna for both transmitting and receiving. To respond HF surface wave radars needs, the antenna should be large band or at least, it should have multiple operational frequencies with a sufficient bandwidth. Concerning the radiating of the antenna, a maximum gain in the sea direction is essential to efficiently propagate and receive surface waves. Finally, it is important to avoid complex structures to allow an easy reproduction of the antenna in series in order to associate them in a phased array. A precise control of the phase shifting between antennas being the basis of the phased array functioning, this point is important. Moreover, by imagining a simple design made of usual material, the antenna can easily be manufactured at low cost.

To respond all these needs, the process is in a first time to choose an antenna technology more compact than usual HF antennas and to model it **(chapter 2)**. A way to compact antenna size can be inspired by designs available at other frequencies, for example in wireless communications, or studied in literature. This departure antenna should be simple and small compared to HF wavelengths to respect two of the important points of the previous specifications. This antenna, called "generic antenna", will then be modeled by an electromagnetic code in order to determine its initial characteristics in terms of impedance, gain, polarization, etc. To obtain an optimum design, this antenna will be optimized thanks to several simulations. A search for parameters influencing antenna performance will be done and will result in a new design **(chapter 3)**. Once the antenna characteristics will be satisfying, a prototype should be manufactured in order to verify its functioning in reality and to validate the design. Several simulations and prototypes would be needed to obtain a final antenna responding every point of the HFSWR specifications. In the end, the final compact HF antenna will be tested and validated in a coastal and shipboard radar configuration.

Another way of improving performance of HF surface wave radars, and mainly detection

capability, is to reduce disturbing impact of sea echoes on radar signals. In fact, when the sea surface is illuminated by a high frequency wave, a portion of the incident energy is backscattered through the source because of a special interaction between HF waves and sea waves. For low elevation angles, a primary scattering mechanism called "Bragg scattering" occurs. This is a selective process in which there is a strong return coming from ocean waves that have a wavelength being half of the transmitted radar wavelength. Spectral analysis of the return signal coming from sea echoes proposes a Doppler spectrum characterized by two predominant peaks (first order Bragg lines) surrounding by a continuum (second order Bragg clutter). Indeed, signals received by the HF antennas of the surface wave radar system have been reflected by targets as ships or low-flying planes but they have also been highly backscattered by the sea surface. So, echoes of potential targets are sometimes hidden by echoes coming from sea surface and their detection is impossible : a target echo can be masked by the first or second order Bragg clutter. The second objective of this thesis is then to reduce the impact of these disturbing sea echoes.

The sea clutter level is proportional to the dimension of the sea surface illuminated by the receiving array of the HF surface wave radar. That is why, to receive less echoes coming from the sea surface, the first idea is to reduce dimensions of the radar cell. But this radar technique is not always feasible that is why other techniques such as signal processing have to be envisaged to solve this problem and will be implemented in the second part of this thesis.

In the reality, real echoes coming from HF surface wave radars are still rare because these kinds of radars are not numerous. That is why, the objective of the **chapter 4** is to obtain simulated sea echoes for any event (frequency, wind force, current velocity...). Indeed, the aim is to create a complete database of sea echoes, based on the models of literature and close to real echoes. This database will be very useful to better understand interactions between sea waves and HF waves for any event and to familiarize with sea echoes. Moreover, a database can be an useful tool to test efficiency of sea clutter reduction algorithms. In this section, a software providing the automatic generation of simulated data will be detailed.

The last chapter is dedicated to the implementation of a filtering algorithm reducing sea clutter. In function of interferences or noise to reduce, different filtering methods can be used. In this study, we decide to use a method of adaptive filtering because of the nature of sea echoes. Mathematical recalling and adaptive filtering principle will be detailed in the **chapter 5**. The adaptive filtering method uses different domains. The choice of the domains is made by having the best separation between useful signals (such as target echoes) and disturbing signals (such as sea clutter), trying to find a coherence between disturbing signals for an optimum efficiency of filter. Thanks to different analysis methods, the spatial coherence of sea wavetrains along distances will be studied. A simple algorithm reducing sea clutter will be implemented and tested on simulated sea echoes but it will have to be improved in a more complicated algorithm to provide a significant reduction of real sea clutter.

The objectives of this thesis can all be summed up in a few words. The HF surface waves radars have the advantage of a greater range detection compared to usual microwave radars. However, the too important antenna size and the disturbing role of sea in detection have not really been tackled in literature and that justifies this work. The study consists in improving detection performance of a HF surface waves radar compacting radiating

elements and reducing sea echoes. To do that, the process is in a first time to choose an antenna technology more compact than usual HF antennas and to model it with usual electromagnetic codes. Then, the design has to be optimized in order to obey specifications and to result in the fabrication of a prototype. Antenna tests in real radar configuration on coast or on ship will be planed to validate the final compact HF antenna. To clean radar echoes from sea influence, a database of simulated sea echoes will be created in order to better understand oceanographic phenomena present in the interaction HF waves / sea waves. Finally, a signal processing algorithm, standard adaptive filtering, will be developed and tested on simulated data and validated on real data in order to filter sea echoes.

Contents

Chapter 1

HF surface wave radars

Contents

The objective of this chapter is to present in detail the context of the thesis which is the HF surface wave radar. A general overview about radar history and over-the-horizon radars will introduce this chapter. Then, particularities and principle of the radar system with its different possible applications will be detailed to better understand the following document. Several drawbacks can be found in the HF surface wave radars and these points have to be improved for better detection capabilities and to try to achieve operational systems.

1.1 Introduction to HFWSR

Use of radars in maritime navigation is an obviousness for a long time. On board or on coasts, they represent today essential elements to guarantee safety in ship navigation, whatever the weather. In general, they are microwave radars, meaning frequencies in the order of a few gigahertz and wavelengths about the centimeter. Such systems provide great quality information for navigators, in particular when they are associated to cartographic software for example. Nevertheless, they are limited by the physical propagation properties of the very high frequency waves. In fact, this propagation occurs in straight line, slightly curved to the ground due to the tropospheric refraction, and that limits radar ranges to the radioelectric horizon, which is located a bit beyond the optical horizon. The range of a microwave radar given in nautical miles can be calculated thanks to this formula :

$$Range = 2,23\sqrt{h_r}$$

with h_r : Height of the observation point of the radar (given in meters above surface).

If the target elevates above sea surface at an altitude h_c, the range will be more important. In fact, in this case, the range becomes :

$$Range = 2,23(\sqrt{h_r} + \sqrt{h_c})$$

As an example, the Stiff tower in Ushant (west of France) and its radar have been sized for a nominal range in the order of 64 nautical miles.

Therefore, in 1982, the United Nations Convention of Montego Bay about sea rights defined the Exclusive Economic Zone (EEZ) as the maritime zone comprising the territorial seas and extending to 200 nm (around 370 km) from their coasts (see figure 1.1).

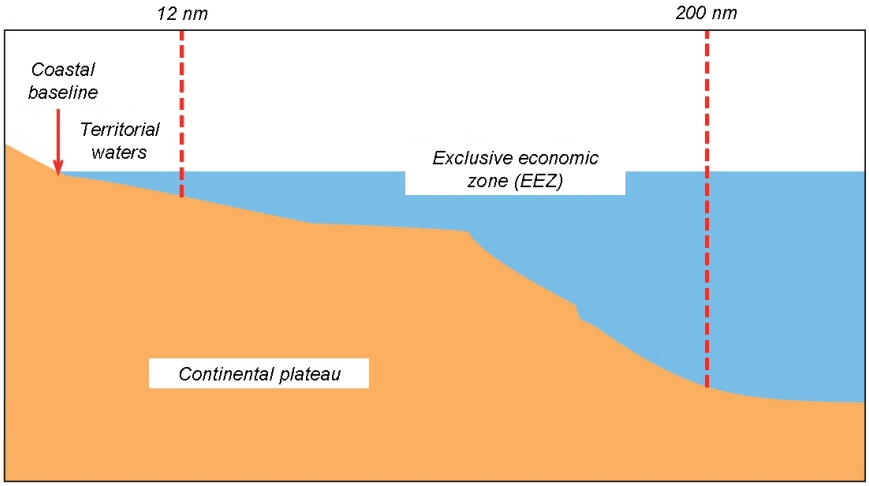

Figure 1.1: Definition of the Exclusive Economic Zone (EEZ)

In this zone, States have new rights, particularly in terms of exploration and exploitation of natural resources (living or not), of surjacent waters, of marine set and of subsoil. These rights are accompanied by obligations concerning protection and preservation of marine environment. So, a surveillance of the EEZ is essential with the possibility of counting and tracking ships sailing in this zone.

The problem is that microwave radars cannot cover the 200 nm of the EEZ. It is always possible to have recourse to aerial or naval surveillance of the zone, but it is expensive and necessarily limited in time and space. And it is the same for the present satellites that cannot have the sufficient spatial and temporal resolution to provide an efficient real-time surveillance. Today, it is feasible to complete it with High Frequency Surface Wave Radars which are better adapted to the coverage of huge maritime areas.

The HF surface wave radars have a lot of applications in the civil domain. First, these are useful instruments for the maritime long ranges surveillance. The surveillance far from coasts allow detection and tracking of potential illegal activities such as drug trafficking, contraband or pirate activities and clandestine immigration. Other applications are the protection of environment and natural resources against excessive fishing or pollution. Finally, these radars can provide information about wind and sea state, that are useful data for oceanographers and scientists. Military applications of HFSWR include the detection of ocean vessels (ranging from large ships to small boats), low-altitude cruise missiles or low-flying aircrafts detection.

1.2 Radar History

The term radar was a code used during the second World War by the US Navy, it is an acronym for *radio detection and ranging*, meaning literally detection and ranging system using radio waves. It is a system that operates by radiating electromagnetic waves from a suitable antenna, striking any target that might be present in that radiation, and then

collecting the backscattered energy. Detection of this energy constitutes detection of the target, analysis of the energy allows target parameters to be established.

Originally defined as a war instrument, radars are now used as surveillance tools for civil or military aims (aerial traffic for example), for help in navigation, as sensors for remote sensing, as scientific instruments (for example in meteorology, geophysics or spatial exploration).

The basic radar concepts are based on equations about electromagnetic waves, formulated by the British physicist James Clerk Maxwell in 1864. These principles were verified in 1886 by experiments of the German physicist Heinrich Hertz. The German engineer Christian Hulsmeyer [1] was the first to suggest, in 1904, the use of radio waves in a detection system in order to avoid collisions in navigation. More than one century ago, he patented the "Telemobiloskop" concept, ancestor of the present radars. A similar device was proposed in 1922 by the Italian inventor Guglielmo Marconi. Afterwards, the radar was developed progressively thanks to the action of several scientists, engineers and technicians.

Three major steps can be distinguished in its history. First, in the twenties, various detection experiments using radio waves were succeeded (Appleton in England in 1924, Breit and Tuve, Hyland, Taylor and Young in the USA, Mesny and David in France). In the middle of the thirties, they resulted in concrete applications thanks to progress of electronics. Thus, continuous wave radars have been implemented in France, on the Ligne Maginot, with a range about tens of kilometers. Moreover, the ocean liner *Normandie* was equipped with detection system using decimetric waves, able to detect icebergs in fog.

From 1935, researches moved towards realization of pulsed radars, as a result of two dissertations of the British R. Watson-Watt. In 1938, two French scientists, Ponte and Gutton, elaborated one of the most important device in this domain : the electronic beam tube, called magnetron with resonant cavity, which transmits high frequency pulses (radar with centimetric waves). Various French firms built then radars for the national defense. The German implemented their own systems but, their strategy being based on the offensive, the third Reich considered radar with less importance and rather developed radio navigation. In parallel, a line with radar stations was installed in England along its East and South coasts in order to detect aerial or maritime attacks. This system played an essential role in the England Battle (August-October 1940), during which the Luftwaffe (German Nazi air force) was not able to be the best in the British sky. From 1940, the collaboration between British and Americans provided to Allies a decisive advance in this technology, a technical superiority maintained until the end of war. Their specialized laboratories employed thousands of engineers, and their factories tens of thousands technicians, building several hundreds of this type of radars for every military use.

On the one hand, since the end of the second World War, the physical radar principles have not fundamentally changed. On the other hand, great progresses have been done in antennas domain with for example the phased array concept. Moreover, signal processing has more and more influence on the improvement of radar systems performances. In parallel, statistical detection theory has been applied successfully to concepts such as adaptive

receiver, ambiguity function or pulse compression. Finally, to go back to the HF radar case, signals digitizing is now used for transmitting and receiving, and it reinforces the role of algorithms compared to the role of analogical device.

1.3 Over-the-horizon radars

High Frequency radars use frequencies between 3 and 30 MHz and the associated wavelengths are from 10 m to 100 m. They are sometimes referred to over-the-horizon (OTH) radars because of their capacity to receive targets echoes over much long distances than microwave radars, which are restricted to distances defined by the line-of-sight of the horizon. Two types of HF radars exist : sky wave and surface wave radars. Both of these radars can measure the range, azimuth, signal amplitude and Doppler characteristics of observed objects.

1.3.1 Sky wave radars

The most common type of HF radars operates in the sky wave mode. It means that the radar system receives echoes through reflection from the ionosphere. In fact, a suitable frequency is selected and the radar bounces radio waves on the ionosphere, receives signals back from reflecting surfaces such as sea, islands, ships and aircrafts which may be hundreds or even thousands of kilometers away. It normally covers the range interval between about 500 and 3,500 km. Sky wave radar depends entirely on the ionosphere for successful operation.

The two following figures 1.2 and 1.3 propose a comparison between the wave path used in classical radars and the one used for sky wave propagation.

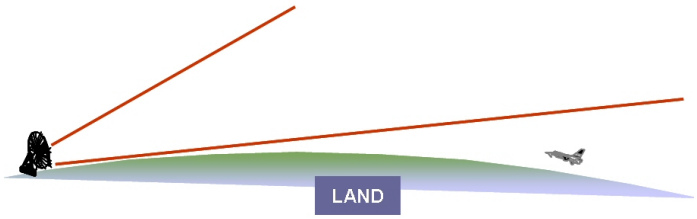

Figure 1.2: Classical radar

On the one hand, it is easy to understand that the ionosphere can be considered as a mirror and then greater ranges can be achieved. On the other hand this reflection condition creates a minimum range under which targets cannot be detected (”blind zone”).

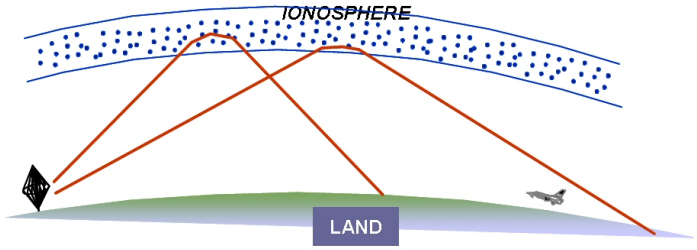

Figure 1.3: HF Sky wave radar

1.3.1.1 Example of HF sky wave radar : Nostradamus

This is an example of a HF sky wave radar called Nostradamus, developed by French researchers in ONERA. This radar is located in France, 100 km away from Paris, near Dreux. It is an experimental system based on an original concept of monostatic radar consisting in 3 branches. This configuration provides a omnidirectional coverage in azimuth. Moreover, a control of the elevation angle is also possible with this radar. A surveillance of many countries is then possible from 500 km to 3,500 km all around the Nostradamus site. An example of a possible surveillance zone is proposed on figure 1.4.

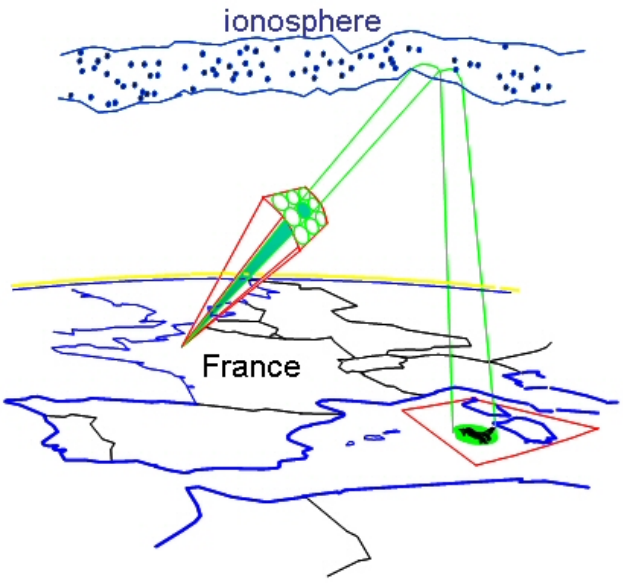

Figure 1.4: Transmitting beam (in red) and receiving beams (in green) of the Nostradamus radar on a potential surveillance zone

1.3.2 Surface wave radars

1.3.2.1 Particularities of the HF surface wave radar

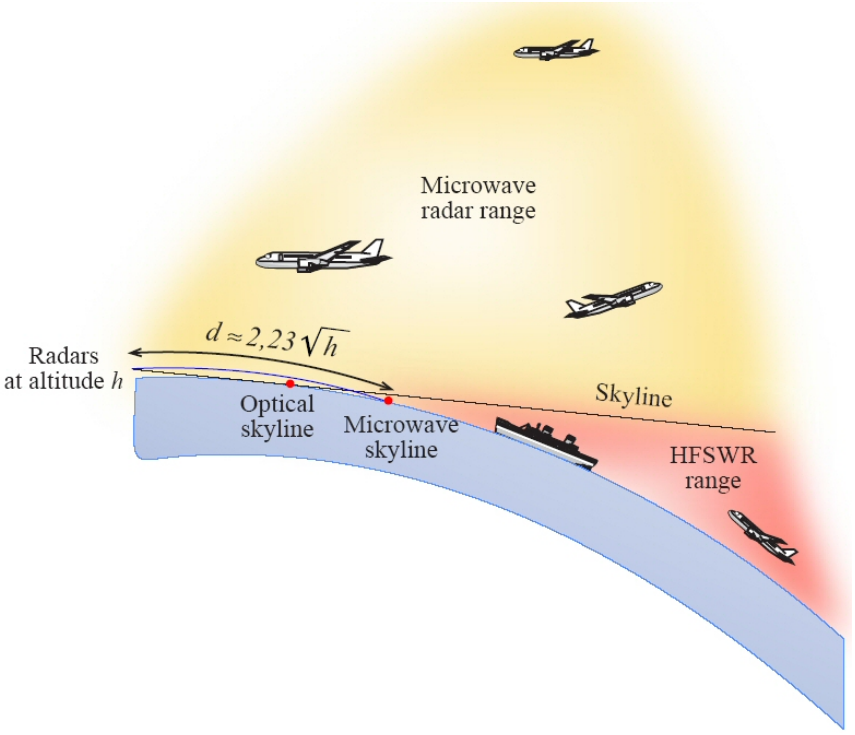

Figure 1.5: Coverages of a HF surface wave radar and a classical microwave radar

The first difference between a surface wave radar and a microwave radar is the carrier frequency which is comprised between 3 and 30 MHz. This corresponds to the "HF" or "High Frequencies" domain. The second difference concerns the electromagnetic field propagation mode : while in the microwave domain, the propagation occurs in free space in a quasi-optic manner, meaning in straight line, in HF, this is the sea surface itself that guides electromagnetic waves, such qualified as surface waves. These waves propagate in vertical polarization above sea surface. Ships or other low flying objects send back through the radar a portion of the incident surface wave as a backscattered surface wave which can be detected. At the considered frequencies, the attenuation of the electromagnetic field is limited because it is guided by the sea surface which is very conductive. Thus, the reflected surface wave can be detected up to ranges about hundreds of nautical miles, which is compatible, for example, with the extent of the Exclusive Economic Zone.

1.3.2.2 At the international level

For countries having great coastal extents, the HF surface wave radar is a very interesting surveillance tool. Several countries are now equipped but these installations are not all operational for the moment.

For Canada, which has one of the longest unpopulated coast line of any country, HF

radar represents a very economical means of providing coastal surveillance and monitoring of the 200 nm economic zone. They have projects directed at developing prototypes for wide area surveillance system with the HFSWR as a principal sensor [2].

Australia has achieved a position of world leadership in OTH Radar, through the development of the Jindalee OTH sky wave radar system at Alice Springs in the center of Australia, by the Australian Defense Science and Technology Organization (DSTO). This success has encouraged the Australian government to expand the Jindalee system to include additional radar sites, in Queensland and Western Australia. The country has also a bistatic HF surface wave radar called SECAR, in the North of the country, to observe the Torres Strait.

The USA are discreet about their surveillance potential but it is well known that the US Navy associated to Lockheed Sanders developed many HFSWR on ships. Moreover, many works on the feasibility of a bistatic or multistatic configuration of the HFSWR are being conducted. They also have HF sky wave radars. In the USA, many universities have projects using these kinds of radars. Most of their published results concern oceanographical applications (marine currents maps for example).

Japan has HF surface wave radars in China sea and their researches are carried out in Okinawa. In Europe, UK and Germany are very active on this subject.

1.3.2.3 At the national level

In France, risks (persons or ships in danger, accidental pollutions) and illicit practices (traffic, fishing, immigration, terrorism) are in constant increase. They can have serious consequences on security and safety of French people, on environment and on interests of the country in general. That is why the French State developed recently the concept of "maritime safeguard" to assure a surveillance of maritime areas, more and more far away from the coasts in order to control every activity. Protection of maritime zones and approaches is then a priority for the national defense and the HF surface wave radar can become a major advantage for it. France is well positioned in the HFSWR research domain and many projects develop nowadays in order to pass from the study and development phase to the operational radar exploitation.

1.4 General description of the HF surface wave radar system

A HFSWR transmits radio waves at frequencies between 3 and 30 MHz which "stick" to the surface of the sea and propagate in vertical polarization over the visible horizon to distances of several hundreds of kilometers. The system exploits this surface mode to collect energy scattered by objects and returned over the same surface path.

This radar system is a sensor that can measure temporal and spatial properties of objects simultaneously over thousands of square kilometers. It can be implemented as a land-based or a ship-based system.

- Coastal HF radar : HFSWR is normally deployed as a pair of land stations with overlapping coverage or, with reduced capabilities, from a single land station.

- Shipboard HF radar : It can also operate from ships and move on ocean.

If the transmitting and receiving parts of the radar are close to each over (up to 100 meters in our case), the radar system is said to be monostatic. If they are separated, the radar is bistatic. Antennas of land-based systems need to be close to the water, about 100 meters or less, to excite efficiently surface waves. This may require installation of a conducting ground screen to the water's edge.

1.4.1 Transmitting area

The radar system is composed of one or several transmitting antennas illuminating the sea surface with an electromagnetic HF wave. The aim of the transmitting is to illuminated every object likely to send back an echo through the receiving site. Antennas with large dimensions are generally used, they are matched to the transmitting carrier frequency to maximize the power transmission from the amplifier to the antenna. Monopole antennas, having a vertical polarization are often used. They illuminate a large area and the directivity is obtained thanks to the receiving antennas.

1.4.2 Receiving area

In general, for the receiving part, an array of antennas is used to have a better beam directivity and consequently a more precise location of targets. On the following figure 1.6, an example of receiving part of coastal HFSWR is proposed. It consists of an array of antennas, monopoles for example, installed parallel to the sea side. The illuminated area on the sea is called a "radar cell" and its size is function of the array length and of the observed range R.

The advantage of using receiving antennas in a phased array is that receiving beams can be formed in different directions. In fact, by applying phase delays between antennas, it is possible to steer receiving beams on both sides of the median position, i.e. perpendicular to the array (theoretical beam position if no phase delay is applied).

The beamwidth θ at 3 dB equals λ/d, meaning the ratio between the transmitted radar wavelength and the receiving array length. Consequently, the more spread the array is, the thinner the beamwidth will be and thus the target location will be more precise.

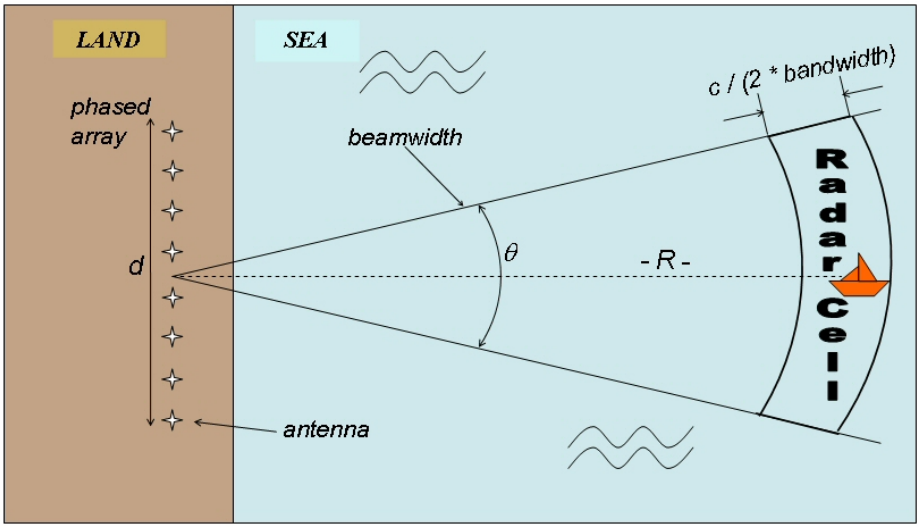

Figure 1.6: Example of the receiving part of a land-based HFSWR

On this example of receiving part of coastal HF radar, there are coherent receivers at the output of each antenna. The radar signal received from each receiver is sampled at an appropriate rate. Then, the signals are digitally down converted to complex baseband, where all the required filtering, beamforming, Doppler analysis, detection, tracking, noise suppression and other signal processing operations are performed. The application of digital signal processing is practical because of rapid advances in both digital hardware and software development.

1.5 Radar Equation

The detection performance of any radar depends upon many factors that are related in what is traditionally known as the Radar Equation.

1.5.1 Radar Equation in the case of a monostatic radar

There are a lot of forms of this equation. One common form equates the ratio of the return signal power, S, to the received noise power, N, as following (in the case of a monostatic radar configuration):

$$\frac{S}{N} = \frac{\bar{P}_t N_t G_t N_r G_r \lambda^2 \sigma}{(4\pi)^3 R^4 F_b k T_0 B L_p^2}$$

with N_t : Number of transmitting antennas
$\bar{P}_t$: Peak power of the transmitter in W
G_t : Gain of a transmitting antenna
N_r : Number of receiving antennas
G_r : Gain of receiving antenna
λ : Wavelength in m
σ : Radar Cross Section (RCS) of the target in m^2 (linked to its dimensions, its shape, its orientation, its material, and to the frequency)

R : Range of the target in m
F_b : External noise factor
k : Boltzmann constant = $1,38.10^{-23}$ J.K^{-1}
T_0 : Temperature in K
ΔF : Frequential resolution in Hz
L_p : Propagation losses on a single path (see the paragraph 4.3.4 about propagation losses in chapter 4 for more details).

This equation means that the probability of detection will be better with a high transmitted power, antennas with good gain and at a low frequency where the wavelength is large and where propagation losses are reduced. Moreover, targets with an important RCS will be well detected.

A target is detected when the Signal to Noise ratio (SNR) is higher than a threshold, which is generally about 13 dB. This is the theoretical value where the probability for the detected echo to be a target equals 90 %. These figures come from the probabilistic aspect of the radar detection. Below this threshold, the received signals are considered as noise.

Thanks to this equation, it is possible to size a radar during its design step in function of the type of targets to detect, the considered ranges, etc. The needs in terms of transmitting power, number of necessary antennas will be amounted and the best frequencies to use will be defined. The key parameter of this equation is the transmitted frequency because it influences the propagation losses, the noise factor, the target RCS and the antennas gain.

Note that the achievable ranges with this type of HF surface wave radar result from this equation and so, they can vary in function of several parameters.

1.5.2 Propagation losses

In the Radar Equation, a penalizing parameter is propagation losses. In fact, the path of electromagnetic field above sea surface affects its level. Bremmer calculated the propagation of ground waves above a spherical Earth in 1949 [3]. The propagation above sea surface occurs only in vertical polarization because it is the only one that satisfies the limit conditions at the interface, due to the high conductivity of sea water. That is why transmitting antennas have to be close to the sea surface to generate an optimum surface wave excitation. The use of a metallic ground plane with extremities plunging into sea water is a good solution to guarantee continuity of the ground plane between land and sea surface.

The propagation losses are variable in function of the frequency, the distance, the sea state (roughness), the intrinsic conductivity and permittivity of sea water. Further explanations about propagation losses are available in chapter 4 (4.3.4).

Millington effect It is interesting to note that the presence of islands or ships on the wave path will strongly attenuate the signal but surface waves can propagate beyond them. This phenomenon is known as the Millington effect [4]. It is then possible to detect targets behind obstacles.

1.6 Radar functioning principle

The radar principle consists in transmitting an electromagnetic wave which is scattered by the target and then collected by the receiver. Measurement of the round trip time of the wave (at the velocity of light) can provide the target range R.

$$Range\ R\ (in\ m) = \frac{\tau c}{2}$$

with τ : Round trip time of the wave in s
c : Propagation velocity of the surface wave (= velocity of light : 3.10^8 m.s^{-1})

Moreover, the radial velocity of a target can be obtained thanks to the frequency carrier shift, called "Doppler effect" and due to the target moving towards the radar. That is why Doppler-range processing can separate echoes distinguished by range R and Doppler frequency f_d.

$$Doppler\ shift\ \Delta f_d\ \ (\text{in Hz}) = \frac{2V_r f_c}{c}$$

avec f_c : Carrier frequency transmitted by the radar in Hz
V_r : Radial velocity of the target in m.s^{-1}

There are a lot of sorts of surface wave radars because different antenna configurations or block diagrams can be possible. To better understand radar signal processing, meaning the way useful information are extracted from returned signal, let us take a precise configuration used for the demonstrator project ONERA / DSTA (see fig.1.7) :

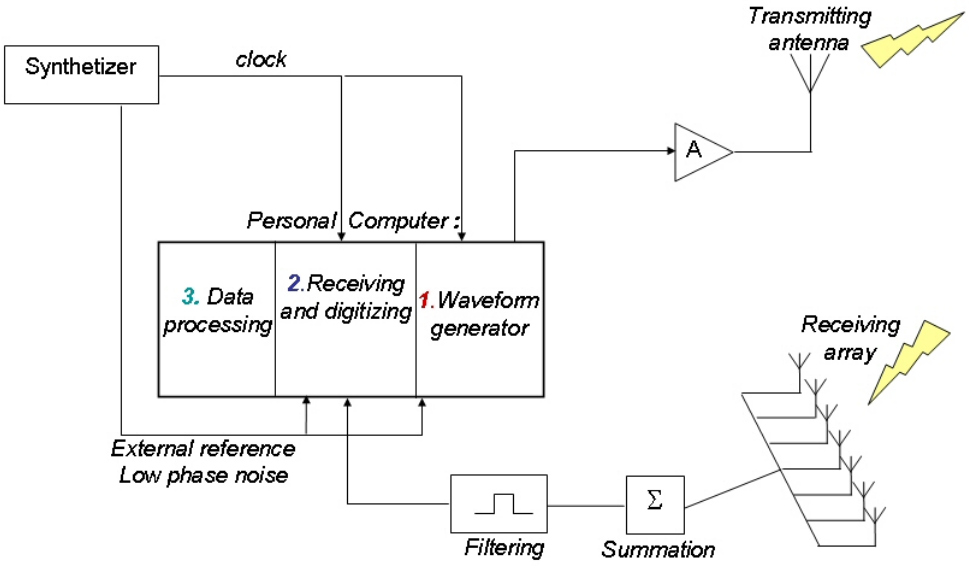

Figure 1.7: Example of a synoptical description of a HF surface wave radar

1. Thanks to a synthesizer and a waveform generator that can be installed on a dedicated personnal computer (PC), a continuous or pulsed signal is transmitted at a precise

frequency, called "carrier frequency" through an amplifier and a transmitting antenna. For this study, we will consider that we have a pulsed system. In this mode, pulses are transmitted regularly at a Pulse Repetition Frequency (PRF). Echoes are received by the array of antennas and coherently summed. Filters are then used to extract signals around the transmitted carrier frequency. A recurrence is the time period that separates two transmitted pulses.

2. Afterwards, the received echoes are sampled and digitized. If the radar transmits, it cannot receive at the same time. That is why, during the transmitting period, the radar cannot receive echoes and is totally "blind". Only backscattered signals arriving in the receiving period will be digitized. This is called the digitizing window, in fact it is the time between two transmitting periods.

3. Finally, signals are processed in the PC : all the required filtering, beamforming, Doppler analysis, detection, tracking, noise suppression and other signal processing operations are performed.

Detailed principle The detailed principle can be explained in the following way : Let e(t) be the transmitted signal and τ(t) the round trip time that the wave takes at the light velocity c (τ depends on time because the target is moving) to propagate through the target and come back. If a signal r(t) is received at the instant t, it has been transmitted at the instant t - τ(t). Then,

$$r(t) = s(t - \tau(t)) \tag{1.1}$$

If the target is in movement with a constant radial velocity V_r (that we consider positive for a target approaching the radar), the radar-target distance is written :

$$D(t) = D_0 - V_r.t$$

where D_0 is the distance at t=0.

Considering the wave has been reflected at $\frac{\tau(t)}{2}$, the length of the round trip of the transmitted wave $c.\tau(t)$ can be written :

$$c.\tau(t) = 2.D(t - \frac{\tau(t)}{2}) = 2.\left[D_0 - V_r.(t - \frac{\tau(t)}{2})\right]$$

So,

$$\tau(t) = \frac{2.\frac{D_0}{c}}{1 - \frac{V_r}{c}} - \frac{2.\frac{V_r}{c}.t}{1 - \frac{V_r}{c}}$$

As c is really greater than V_r, the delay is now :

$$\tau(t) \approx 2.\frac{D_0}{c} - 2.\frac{V_r}{c}.t \tag{1.2}$$

1.7 Radar processing

Signals coming from the receiving radar system have several dimensions :

- A spatial dimension corresponding to the output of different sensors,
- A temporal dimension in the digitizing window , that is called "fast time",
- A temporal dimension from a recurrence to another, that is called "slow time".

These data can be represented in a volume :

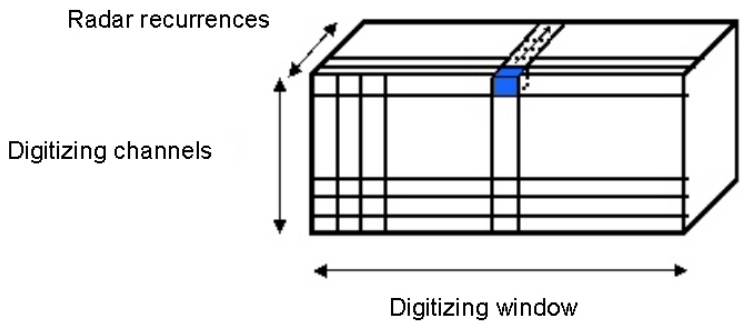

Figure 1.8: Data cube

The manner of which a wave of energy is transmitted (the waveform) and received is a choice that is always fitted to the intended use of radar equipment. Generally, if one particular measurement, such as range, is more desired, other information (velocity, elevation, etc) may be compromised as less important objective. For each dimension, a process can be applied in function of the desired information :

- To obtain angular dimension (azimuth, elevation), a Fast Fourier Transform (FFT) or a Digital BeamForming (DBF) is applied on the spatial dimension.
- To obtain the spectrum of the digitizing window, a FFT is processed on the "Fast time" dimension.
- Range information are obtained after correlation on the "Fast time" dimension.
- And finally, the Doppler spectrum (from which the radial velocity is deduced), is obtained by FFT on the "Slow time" dimension.

All these dimensions are available. Moreover, polarization of signals (horizontal and vertical) can also be used to study signals. In this thesis, we will particularly be interested in the range and the radial velocity of targets.

After acquisition of the signals coming from the illuminated radar cell, we need to extract information from these data. It means extraction of the range of echoes and their Doppler shifting. In the previous paragraph, we have a simple explanation of the way range and

Doppler shifting can be obtained. In reality, the processing step is a bit more complicated because we transmit more than one pulse.

In fact, the radar transmits a signal with a bandwidth B and a transmitting time Tx. After transmitting, it switches in receiving mode during Tr - Tx (where Tr is the total duration of the radar recurrence). A wave train is transmitted as shown on figure 1.9 and it is composed of N recurrences. The backscattered signals acquired by the radar are analyzed on these N recurrences, meaning an analysis time of N × Tr.

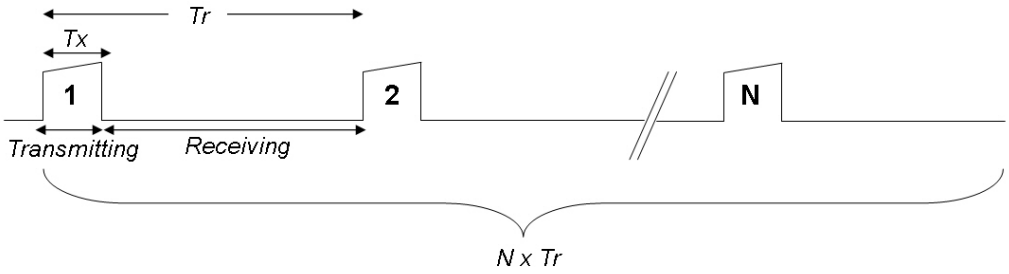

Figure 1.9: Details of transmitting and receiving modes in radar recurrences

Consider that the transmitted signal e(t) is :

$$e(t) = e^{j2\pi f_c t + jC(t)}$$

with f_c is the carrier frequency of the radar and C(t) is the transmitted code of bandwidth B and duration Tx.

Transmitted code It is possible to transmit a non coded pulse but for the same energizing results, coded and non coded pulse have different resolution power. It is better to code the transmitted signal. In our radar applications, we generally use a chirp code, which is a linear frequency modulation that can be written $C(t) = e^{j\pi \frac{B}{T_x} t^2}$. This waveform is the easiest to generate (see this code on figure 1.10), other codes such as Barker code or others can be also used.

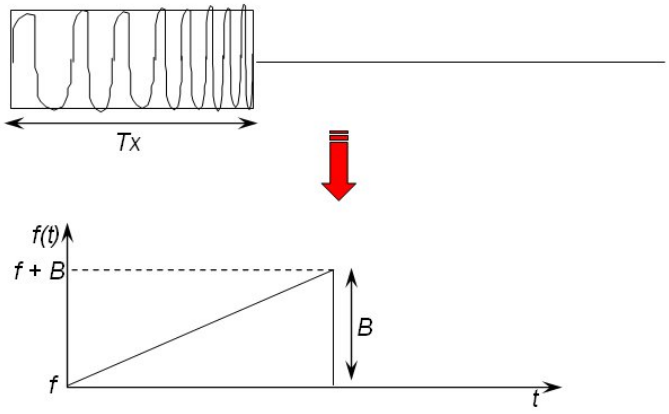

Figure 1.10: Transmitted chirp and evolution of its frequency in function of time

The signal received at the recurrence i is (cf equation 1.1) :

$$r_i(t) = A.e(t - \tau_i(t))$$

Note that the signal received is reduced compared to the transmitted signal, this attenuation is represented by the factor A. In the following explanations, this factor will not be taken into account.

Calculation of $\tau_i(t)$ At the first recurrence, a target echo is characterized by an initial delay t1. At the second recurrence, the target moves of $V_r \times T_r$ and it corresponds to a round trip time of $\frac{2V_rT_r}{c}$. The echo delay compared to the beginning of the second recurrence is $t2 = t1 - \frac{2V_rT_r}{c}$.

Then, for the recurrence i, this delay will be : $ti = t1 - \frac{2V_rT_r}{c}(i-1)$.

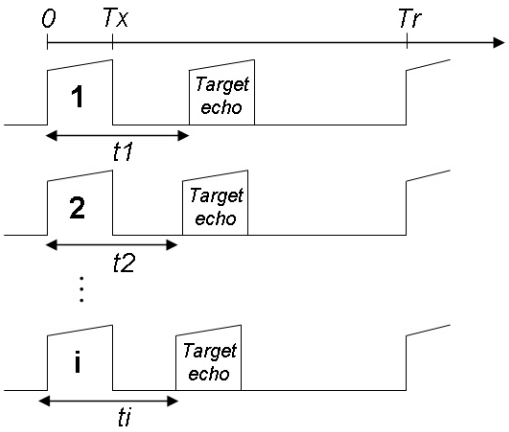

Figure 1.11: Position of a target echo among recurrences

The delay $\tau_i(t)$ can then be written by analogy with the previous equation 1.2 :

$$\tau_i(t) = t_i - \frac{2.V_r.t}{c}$$

where t_i is the delay accumulated from a recurrence to another and $\frac{2.V_r.t}{c}$ is the delay related to target's motion during the recurrence i (the time origin is set for each recurrence at the beginning of the transmission).

Moreover, as we know the duration of the transmitted code is Tx, the signal has been transmitted between 0 and Tx. It comes :

$$0 \leq t - \tau_i(t) \leq T_x$$

$$\Rightarrow \frac{t_i}{(1 + \frac{2.V_r}{c})} \leq \frac{t_i + T_x}{(1 + \frac{2.V_r}{c})}$$

Then, it is now possible to find the signal received at the instant t for each recurrence i.

$$r_i(t) = e^{j2\pi f_c(t-\tau_i(t))} \times e^{jC(t-\tau_i(t))}$$

$$= e^{j2\pi f_c t} \times e^{-j2\pi f_c t_1} \times e^{j2\pi f_c \frac{2.V_r}{c}(i-1)T_r} \times e^{-j2\pi f_c \frac{2.V_r}{c}t} \times e^{jC(t-\tau_i(t))}$$

After demodulation by the carrier frequency (multiplication by $e^{-j2\pi f_c t}$) and considering for the Doppler shifting : Δf_d (in Hz)$=\frac{2\mathrm{V_r}f_c}{\mathrm{c}}$, it comes :

$$r_i^{'}(t) = e^{-j2\pi f_c t_1} \times e^{j2\pi \Delta f_d(i-1)T_r} \times e^{-j2\pi \Delta f_d t} \times e^{jC(t-\tau_i(t))}$$

That we can express as a four-terms product :

$$r_i^{'}(t) = A_1 \times A_2(i) \times A_3(t) \times A_4(t,i) \tag{1.3}$$

- First term : $A_1 = e^{-j2\pi f_c t_1}$, it expresses the signal phase under carrier frequency at the recurrence number 1.
- Second term : $A_2(i) = e^{j2\pi \Delta f_d(i-1)T_r}$, it allows the observation of the phase evolution in function of time of a signal that has a Doppler shifting Δf_d all along the recurrences.
- Third term : $A_3(t) = e^{-j2\pi \Delta f_d t}$, it expresses the phase associated to a Doppler shifting of the target at the instant t.
- Fourth term : $A_4(t,i) = e^{jC(t-\tau_i(t))}$, it indicates that the transmitted code is modified.

In practice, the code compression or expansion from a recurrence to another is insignificant, this fourth term can then be written (supposing that c is really greater than $\mathrm{V_r}$):

$$A_4(t,i) = e^{jC(t-\tau_i(t)} = e^{jC(t(1+\frac{2.V_r}{c})-t_1+\frac{2.V_r}{c}T_r(i-1))}$$
$$\approx e^{jC(t-t_1)} = A_4^{'}(t)$$

The radar processing can now be divided into two distinct steps. The first step is for Doppler shifting extraction and the second a range extraction. They are interchangeable and the order we process has no importance.

1.7.1 Doppler processing

For each recurrence, a signal $r_i^{'}(t) = A_1 \times A_2(i) \times A_3(t) \times A_4^{'}(t)$ is received. If the time t is fixed and if we consider all the values of the received signal at each recurrence $(r_1^{'}(t), r_2^{'}(t), ..., r_N^{'}(t))$, only the second term $A_2(i) = e^{j2\pi \Delta f_d(i-1)T_r}$ varies in function of the recurrence number.

Thanks to a simple Fourier transform applied on the terms $r_1^{'}(t), r_2^{'}(t), ..., r_N^{'}(t)$ with t fixed, we obtain a curve where the maximum is at the Doppler shifting Δf_d. In fact, from

a pulse to another for a fixed time t, the received signals are dephased of $2\pi\Delta f_d T_r$. The optimal processing, meaning the one that provides the best gain in terms of signal to noise ratio, consists in putting back theses successive samples in phase, in summing them and finally in squaring its modulus (in order to cancel the unknown phase at the origin). This is called the "coherent summation".

The operation to apply for the optimal processing consists in calculating the value of :

$$J_t(n) = \left| \sum_{i=1}^{N} r_i(t) \cdot e^{ji\varphi} \right|^2$$

As it is necessary to explore all the Doppler shiftings, the calculation has to be done for all the possible φ. That amounts to doing the Fourier transform of the samples continuation $r_i(t)$. In fact, it is the Fourier transform of $A_2(i)$. These successive samples are at least spaced out with a recurrence, the Fourier transform consists then in applying a discrete Fourier transform where the sample period is T_r. If φ is equal to $2\pi n/NT_r$, we obtain the FFT formula.

The Fourier transform is able to put back the received samples in phase, and that for each Doppler shifting. The function $S_t(f) = J_t(n)$ will be maximum when the Doppler shifting will be exact, meaning for a Doppler shifting equal to the Doppler shifting Δf_d of the target.

This processing is applied for each t and so for each range cell.

In conclusion, for the Doppler processing, the function $S_t(f)$ has to be calculated :

$$S_t(f) = A_1 \times DFT[A_2(i)] \times A_3(t) \times A_4(t)$$

This processing can also be summed up in the following figure :

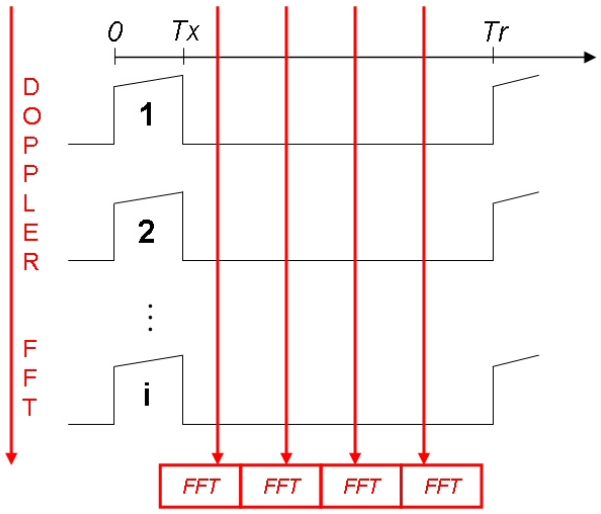

Figure 1.12: Illustration of the Doppler processing

1.7.1.1 Frequency resolution

As the Doppler processing uses a discrete Fourier transform, the frequency resolution depends on the integration time T_i ($T_i = N \times T_r$) and is then equal to $1/T_i$. This frequency resolution is just function of the number of recurrences and of the recurrence duration. In order to improve the Doppler shifting resolution, the best possible choice is to increase the integration time of the Doppler processing.

We have to be careful because targets position and velocity and sea state have to be stable during the integration time. A too long integration time is a risk because a lot of parameters may change during this temporal interval. A compromise has to be found about this integration time to obtain a good Doppler shifting resolution and steady observed objects.

1.7.1.2 Weighting window

Every measurement made in the temporal domain has a beginning point and an ending point. That means that the real signal is multiplied by a square function which is null everywhere except in the time interval where it is equal to 1. The spectrum of the measured function is then convoluted with the Fourier transform of the square function which is a cardinal sinus. This function has sidelobes at -13 dB as shown of figure 1.13.

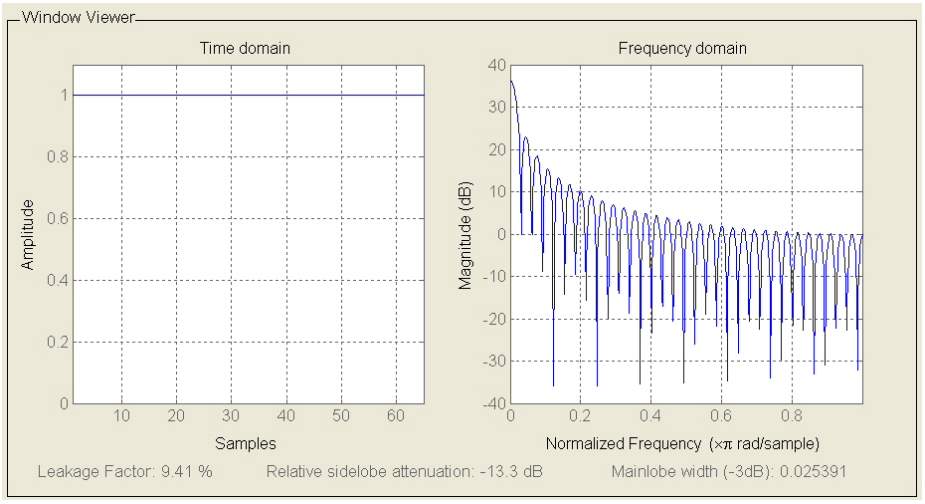

Figure 1.13: Square window (in temporal and frequency domain)

The process of shaping a Doppler response by control of a waveform envelope shape is called *time weighting*. The primary objective of weighting windows, used in either domain, is to reduce sidelobes in the other domain. Sidelobes can severely limit resolution when the relative magnitudes of received signals are large. In our process, we usually use a Blackman window (cf. figure 1.14). The consequence is that primary lobe is larger than the one obtained without weighting but the advantage is the reduced level of sidelobes (-58 dB instead of -13 dB). Other windows such as Hamming or others can also be used.

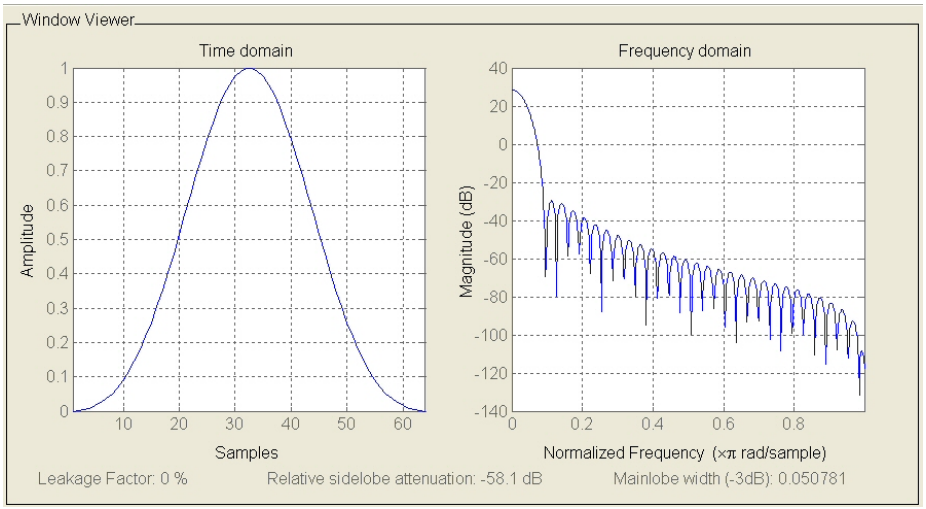

Figure 1.14: Blackman window (in temporal and frequency domain)

1.7.2 Range processing

As previously explained, the target distance to the radar is given by the round trip time taken by the wave to travel at the light velocity. In the case where a code $C(t)$ is transmitted, a correlation between the received signal with the transmitted signal $e^{jC(t)}$ is sufficient to

obtain the transmitted wave delay. In fact, we notice, in the equation number 1.3, that the term A_4 corresponds to the replica of the transmitted code temporally shifted with the delay of the target echo (we previously supposed that the received code is not distorted by the target velocity). If we correlate this term with the initial code, the maximum obtained will correspond to the target delay.

In practice, at the end of the Doppler processing, we obtain a frequency signal $S_t(f) = A_1 \times DFT[A_2(i)] \times A_3(t) \times A_4(t)$ for each t. In the temporal domain, we obtain then for each frequency a signal $S_f(t) = A_1 \times DFT[A_2(i)] \times A_3(t) \times A_4(t)$.

The term $A_3(t)$, that expresses the variation of the target Doppler shifting during the recurrence, depends on time and must be canceled in order to keep only information about the received code shifting. We then have to multiply the signal $S_f(t)$ by $e^{j2\pi\Delta f_d t}$ for each frequency line f obtained after the Doppler processing (we suppose that, for each frequency line f, we have an echo with a Doppler shifting Δf_d equal to f).

We then obtain a signal $S'_f(t) = A_1 \times DFT[A_2(i)] \times A_4(t)$. After correlation between $S'_f(t)$ and $e^{jC(t)}$, a time maximum appears corresponding to the target or ground delay having a Doppler shifting equal to f. With this delay, the target distance can then be deduced.

It is also possible to sum up the Doppler range processing with a figure (cf. figure 1.15):

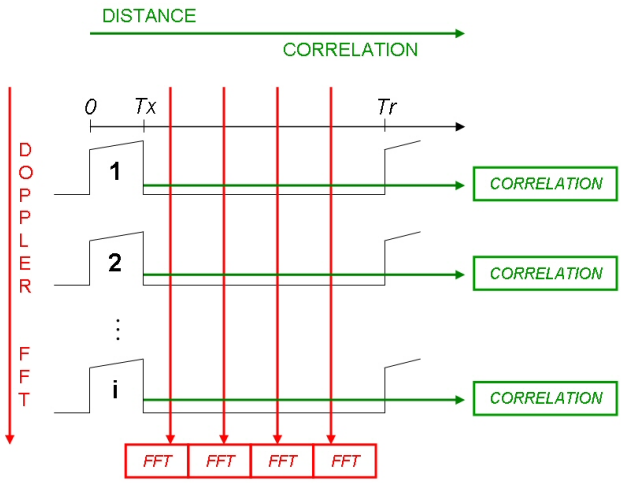

Figure 1.15: Illustration of the Doppler range processing principle

1.7.2.1 Correlation sidelobes

When we correlate the transmitted chirp with the received signal, we obtain correlation sidelobes. In fact, these sidelobes are due to the multiplication of the DFT of two square functions (replica and received signal), that is why we obtain correlation sidelobes of a square cardinal sinus. As presented on figure 1.16, sidelobes are 26 dB above the highest correlation peak, which is well the double of a simple cardinal sinus (cf. figure 1.13).

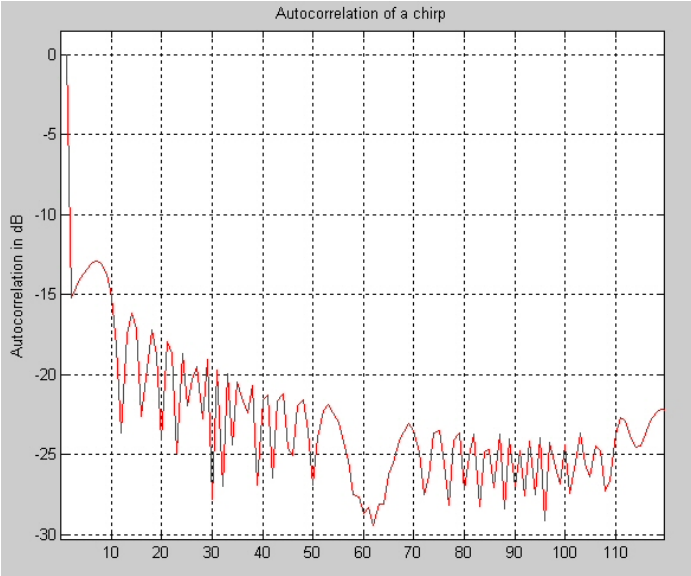

Figure 1.16: Autocorrelation of a chirp

1.7.2.2 Pulse compression and range resolution

This range processing is also known as pulse compression. In fact, as technology is sometimes limited to provide short pulse with high amplitude, the pulse compression has been imagined. By transmitting a coded pulse (linearly modulated in frequency for the chirp code) and correlating it with the received signal, the resulting effect is that a punctual target will produce a square cardinal sinus, as explained in the previous paragraph.

The higher the bandwidth is, the more narrow the cardinal sinus beamwidth will be. The time duration of the compressed pulse is then : $\tau = 1/B$ (cardinal sinus beamwidth at 3 dB).

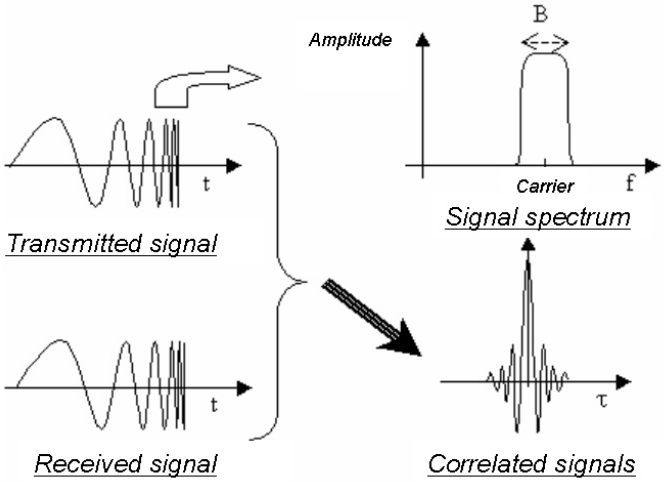

Figure 1.17: Explanation of the pulse compression

Range resolution The range resolution corresponds to the minimum distance between two target (or clutter) echoes for the radar to distinguish them. The transmitted code has a bandwidth B and a duration Tx. If we do not code the transmitted pulse, the range resolution will be : $\Delta R = c.Tx/2$. If we code the transmitted pulse, we will achieve, by pulse compression, a resolution given by :

$$\Delta R = \frac{c \times \tau}{2} = \frac{c}{2 \times B}$$

This range resolution fixes then the size of the radar cell in range. It will define the space in range between two consecutive points on the Doppler range image.

It means that, for example, for a given energy, the pulse compression does not modify the radar range but can improve its range resolution. The compression ratio obtained is $B \cdot Tx$. These operations are equivalent to transmit a short pulse with high power instead of a long pulse with low power (see illustration on figure 1.18) :

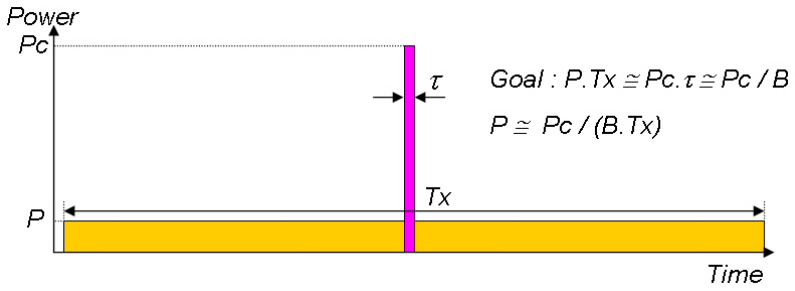

Figure 1.18: Pulse compression principle

1.8 Results available after radar processing

1.8.1 Doppler-range images

Results from signal processing of a surface wave radar can be displayed on a Doppler range image on which each backscattered signal has been placed on a map, thanks to the determination of its range and its Doppler shifting (linked to its radial velocity).

Example of a Doppler range image is given in figure 1.19. Maxima of the image (in red color on the graph) correspond to the presence of a target or of a clutter echo. On this picture, we can see three central line that correspond to ground and sea clutter. Every other point with high level is a potential target. The blue pixels represent noise which is essentially external in HF. We also notice correlation sidelobes around strong targets. For echoes with a lower level, correlation sidelobes are not distinguished because they are hidden by the noise. Doppler sidelobes are not really visible except for strong echoes where their signal to noise ratio is higher than 58 dB (see explanation of this value in the weighting windows paragraph 1.7.1.2).

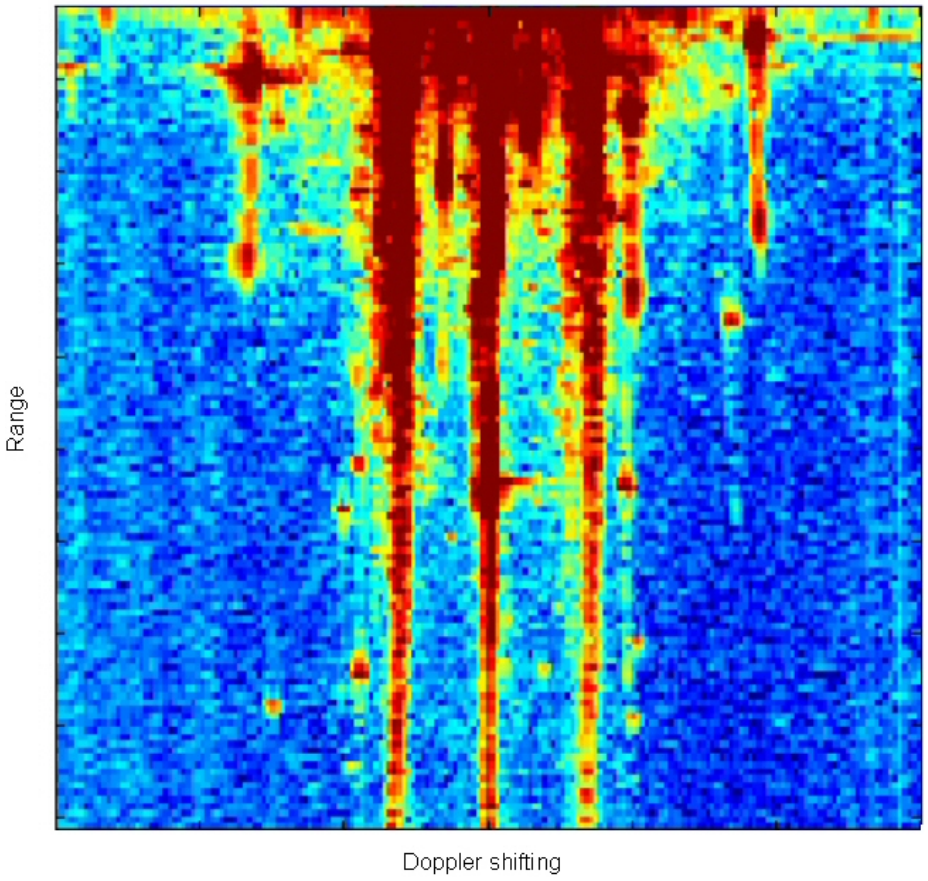

Figure 1.19: Example of results after Doppler range processing

Sea clutter is represented on the image by two lines on both sides of the central line which is associated to ground clutter and immobile echoes. Echoes coming from sea clutter appear as two lines, called Bragg lines[1](interaction between HF waves and sea waves will be detailed in the chapter 4).

By accumulating information coming from successive images, we clearly notice target motion. It is practical to position these successive echoes on a geographical map for more legibility and to display evolution of target trajectory in course of time (this is called tracking).

[1]When the sea surface is illuminated by a high frequency wave, a portion of the incident energy is backscattered through the source. For low elevation angles, this primary scattering mechanism occurs, it is called "Bragg scattering". This is a selective process in which there is a strong return coming from ocean waves that have a wavelength being half of the transmitted radar wavelength. Spectral analysis of the return signal coming from sea echoes proposed a Doppler spectrum characterized by two predominant peaks surrounding by a continuum.

1.9 Major constraints of the HF surface wave radar

1.9.1 Limited resolution power

The maximum range of a radar system is important but its location resolution is also a key parameter. Targets separation first depends on the range and angular resolution of radar cells. These resolutions are given by dimensions of the elementary sea cell illuminated by the receiving array (see illustration on figure 1.20).

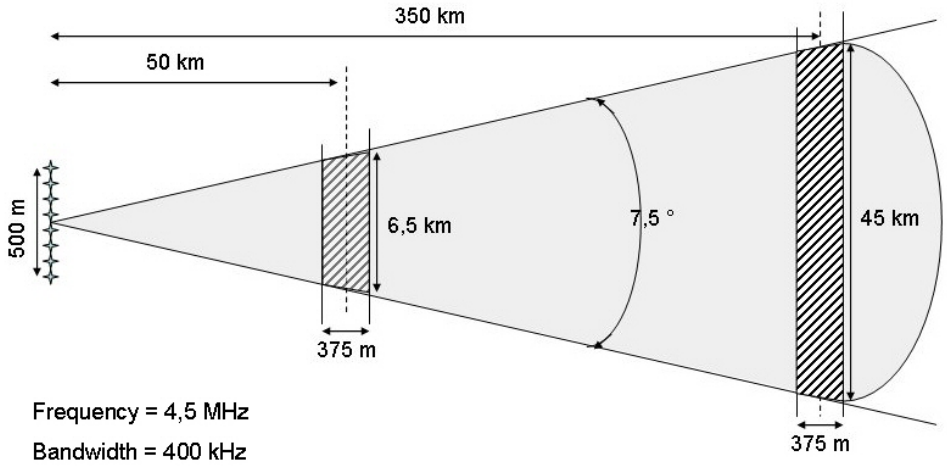

Figure 1.20: Example of an elementary radar cell for a low frequency of 4.5 MHz and a bandwidth of 400 kHz

With the range resolution of this precise example, it is possible to separate targets that are 375 m away from each other. The beamwidth is about 7 °, that means that the angular separation is limited but thanks to "ecartometrie" methods (*monopulse* technique well known in radar domain), this angular resolution can be improved by a factor 10.

If targets are not separated because they are too close to each other, they can be separated thanks to their radial velocity. The Doppler frequency, from which is deduced the velocity, has a resolution linked to the integration time, i.e. the signal duration used for the measurement. This frequential resolution is inversely proportional to the coherent integration time. So the higher the integration time is, the better the target discrimination will be. A compromise has to be found between a long integration time and the maintain of a stable state of targets to detect (position and velocity have to be unchanged during the measurement).

This example has a quite good resolution but in general, we use a smaller bandwidth and the resulting minimum radar cell has dimensions in the order of a few square kilometers. In case of an important ship traffic, safety distances between two ships in a sea lane are smaller than the resolution power of the radar. Moreover, for the moment, it is still difficult to detect small boats because of their poor RCS unless the radar is equipped with powerful transmitter and antennas.

1.9.2 Electromagnetic problems

In the case of shipboard radars, there can be electromagnetic problems between the radar system and the HF equipment of the ship. In fact, there are critical issues about compatibility of the radar with other shipboard HF systems and about the effects of the complex shipboard scattering environment on target detection and tracking. It is also important to take into account matching problems linked to coupling effects between the metallic environment of the ship and the antennas.

1.9.3 Important antennas size

Wavelengths associated to low frequencies used for HF surface wave radars are comprised between 10 and 100 m. Now, radiating elements used to transmit and receive HF waves are generally sized at a quarter wavelength for an optimum matching. It means that the antennas have heights comprised between 2.5 and 25 m. In general, we use a quarter-wavelength monopole, matched at one frequency for transmitting and receiving. This is a simple and low-cost solution for antennas of a HF surface wave radar but that is not the optimum solution.

It is possible to use active monopole antennas for receiving. They have a smaller size in the order of 1 m but these kinds of antennas, employing active device, are not really stable in phase. The phase control being the base of the phased array, passive antennas are prefered to active ones.

Consequently, it is impossible to have this large antennas shipboard because of their too important dimensions. Moreover, their size pose a problem for a question of discretion and furtivity on coastal or shipboard installations. Finally, huge elements arranged in array can be disturbed by coupling effects between antennas. All these drawbacks caused by important antennas size compromise detection possibilities.

1.9.4 Disturbing sea clutter

Another drawback to notice is the disturbing effect of sea clutter. Echoes coming from sea waves can disturb target detection if their level is high compared to the level of targets to detect. In fact, a target echo can be masked by the first or second order Bragg clutter. It is mainly the case for echoes of slow ships that have a Doppler shifting close to the one of Bragg lines. On the contrary, aircrafts or missiles have higher velocities and then, they will less be affected by sea clutter.

This disturbing effect of sea clutter deteriorates the detection capabilities of HF surface wave radars and Bragg lines are considered as interferences. The problem is that if we use an ordinary filter to delete these interferences (Bragg lines due to the Doppler effect of sea waves) it will delete at the same time Doppler frequencies of a useful part of the spectrum where targets appear. This is really problematic.

1.9.5 Disturbing ionospheric clutter

Another disturbing clutter concerns the ionospheric one. In fact, the ionosphere is efficiently used as a "mirror" for HF sky wave radars. But, this atmospheric layer can be a source of perturbations for a HF surface wave radar. Under certain conditions, because of ionospherical irregularities (motion of ionosphere, electronic density variation, etc), a portion of the incident surface wave is sent back to the radar. The problem is that antennas of surface wave radars have a radiation pattern that is not always directive in elevation in the sea direction. They can then receive unwanted signals coming from the ionosphere. This causes signals disturbance.

A possible solution to solve this problem could be the design of very directive antennas that would mainly illuminate sea surface and less the high elevation angles. It is also conceivable to use antennas detecting different polarizations in order to distinguish signals coming back from ionosphere and signals coming from sea surface thanks to their different polarization. It is also possible to select a radar frequency that can go through the ionosphere and avoid backscattered signals. Another way to reduce ionospheric clutter would be the implementation of filtering algorithms. These solutions are studied at the present time in ONERA in the frame of the thesis of Florent Jangal.

1.9.6 Congested HF spectrum

According to the used frequencies, the HF spectrum is more or less congested and this is not always easy to find clear channels (i.e. free frequencies) that are authorized. Finding a large bandwidth in the HF spectrum is often difficult. In practice, performance of HF surface wave radars are then limited by external noise due to the world-wide high natural and man-made ambient conditions in the HF spectrum, unwanted signals (sea clutter, ionospheric interferences) and by propagation losses attenuating signals level.

1.10 Conclusion about HF surface wave radars

Many countries have strategic policies with high priority on achieving continuous, effective, real-time surveillance of aircraft and ships in their maritime approaches. Technologies such as HF surface wave radars offer a significant potential for over-water detection and tracking capability against ships and low-flying aircrafts from shore-based sites or ships. Oceanographers can also find a lot of information about winds and currents.

The system requires transmitting and receiving antennas close to the sea surface and appropriate receivers and digitizers to compute sea echoes signals. Signal processing techniques are then used to extract useful information from these signals. Range or target size detection capability is function of a lot of parameters (external noise, sea state, hardware quality, system configuration, etc). It is typically proposed for ranges up to a few hundreds of kilometers using surface waves that follow the curvature of the earth beyond the horizon.

This system is almost operational or in development phase in the U.S.A, Australia, Canada or France. All these countries want to benefit from reliable and available means

providing real time information for the surveillance of their maritime approaches. To respond this need, a system such as HF surface wave radar can be an efficient solution, complementary to existing microwave radar systems. They can be efficient for targets detection and tracking such as ships and low-flying planes or missiles. Oceanographers and scientists are also very interested in this measurement mean to obtain information about seas, winds and currents, over great maritime areas.

In conclusion, there is an increasing interest for maritime surveillance up to great distances from coasts and then radar systems such as HF surface wave radars will certainly develop in the coming years for many civil or military applications. One of their principal constraints is the important antenna size that prevents the radars from being shipboard or used in limited coastal areas. Moreover, sea clutter that disturbs target detection is very penalizing. The aim of the thesis is to propose solutions to these two major drawbacks. The following chapters 2 and 3 deal with the problem of small antennas and researches lead on this point in order to find a new design with a good trade off between compactness and performance. The chapters 4 and 5 are dedicated to a better knowledge of the disturbing sea echoes and to the development of a signal processing algorithm that can reduce them.

Chapter 2

Choice and simulation of a compact antenna for a HFSWR

Contents

This chapter has the objective of selecting a technology to compact the size of classical HF antennas in order to conceive a compact HF antenna. First, a list of required characteristics to respect will be detailed and several examples of usual HF antennas will be presented to well understand the problematics. A part dealing with theory of small antennas will be proposed. Then, a basic antenna will be imagined and modeled in order to estimate if its initial performance respect required specifications. For that modeling, various electromagnetic codes will be used.

2.1 Definition of specifications needed for HFSWR antennas

The aim of the first part of this thesis is to find a design of antenna, more compact than usual HF antennas. The size objective is not the only specification needed. In fact, for HFSWR applications, the antenna to design has to respond several criteria. A perfect antenna does not exist but we can try to achieve the following objectives.

2.1.1 Compactness

Antenna size is the principal parameter that should be significantly be improved, i.e. reduced. Low frequencies used for HFSWR applications imply large antennas, that measure several meters high. This is a really important problem when you want to install it on ships or in limited areas. To make progress in compactness, we need to have a structure smaller than $\lambda/4$, which is the usual height of HF antennas.

Moreover, with smaller antennas, the coupling effect between elements in the receiving phased array will be minimized. It is also the case for coupling with surrounding environment of shipboard antennas that are generally metallic structures. An other advantage is a gain in the discretion and furtivity. In fact, thanks to a smaller antenna, radar system installations would be less visible along coasts or from the seaside.

In the middle of the HF band, for example at 15 MHz (λ=20 m), a quarter-wavelength monopole would be 5 meter high. As only one antenna is desired whatever the HF used frequency, the center of the HF band will be a reference for the size reducing. In fact, an objective for the new antenna about **1 meter high maximum** seems to be an ambitious objective. With this height, the antenna would be easily transportable, shipboard without problems and also it can be deployed rapidly. If the antenna can be more compact than 1 m, it would be better but it is also important that its performance are not affected by this size reduction.

Such a small structure does not need to be guyed or placed on a concrete base. This is a real economy for the radar system owner. That is why it would also easily been installed on coasts; from an environmental point of view, small antennas are preferable to huge structures that misrepresent coastal sites.

Finally, a compact size would be great to provide a good resistance to wind. That is important mainly for coastal or shipboard installations where wind can be strong and damage radar equipment.

A good trade off has to be found between this compactness (1 meter high maximum) and other following characteristics required for these applications.

2.1.2 Passive antenna

The aim is to design a compact antenna that could be used for receiving. This is the principal requirement. If the antenna can also function in transmitting, it would be an

advantage but we know that for small antennas, the radiating power being low and due to a lot of reactive energy, matching is difficult.

The aim of matching is to transfer the maximum of power from the amplifier to the antenna via the feeding line. It is less critical to have an imperfect matching in receiving rather than in transmitting. Usually, for efficient matching of small elements, active components are used to compensate this lack of size. The problem is that active components cannot be used for transmitting because they could not resist to high powers. That is why if we envisage a possibility of using the compact antenna in transmitting also, the objective is to create a passive antenna, with no active elements.

Moreover, a **passive antenna** is an advantage, mainly in a phased array because it is not composed of active elements that can create phase instabilities.

2.1.3 Frequency and bandwidth

A wideband antenna is a difficult specification that is why multiple bandwidths are acceptable. In general, for HFSWR applications, we need multiple operating bandwidths, at least two : one at **low frequency around 5 MHz** to detect boats with low velocity and high RCS and one at **high frequency around 15 MHz** to detect planes and missiles, with high velocity and low RCS.

Concerning the bandwidth, the problem to find bands of clear channels in the HF spectrum will be developed in the paragraph 5.1.1. In fact, there are no precise frequency bands allocated for HFSWR applications. It means that we cannot design a compact antenna functioning at a certain frequency with a narrow band because if this frequency is jammed, we have to tune it to find a possible band elsewhere. The antenna has to present several operational bands with sufficient bandwidths to adapt to the spectrum congestion.

In the chapter 1 (1.7.2.2), the range resolution has been defined inversely proportional to the bandwidth. In the second part of the thesis, a method using coherence of the sea echoes from a range cell to another will be used. The success of this method is based on the fact that range cells are not very big in order to keep stable sea state. A few hundreds of meters could be a very good range resolution for the radar system and morever this is a very acceptable value for the signal processing method.

To obtain, for example, a range resolution about 375 m, the associated bandwidth is 400 kHz. The compact antenna should then have a **bandwidth of a few hundreds kHz**, at least at a low and a high frequency.

2.1.4 Impedance

A "perfect" antenna (consisting in elements without any losses) does not exist. When an antenna receives energy, currents travel through its structure. A part of the incident energy is radiated back and the created wave comes localy to disturb the incident wave. So, there are losses due to radiation and they create a real part in the equivalent impedance of the antenna.

In this thesis the aim is to conceive a compact antenna with an **impedance of 50 ohms** in order to be compatible with coaxial cables or measurement equipment that would be connected to it. To do that, we will try to conceive a compact antenna with a good VSWR. The VSWR stands for Voltage Standing Wave Ratio and it is a measure of impedance mismatch between the transmission line and its load. The higher the VSWR, the greater the mismatch. The minimum VSWR, i.e. that corresponds to a perfect impedance matching, is unity. Optimizations of the antenna will search for a VSWR as close to 1 as possible.

2.1.5 Polarization

When a surface wave is horizontally polarized, the electric field of the wave is parallel with the sea surface and, therefore, is constantly in contact with it. The wave is then completely attenuated within a short distance from the transmitting site. On the other hand, when the surface wave is vertically polarized, the electric field is vertical to the sea surface and merely dips into and out of the surface. For this reason, vertical polarization is vastly superior to horizontal polarization for surface wave propagation.

For the antenna design, the antenna should then be **linearly and vertically polarized** to provide the best propagation mode for surface waves.

2.1.6 Radiation pattern

The HFSWR uses sea surface to propagate surface waves up to great distances and to detect objects low at horizon. It means that the zone illuminated by the compact antenna has to be maximum at low elevation angles. The **radiation pattern** of the antenna has then to be **directional with a maximum gain obtained in the sea direction** for an optimum functioning.

2.1.6.1 Gain

Gain of an antenna is the ratio between power you should give to a reference antenna and power you give to the considered antenna to produce the same radiating intensity in a given direction. It is defined for a specific frequency. If the antenna does not have losses, gain and directivity are equal. Note that directivity characterizes the way an antenna distributes its radiation in different space directions. It is the ratio between the radiating intensity in a given direction and the mean value of this radiating intensity in each direction of space. The unit is the decibel (dB).

2.1.7 Material and fabrication

For convenience and cost, fabrication of the compact antenna has to be easy. It means that complex structures, strip antennas or precious materials should be avoid and the objective to prioritize is the use of **common material**, such as metallic wires in copper for example.

In this study, it is obvious that several specifications are more difficult to obtain than others and we have to find a good trade off between all these constraints in the conception of the compact element.

2.2 Compacting usual HF antennas size

2.2.1 Usual HF antennas

You will not find here an exhaustive list of all kind of antennas used in HF but several examples of large antennas that can be used for HFSWR applications.

Usually, HF antennas are sized at 1/4 of the wavelength to optimize matching. The common type of antennas used for HF Surface Wave Radars are monopoles antenna. On the following figure 2.1, you can see examples of two monopoles antennas that are 11 m high. This kind of antenna is separated in several elements that need to be mounted together before erection. The advantage is that this structure does not need a support post or special guys to be maintained : this structure can be self-supporting. If the height is higher, guys will be needed.

Figure 2.1: Example of HF quarter wavelength monopole antennas

The skywave radar Nostradamus (see details in 1.3.1.1) is composed of 288 large biconical antennas. An example of this antenna is available on figure 2.2. A single element measures about 8 m high and need to be guyed. This antenna is broadband and can be used between 6 and 24 MHz. For HFSWR applications, this antenna is too large and moreover would need a very important ground plane to lower its radiation pattern because its pattern tends to raise with frequency, which is not favorable to the use of surface wave.

Figure 2.2: Biconical antenna of the HF skywave radar Nostradamus

On the following figure 2.3, commercial antennas used in the SeaSonde system developed by CODAR Ocean Sensors are presented. On the left part of the image, the receiving antenna is composed of three elements associated to a passive vertical monopole mounted on a support post. This antenna measures 6.5 m high. On the right of the figure, the transmitting antenna is a vertical fiberglass whip. Its total height mounted its the support post is about 9 m.

Figure 2.3: Example of antennas used in Sea Sonde system developed by CODAR Ocean Sensors. On the left, the receiving antenna and on the right the transmitting antenna

Another HF antenna, developed by CODAR Oceans Sensors, consists in using the superdirectivity principle[1]. In fact, they create a kind of receiving array at the top of mast.

[1]Superdirectivity in used to obtain a directive gain greater than ordinary gain obtained with a classical phased array. The conventional method for obtaining high directive gain is to feed the array elements with a constant amplitude and a proper phase so that the radiation from each element adds in phase in the direction

The total size of this superdirective antenna is not specified on the advertising brochure. CODAR Ocean Sensors patented this concept a few years ago.

Figure 2.4: Example of a superdirective antenna patented by CODAR Ocean Sensors

2.2.2 How to compact antenna size?

Small HF antennas responding to HFSWR specifications are not available off-the-shelf. That is why a new antenna has to be imagined, designed and optimized to fil this lack and improve performance of the HFSWR in this way. A passive antenna being needed, tricks as active elements are prohibited. The only way to reduce antenna size is to find smaller structures with the same performance than large ones. The idea is to combine radiation and matching in a small antenna. Based on fractal concept, we can imagine that bending a wire structure to obtain a smaller one is a right track. Inspired by an American patent using meanders to create compact antennas for wireless communications, we decide to adopt this departure point.

2.2.2.1 Meander Line Antenna technology

History Meander Line Antenna (MLA) is the name of a new generation of compact antennas. It is a new type of 3-dimensional radiating element, made from a combination of a loop antenna and frequency tuning meander lines. This structure results in an antenna element that is more efficient than currently-used elements in wireless applications.

of interest. It is possible to find designs that result in a directive gain greater than the ordinary gain by reducing space between elements and by feeding them with a non constant phase law. These surperdirective arrays are difficult to implement because phase differences have to be very precise. Moreover, they usually lead to extremely small bandwidths and efficiencies as well as impractical tolerances. Finally, they are very difficult to match.

MLA technology was originally developed by BAE Systems, Information and Electronics Warfare Systems (IEWS), formerly Lockheed Sanders Corporation, for military applications where unobtrusive, high performance antennas are required for both satellite and terrestrial communications. The technology was patented in 1998 (patent Nr.US6790080, Aug. 4, 1998, inventor : Dr. John Apostolos). Today, SkyCross Inc., formed by Milcom Technologies which commercializes military technology, has an exclusive worldwide license to improve this invention. The patented meander line antenna is being used in a wide range of military applications from HF direction-finding to UHF communications and also commercial applications. Sky-Cross antennas are based on the MLA technology that allows engineers to design high performance, multi-mode, multi-frequency antennas that can be hidden inside a mobile casing. These elements have a very low radiation profile and offer much better gain characteristics than existing solutions. Typical applications for the antennas include mobile and fixed wireless communications, automotive and mobile computing markets. For example, it can be used with cellular phones, satellite communications or Personal Communications Services (PCS) applications.

The patent proposed in 1998 defined a Meander Line loaded Antenna and presented a structure comprising :

- a multiplicity of conductive elements adapted for acting as radiating antenna elements,
- a slow wave meander line,
- conductive elements connected to form a loop antenna.

The patent is really complicated to understand because of the number of pages and confusing explanations of each part of the antenna. Americans must have been woolly and complicated in order to preserve their invention.

From this confusing patent, it emerges that meanders could be a good solution to the compactness problem of HF antenna. Giving up the rest of the patent, we will try to use meander lines in the design of an HF compact element.

Principal characteristics of MLA in wireless communication The patent, presented in the previous paragraph, is one precise realization of Meander Line Antenna. There are many studies on the subject and from all this works, based on articles available on the Internet [5] it is possible to present the principal characteristics of antennas based on the MLA concept.

Physically small, electrically large With the MLA technology, engineers can combine smaller, antenna-radiating elements with a meander line structure and geometry to achieve broadband performance in a small envelope. They can electrically couple the fields of different segments of the antenna lines to significantly enhance their performance. The result is an antenna that can resonate broadband and, produce circular as well as horizontal and vertical polarization, and achieve high gain typically a few dB greater than other antennas on the market today.

Narrowband and broadband MLA MLA antennas are configured into two distinct classes :

- The **Narrowband class** exhibits extreme compactness for a given operating bandwidth;
- The **Broadband class** boasts extreme bandwidth capability, capable of covering multiple frequencies without the need to tune it.

Volumetric efficiency The MLA has a number of significant advantages over more conventional antennas. One, which is very important in this study, is a high volumetric efficiency. Compared to other antennas, the Narrowband MLA is demonstrated to provide the most effective use of physical volume for narrow bandwidths.

Multimode operation Another advantage of the MLA is the ability to achieve multimode operation in one antenna structure. The MLA can be used in two radiation modes that may can be excited simultaneously or that can be switched electrically.

- The fundamental mode is that of a monopole, the so-called "**monopole mode**" producing a linear polarized radiation field resembling that of two closely paced monopole antennas. In the monopole mode, the primary antenna current is perpendicular to the antenna ground plane. For a use in HF Surface Wave Radar, we will prefer this mode.
- The second mode of operation is the "**loop mode**" where the primary antenna current is parallel to the antenna ground plane and the maximum radiation is perpendicular to the ground plane. The loop mode can be used for satellite communications since one or the other linear or circular polarization may be obtained through the use of a "crossed" radiating structure.

Portable and handsets The MLA is truly suited to next generation wireless products due to its small size and excellent performance characteristics. Nowadays, there is an important development of handsets requiring multiband operation from 824 to 950 MHz and from 1850 to 1990 MHz. Existing plans for incorporation of GPS to allow user localization require additional frequency coverage at 1,575 MHz. For example, a broadband MLA measuring 2 x 1.2 x 3.1 cm is able to cover all three required bands simultaneously from 800 to 5,000 MHz because it can cover a large band. Coverage of the different frequency bands is also possible with multiband conventional antenna designs. A disadvantage of currently used multiband embedded antennas is detuning when held in proximity to the body. It is common to observe resonance shifts completely out of band with some embedded cellular handset antennas. The broadband MLA, however, does not exhibit measurable proximity detuning under similar conditions.

MLA handset antennas also feature reduced SAR (Specific Absorption Rate) due to their distributed near-field radiation. It has been shown statistically that signal strengths can be increased on the average by as 2 or 3 dB with the use of embedded, reduced SAR antennas such as the MLA. The advantage gained is due in part to a reduction of absorption

of the radiated signal by the human body. Studies have shown that conventional high SAR antennas, such as the dipole and its derivatives, lose approximately 40-50% of their radiated signal to absorption in the head. The increased effective gain available with low SAR antennas provides a number of advantages toward problems that are currently experienced by cellular users and service providers. The advantages are : improved reception quality at the cellular tower receiver (fewer dropped calls), lower power consumption in the handset (longer battery life).

Engineers have begun leveraging advanced technology, such as the MLA to create nearly invisible antenna solutions that not only reduce the size of devices but also significantly improve performance. In wireless communication, this antenna seems to be revolutionary because it operates over large bandwidths, is compact and easily tuned electronically, can be configured for multiple polarizations and has a very high efficiency. It seems to be the best candidate to respond our needs.

2.2.3 Theory of small antennas

After this state-of-the-art about MLA technology, it is interesting to present theory of small antennas because they have particular properties that can be useful to know.

2.2.3.1 Definition of a electrically small antenna

First, the meander line antenna used in HF will be a simple structure with only meander lines, so it has an electric nature. Referring to the desired antenna size, can this compact antenna be considered as an electrically small antenna? To find the definition of an electrically small antenna, we can refer to the pioneers of these questions. The first work about the fundamental limits of electrically small antennas was done by Wheeler in 1947 [6]. He defined an electrically small antenna as one whose maximum dimension is less than $\frac{\lambda}{2\pi}$. This relation is often expressed as :

$$ka < 1$$

where k is the wave number corresponding to $\frac{2\pi}{\lambda}$ in radians/meter. λ is the wavelength in meters and a is the radius of an imaginary sphere enclosing the maximum dimension of the antenna given in meters. This sphere can be represented on the following figure 2.5.

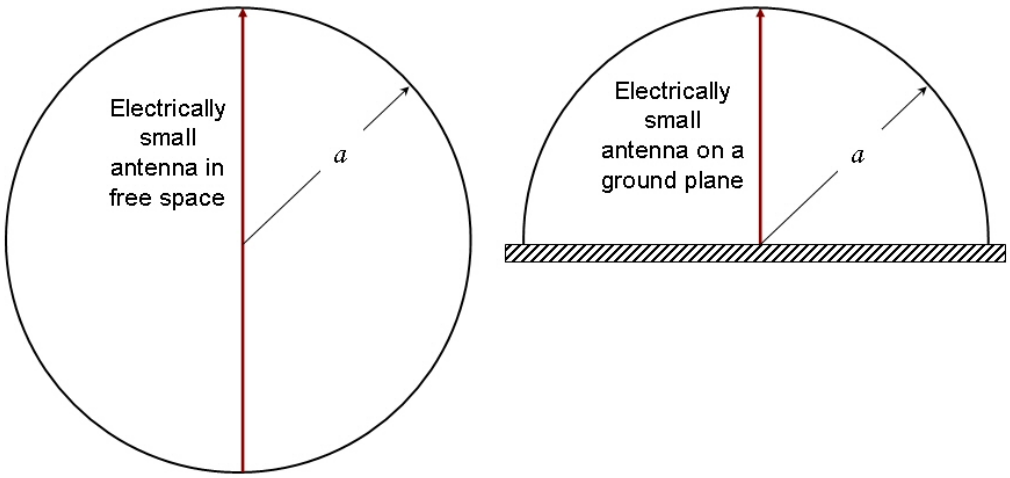

Figure 2.5: Illustration of the imaginary sphere enclosing an electrically small radiating element

In our study, HF frequencies imply decametric wavelengths between 10 and 100 m, and then we have small associated wave numbers. They are comprised between 0.06 and 0.6 radian/meter. According to the size specification previously mentioned (1 m maximum), the needed compactness is such that the antenna to design has to be enclosed in a sphere that has a radius a about 1 m.

By the fact, we obtain a product ka that is well inferior to 1. The future antenna is then considered as an electrically small element.

2.2.3.2 Limitations of quality coefficient

Electrically small antennas have been studied by many scientists. The first works date back to 1948 with Chu studies [7]. A few years later, Harrington [8] was also interested in the small antennas subject. They both tried to find limitations of parameters of small antennas such as the maximum bandwidth for given small dimensions characterized by a quality coefficient Q_a.

This coefficient is very important because many parameters can be deduced from it (bandwidth, radiation efficiency, etc). Thus, the knowledge of the minimum Q_a for a given antenna is useful for design. A general definition of the quality coefficient Q_a can be expressed as :

$$Q_a = \omega_c \frac{Stored\ energy}{Radiating\ power}$$

where $\omega_c = 2\pi f_c$, f_c being the considered frequency. The stored energy can be decomposed in the sum of an electrical stored energy and a magnetic stored energy. If the antenna has a nature purely electric, the stored energy will only be electric. If the antenna has a nature purely magnetic, the stored energy will be magnetic. A priori, the antenna

to design, based on the MLA technology, will be purely electric because it will use only meanders and no magnetic loop, as proposed in the American patent.

Chu and Harrington found the concept of the sphere enclosing the antenna in order to calculate the stored energy and the radiating power. Then, they used a decomposition of the electric field in spherical harmonics. They made works to find a minimum quality coefficient providing the maximum bandwidth. In fact, the quality coefficient of small antennas is inversely proportional to the bandwidth :

$$Q_a \propto \frac{f_c}{\Delta f}$$

At the time, these works from Chu and Harrington were only reflections but nowadays the miniaturization aspect is very important in many domains. That is why many studies have been published in the last decades. In 1996, Mac Lean [9] proposed a simple formulation for the minimum quality coefficient that can be reached with an electrically small antenna.

$$Q_{a\,min} = \frac{1}{k^3a^3 + \frac{1}{ka}} \approx \frac{1}{k^3a^3}$$

where k is always the wave number and a the radius of the sphere enclosing the antenna. This formula is given for an antenna with a rectilinear polarization in free space. Moreover, this equation assumes a perfect lossless matching network.

2.2.3.3 Gain of small radiating elements

Harrington showed that the maximum gain of an electrically small antenna is given by :

$$G_{max} = (ka)^2 + 2ka \approx 2ka \tag{2.1}$$

This gain would be a theoretical limit that we could not pass because it is linked to the fundamental Maxwell equations and also linked to the nature of currents. This gain is given is free space.

2.2.3.4 Bandwidth of small radiating elements

The MLA can be considered as a RLC type circuit and it is then possible to calculate its bandwidth linked to its quality coefficient and its VSWR with the following formula :

$$BW = \frac{\Delta f}{f_c} = \frac{S-1}{Q_a\sqrt{S}} \tag{2.2}$$

where BW is the normalized bandwidth and S is the VSWR. The demonstration of this formula is available in annexe 5.6.3.

2.2.3.5 Efficiency of small radiating elements

The efficiency of an electrically small antenna is determined by the amount of losses in the conductors, dielectrics and other materials out of which the antenna is constructed compared with the radiation loss. This can be expressed as :

$$\eta_a = \frac{R_r}{R_r + R_m}$$

where η_a : Efficiency of the antenna
R_r : Radiation resistance (in ohms)
R_m : Material loss resistance (in ohms).

The dissipative loss resistance can be separated from the radiation resistance using S-parameter measurements.

The input impedance of an electrically small antenna is capacitive and in order to provide the maximum transfer of power into the antenna, a matching network may be required. The efficiency of the antenna and its matching network is expressed as :

$$\eta_s = \eta_a \eta_m$$

with η_s : Efficiency of the system (i.e. antenna and matching network)
η_m : Efficiency of matching network

The efficiency of the matching network is approximately :

$$\eta_m \approx \frac{\eta_a}{1 + \frac{Q_a}{Q_m}}$$

where Q_a : Quality coefficient of the electrically small antenna
Q_m : Quality factor of the matching network

All these theoretical formulae will be useful in this document to verify performance of the designed antenna.

2.2.4 Choice of a departure geometry : the generic antenna

First, in a logical way, the design must present a simple geometry and evolutions will lead to more complicated designs. Based on many designs examples of antennas used in cellular phones, mainly microstrip antennas as presented on figure 2.6, the departure point of this study is a simple structure with meanders. Microstrips would be to large in HF, that is why we decide to imagine a wire structure with bended parts.

Figure 2.6: Example of a microstrip meander line antenna used for wireless communications

The departure point was not chosen at random. The structure was chosen to have a maximum size of 1 m with ressemblance to antennas tested in articles (e.g. number of meanders, distance between horizontal branches, proportion between length and width, etc). Based on the similitude principle transfered to HF frequencies, we define a basic antenna that will be optimized and name it "generic antenna". The generic antenna has these geometrical parameters :

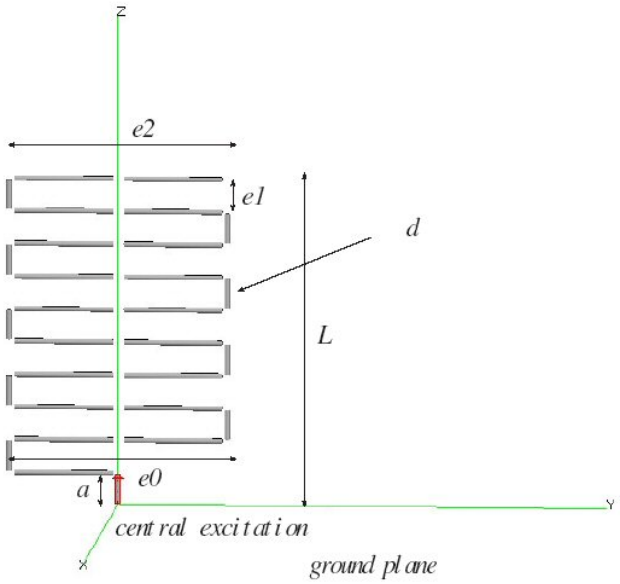

Figure 2.7: geometrical parameters of the generic antenna

- Total height = L = 1 m
- Straight shape
- Bottom width = e0 = 0.7 m

- Top width = e2 = 0.7 m
- Central excitation
- Diameter of wires = d = 0.005 m
- Distance from the ground = a = 0.1 m
- Distance between horizontal branches = e1 = 0.1 m

The generic antenna is presented in figure 2.7 and its dimensions are in accordance with specifications. The total deployed length of this antenna is about 7.5 m.

2.2.5 Theoretical functioning of the generic antenna

The functioning of a MLA can be simply explained thanks to a monopole antenna. In fact, in a monopole antenna, the total vertical structure will take part in the radiation. Imagine that you separate a monopole antenna in several short segments, as presented on the left part of figure 2.8, and you arrange them in staggered rows. These short radiating segments can be linked by horizontal segments to have a continuity in the feeding. The meander line antenna is born. Currents that travel in the structure will be in phase from a vertical part to another while they will be opposed from an horizontal branch to another. With a few phase differences, effect of horizontal segments will compensate and will not contribute to the radiation. Moreover, as only vertical parts radiate efficiently, the polarization of this kind of MLA will be rectilinear and vertical.

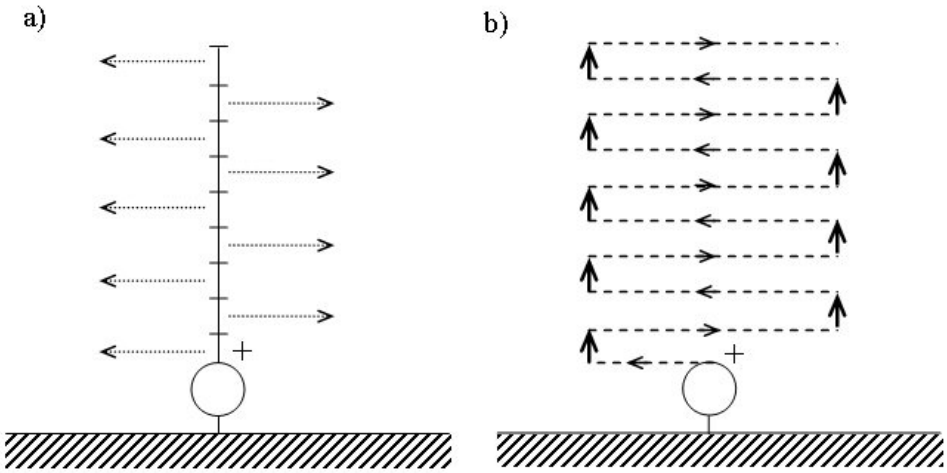

Figure 2.8: Derivation from a monopole (a) to a meander line antenna (b)

The impedance of an antenna is composed of an active part and a reactive part. For a meander line antenna, the active part is due to the sum of active power radiated by each vertical dipole. The reactive part has a value linked to the total length of the structure. It means that the small size of the antenna will be taken into account in the radiation implying weak radiating performance. But for matching, the total deployed length of the

structure will be taken into account to find resonant frequencies. And so, the longer the antenna is, the lower the resonant frequencies will be. The aim will be to obtain a long deployed length comparable to the usual size of HF antennas (for a question of matching) while minimizing overall dimensions of the antenna.

To verify this functioning principle, this is an example of works, made by an American called Randy Bancroft (Centurion Wireless Technologies) [10]. He studied the case of a microstrip meander line antenna, used for mobile design device at 1.5 GHz. He proposed the following results, available on figure 2.9, which are results given by FDTD method (the Finite Difference Time Domain (FDTD) method provides a numerical solution of Maxwell's equations in the spatial and time domains). This figure presents magnitude of currents measured with a small prototype of meander line antenna. Patches of current are in phase with the four vertical high current radiating sections on the meander line. Horizontal currents on the meander line section cancel each other. In fact, vertical sections are essentially the only sources of radiation.

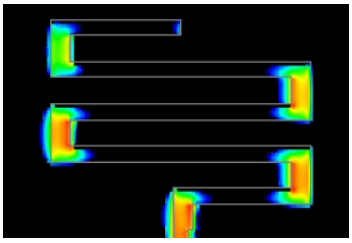

Figure 2.9: Current magnitude plot for a microstrip meander line antenna designed for mobile communication

According to Japanese scientists (Endo et al [11]), a meander line antenna can be decomposed in short-terminated transmission lines, whose number is equal to the number of turns of the antenna, and a linear conductor whose length is equal to the antenna height. In other words, a model consisting of a linear monopole antenna with inductance is considered. Their analytical model can be represented by figure 2.10.

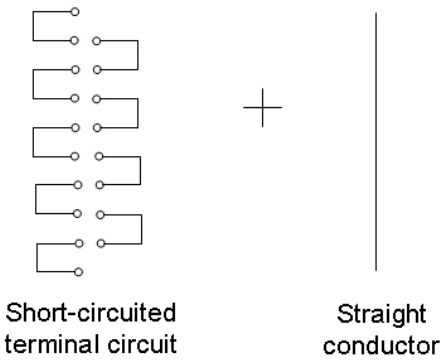

Figure 2.10: Analytical model of the meander line antenna

Thanks to this model, they made comparison between meander line antenna and a

dipole antenna. They assume that the MLA self-inductance and a dipole self-inductance have the same resonant frequency. This assumption was verified by construction of several prototypes. Then, they deduce for example, the number of meanders needed to have resonance at a precise frequency.

$$N_{meanders} = \frac{\frac{\lambda}{4}\left(log\frac{2\lambda}{d} - 0.5L\right) - 0.5L\left(log\frac{4L}{d} - 0.5L\right)}{e0\, log\frac{L}{Nd}\left(0.5L + \frac{0.5L}{3}\left(\beta\frac{e0}{2}\right)^2\right)}$$

with L : Antenna height
d : Diameter of wires
$e0$: Width of the MLA
$\beta = 2\pi/\lambda$.

This is a transcendental equation[2] that can be solved by mathematical softwares such as Mathematica or Maple. To obtain a resonance at 5 MHz, the number of turns is an imaginary number and for 15 MHz, 25 meanders would be needed. These results have to be considered carefully because the Japanese scientists used a meander line dipole antenna (feeded at its center) in their calculation while the generic antenna that we study is rather considered as a meander line monopole antenna.

We then decide to maintain the number of meanders of the generic antenna and to model it to have an estimation of its performance.

2.3 Modeling of the generic antenna

This chapter would be incomplete without a presentation of the method used to simulate the antenna. For this thesis, the available electromagnetic code was NEC-2.

2.3.1 Principal electromagnetic code used

2.3.1.1 NEC-2

When we are interested in wire antennas, the famous modeling software NEC become obvious. NEC stands for Numerical Electromagnetics Code. It has been developed by the Lawrence Livermore National Laboratory of California, under the sponsorship of the Naval Ocean Systems Center and the Air Force Weapons laboratory. It dates back to 1981 and has then originally been developed for the military domain.

This code is used to model thin wire antennas and 3-D models constructed of thin wires. You can derive the input impedance of an antenna, add a matching network if desired, then calculate the near or far electric and magnetic fields in any direction or at any distance from the antenna. The program breaks the wires of the model into short segments and

[2]Transcendental relates to a real or complex number that is not the root of any polynomial that has positive degree and rational coefficients. A transcendental function is a function which does not satisfy a polynomial equation whose coefficients are themselves polynomials. Saying it more technically, a function of one variable is transcendental if it is algebraically independant of that variable. The logarithm and the exponential functions are examples of transcendental functions.

calculates the current and phase in each. It then uses integral equations to compute the fields at any distant point.

NEC has been improved over the years. NEC-2 is widely available, even for free, and can model wire structures in free space, especially at HF and VHF. NEC-3 does the same but can also model wires buried in the ground or penetrating from the air into the ground. Both versions suffer loss of precision when modeling electrically small structures such as low frequency radio antennas. NEC-4 uses revised algorithms which will (with some limitations) model electrically small structures in, on, and above real earth with finite conductivity and permittivity. It also can model insulation around the wire, which is very useful for modeling antennas in water. NEC-4 is not (in theory) available to the public.

NEC-2 Version 4 On the internet, NEC-2 is available for free. A simple download[3] is necessary to model wires antenna. NEC-2 Version 4 is the last version of the code that can be downloaded. This version has been used to model the compact antenna of this thesis. The advantage is that it has now a graphic interface, but that was not the case 3 years ago. This interface is practical and simplifies geometry editing, computing and results visualization compared to previous versions devoid of tools.

To sum up, NEC is a computer code analyzing the electromagnetic response of an arbitrary structure consisting of wires and surfaces in free space or over a ground plane. The analysis is accomplished by the numerical solution of integral equations for induced currents. The excitation may be an incident plane wave or a voltage source on a wire, while the output may include current and charge density, electric or magnetic field in the vicinity of the structure, and radiated fields.

2.3.2 Integral equations

To simulate functioning of the antenna and to calculate all interesting values for its characterization, we use the integral representation of the electric field, associated to the Method of Moments.

2.3.2.1 Integral representation

The aim is to calculate the current in the antenna to obtain impedance, radiation patterns, etc. The integral representation of the radiated field is given by :

$$\vec{E}(\vec{r}) = -\frac{j\eta}{4k\pi}\int_V \vec{I}(\vec{r})\bar{G}(\vec{r},\vec{r'})dV'$$

where : $\bar{G}(\vec{r},\vec{r'}) = (k^2\bar{I} + \nabla\nabla)\left|\frac{exp(-jk\left\|(\vec{r}-\vec{r'})\right\|)}{\left\|(\vec{r}-\vec{r'})\right\|}\right|$ is the Green's function in free space. r is the distance between the voltage source and the observation point.

$k = \omega\sqrt{\mu_0\epsilon_0}$ and $\eta = \sqrt{\mu_0/\epsilon_0}$ where μ_0 is the vaccum permeability (=$4\pi e^{-7}$ H/m) and ϵ_0 is the vacuum permittivity (=$8.8541e^{-12}$ F/m).

[3]Download available on the site http://www.si-list.org/swindex2.html

For a wire structure, we can present the Pocklington integral equation, which is the integral equation of the radiated field. It is given by :

$$\int\int_{L\times C} \frac{I(s^{'})}{2a\pi}\left[\frac{\partial\partial}{\partial s\partial s'} - k^2 ss^{'}\right] C(s,c,s^{'},c^{'})dsdc = j\omega\epsilon E_i(s)$$

where : a : Radius of wire
s : Curvilinear abscissa along the wire structure
C : Wire contour
L : Total length of the wire

In this equation, we can notice that the term I, we are interested in, is in the integral. So, we use the Method of Moments in order to extract it and determine its value.

2.3.2.2 Method of Moments (MoM)

This method was developed by Harrington in 1968 and its aim is to provide a unified treatment of matrix methods for computing the solutions to field problems. The basic idea is to reduce a functional equation to a matrix equation, and then solve the matrix equation by known techniques. These concepts are best expressed in the language of linear spaces and operators.

The integral equation can be written :

$$L(f) = g$$

We consider equations of inhomogeneous type where L is an operator, g is the source or excitation (known function), and f is the field or response (unknown function to be determined).

You have to respect some steps to find the solution. First, let f be expanded in a series of functions f_1 , f_2, f_3 in the domain of L, as :

$$f = \sum_n \alpha_n f_n$$

where the α_n are constants.

We shall call the f_n expansion functions or basis functions. For approximate solutions, f is usually a finite summation. With the linearity of L, we have :

$$\sum_n \alpha_n L(f_n) = g$$

It is assumed that a suitable inner product has been determined (scalar product). Now define a set of testing functions w_1 , w_2, w_3 in the range of L, and take the inner product of g for each w_m . The result is :

$$\sum_n \alpha_n \langle w_m, Lf_n\rangle = \langle w_m, g\rangle$$

m=1, 2, 3, etc, this set of equations can be written in matrix form as :

$$[l_{mn}]\,[\alpha_n] = [g_m]$$

where :

$$[l_{mn}] = \begin{bmatrix} \langle w_1, Lf_1\rangle & \langle w_1, Lf_2\rangle & \cdots \\ \langle w_2, Lf_1\rangle & \langle w_2, Lf_2\rangle & \cdots \\ \cdots & \cdots & \cdots \end{bmatrix}$$

$$[\alpha_n] = \begin{bmatrix} \alpha_1 \\ \alpha_2 \\ \cdots \end{bmatrix}$$

$$[g_m] = \begin{bmatrix} \langle w_1, g\rangle \\ \langle w_2, g\rangle \\ \cdots \end{bmatrix}$$

If the matrix $[l]$ is non singular, its inverse $\left[l^{-1}\right]$ exists. The α_n are given by :

$$[\alpha_n] = \left[l_{mn}^{-1}\right]\,[g_{mn}]$$

And the final solution for f is given by :

$$f = \sum_n \alpha_n f_n$$

One of the main tasks in any particular problem is the choice of the f_n and w_n . The f_n should be linearly independent and chosen so that some superposition, as above, can approximate f reasonably. The w_n should also be linearly independent and chosen so that the products depend on relatively independent properties of g.

Some additional factors which affect the choice of f_n and w_n are :

- the accuracy of solution desired,
- the ease of evaluation of the matrix elements,
- the size of the matrix that can be inverted and,
- the realization of a well-conditioned matrix.

2.3.2.3 Meshing

In the code NEC-2, meshing is an important step. In fact, it is a concrete application of Method of Moments. First, you have to divide a wire structure in segments and define basis functions on these segments.

In fact, meshing is not a simple step because there is a precise number of segments where you have a stabilized solution (for the impedance, for example). The aim is to find the optimum number of segments, enough to have a reliable solution and not too much to avoid problems of convergence and long computation time. Usually, we use a maximum length segment of a $\lambda/10$ or $\lambda/20$. In our case, with frequencies between 3 and 30 MHz, meaning wavelengths between 10 and 100 m, the number of segments is the same for each frequency because antenna size is 1 meter high to a maximum. So all wires will be meshed with with one segment.

The problem is that NEC may have too less segments for its calculation or length of these segments can be to small compared to the radius of wires. In these cases, a few hypothesis are not respected during the computation. That is why results can be different and far from reality if the defined meshing is not well adapted or if segments size is too small compared to $\lambda/20$. This point will be important at the end of the study to compare modeling results with real measurements data.

2.3.3 Results of the generic antenna modeling

2.3.3.1 NEC-2 results

This antenna has been modeled with NEC-2, based on the Method of Moments, and it is assumed to be placed on a perfect electric conductor ground plane.

To be faithful to reality, we have to take losses into account in the simulations. In fact, with NEC, it is possible to define a wire conductivity for the whole structure. Thus, it is possible to create a wire structure made of various material. For our study, we take the example of an antenna made of copper, which is a good conductor and it is also flexible. Its conductivity is 5.8e7 S/m.

The quality coefficient of the generic antenna is about $\frac{1}{k^3a^3}$ at 17 MHz, i.e. about 19. It means that for an optimistic VSWR equals to 2 around 17 MHz, this antenna should have a bandwidth about :

$$\Delta f = \frac{(S-1)f_c}{Q\sqrt{S}} = 632\ kHz$$

The simulated VSWR is really bad compared to the predictions. In fact, the VSWR is not good at all because its best value is 20.33 at 17 MHz, corresponding to a reflection coefficient of -0.8 dB as shown on figure 2.11.

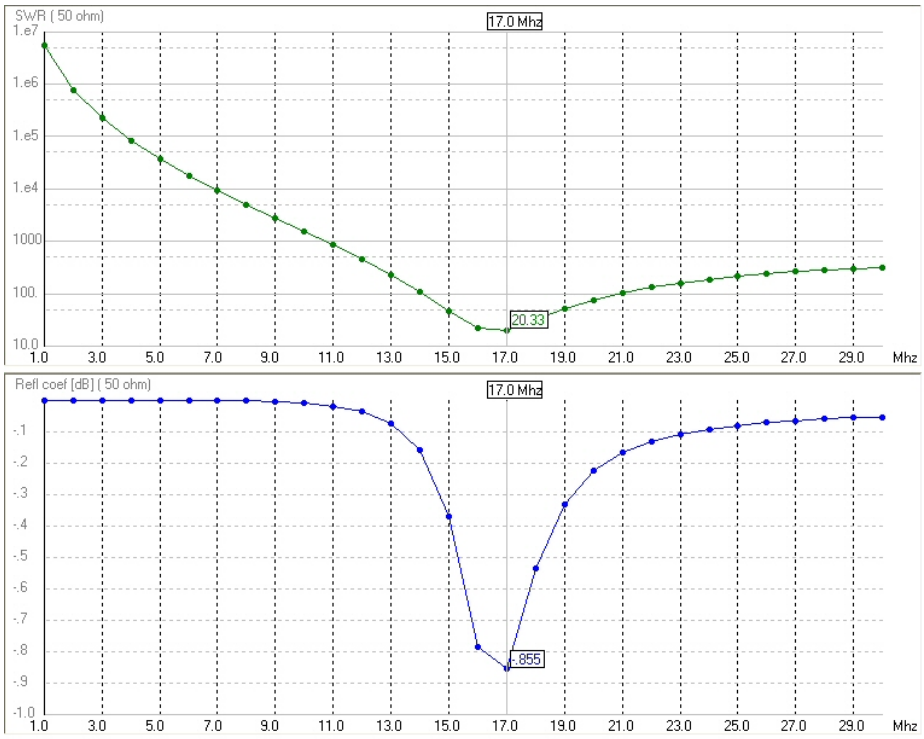

Figure 2.11: VSWR and reflection coefficient of the generic antenna simulated with NEC-2

The theoretical maximum gain of the MLA can be calculated thanks to the Harrington formula (see 2.1).

$$G_{max} \approx 2ka$$

This formula is obtained by using several orders of spherical wave functions as well explained by Harrington [8]. This formula is valid if we use a number of orders inferior to ka. Let us take the example at 17 MHz. At this frequency, the wave number k is about 0.356 radians/meter. The dimensions of the generic antenna can be enclosed in a sphere that has a radius a about 1.059 m as shown on figure 2.12. It means that the product ka is inferior to 1, meaning that the approximation of the maximum gain cannot be used in our case because it would have been obtained with less than one order of spherical wave function, which is a nonsense. That is the reason why, we cannot conclude about a theoretical gain for this antenna.

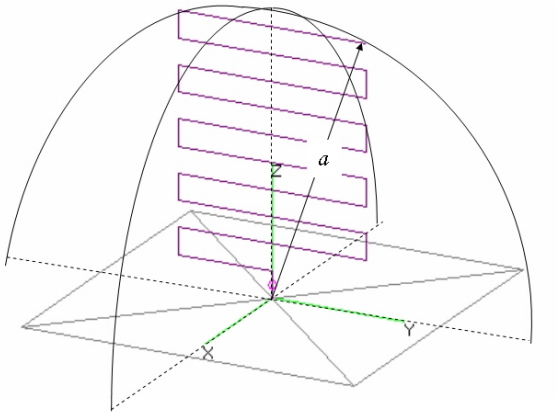

Figure 2.12: Illustration of the sphere enclosing the generic antenna

To better understand radiation pattern displayed by NEC, this a presentation of conventional angles used in this document on figure 2.13. By exciting the antenna with a voltage source, NEC-2 can compute the radiated field for a set of directions of space. Generally, we will be interested in the vertical plane containing the antenna (vertical section at phi = 0°) and in the horizontal plane (horizontal section at theta = 0°) to study the radiation all around the antenna.

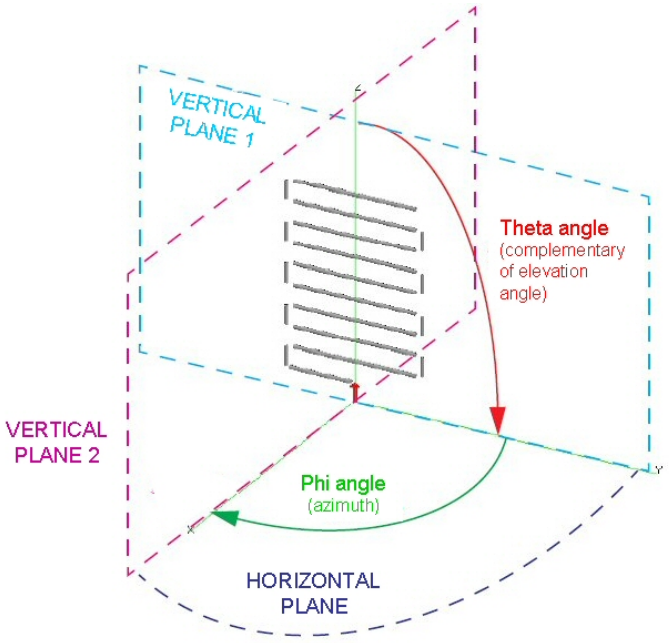

Figure 2.13: Conventional angles and planes

The simulated result for the gain calculation at 17 MHz proposes a maximum gain about 5 dBi[4] as shown on figure 2.15. This value is comparable with the gain of a quarter

[4]In the expression of antenna gain, the number of decibels of gain of an antenna is referenced to the zero dB gain of a free space isotropic radiator and this unit is called dBi

wavelength monopole antenna placed on a perfect infinite ground plane. A practical tool available with NEC-2 version 4 is the 3D viewer that represents radiation pattern results in 3 dimensions (see figure 2.14). By this way, it is easier to imagine the radiating around the antenna. The generic antenna has a radiation pattern strongly ressembling to the one of a monopole antenna, for each frequency.

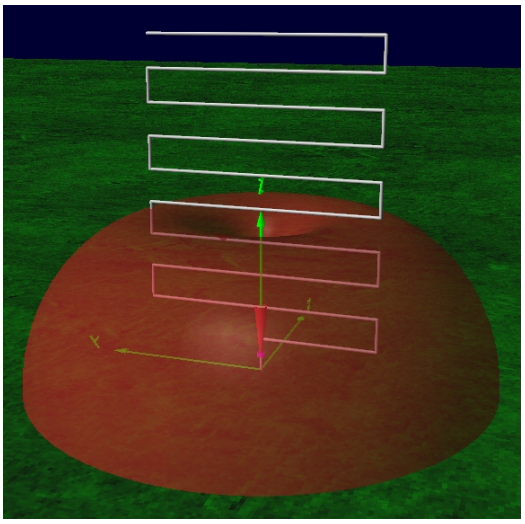

Figure 2.14: 3D viewer of the generic antenna radiation pattern

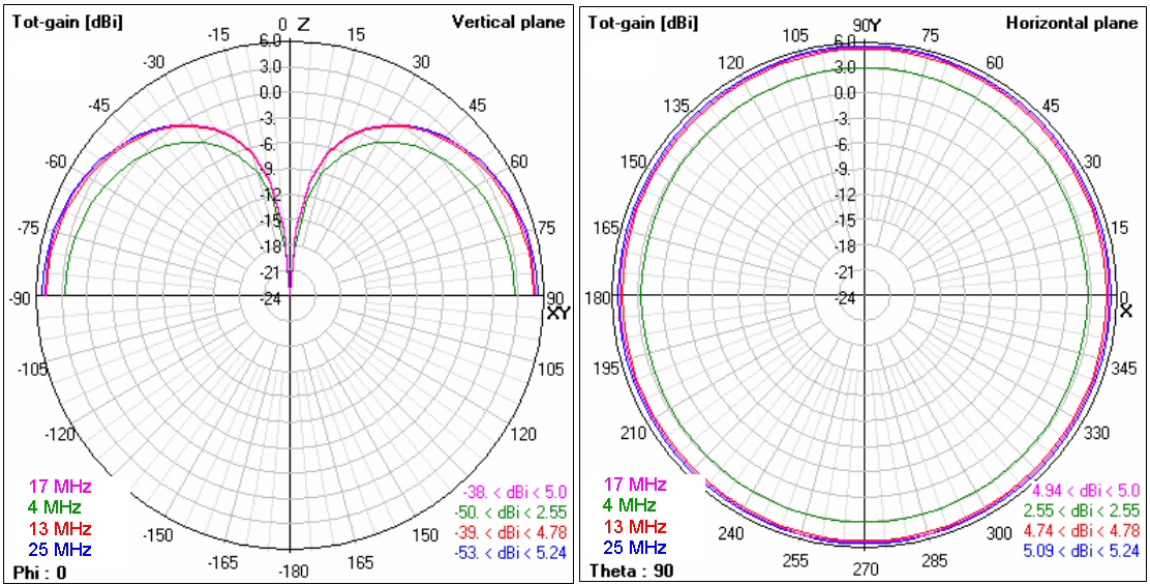

Figure 2.15: Radiation pattern of the generic antenna

2.3.3.2 Simulations results by France Telecom

To validate these simulation results, we decide to compare them with results coming from powerful tools that have proved themselves. An help has then been asked to the Research and Development center of France Telecom. This is a research center of repute that is third on a worldwide scale in the telecommunications domain. They are known to be well equiped and are often confronted with sensitive problems, such as miniaturization problems. For their antenna simulations, they use a code called SR3D, which is based on the same principle as NEC with one exception the use of a Galerkin method in the Method of Moments. They accept to simulate the generic antenna to prove their code efficiency and check the code capability for this type of structure comprising small elements compared to the wavelength. The software is not able to simulate very infinite thin wires. Moreover, every elements of the structure such as the ground plane must have finite dimensions.

They made simulations on the complete structure, without thin wires approximation, including a circular ground plane with finite dimensions. The antenna is feed thanks to a coaxial cable of 50 ohms in TEM mode. They have to mesh the structure and the meshing density is usually 2,000 points/λ for wires and 500 points/λ for the coaxial and the external contour of the ground plane. An example of this meshing is presented on figure 2.16.

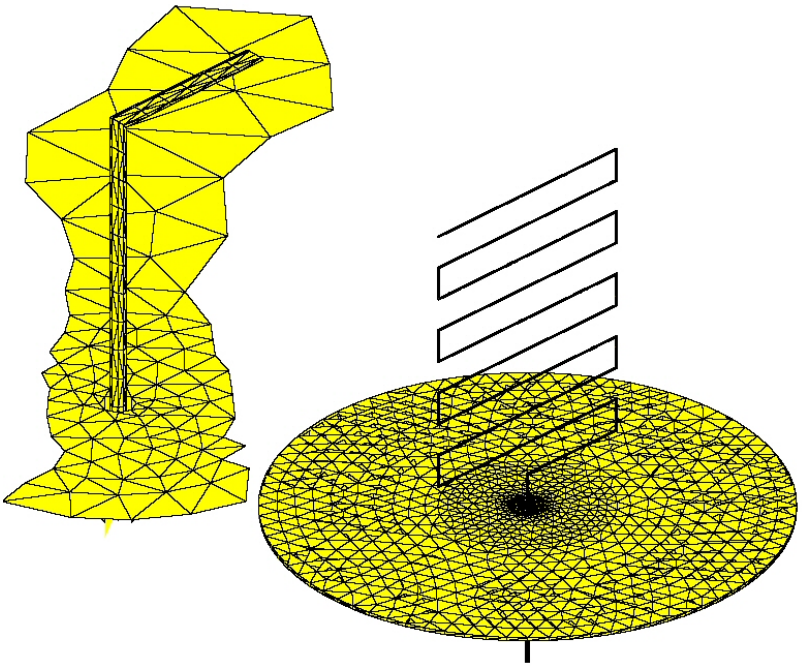

Figure 2.16: Meshing of the antenna and its small circular ground plane

For a ground plane with a diameter of 1.5 m, the structure has been meshed with 16,800 triangles meaning 25,100 degrees of freedom. Tests have also been done with a ground plane having a diameter of 3.5 m (25,900 triangles meaning 38,800 degrees of freedom).

Simulations show an instability of results concerning the input impedance of the antenna

in function of the ground plane size. These results are displayed on figure 2.17. The instabilities are due to the small dimension of the ground plane, which is $< \lambda/10$. The green curve corresponding to the smallest ground plane is really chaotic while it is better on the red curve corresponding to the bigger ground plane. It seems to be a resonance around 19.5 MHz but the VSWR value of 25 is really bad. With NEC, the best VSWR was obtained about 20 at 17 MHz. Both results are close to each other.

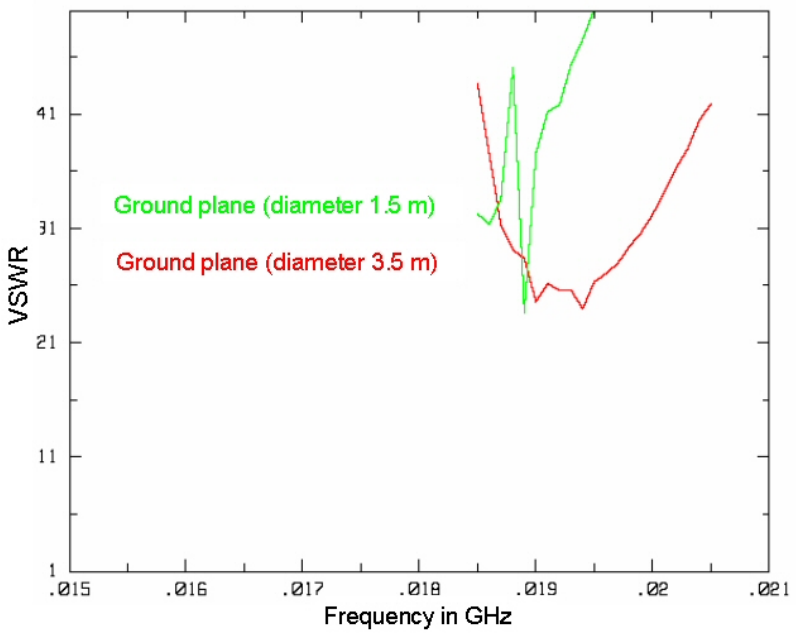

Figure 2.17: VSWR of the generic antenna simulated by SR3D with a finite ground plane

Concerning simulations of the radiation pattern, it has been done for 19.5 MHz with the 3.5 m diameter ground plane. Results are presented on figure 2.18. The continious curve represents the component Eθ and the dotted lines represent Eϕ. These plane correspond to the conventional planes "vertical plane 1" and "vertical plane 2" defined previously. The plane $\phi = 0$ ° is displayed in green, the plane $\phi = 90$ ° in blue and the planes $\phi = 45$ ° in red. For our study, we are interested the continious red line, it confirms that the generic antenna has the same radiation pattern than a monopole antenna. That confirms the results of NEC simulations.

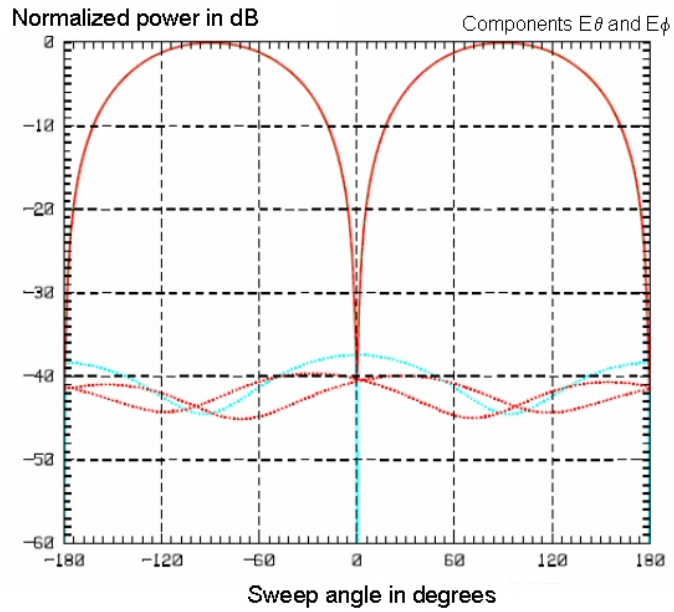

Figure 2.18: Radiation pattern of the generic antenna simulated by SR3D with a finite ground plane (diameter 3.5 m) at 19.5 MHz

A second step consisted in increasing the ground plane dimensions. To do that, they extended the circular ground plane with 8 wires being 8 m long all around the structure. This ground plane extension is shown on figure 2.19.

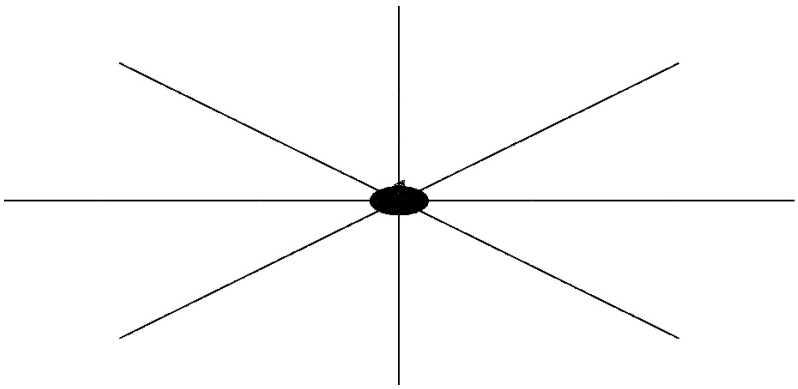

Figure 2.19: Illustration of the extended ground plane considered in SR3D simulations

These long wires have also been meshed. For this configuration, two circular ground planes (diameter 1 and 2.8 m) have been simulated. For the 2.8 m diameter ground plane, the meshed structure has 27,400 triangles, meaning 38,700 degrees of freedom. A zoom on the final meshed structure with extended ground plane is displayed on figure 2.20.

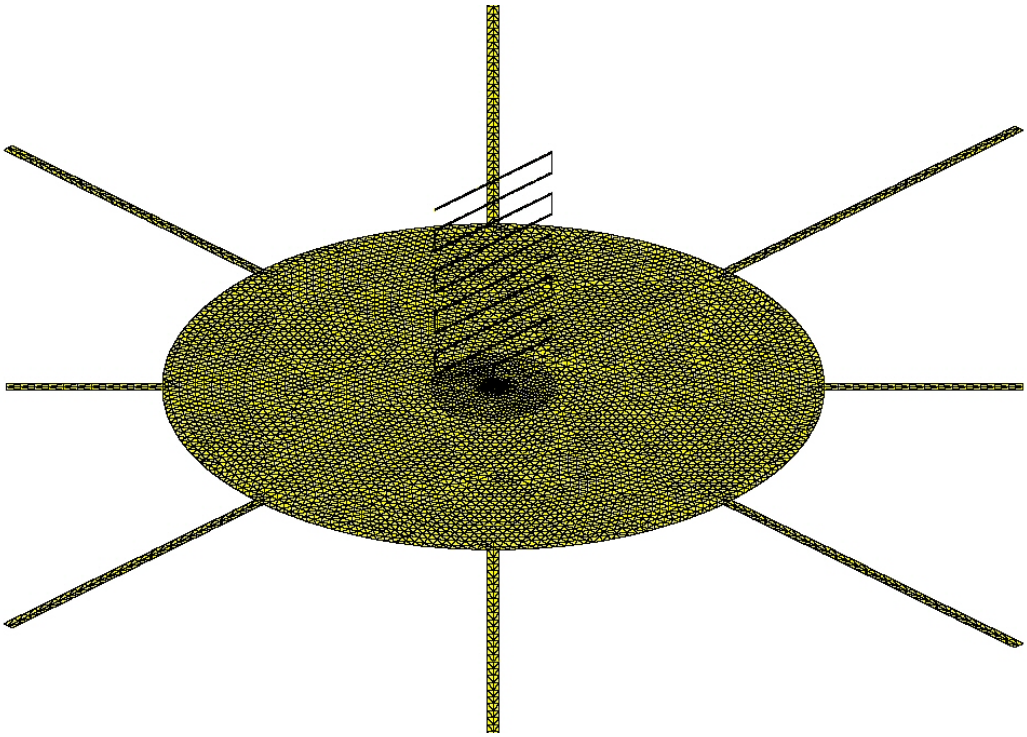

Figure 2.20: Zoom on the extended ground plane considered in SR3D simulations

This time, results are more stable, even the test with the small extended circular ground plane. The resonance seems to be shifted around 16.5 MHz. This is close to NEC results in terms of resonant frequency. In fact, there is a matching point at 16.4 MHz. At this frequency, with an extended 2.8 m diameter ground plane, the VSWR is about 1.97, which is a good value.

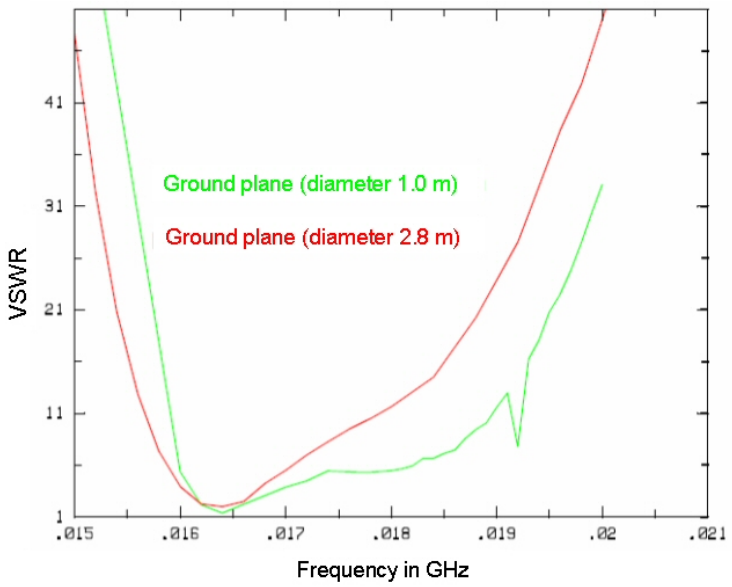

For the radiation pattern, displayed for the extended 2.8 m diameter ground plane on figure 2.21, we notice that it is totally disturbed by the ground plane configuration. In fact, the radiation pattern has several lobes. This is not really coherent with the functionning principle that has been explained in 2.2.5. Normally, this antenna should have a radiation pattern resembling to the one of a monopole antenna.

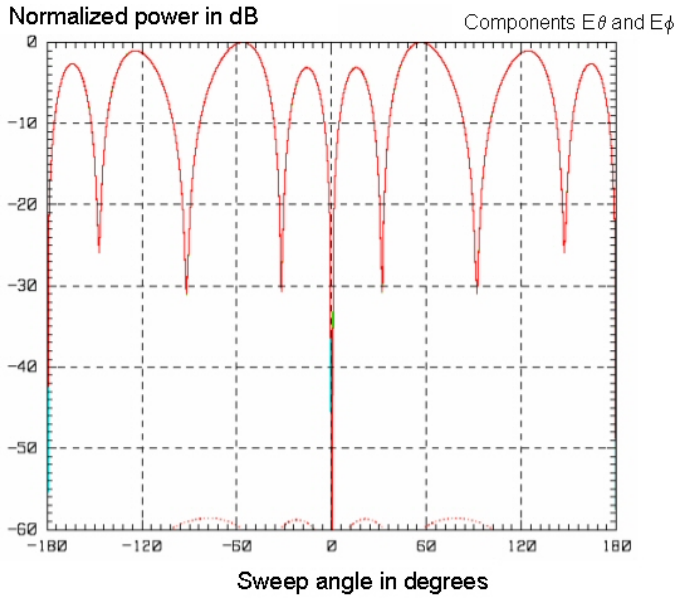

Figure 2.21: Radiation pattern of the generic antenna simulated by SR3D with a extended ground plane (diameter 2.8 m) at 16.4 MHz

In conclusion for the simulations made by France Telecom, it appears that the addition of the 8 long metallic wires creates a ground plane around 2.5λ and by the way, results are stabilized. The matching of the generic antenna is then around 16.4 MHz with a VSWR inferior to 2.

This simulations results confirm NEC-2 result, except that the influence of the ground plane can be better studied whith SR3D. Simulations have to be continued to find a design responding perfectly to all specifications and a prototype is envisaged to validate simulation results.

In this chapter, precise specifications for HFSWR have been detailed to well understand the need in terms of antenna. Then, after a presentation of usual HF antennas that can be used for surface wave radars applications, it emerges that compact antennas does not exist on the market today and it is a problem for many HF users. To fil this lack, a compact HF antenna is defined with similitudes with antennas used in wireless communications. A generic antenna composed of simple meander lines is the departure point of this study. This antenna is considered as an electrically small element and then it has special properties that it is interesting to know to well size the compact element. This generic antenna has been

modeled with an electromagnetics code called NEC-2, based on the Method of Moments, which is generally efficient for wire structures simulations. The generic antenna has also been simulated with a powerful research code to confront several simulation results. The basic antenna has already interesting characteristics : its radiation pattern is quite similar to the one of a monopole with vertical polarization and its size respects specifications. The problem is that this first antenna is a departure point but it does not correspond perfectly to specifications needed for HF Surface Wave Radars mainly in terms of impedance. An optimum geometry has to be found. Next step of the study will concern optimization of the design of the generic antenna to obtain the best possible performance in the smallest possible dimensions.

Chapter 3

Optimization, manufacturing and validation of a compact HF antenna prototype

Contents

In spite of slight differences between modeling results of the two codes previously used for the generic antenna, we have its general trend. A resonance can be obtained around 17 MHz, but the associated VSWR value is not always concordant in both simulations. The way the ground plane is modeled seems to strongly influence results. The radiation pattern has the same characteristics than a monopole antenna and this is faithful to the theoretical MLA functioning. An important specification to obtain is at least two operating band with a bandwidth of a few hundreds of kHz. With this objective, we will modify the generic antenna in order to obtain the most compact HF antenna having the same performance than usual HF antennas in terms of gain, impedance, polarization, etc. First, a search for geometrical parameters influencing the antenna performance will be done. These parameters will be optimized to find a compact design responding HFSWR specifications. Then, the final antenna will be modeled and a prototype fabricated to check modeling results.

3.1 Search for parameters influencing antenna performance

Based on NEC-2 simulations results, all possible modifications have been tested to obtain the best antenna configuration. In fact, we modified the antenna size, its voltage source location, its shape, diameter of its wires, etc. We modified parameters one by one to better estimate their influence on the antenna performance. In fact, the important point for this study was to obtain at least two matched frequencies with a sufficient bandwidth and a radiation pattern comparable to the one of a monopole. That is why we observe effects of all these modifications principally on the VSWR and on the radiation pattern.

3.1.1 Geometrical factors

To find factors influencing the MLA performance, we present here a list of potential geometrical factors. All results are not developed here but a description of their effects is presented in the following paragraphs.

3.1.1.1 Antenna size

The antenna size is a critical parameter for this study because the size reduction is an important point. To test size influence on MLA characteristics, various tests have been made.

First, the height of the antenna has been increased to L=1.5 m and 2.0 m, maintaining other parameters unchanged. Results for impedance were globally improved with a normal shift of the resonance frequency to the lower frequencies. Nevertheless, the VSWR values were still high.

By reducing the height at L=0.7 m and 0.5 m, the obtained impedances were not good at all : this antenna size would be really difficult to match.

As a conclusion, it is clear that increasing the height of the antenna is beneficial to the MLA performance. The problem is that a compact size has to be maintained so this improving factor seems to be problematic.

3.1.1.2 Shape of the structure

We can say that the generic antenna has a straight shape because its top and bottom widths are equal. We can imagine that this width is variable. In fact, we have tested ascending and descending design.

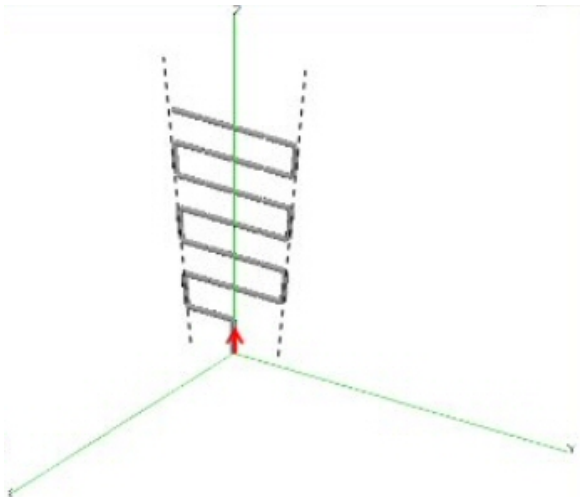

Figure 3.1: Example of a tested ascending shape

For ascendant antenna (see figure 3.1), we keep its top width constant (e2=0.7 m) and reduce its bottom width (e0=0.1 m). No improvements have been made with this shape. We can just notice that the antenna is capacitive most of the time. For another tests with e2=0.9 m and e0=0.3 m, results are better than the generic antenna in terms of VSWR, but they values are still weak for our objectives.

By considering same widths as previous geometry but in the descending configuration, we obtain disappointing results.

When we have a variable width between turns, we can test if biased wires instead of vertical parts can improve results. Unfortunately, this change has no effect, the vertical branches seem to better radiate than biased ones and it is comprehensive if we refer to its functioning.

Finally, a rhombic shape has been tested without success.

3.1.1.3 Feeding point position

In the generic antenna, the feeding point is in the middle of the antenna and it has the advantage of a symmetry in the structure. If we try to change the source voltage position, we observe that lateral feed breaks a kind of equilibrium in the structure and the radiation pattern is not omnidirectional anymore.

Impedances are a little bit better, mainly for high frequencies, but the radiation pattern is distorted by this dissymmetry. Moreover, we have to take into account the practical use of the antenna. In fact, if we want to maintain the antenna in a vertical position, it is better to keep a symmetrical shape to avoid supplementary wires or strings to maintain it because that may change its functioning.

3.1.1.4 Diameter of metallic wires

Diameter of wires in the generic antenna are quite small but they cannot be physically too big because of the turns that must be realizable in practical. By increasing diameter (d=0.01 m), we have bad impedances. If we go on increasing diameter (d=0.02 m), results are worse.

By reducing wires diameter to d=0.04 m, we notice improvements only for high frequencies. The problem is that we cannot have a too small diameter, always for a question of realization.

3.1.1.5 Distance from the ground

When the first meander is close to the ground (a=0.05 m), we have a good VSWR for frequencies higher than 16 MHz with no significative effects on the other frequencies. If we increase the distance between the first turn and the ground (a=0.2 m and 0.3 m), results are not improved.

Note that when you have a great distance from the ground, number of meander lines will be reduced and by the fact we loose advantages of meander lines.

3.1.1.6 Distance between horizontal branches

For a regular increment between meanders greater than the basic one (e1=0.2 m and 0.3 m), VSWR values stay weak. When the step is reduced (e1=0.05 m and 0.025 m), results are mediocre and by testing irregular step, meaning a variable distance between branches, we do not have good surprise.

To synthesize all these experiments, we can say that the generic antenna was not a so bad departure point because very few changes in the geometric factors managed to improve its VSWR, except maybe an height increasing or a reduction of wire diameter. Moreover, it is very difficult to analyze results because a parameter can improve high frequencies and worsen low ones. For the moment, any modification of parameters gave us satisfaction. The VSWR values are still too high.

3.1.1.7 Interdependence between geometrical parameters

The first step is to study each factor separatly. But, in reality there are interdependence between all these geometrical factors and we cannot change one of them without affecting the others. The next step is to study the interdependence between geometrical parameters. By changing two or more parameters at the same time, we hope to find a good configuration but this is more a question of chance.

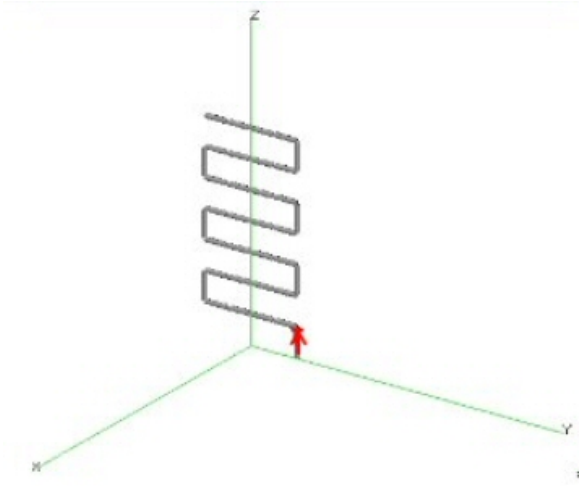

Figure 3.2: Example of an antenna comprising less turns than the generic antenna with a lateral feeding point

But we prefer go on searching factors capable of really increasing impedance for each frequency.

As shown on the example of figure 3.2, we tried to modify the generic antenna geometry combining different factors. We will not make here an exhaustive list of each test because there were no encouraging results. Sometimes, impedances are better but only on a small frequency scale. We can have few ohms more than resistance of generic antenna but that is all we can hope.

3.1.2 Further tests

As geometrical parameters are not satisfying, researches take another direction. We try to find other improvements, for example adding coils in the antenna. In fact, previous tests have shown that increasing the antenna size is beneficial to its VSWR. It is well known that we can increase antenna size by means of a coil. Different configurations have been imagined for different frequencies between 3 and 30 MHz. First, in the antenna model entered in NEC, 20 cm-long coils are placed on each horizontal part of the MLA. It improves impedances for high frequencies only. Then, coils are placed on the vertical branches reduced to 5 cm and every frequency seems to take advantage of this change. For low frequencies, it is very difficult to have a good resistance, it is always less than 1 ohm (the antenna size is too small to be efficient at these frequencies). Finally, to obtain significative results, coils to add should have inductances of a few henrys which are very difficult to do.

3.2 Optimization of the influencing parameters in order to combine compactness and performance

This geometrical study results in an obvious observation : the antenna length seems to be the most important geometric parameter influencing the MLA performance. The idea is to take it into account and to imagine a longer antenna in the same compact space. The MLA

concept is already based on the bend of the total length thanks to meanders. We have to advance and search in that direction.

3.2.1 Double MLA

According to articles about MLA, they consider it possible to mirror the antenna in order to increase the bandwidth. Japanese scientists (Noguchi et al. [12]) made researches about a meander line antenna consisting of two strips. The used frequencies were higher and then their antenna is small enough to be stripped. The first structure is fed at its bottom and the second structure is linked to the ground plane. These two parts are linked by a wire at their top. Because of the radiating resistance which can be stepped up, the reactances can be made to cancel each other in the balanced and unbalanced current modes.

Based on this principle, a double MLA has been imagined in order to have a longer structure and then better characteristics. The generic antenna has been imaged. We tested the distance between the two parts of the antenna (10, 20 and 50 cm), tried to set off the second structure and finally add a metallic wire between both. Finally, we obtained good results in terms of impedance for a double antenna, 50 cm-wide where antennas are linked at the top (the double MLA design is displayed on figure 3.3). Good results mean that all frequencies have their impedances significantly improved, more than by addition of coils in the structure. We managed to have acceptable resistances and reactances that could be easily compensated to obtain a perfect matching.

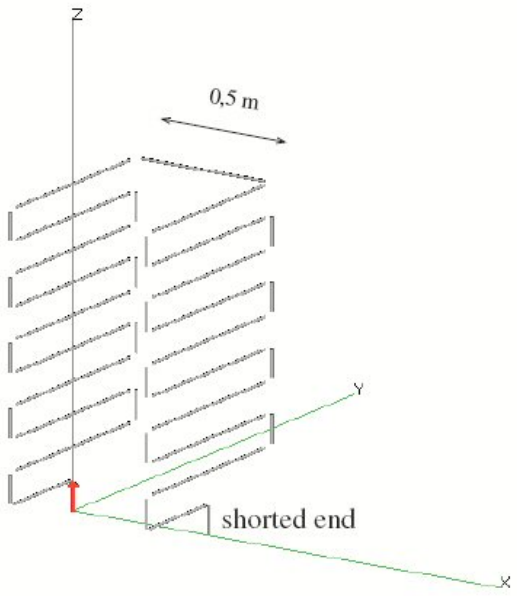

Figure 3.3: Design of the double MLA

Once a global shape is available, little adjustments in the geometry have been done in order to obtain favorable effects. The following design seems to be the best configuration :

- Total height = L = 1 m
- Straight shape

- Bottom width = e0 = 0.7 m
- Top width = e2 = 0.7 m
- Central excitation on the first antenna, second is linked to the ground plane
- Diameter of wires = d = 0.005 m
- Distance from the ground = a = 0.1 m
- Distance between horizontal branches = e1 = 0.1 m
- Distance between structures = 0.5 m
- Structures are linked with a wire

The VSWR of the double MLA has been simulated with NEC-2. Results are available on figure 3.4. On this figure, we notice that the resonant frequency is shifted compared to the resonant frequency of the generic antenna. It is now around 18 MHz instead of 17 MHz and this is a strange observation because the antenna is longer and should resonate at a lower frequency. A positive effect is the improvement of the value of the VSWR which is around 4.87 instead of 20. It is interesting to note the presence of a second frequency peak around 28 MHZ with a bad VSWR around 55.

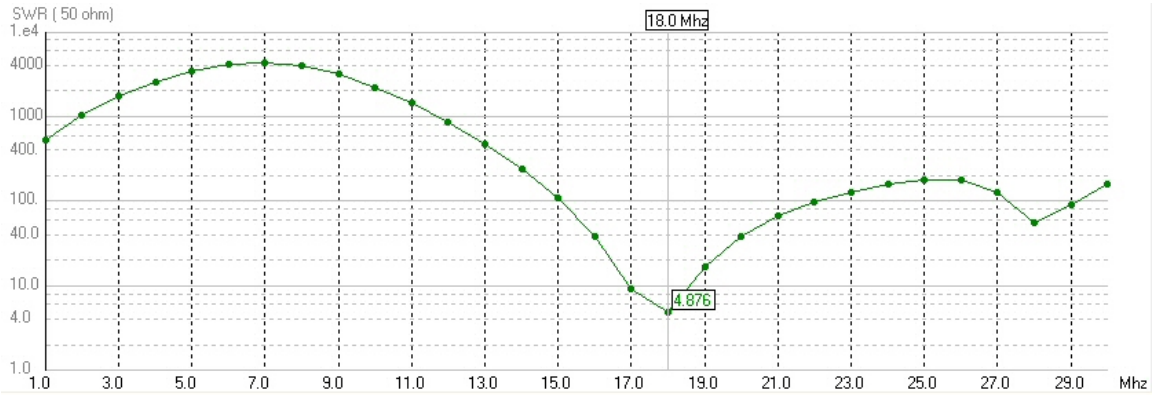

Figure 3.4: VSWR of the double MLA simulated with NEC-2

Even if a structure has been added to the simple generic antenna, the radiation pattern is still omnidirectional (see figures 3.5 and 3.6). Compared to the important wavelengths, the 50 cm extent is small and does not desequilibrate the radiation.

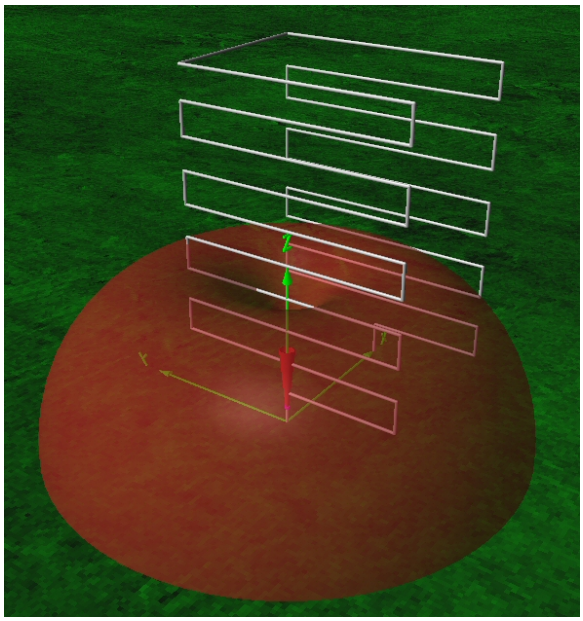

Figure 3.5: 3D viewer of the radiation pattern of the double MLA

The radiation pattern is still ressembling to the one of a monopole antenna, with a maximum gain of 5.22 dBi in the sea direction.

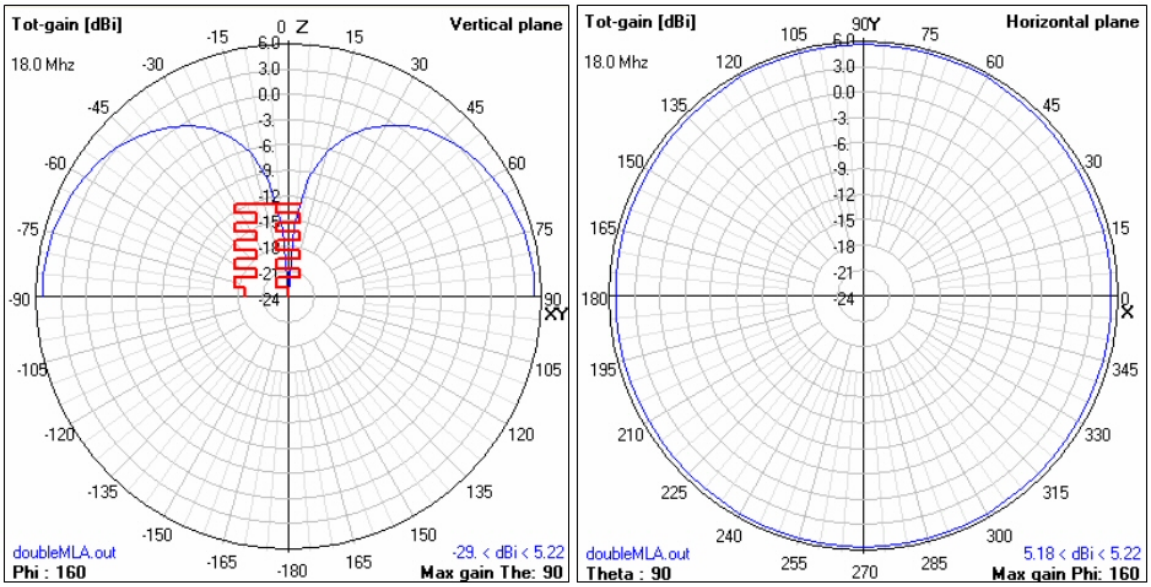

Figure 3.6: Radiation pattern of the double MLA at 18 MHZ

The doubling of the structure had a favorable effect on the VSWR value but not on the resonant frequency. Nevertheless, this antenna has characteristics satisfying enough to confront these simulations results to real measurements. And the best way to compare results is to manufacture a prototype of this model and to measure it.

The double MLA prototype has then been built by a French firm, specialized in antennas, that has many contracts with ONERA. It is made of copper wires. It has a ground plane made of aluminium and there is a proctecting Plexiglas radome all around the structure. A picture of the prototype is available on figure 3.7. In reality, the antenna has important dimensions compared to a human body but it is smaller than usual HF antennas so there is a plus. One part of the antenna is connected to a N-connector while the other is linked to the ground plane.

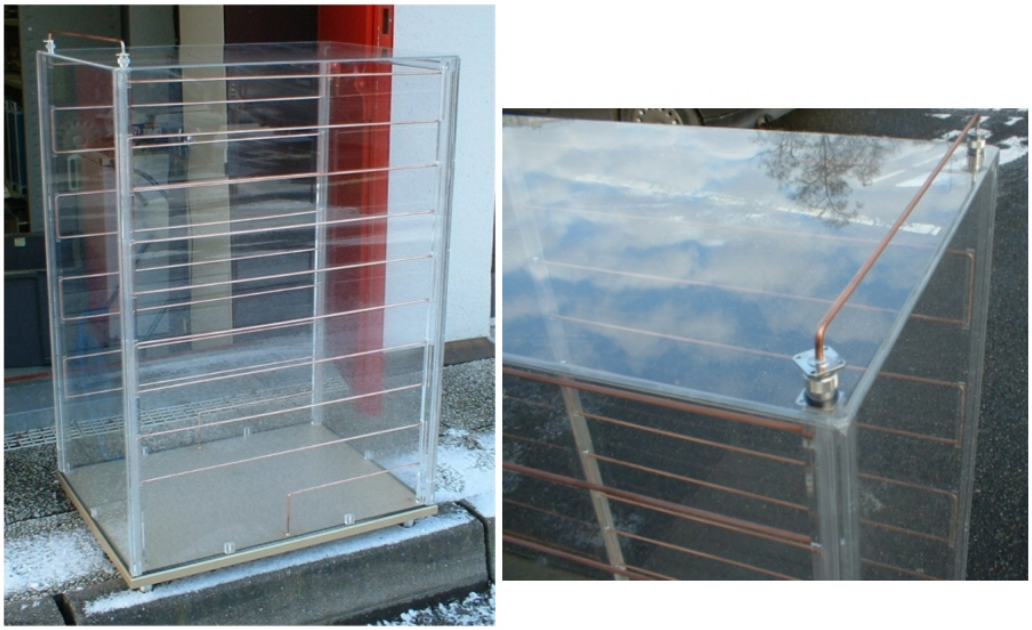

Figure 3.7: Prototype of the double MLA and view of the link at the top of the antenna

Small differences can exist between simulations and real measurements. In fact, they are due to small differences between the prototype and the modeled antenna. In fact, it is not exactly the same antenna. For example, the link at the top is a little bit surelevated as shown on the right part of figure 3.7 and it has been done to make tests with and without the link. Moreover, the aluminium ground has not been taken into account with NEC where we assume a perfect conducting ground plane. Finally, the Plexiglas radome can also influence the functioning of the antenna.

Tests have been made in open space on the HF skywave radar site (Nostradamus). This site is located at 100 km away from Paris. It has the advantage to be remote from cities, with any obstacles such as buildings or trees and there is an existing ground plane in copper that can be useful for MLA tests. The first step of these experiments was to check the VSWR of the double MLA. Thanks to a network analyzer correctly calibrated, we rapidly obtained measurements of the VSWR. To be close to simulation conditions, the existing ground plane of the antenna has been prolongated thanks to 8 very long copper wires (20 m long), all around the antenna and linked to the existing Nostradamus ground plane. Results are displayed on figure 3.8. We notice that a peak is visible between 18 and 20 MHz, with a VSWR value around 5. VSWR measurements are quite the same than

simulation results. It confirm that NEC can be used to model the compact HF antenna.

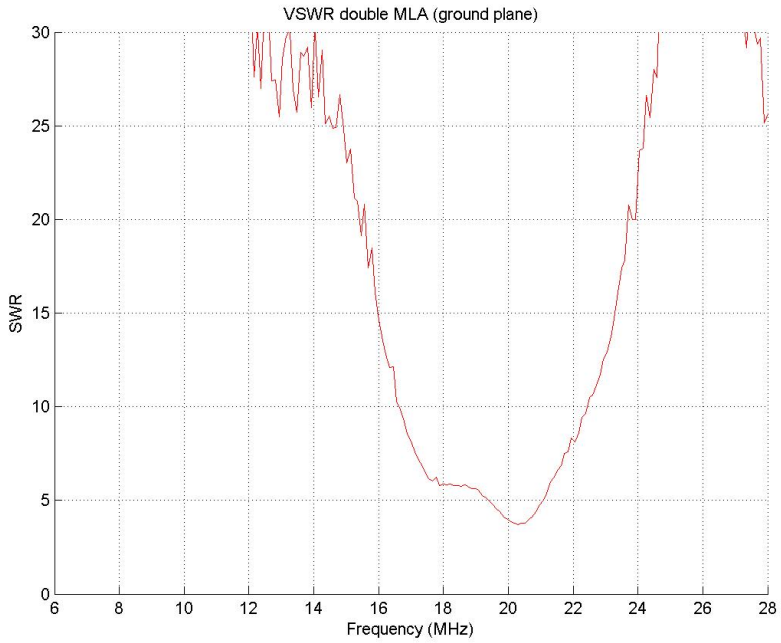

Figure 3.8: VSWR measured with the double MLA prototype

This antenna needs an external matching to have an impedance equals to 50 ohms. Moreover, compared to HFSWR specifications, this antenna should be modified for a functioning in the low frequencies of the HF band. It seems to be the most difficult specification to achieve.

To measure its radiation pattern, we should have used an helicopter to have the radiation level in every direction all around the antenna. It was impossible to put that in place for a question of cost. Nevertheless, by transmitting a signal with the MLA thanks to a synthetizer, it was possible to measure on a spectrum analyzer the received signal level received by a simple monopole antenna. By turning the antenna around its axis in different directions, we check that the level received by the receiving element was always the same, confirming the omnidirectional characteristic of the radiation pattern in the azimuthal plane.

3.2.2 Sinusoidal antenna

The double structure improved the VSWR value and it has been confirmed by real measurements with the prototype. The problem is that the compact antenna has to function at low frequencies around 5 MHz. The only way to shift the resonant frequency in a significative way is to increase significantly the total length of the antenna. That is why another way is studied in the following paragraph.

The new idea, studied with Singaporian engineers, is to add length on the horizontal

parts of the antenna by means of kind of zigzags. In fact, horizontal wires do not contribute so much to the radiating part of the impedance so we can increase their length without a lot of modifications on the radiation pattern. Vertical parts must stay straight and vertical to provide an efficient radiation and to maintain the vertical polarization. To avoid a bigger structure, the idea is add sinusoids on the horizontal branches only. The sinusoids will make the straight lines longer and if they have the same position on each branch, the compensation principle is still the same.

The aim is to have a longer electric length by replacing horizontal straight wires of the generic MLA by sinusoids to improve the lower frequency performances. The curvilinear abscissa of a sinusoid is given in terms of its amplitude A and its period L by the following elliptic integral :

$$s(t) = \int_0^t \sqrt{1 + A^2 \frac{4\pi^2}{L^2} cos^2(\frac{2u\pi}{L})} du \tag{3.1}$$

If the departure point is the generic MLA, amplitude of sinusoids should not be greater than 10 cm, which is the space between two horizontal branches. Moreover, if this amplitude is two important there will be disturbing coupling effects between branches because they will be too close from each other. A mean value, which is enough to have a significative length improvement avoiding coupling effects is chosen. The amplitude is then A =10 cm and the period also L =10 cm. Using these values in the equation 3.1, a sinusoidal line instead of a straight line, will have a length 60 % higher. This is a great value. Instead of 7.5 m for the total deployed length of the generic antenna, the sinusoidal MLA will measure about 12 m.

This antenna will be called sinusoidal MLA. Figure 3.9 represents the structure as modeled with NEC-2. Note that in reality, sinusoids are wished but this shape is too difficult to model in NEC-2 so triangles will be used to replace them. Moreover, a wire with a diameter of 5 mm is difficult to bend that is why we choose to simulate this antenna with thiner wires being 2 mm diameter.

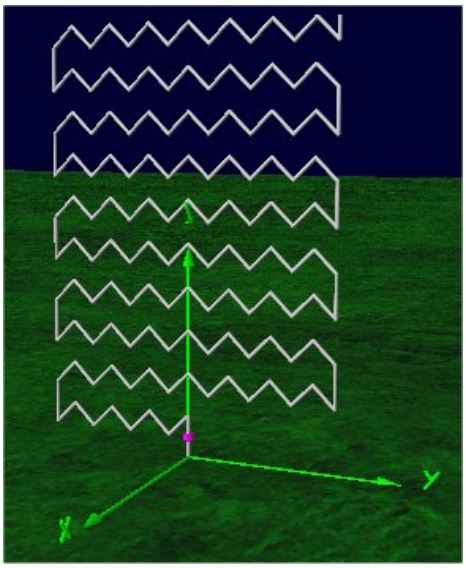

Figure 3.9: Model of the sinusoidal MLA simulated with NEC-2

Simulations results with NEC-2 are desapointing. In fact, the resonant frequency is well shifted to the lower frequencies as shown on figure 3.10, meaning a frequency of 14 MHz but the associated VSWR value is about 32.

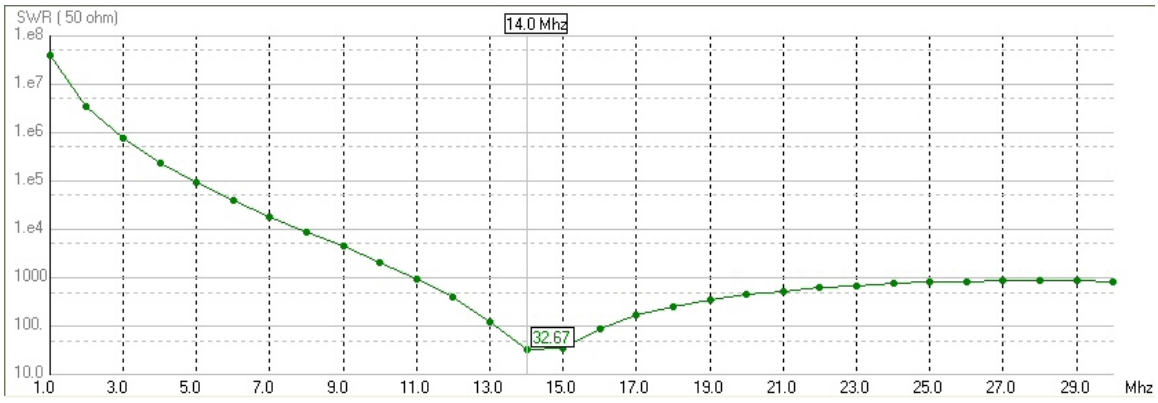

Figure 3.10: VSWR of the sinusoidal antenna simulated with NEC-2

If we simulate the radiation pattern of the sinusoidal antenna at 14 MHZ, we have usual patterns with a maximum gain of 4.61 dBi in the sea direction. Results are displayed on figures 3.11 and 3.12.

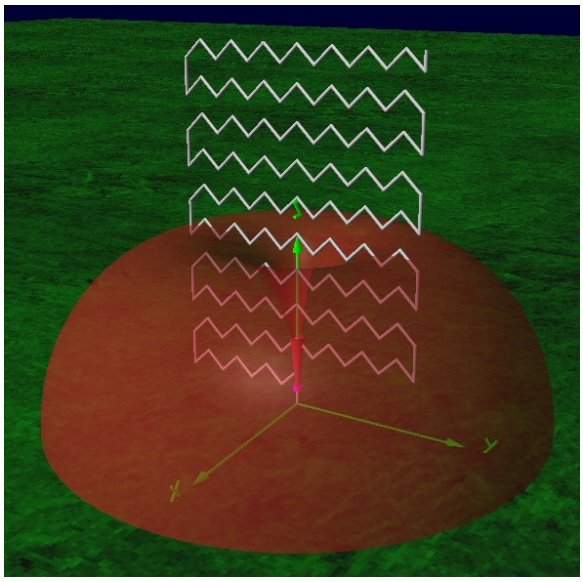

Figure 3.11: 3D viewer of the radiation pattern of the sinusoidal antenna

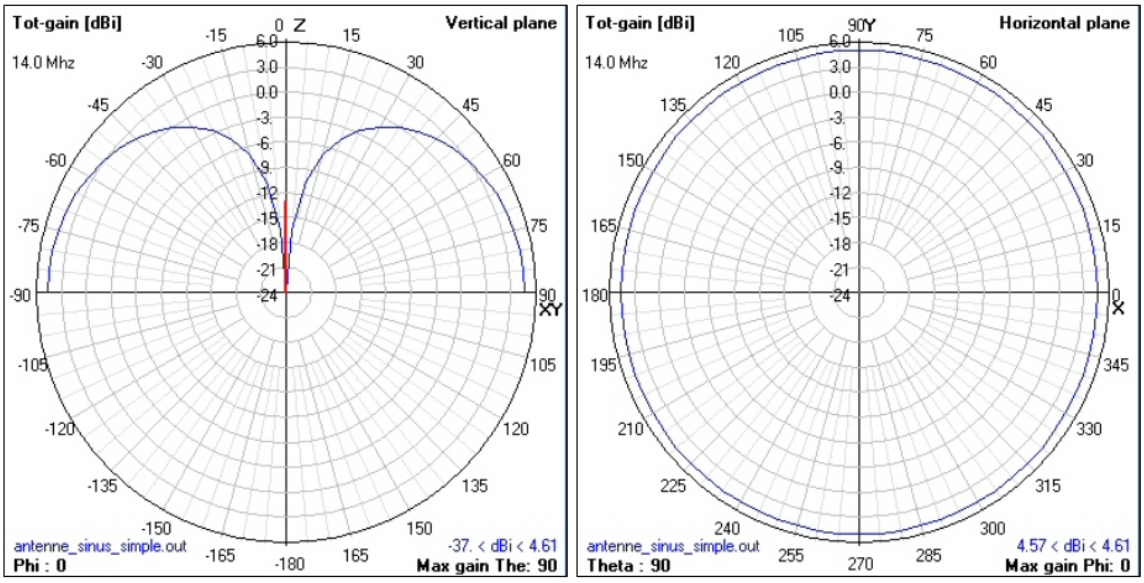

Figure 3.12: Radiation pattern of the sinusoidal antenna

For this antenna, a prototype has also been realized as presented on figure 3.13. This antenna has been made manually in ONERA. A copper wire has been bended on splinters mounted on a Plexiglas panel. The base of the antenna is made of aluminium and the copper wire has a diameter of 2 mm. It is connected to a N-connector.

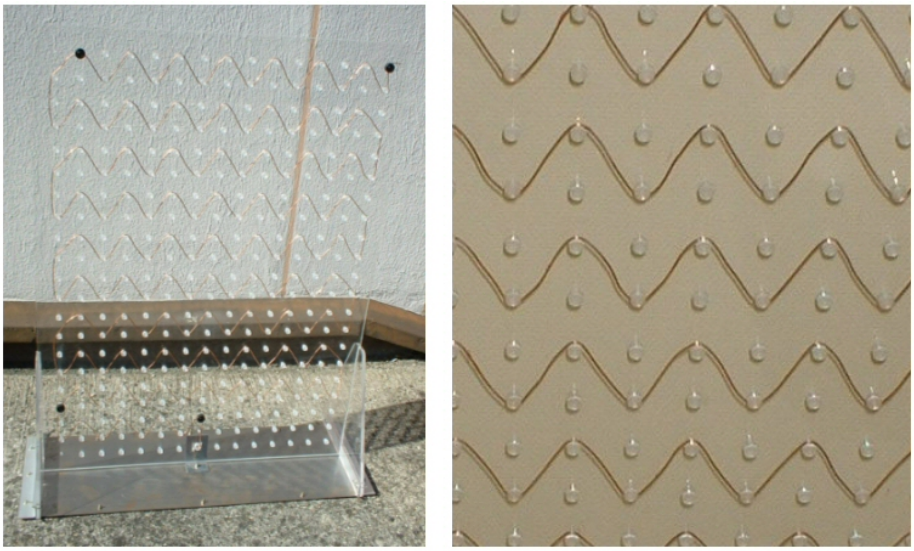

Figure 3.13: Prototype of sinusoidal antenna and zoom on the mounting of its sinusoids

Compared with the double prototype, we can considered that the length of the double structure has been bended to obtain the sinusoidal antenna (see figure 3.14).

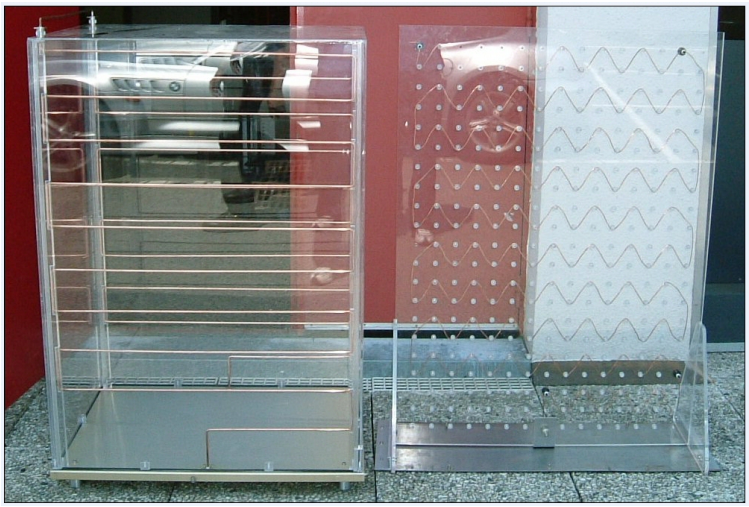

Figure 3.14: Comparison between double and sinusoidal MLA

New experiments have been made with this prototype, with an extended ground plane of 8 long copper cables, and there is a natural impedance matching around 13 MHz as shown on figure 3.15. The associated VSWR is about 1.9 and this is a really better VSWR than in NEC simulations where it was 32. This problem deserves to be raised because it deals with the limits of usual codes.

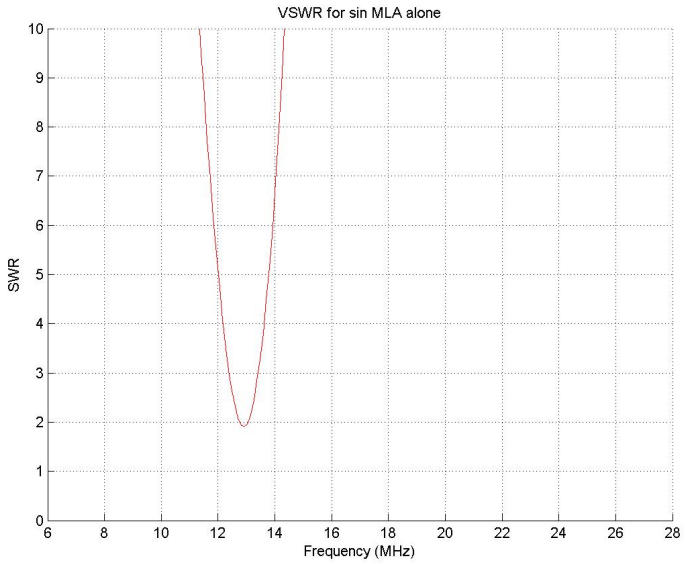

Figure 3.15: VSWR measured with the sinusoidal antenna

Thanks to measurement of sinusoidal antenna VSWR, the bandwidth at a precise frequency is available. In chapter 2, a recall about formulae refering to electrically small antennas have been presented (see 2.2.3). It is interesting to verify the measured bandwidth compared to theoretical predictions.

The sinusoidal antenna can be enlcosed in an imaginary sphere of radius a=1.059 m like the generic antenna. It is then possible to calculate its quality coefficient, at 13 MHz for example, thanks to the formula : $Q_a \approx \frac{1}{k^3 a^3} \approx 41$.

Refering to the equation 2.2, the maximum bandwidth Δf that can be reached with this quality coefficient for a given frequency f_c of 13 MHz and for a given VSWR S (for example 2).

$$\Delta f = \frac{(S-1)f_c}{Q_a\sqrt{S}} = 220.3\ kHz$$

If we refer to figure 3.15, we have a bandwidth about 200 kHz at 13 MHz for a VSWR of 2. Theoretical limitations of this antenna seem to be reached.

3.2.2.1 Computation limits of usual codes

On the one hand, simulation results and real measurements do not agree at all about the VSWR value while the resonant frequency is approximately exact (13 MHz in reality compared to 14 MHz in simulations). Various causes could explain these differences.

First, real sinusoids are represented in NEC-2 by triangles with 5 cm long segments. It means that the shape is not exactly the same. It would take too much time to divide sinusoids in tiny segments to adapt perfectly to the prototype design.

Moreover, the segment length is very small compared to the wavelength. In fact, NEC-2 needs to mesh wires in segments being approximately $\lambda/20$ long while size of the triangular segments (5 cm) is comprised between $\lambda/200$ and $\lambda/2,000$ depending on the HF frequency. The meshing condition required by NEC for an optimum computation is then not respected. It means that a few hypothesis are not available anymore.

Apart from the fact that the segment length of the sinusoidal antenna is too small, a supplementary problem concerns the low frequencies used in this study. The electromagnetic code NEC is not dedicated to low frequencies. In fact, in the electric field calculation with Integral Equation, there is an integration by parts to find electric field radiated. For that reason, a few terms appear. The original code does not take these terms into account but they become important at low frequencies and cannot be neglected.

Moreover, there can be a code precision trouble but NEC-2 has a double precision and that should be sufficient for such electromagnetic problems. It is well known that the code proposed on the Internet is restrainted, for example in the number of segments to take into account in the computation. Other restrictions of original code modifications may have been made in this version and it can affect the results.

This measurement is very interesting because on the one hand, simulation results and real measurements do not agree about the VSWR value but on the other hand, the real VSWR is really better than in simulation and the matching is almost achieved. So is it preferable to have concording results or an efficient prototype responding specifications? It is obvious that the second choice is the best.

Under those circumstances the question is : are other codes, such as commercial codes or efficient code from research centers, able to model correctly the compact antenna to be faithful with the reality? Whatever the answer, real measurements are encouraging but even with sinusoids, it is still difficult to obtain satisfactory performances around 5 MHz. The ideal solution seems to be a mix between the double MLA concept associated to the idea of sinusoidal wires.

3.2.2.2 Antenna matching

The VSWR of the different tested prototypes have sometimes good values but they are not perfectly matched at 1. That is why, to function in the best conditions, a matching is needed. In fact, an unmatched load as the prototype, on a lossless transmission line (considered short), generates a reflection. It is possible to cancel out this reflection by adding an equal and opposite reflection from a matching cell, at least over a narrow range of frequency close to the design point. One of the specifications for the design of a small HF antenna is to design a passive antenna. For that reason, the matching cell will be made with stubs because they are non active device.

A stub consists of a side section of line attached in shunt with (or in series with) the main transmission line, at a point to be determined. The length of the line, and the point of attachment, both need to be calculated from the load impedance. The stub needs

to be nearly lossless; it may be open circuit, or short circuit, or indeed terminated in a pure reactance. In our experiments, stubs will be coaxial cables used in shunt with the transmission line which is connected to the load. See examples of stubs on figure 3.16.

Figure 3.16: Stubs of different length prepared for matching experiment

In fact, a stub is a piece of cable which is short-terminated or open with a length l_{stub}. It is connected in parallel on the principal line at a distance d_{stub} from the load (see illustration of these parameters on figure 3.17). In transmitting configuration, this load will be the antenna impedance and in receiving configuration it will be the internal impedance of the measurement system.

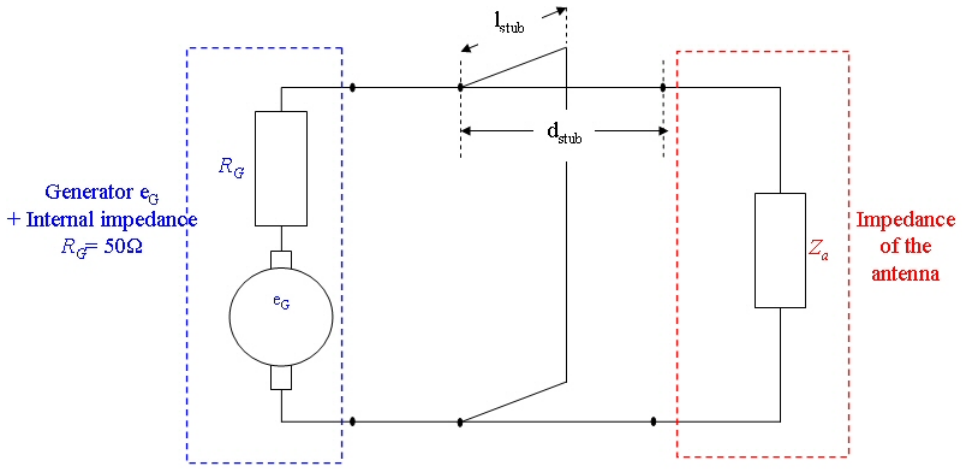

Figure 3.17: Illustration of the stub position and parameters used for the matching calculation

The matching with stub is only valid at the frequency for which the stub has been calculated : it is a narrowband matching device. This is a problem for the design of the compact HF antenna because the element needs to function at several frequencies with a bandwidth of a few kHz.

When they are used at microwave frequencies, stubs measure a few centimeters while in HF their length can rapidly reach a few meters.

In the case of a single stub matching, for the calculation of the parameters d_{stub} and l_{stub} of the stub system, three parameters have to be known :

1. The frequency f_0 (in MHz) where the matching is needed. Generally, this frequency will be chosen where the VSWR is not too high, meaning the matching will be possible and relatively easy.
2. The real part of the reflection coefficient Re measured at the frequency f_0
3. The imaginary part of the reflection coefficient Im measured at the frequency f_0

First, we need to calculate the impedance of the antenna :

$$Z_a = \frac{50 * (1 + Re + jIm)}{(1 - Re - jIm)}$$

The resistance R is the real part of that impedance and the reactance X is the imaginary part of that impedance.

The stub position d_{stub} is the distance d_{stub} that makes the resistance be equal to 50 ohms. It is given by the following formula :

$$d_{stub} = mod(\frac{\frac{\pi + atan(X.Z_c + \sqrt{R.Z_c.(X^2 + (R - Z_c)^2)}}{Z_c.(R - Z_c)}}{K}, \frac{\pi}{K})$$

where Z_c is the matching impedance (50 ohms).

The length l_{stub} makes the reactance be zero. It can be calculated by this formula :

$$l_{stub} = mod(\frac{\pi + atan(\frac{1}{Z_c.imag(\frac{Z_c + j(R+jX).tan(K.d_{stub})}{Z_c(R+jX+jZ_c tan(K.d_{stub}))})})}{K}, \frac{\pi}{K})$$

with :

$$K = \frac{2\pi\sqrt{\epsilon_r} f_0}{300}$$

where $\epsilon_r \approx 2.38$ is the coaxial cable relative permittivity.

To verify the efficiency of the single stub matching, we made experiments with the sinusoidal antenna. It has a VSWR about 2 at 13 MHz but we would like to improve it to have a perfect matching at this frequency. With a network analyzer, we measure real part and imaginary part of its reflection coefficient. Using the previous formulae, we find that a stub with a length l_{stub}=2.50 m is needed at a distance d_{stub}=4.62 m from the antenna to obtain a perfect matching. A measurement of the sinusoidal antenna VSWR with its stub is displayed on figure 3.18. On this figure, the measured VSWR is well equal to 1 at

13 MHz, the single stub matching is efficient. Moreover, we notice that another resonance appears at lower frequencies around 7 MHz. It has to be improved but this can be helpful to obtain several operational bandwidth with a sufficient bandwidth.

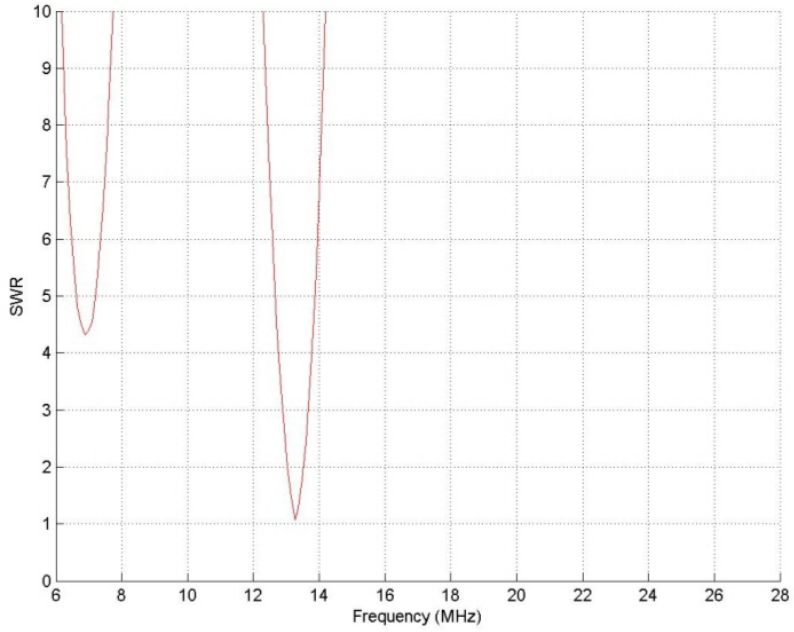

Figure 3.18: VSWR of the sinusoidal antenna with one stub

Most of the time, stub length and position calculated with the previous formulae are not exactly the ones needed to have a perfect matching. In fact, in practise, these lengths have to be adjusted by trial and error. Moreover, we do not have very small coaxial cables to respect exactly the calculated dimensions. In HF band, due to decametric wavemengths, a difference on the stub length or position of a few centimeters is not very influential.

Thanks to Patrick Delavictoire, who took part in that thesis project in 2003 through a training period, other ways to improve matching for multiband functioning have been explored. One of the interesting topics of his study was the use of a double stub matching. In fact, a first stub is used to obtain another reflection coefficient at a point of the transmission line and then a second stub matches this new obtained impedance to 50 ohms. The principle is exactly the same than in the previous paragraph in two steps. The two stubs calculation will not be detailed here. Experiments have been made, as shown on figure 3.19 to verify this new matching possibility. Results were quite encouraging (see figure 3.20).

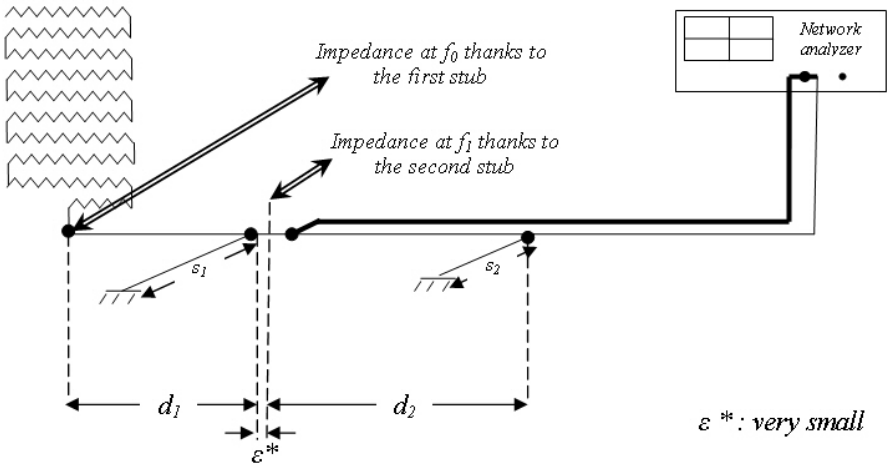

Figure 3.19: Principle of matching with two stubs

On this figure 3.20, we notice a real improvement of the VSWR value of the sinusoidal antenna at various frequencies. There are 4 matched frequencies at 7.5 MHz, 13 MHz, 21.5 MHz and 26.5 MHz instead of 13 MHz only with one stub. They have a narrow bandwidth, meaning about 300 or 400 kHz (for a VSWR=2). The stubs used measure ($d_{stub}1$=4.66 m; $l_{stub}1$=1.95 m) and ($d_{stub}2$=4.20 m; $l_{stub}2$=0.40 m). These dimensions have been found empirically. In fact, it was quite difficult to predict the final matched frequencies using two stubs because some of them appear while other wanted frequencies do not. This method is not totally finalized but there are good experimental results.

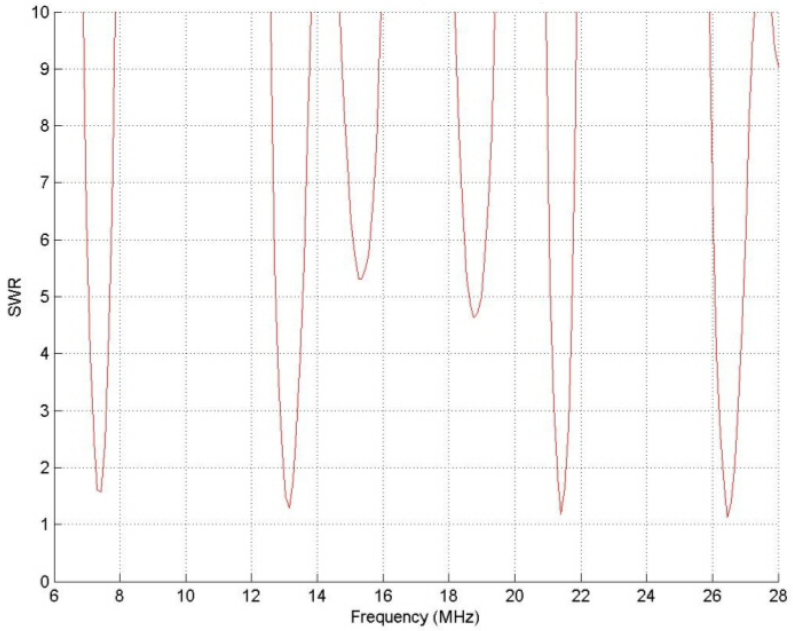

Figure 3.20: VSWR of the sinusoidal antenna with 2 stubs

This sinusoidal antenna has quite good characteristics so far, mainly when used with stubs, but due to unfortunate experiments (breaking of the prototype because of strong wind), we wonder if this design on one panel can resist to mechanical constraints. This point has to be improved.

3.3 Simulation and realization of final antenna prototype fitting specifications

3.3.1 Mix between double MLA and sinusoids

In this part, the idea is to combine the concept of double structure with the one of sinusoids in order to a compact antenna and better respond specifications while having doubts about simulation results proposed by NEC-2.

3.3.1.1 Compact antenna for low frequencies

To benefit from advantages of a double structure and a sinusoidal antenna, a design mixing both ideas is imagined as shown on figure 3.21. The problem is that the antenna length has to be really increased to shift resonant frequencies in the lower part of the HF band. That is why the new antenna is a little bit higher than 1 m and wider than 70 cm. It total dimensions are then : 1.35 x 0.85 x 0.50 m. All other geometrical parameters are the same than sinusoidal antenna in terms of wire diameter, dimensions or space between horizontal branches, the only difference is that the structure is doubled and is not connected to the ground plane anymore. The total deployed length of this antenna is about 40 m, which is comparable to the used decametric wavelengths.

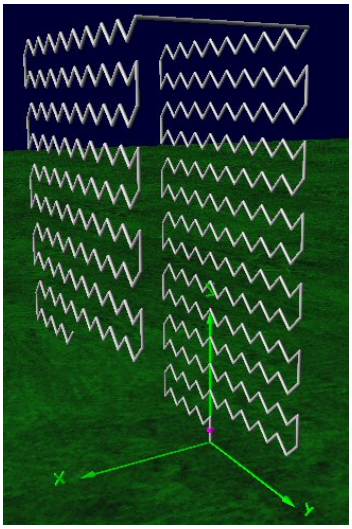

Figure 3.21: Design of a mix antenna made of a double structure and sinusoids simulated with NEC-2

According to NEC-2, as displayed on figure 3.22, this antenna seems to have four resonant frequencies in the HF band : 6 MHz, 14 MHz, 23 MHz and 28 MHz. The associated

VSWR are about 10, wich is not a very good result but in reality, these values can be better as in the case of the sinusoidal antenna. Limits of calculation of NEC-2 may cause errors on the VSWR value. The resonant frequency around 6 MHz is the most interesting because of the possibility to respond specifications. Low and high frequencies of the HF band could be reached with this antenna.

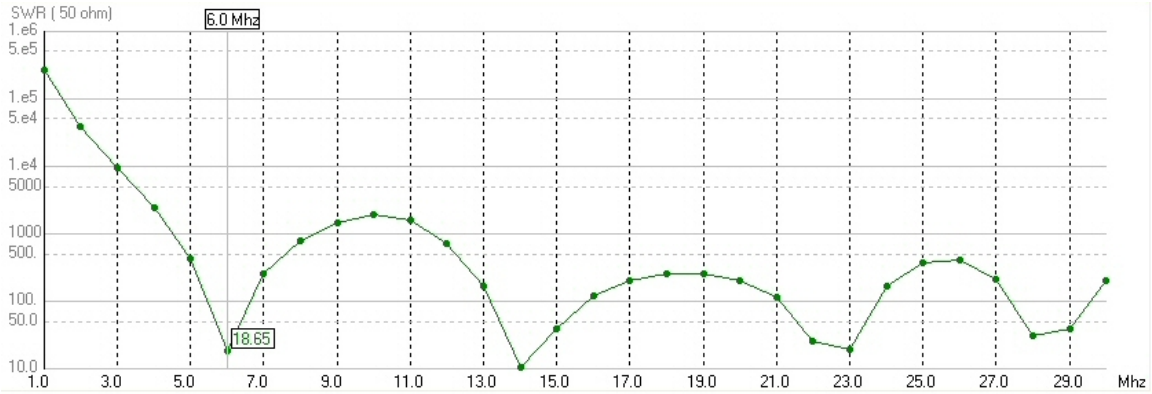

Figure 3.22: VSWR and reflection coefficient of the mix design simulated by NEC-2

To verify this result, a prototype has been made manually with Plexiglas pannels, copper wires and aluminium ground plane. On the following picture 3.23, we can see height difference between the biconical antenna of the HF skywave radar Nostradamus (height : 8 m) and the new prototype (height : 1.35 m). This picture is very impressive because even if the prototype seems to be imposing, the compactness gain compared to this HF antenna is very flagrant. The size is 6 times smaller than the biconical antenna.

Figure 3.23: Comparison between the size of the compact HF antenna for low frequencies and a biconical antenna

As expected, the measured VSWR are really better than those predicted by simulations results and the resonant frequencies are close to the one expected. Results of measurements

on figure 3.24 show that 5 resonant frequencies can be found : 5 MHz, 12.5 MHz, 18 MHz, 23.5 MHz and 28 MHz. At 5 MHz, the associated VSWR is about 1.5 and at 12.5 MHz, it is about 1. Others VSWR are all above 2. These results are obtained naturally whitout any matching cell.

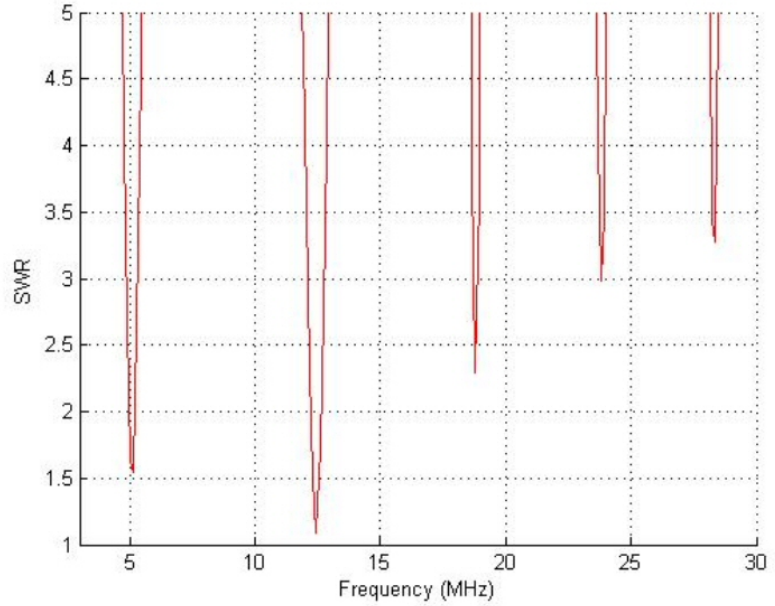

Figure 3.24: Measured VSWR of the mix antenna prototype

These results are satisfying but the prototype dimensions are too large for HFSWR users. In spite of the obvious compactness gain, this kind of design cannot be easily shipboard and it is too large even for coastal radars. Efforts have to gather on the size reduction.

3.3.1.2 Final design proposed : small mix structure

A dilemna is posed : on the one hand, the previous prototype has good characteristics but its size is too large and on the other hand, the usual code NEC-2 has problems to simulate this kind of antenna. Nevertheles, to reduce antenna size, we need efficient simulations tools, meaning valid at low frequencies and where small segments compared to wavelength can be correctly simulated. At this stage of the thesis, no other codes were available. The decision was then to conceive a prototype smaller than the previous one and to optimize it in practice.

A restricting factor is antenna height. An ideal height for the HF compact antenna would be 50 cm high for transport, furtivity and discretion reasons. That is why the final design proposed in this study is a mix structure between double and sinusoidal antenna, being only 50 cm high as proposed on figure 3.25. The compactness is maximum compared to usual HF antennas.

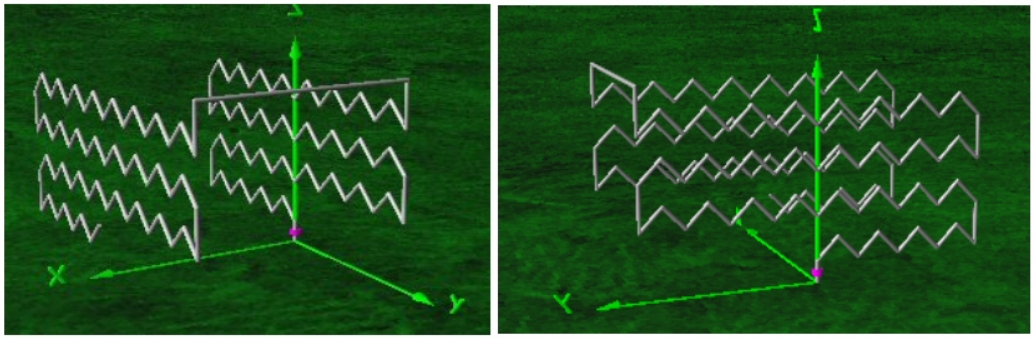

Figure 3.25: Design of the final version of the compact HF antenna

The antenna has been manufactured by a French firm called DAPA, located in France, near ONERA. This antenna has dimensions being 0.50 x 0.85 x 0.5 m and presents as a box (see figure 3.26). You can find precise design of the prototype in the annexe 5.6.4 at the end of the document.

Figure 3.26: Prototype of the final compact HF antenna

The wires are made of copper and they are encrusted in a panel and recovered by a kind of resin which is fiberglass. This material is specially dedicated to marine use so the prototype can easily be used near sea. Wires are sandwiched between two mediums and then they cannot move during transport. The fiberglass panel can be removed to see the understructure. Pictures of all these details are shown on figure 3.27. The radome material will surely have effect on the antenna radiating but not so much. It may only shift the resonant frequencies but not totally misrepresent the antenna funtioning.

The box is painted in white but we can imagine other colors such as dark green being more camouflage painting.

Moreover, the antenna is now really small and very solid. It can easily resist to mechanical or wind constraints.

The ground plane of the box is made of aluminium and there are practical handles to carry the box. These handles are practical for antenna tests but they may be not necessary for an operational antenna that should not be handled or moved very often.

The connector is either a type 7/16, either a type N to connect easily the antenna to usual cables.

The interior of the antenna is totally empty and we can envisage to stow a matching cell in this free space.

Figure 3.27: Pictures of the prototype and details of the final version of compact HF antenna

This antenna has been simulated with NEC-2 and also with a code called Elsem 3D, used in ONERA. Vincent Gobin from ONERA in Toulouse kindly help us to simulate this final design with this powerful code but results confirm those of NEC-2 as shown on figure 3.28. Both codes find a resonant frequency around 13 or 14 MHz but with an astronomical VSWR (58 for NEC-2 and 100 for Elsem 3D). On this figure, the VSWR proposed by Elsem 3D is about 100 at 14.5 MHz, while NEC-2 proposes a VSWR about 59 at 13 MHz. These are really bad predictions that have to be confronted to reality.

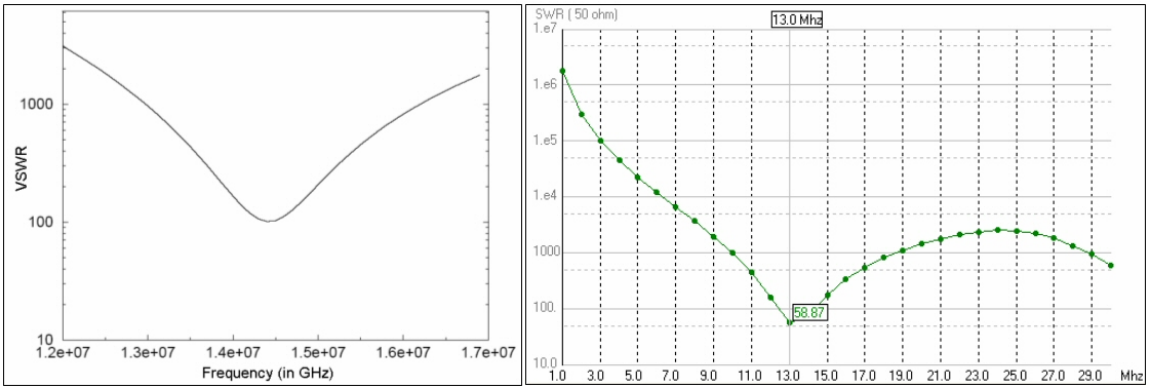

Figure 3.28: VSWR simulated with Elsem 3D (ONERA code) on the left and VSWR simulated with NEC-2 on the right

As expected, in reality, the small prototype has better characteristics than in simulations as displayed on figure 3.29 where the VSWR value is 2 at 10 MHz or 1.5 at 29 MHz. These are natural VSWR, no matching cell has been used for this measurement.

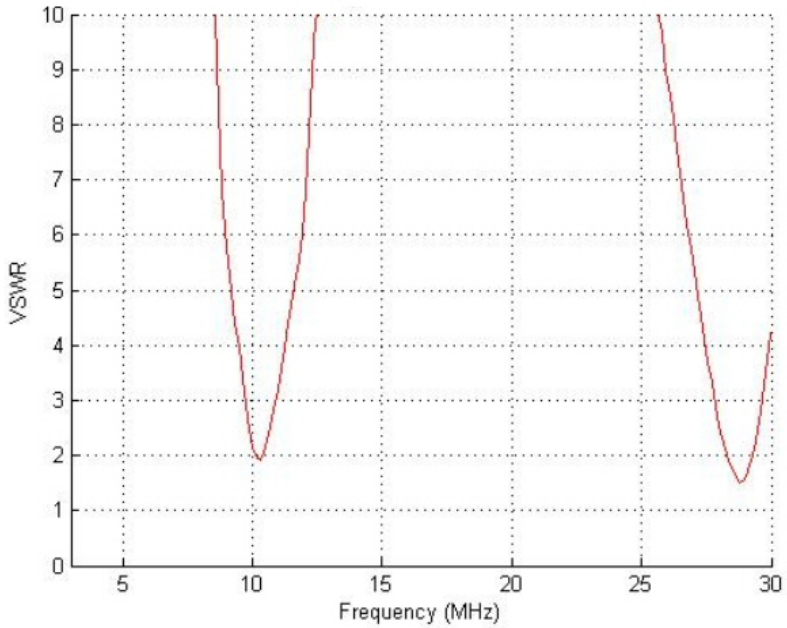

Figure 3.29: Measured VSWR of the prototype of final compact HF antenna

It seems evident that a very small antenna will not have natural impedance matching at low frequencies. The only way to able its functioning in the lower part of the HF band is to use stubs, hoping that matching will be possible.

3.3.2 Validation of the prototype in a classical radar configuration

The objective of the antenna to design is to be used as a receiving antenna in a HF Surface Wave Radar system. If the antenna can be used for transmitting also, it will be a supplementary quality and we will test this possibility also. To valid the final design, the prototype has to be tested in a radar configuration to verify its ability to detect targets. What we call a classical radar configuration is the detection of targets in a direct view. Moreover these tests are the opportunity of comparing the small prototype to a large HF antenna. Do the size reduction have negative effects on the antenna performance required for HFSWR applications?

The first experiment conducted with the final prototype was a simple test of its "radar performance". The ideal would have been experiments on a piece of land near sea in order to test surface wave propagation. But a coastal terrain is very difficult to find that is why the first series of tests have been planed in Dreux in a first time. The Nostradamus site is located not far away from Paris, in countryside where radar tests are often performed when needed. This site has the advantage of being distant from housing estate and the HF spectrum is not so congested as it is in Paris. This place being far away from sea, radar tests will occur with planes that fly directly in the beam of the receiving antennas.

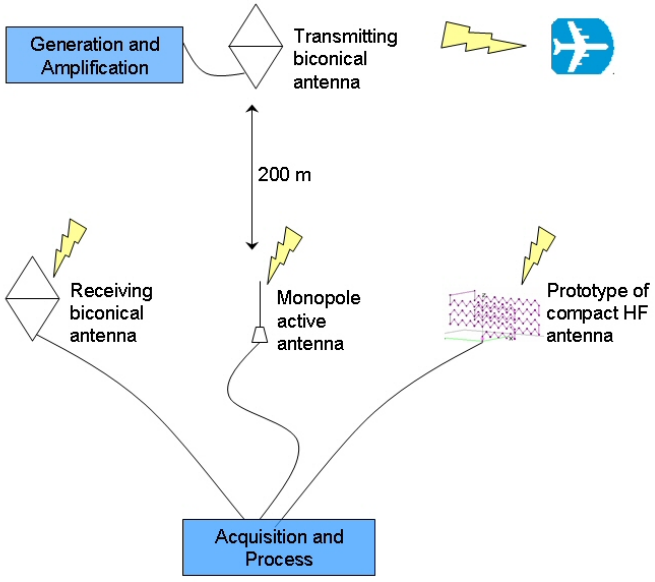

Figure 3.30: Simple illustration of the experiment in Dreux

In fact, the aim of this first experiment is to valid the functioning of the final compact HF antenna prototype in a radar system and to compare its performance with those of usual large HF antennas. In Dreux, there is already a large part of the equipment needed for trials. The previous figure 3.30 illustrates the experiment. In fact, a personal computer has been installed for transmitting. This PC generates a waveform thanks to a digital generation card and transfers it to an amplifier and then to a transmitting biconical antenna. This antenna belongs to the Nostradamus radar, it is 8 m high and can function between 6 and

28 MHz for transmitting and receiving.

Potential targets as planes are illuminated by the HF wave transmitted by the transmitting biconical antenna and they backscatter a portion of this incident wave to the receiving system of the radar. In the experiment, targets signals are received by another large biconical antenna, a monopole active antenna (1 m high) and by the compact HF antenna prototype. About 200 meters separate transmitting area from receiving area. Signals received by the three receiving elements are digitized and processed simultaneously in order to have an exploitable comparison between signals received at the same moment.

First, note that the compact HF antenna has been matched with a stub to obtain three interesting resonant frequencies that are authorized on the Nostradamus site. These frequencies are 9.76 MHz, 14.80 MHz and finally 19.60 MHz. At 14.80 MHz, the antenna is almost perfectly matched at 50 Ohms that is why interesting results in this document will be presented at this optimum frequency.

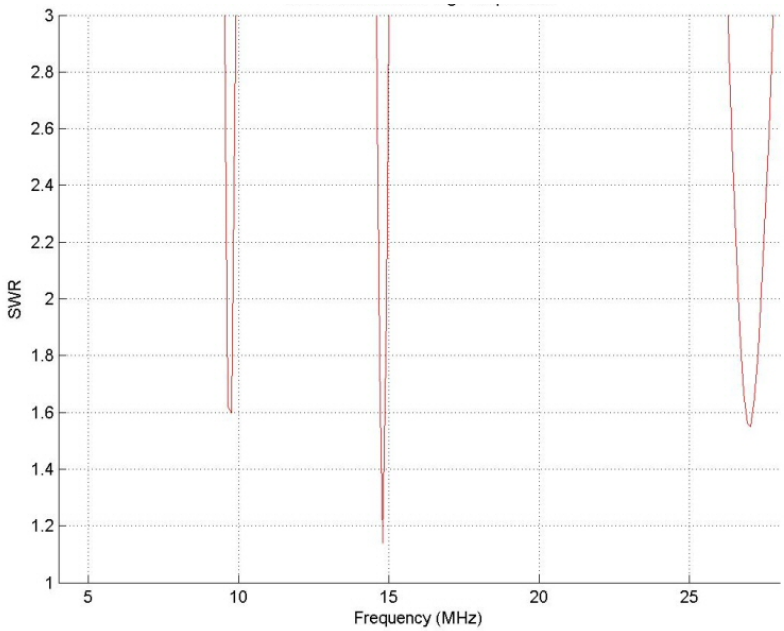

Figure 3.31: VSWR of the final compact HF antenna prototype with a stub

It is very interesting to compare the small prototype to a biconical antenna because it is 16 times smaller as shown on figure 3.32. Moreover, a biconical antenna is very bulky because it is too large to be self-supporting and then the prototype seems to be really tiny compared to this giant.

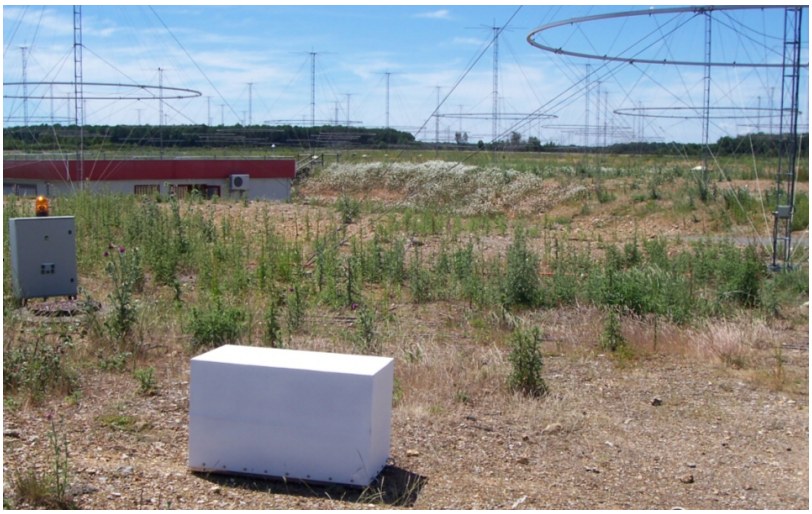

Figure 3.32: Comparison between a biconical antenna and the final compact HF antenna prototype

In radar, what is important to compare is the SNR (signal to noise ratio) of detected targets measured by each antenna. The three following figures (from 3.33 to 3.35) propose a Doppler range image obtained after radar processing for each antenna at the frequency 14.80 MHz. Data have been processed the same manner on the three channels and then observed targets are physically the same on the three images.

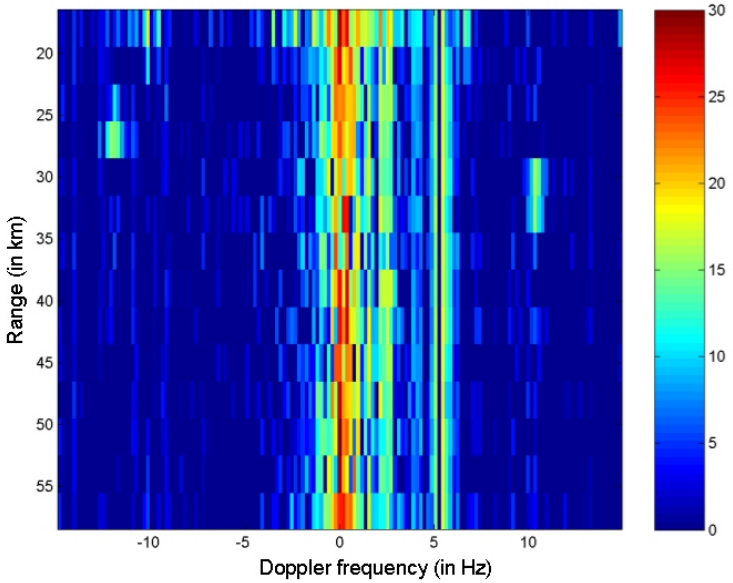

Figure 3.33: SNR level (in dB) detected by the biconical antenna at 14.80 MHz

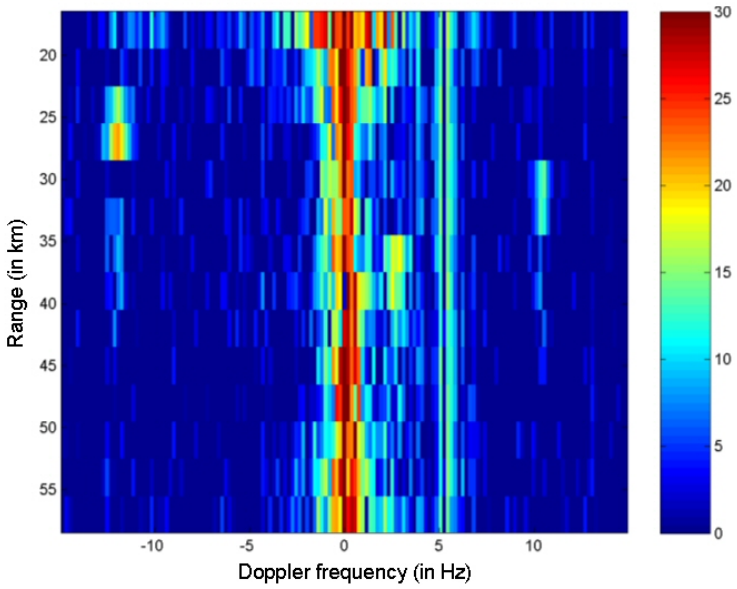

Figure 3.34: SNR level (in dB) detected by the prototype of compact HF antenna at 14.80 MHz

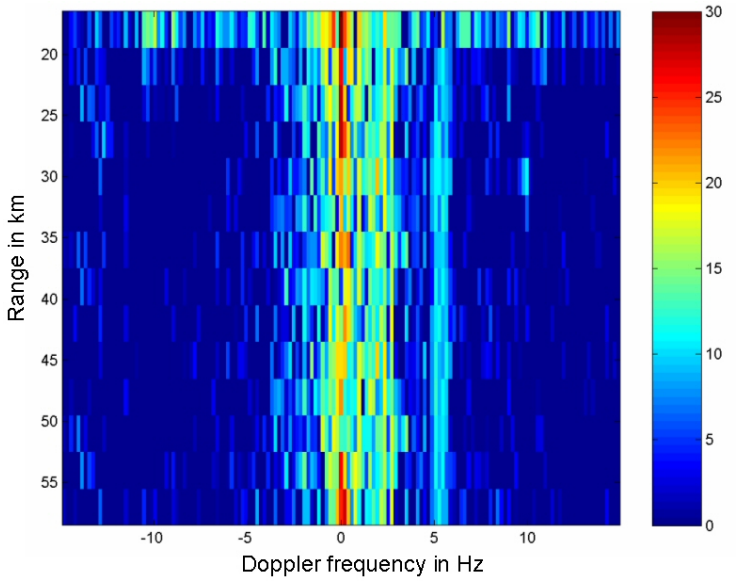

Figure 3.35: SNR level (in dB) detected by the monopole active antenna at 14.80 MHz

By comparison between these Doppler range images, we note that the compact HF prototype is as efficient as the biconical antenna (or even more) because they have a competitive performance in terms of SNR on the observed objects. Differences between SNR are not the same between antennas for each target as shown on the resulting figures. It may be due to the radiation patterns of the antennas that are not exactly the same. The target on the right is more visible with the biconical antenna and less with compact prototype or monopole antenna. While the target on the left is really well visible on the central

image corresponding to the compact HF antenna and less visible or totally absent on other images. Mean values can be calculated for different targets and the following table 3.1 presents comparison between average SNR for 3 frequencies and 3 antennas.

Frequency (MHz)	Biconical antenna	Compact antenna	Active monopole
9.76	20	26	22
14.80	18	16	17
19.60	17	22	20

Table 3.1: Average Signal to Noise Ratio (in dB) on detected targets

The compact HF prototype has a SNR as good as the one of a large antenna such as biconical antenna and compared to an active antenna. This can be explained by the fact that the prototype receives less signal due to its small size but it receives also less noise and then SNR are equivalent. This can be confirmed by the measurement of noise level received by each antenna. The table 3.2 presents the average noise level measured by the three antennas at 3 frequencies. The biconical antenna measures more noise level than others because it is an efficient and large antenna. The monopole antenna uses active device to compensate its small size and then it is often a very noisy antenna. The compact HF antenna is small and passive so it cannot detect very high signals or noise levels that is why it measures less noise level than others.

Frequency (MHz)	Biconical antenna	Compact antenna	Active monopole
9.76	-112	-128	-123
14.80	-116	-136	-126
19.60	-121	-142	-130

Table 3.2: Average noise level measured (in dBm, ref : 1 mW)

It would be interesting to know the gain of the prototype to envisage its use for transmitting. It is difficult to evaluate the absolute gain of the prototype but it is possible to find its gain relative to the one of the biconical antenna for example. In fact, by measuring a signal or noise level (voltage measurement), the gain ratio between antennas can be deduced. To find relationship between gain and noise level measured by the antennas, the following demonstration can be useful.

$$|Vs| = \left| \frac{E_{inc}}{AF} \right|$$

AF : antenna factor, E_{inc} : incident electric field, Vs : voltage measured by the antenna.

The antenna factor can be expressed as :

$$AF = \frac{\eta k}{4\pi} \frac{|Z_0 + Z_a|}{Z_0} \frac{1}{|F_r|}$$

with : Z_0= 50 Ohms and Z_a : impedance of the antenna ($Z_a = R_a + j.X_a$).

$$F_r = \sqrt{30.R_a.G}$$

where G is the gain of the antenna.

Then the measured voltage can be written :

$$|Vs| = |E_{inc}| \frac{4}{\eta k} \sqrt{30.R_a.G} \frac{Z_0}{|Z_0 + Z_a|}$$

If two antennas are perfectly matched at 50 Ohms, we can compare them and directly obtain the gain ratio :

$$\left| \frac{Vs_{ant1}}{Vs_{ant2}} \right| = \frac{G1}{G2}$$

If the antennas are not exactly matched at 50 Ohms, as in this example, we have to take into account their real impedance before comparing their gains :

$$\left| \frac{Vs_{ant1}}{Vs_{ant2}} \right| = \frac{\frac{\sqrt{R_{a\ ant1}.G1}}{|Z_0+Z_{a\ ant1}|}}{\frac{\sqrt{R_{a\ ant2}.G2}}{|Z_0+Z_{a\ ant2}|}}$$

As the impedance is different for each frequency, we will have a different gain ratio for each frequency.

Thanks to the measured noise levels and after calculation of the gain ratio, we assume that the compact HF antenna prototype has a gain which is about 20 dB less than a large biconical antenna and about 10 dB less than an active monopole. Assuming than a biconical antenna has an absolute gain of a few dB, it means that the prototype has a really low gain and then it can be used without problems for receiving but its size is too penalizing to be competitive for transmitting.

3.3.3 Validation of the prototype in a surface wave radar configuration

To validate completely the functioning of the compact HF antenna in receiving configuration, it is necessary to make experiments near sea. Thanks to the collaboration DSTA and NTU Radar Laboratory of Singapore, we had the opportunity of testing the antenna on near sea and on a ship. These tests are confidential that is why many information have to be kept secret and then many results or pictures cannot be presented in this report.

3.3.3.1 Coastal configuration

If compact HF antennas are settled on coasts, their performance have to be studied to see influence of sea near the antennas. The most important part of a HFSWR is to well propagate surface waves. Once the wave is transmitted, the antenna has to radiate at grazing angles to excite correctly the surface waves.

We made tests with the compact prototype in receiving configuration near sea but the amplifier used for the experiment broke down. Normally, it could amplify up to 2 kW but during experiments, it supplied only a few watts and then the range achieved by signals were very short and no target was detected. The amplifier was then unavailable during all the experiments so comparison between SNR received with the compact HF antenna prototype and with an active antenna was then impossible. We only noticed sea echoes detected by the two antennas meaning that surface wave propagation is quite good.

The only important conclusion that we have to remember about these series of experiments is the vulnerability of a demonstrator equipment. The repair of the amplifier was quite long and then no conclusions could have been established or verified during this mission. Nevertheless, we made many measurements of the VSWR of the prototype and many conclusions are interesting to present here. In fact, to have a good and reproducible VSWR measurement, it is advisable to screen cables going to the antenna otherwise they can be affected by the antenna radiating and disturb the measurement. Typically, cables linked to the antenna should be hidden under the ground plane or settled in metallic tubes to receive the less radiating possible from the antenna as shown on figure 3.36. Moreover, it is important to avoid the creation of a "loop" between the supply of the network analyzer and the measurement cable, otherwise it can also disturb measurements. Respecting these two important advice and avoiding moving cables, the VSWR measurement is reliable and reproducible.

Figure 3.36: Final prototype with screened cables tested near sea in coastal configuration

3.3.3.2 Shipboard configuration

One of the principal interest of the compact HF antenna is to allow shipboard configuration that is why it is very important to know effects of a metallic structure on the radiation of the antenna and also impact of sea surface all around the antenna.

Comparisons between compact HF antenna prototype and monopole active antenna on a ship have been made by Singaporian teams but their results are confidential and then

cannot be presented in this report. The only thing we can say is that their results confirm measurements made on the Nostradamus site : the prototype has performance competitive with active HF antennas in terms of SNR but its gain is about 10 dB inferior. In this series of tests, the amplifier was repaired and then the antennas received sea and target echoes up to great distances. On the resulting Doppler range images, sea echoes were very visible.

After many design tests, a compact antenna corresponding to specifications has been modeled and a prototype has been realized to validate this final design. Its performance are quite the same than those of usual bulky HF antennas but its size is really reduced. The compacity gain can easily reach a factor 20. Tests with the final prototype in real radar conditions validate its radar performance in receiving configuration. Signals received by this compact element are similar to signals received by usual antennas. The problem of these signals is that they are affected by sea echoes and it causes detection problems. Influence of external interferences such as sea surface scattering should be reduced to obtain clean radar signals and to improve detection capabilities of HFSWR. In order to understand effects of sea backscattering on radar signals and to know its characteristics for any event, an algorithm that simulates sea echoes will be created in the following chapter.

Chapter 4

Creation of a simulated sea echoes database

Contents

In the reality, real echoes coming from HF Surface Wave Radars are still rare because these kind of radars are not numerous. The objective of this part is to obtain simulated sea echoes for any event (frequency, wind force, current velocity, etc). Indeed, the aim is to

create a complete database of sea echoes, based on the models of the literature. The first step is to study characteristics of sea echoes and better understand interactions between HF waves and sea surface and then to implement an algorithm for the automatic generation of simulated data.

4.1 Characteristics of sea echoes

4.1.1 Interaction between HF wave and sea surface : Bragg scattering

4.1.1.1 First order Bragg lines

The illumination of the sea surface by an HF radar reveals a particular phenomenon that it is necessary to understand to better exploit the data given by the radar system : this phenomenon is called the Bragg scattering.

The physical phenomenon of the coherent scattering of decametric waves on the sea surface was studied for the first time in 1955 by Crombie [13]. After, in the seventies, Barrick [14] elaborated a model that can be explained as a "resonant Bragg scattering". This phenomenon, originally discovered by the English physicist William Bragg, is also responsible for the scattering of X-rays in crystals. It can be explains by the following demonstration.

Far from coasts, the visible roughness of sea surface is the superposition of a great number of irregular elementary undulations that differ in their lengths (distance between two successive crests or troughs), their heights (vertical distance between the crest level and the trough level), their periods (time for two successive crests to go through the same fixed point) and their directions. They all result from the propagation of an initial disturbance generated by the wind.

To describe the sea state, we generally distinguish the wind sea and the swell, but they are only two successive steps of the same phenomenon. The wind sea, uncoordinated, corresponds to the short term and local response of the sea to the wind action. The swell, apparently regular and simple, is generated out of the observation area that it reaches propagating from its development zone.

Swell and waves are gravity waves, i.e. waves for which the return force of the water particles to their equilibrium position is the gravity. It has been shown that, in ocean depths, the phase velocity of a gravitational wave, meaning the velocity of displacement of a crest, is given by :

$$V_i = \left(\frac{gL_i}{2\pi}\right)^{1/2}$$

where g is the gravity acceleration (= 9.81 m.s^{-2}) and L_i is the wavelength of the wave in m.

The oscillation echo is affected by a Doppler shift Δf_{di} such as :

$$\Delta f_{di} = \pm \frac{2V_i}{\lambda} = \pm \left(\frac{2gL_i}{\pi \lambda^2} \right)^{1/2}$$

Note that an ambiguity on the propagation way exists.

When the wavelength of an oscillation corresponds to the half of the wavelength of the electromagnetic waves transmitted by the radar, the Bragg resonance phenomenon occurs : echoes coming from successive crests of this oscillation are in phase. In fact, we observe on figure 4.1 that the phase delay $\Delta\phi$ between the round trip waves at point P, that can be expressed : $\frac{4\pi L_i}{\lambda}$, equals 2π.

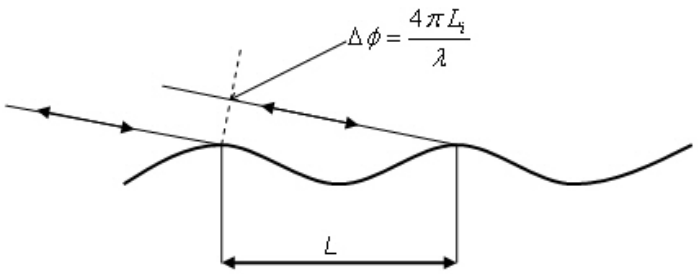

Figure 4.1: Illustration of the Bragg scattering phenomenon

Thus, if $L_i = \lambda/2$, a resonance frequency appears, it is called the Bragg frequency and is noted f_b. Its expression is :

$$f_b \ : (\text{in Hz}) = f_c \pm \left(\frac{g}{\pi \lambda} \right)^{1/2} = f_c \pm 0,102\sqrt{f_c}$$

where f_c is the carrier transmitted frequency of the radar system.

Observing a sea echo spectrum as shown on figure 4.2, we notice two distinct peaks at the two Bragg frequencies representing the strong return coming from the waves or the swell of wavelength $L_i = \lambda/2$. They are first order peaks of the Bragg phenomenon. But the sea surface is composed of many oscillations with various amplitudes, different velocities, different directions and they produce a second order continuum. Its shape and its level depend on the sea state.

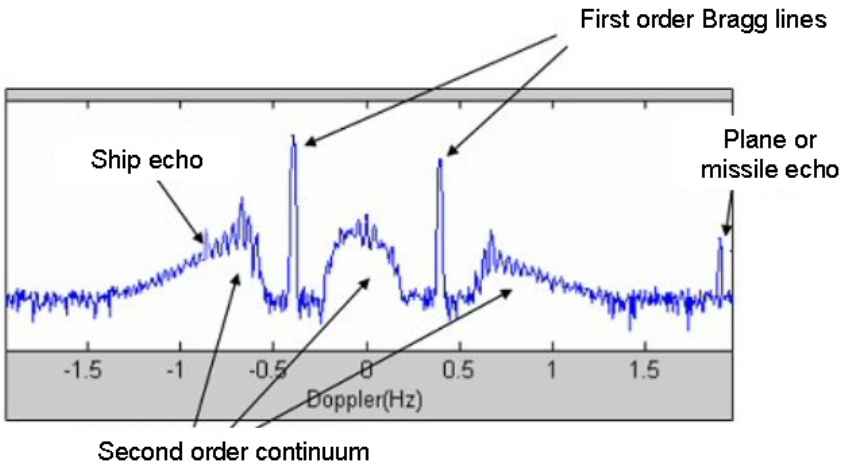

Figure 4.2: Example of a modeled sea echo spectrum

To detect a target, the useful signal is its echo. Sea echoes become then useless, even disturbing, and we often use the term "clutter" to characterize them.

For studies of the marine environment, sea echoes become the useful signal. Bragg lines analysis results in information about winds and currents, that are interesting for oceanographers and seamen.

4.1.1.2 Second order Bragg clutter

As sea surface is composed with a multitude of waves with different amplitude, direction and velocity, we have various interactions between them that produce a second order Bragg clutter. This is illustrated in figure 4.3 showing the superposition of waves. This second order continuum can throw the spectrum into confusion and make the detection impossible. If an appropriate signal processing can reduce impact of this second order Bragg clutter, radars will be able to detect smaller boats or low-flying planes. In fact, it is interesting to present major origins of this second order.

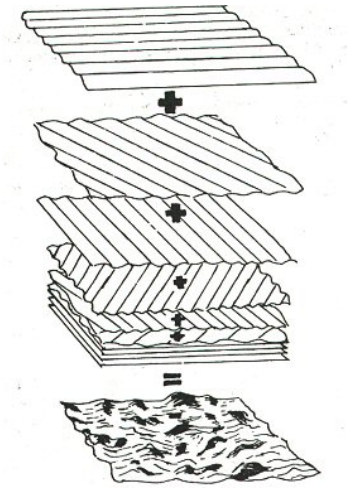

Figure 4.3: Decomposition of sea surface

These are the 3 major origins of second order Bragg clutter :

- **Waves are trochoidal** : It means that they result from the superposition of harmonic sinusoids moving at the same velocity.

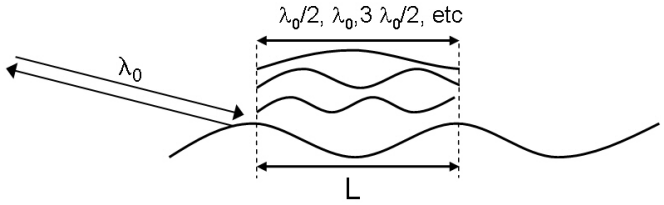

Figure 4.4: Trochoidal waves

- **Horn reflection** : A part of the backscattered signal results from two first order wave trains. It happens a kind of double scattering. The measured Doppler shift is the sum of the two reflections Doppler shifts.

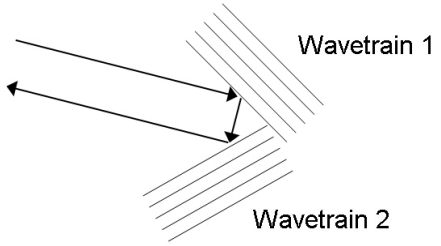

Figure 4.5: Horn reflection

- From the interaction of two first order waves, a **third wave** appears propagating in the radar direction. This wave does not obey the dispersion relationship of gravity waves but its velocity is a composition of the velocities of Bragg waves that create it.

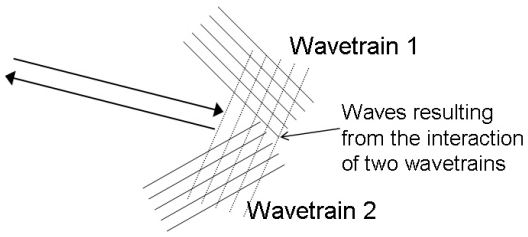

Figure 4.6: Combination of waves

4.1.2 Oceanographic parameters deduced from sea echoes

The spectral analysis can provide information about oceanographic parameters :

- Wind direction
- Waves height
- Wind force, meaning wind velocity
- Current velocity

4.1.2.1 Wind direction

The average waves direction is assumed to be in line with the wind direction at sea surface. This wind direction can be obtained thanks to the ratio between first order Bragg lines in the sea spectrum.

From the HF spectrum, Georges et al.[15] used a simplified, linear inversion method resulting in this formula :

$$\theta = 90(\frac{\Delta S - 24}{24})$$

where ΔS is the ratio between the two first order Bragg lines (in dB). θ is the angle in degrees between the observation direction and waves direction (wind direction). This is an empirical formula.

A problem has to be mentioned : θ presents an ambiguity about its angle sign. In fact, for the same angle $\pm\theta$, the received spectrum is the same. This is due to the symmetry in the directional distribution of waves around the propagation direction (see details in the following section 4.2.1).

4.1.2.2 Waves height

According to Barrick and Maresca [16], there is a link between the Doppler spectrum and the average quadratic waves height. The following formula 4.1, elaborated by Maresca, relates the ratio between energies contained in the second order and in the dominant first order Bragg lines to the average quadratic height of sea waves.

$$k_0 h = 0.8 r^{0.6} \tag{4.1}$$

with k_0 : Radar wave number
h : Average quadratic height of sea waves
r : Energy ratio between second and first order

Nevertheless, the power levels are defined in such a manner :

- The energy of the first order Bragg line is calculated, according to Maresca, for a band of 0.14 Hz around the predominating Bragg line,
- the energy of the second order is contained in the continuum surrounding the predominating Bragg line.

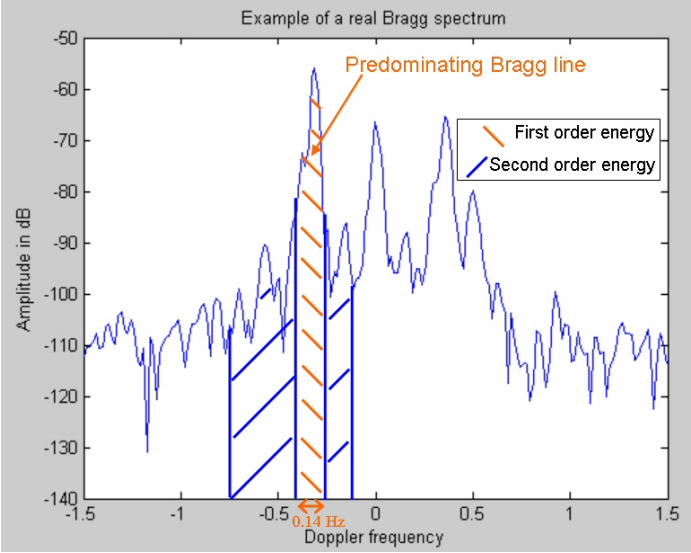

Figure 4.7: Repartition of the energy around the predominating Bragg line in a real sea spectrum

Once h is known, it is possible to calculated the significant wave height (SWH) of sea waves. The SWH is the average height of 1/3 of the highest waves. According to Barrick's works [17], h and the SWH can be relates by :

$$H_{1/3} = 2.83\ h$$

with $H_{1/3}$: Significative wave height
h : Average quadratic height of sea waves

Waves height maps can then be drawn.

4.1.2.3 Wind velocity

Many scientists (for example Long and Trizna [18]) have studied the determination of wind velocity and its effects on waves formation. Waves are generated by the wind. In fact, when the wind blows on a calm sea, it first produces small waves with wavelengths of a few centimeters. Next, the wind acts on the small waves, causing them to become larger. Finally, the waves begin to interact among themselves to produce longer waves.

Assuming that sea waves are generated by the wind at the sea surface, it is possible to relate the average quadratic wave height to the wind velocity :

$$h = 6.57.10^{-3}.U^2$$

where h : Average quadratic height of sea waves (in m)

U: Wind velocity (in m/s)

Thanks to this empirical relationship, wind maps can be drawn, typically wind directions are represented by arrows on a geographical map, the size of the arrow being proportional to the wind velocity.

4.1.2.4 Current velocity

When there is current, the sea echoes spectra are shifted from their theoretical position. In fact, to determine the current velocity, it is necessary to find the central frequency of the two Bragg lines. Thanks to this frequency shift, the radial current velocity in m/s can be easily deduced with :

$$V_{r_{current}} = \frac{\Delta f_c.c}{2.f_c}$$

where f_c : Transmitted carrier frequency in Hz

Δf_c : Doppler frequency shift in Hz.

Apart target detection, as previously mentioned, we can use information contained in the sea spectrum to draw current maps (see figure 4.8).

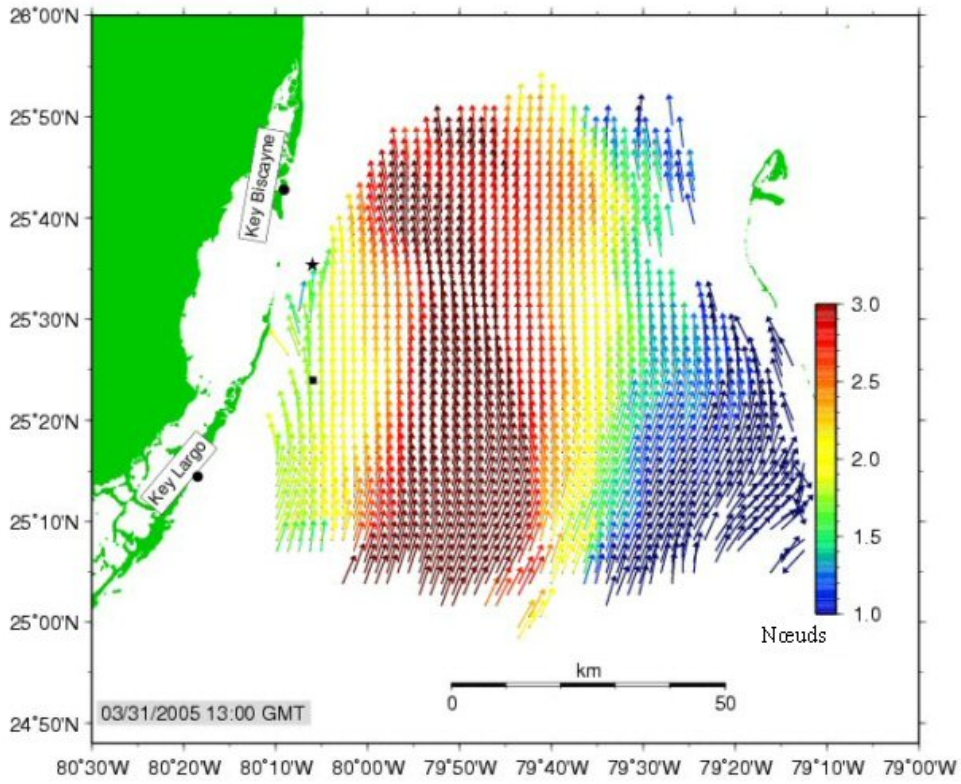

Figure 4.8: Current map off Florida (map drawn with data coming from a surface wave radar called WERA and developed by the Hamburg university [19]).

4.2 Sea spectra modeling

4.2.1 Model of sea spectrum : Pierson-Moskowitz spectrum

The Pierson-Moskowitz spectrum is a semi-empirical model for a fully developed sea, i.e. not limited by fetch or duration.

$$S(k,\theta) = S(k) \cdot g(\theta)$$

with S(k) the scalar spectrum and $g(\theta)$ a function of directional distribution of waves.

In fact, there is a relationship between wind and the locally generated waves. In the equilibrium model generally assumed, the seas are "fully developed" and the horizontal distribution of the wave energy is described by the cardioid model proposed by Longuet-Higgins in 1963 [20] :

$$g(\theta) = a.cos^s(\frac{\theta}{2})$$

where the exponent s is a spreading parameter that takes into account the spatial distribution of waves around the wind direction. a is a normalization coefficient and θ is

the angle from the direction of maximum wave energy (the wind direction) compared to the radar direction.

This cardioid pattern gives the relative values of receding (A-) and approaching (A+) waves components as shown on figure 4.9.

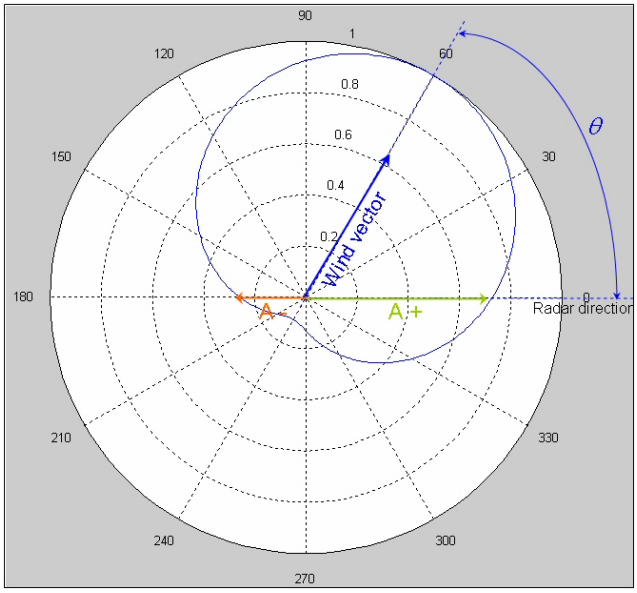

Figure 4.9: Wind cardioid representing the directional wave spectrum

From this pattern, the relative amplitude of Bragg lines are known, as shown on figure 4.10.

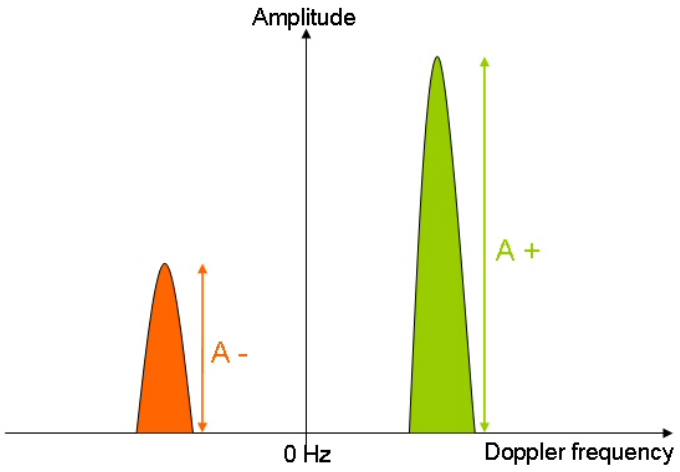

Figure 4.10: Relative amplitude of Bragg lines deduced from the wind cardioid

See also figure 4.11 representing various examples of wind cardioids. All these examples illustrate the ambiguity on the sign of θ in the calculation. The direction can be found but

the way of propagation on this direction can not. The way of getting round this problem is to consider a temporal and spatial continuity in wind direction. The direction ambiguity could also be resolved using two radar sites to provide two different radar look angles.

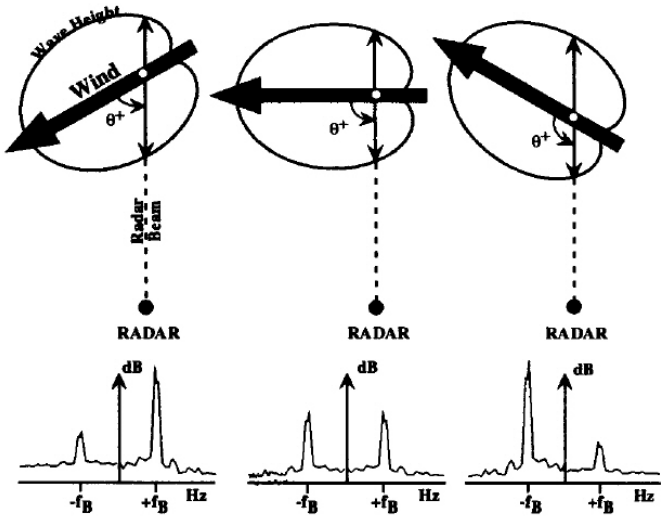

Figure 4.11: Examples of different wind cardioid and associated Bragg lines relative amplitude

The Pierson-Moskowitz scalar spectrum is given by the following formula:

$$S(k) = \frac{0.005}{k^4} \cdot e^{-0.74\left[\frac{g}{U^2 k}\right]^2}$$

where : U = Wind velocity above sea surface
g = Gravity
k = Wave number
θ = Angle between radar direction and direction of waves propagation

4.2.2 Reflectivity of sea waves : Robson method

The total backscatter coefficient σ_0 of the sea is mainly related to the first and second order reflectivity (σ_1 and σ_2) :

$$\sigma_0 = \frac{1}{2} \int_{+\infty}^{-\infty} [\sigma_1(\omega) + \sigma_2(\omega)] \cdot d\omega$$

4.2.2.1 First order reflectivity

The Doppler spectrum of an electromagnetic wave backscattered by the sea was first studied by Crombie in 1955 [13]. He noticed two dominant spectrum lines that are symmetrical around the carrier frequency. The Doppler shift of these lines corresponds to the velocity

of a wave with a wave vector K being the double of wave vector $\vec{k_0}$ of the incident radar wave.

$$\vec{k} = 2\vec{k_0}$$

To a mathematical point of view, Barrick studied the scattering of sea surface, which is considered as a surface with a low roughness. Barrick determined the first order cross section per area unit in vertical polarization :

$$\sigma_1 = 16\pi k_0^4 \cdot W(-2k_0, 0)$$

where $W(-2k_0, 0)$ is the value of the bidimensional wave spectrum $W(k_x, k_y)$ in the case of the backscatter ($k_x = -2k_0, k_y = 0$). In this relationship, W is defined in the wave vectors space from $-\infty$ to $+\infty$. The backscatter coefficient σ_1 can also be expressed in function of the wave spectrum S, often used by oceanographers.

Robson continued Barrick researches and we use his method to calculate reflectivity of the different Bragg orders. It is a model of diffuse scattering radio waves on a rough surface that takes into account multiple reflections on waves.

For the first order reflectivity $\sigma_1(\omega)$, only waves vectors being multiple of $2K_0$ will be considered :

$$\sigma_1(\omega) = C_1 \cdot k^4 \cdot S(2k_0) \left\{ \delta(\omega + 2k_0 \cdot V - \sqrt{g \cdot |2k_0|}) \cdot g(\theta) + \delta(\omega + 2k_0 \cdot V + \sqrt{g \cdot |2k_0|}) \cdot g(\theta + \pi) \right\}$$

In this formula, a scalar spectrum $S(k)$ is needed, the Pierson-Moskowitz spectrum presented in the previous paragraph is used.

4.2.2.2 Second order reflectivity

The first order scattering mechanism is quite simple to understand physically but that is not the case for the second order mechanism that makes interact the whole waves spectrum.

To calculate second order cross section, two infinities of waves vectors $\vec{k_1}$ and $\vec{k_2}$ are used such as $\vec{k_1} + \vec{k_2} = -2\vec{k_0}$.

In this case, the second order reflectivity $\sigma_2(\omega)$ is given by :

$$\sigma_2(\omega) = C_2 \cdot k_0^4 \cdot \int dk_1 \cdot dk_2 \sum_{m=\pm 1} \sum_{p=\pm 1} S_{mk_1} \cdot S_{pk_2} \cdot |\Gamma(k_1, k_2)|^2 \cdot \delta(\Delta\omega + 2k_0 \cdot V - m\sqrt{g\,|k_1|} - p\sqrt{g\,|k_2|})$$

with $|\Gamma(k_1, k_2)| = \frac{\{(k_0 \cdot k_1)(k_0 \cdot k_2) - 2(k_1 \cdot k_2)\}}{\sqrt{|k_1 \cdot k_2|}}$ is the coupling coefficient. This coefficient includes hydrodynamic and electromagnetic effects.

It is then possible to plot reflectivity of first and second order Bragg clutter in function of the Doppler frequency. The following figure 4.12 presents a model of sea spectrum for

a low frequency of 4 MHz and a wind velocity of 4 m/s. Other considered parameters are printed in the upper part of the image. On the upper right corner, the wind cardioid present the wind orientation compared to the radar direction. On the lower part of the figure, we notice the two predominating Bragg lines (first order) and the second order between them. They have a low level.

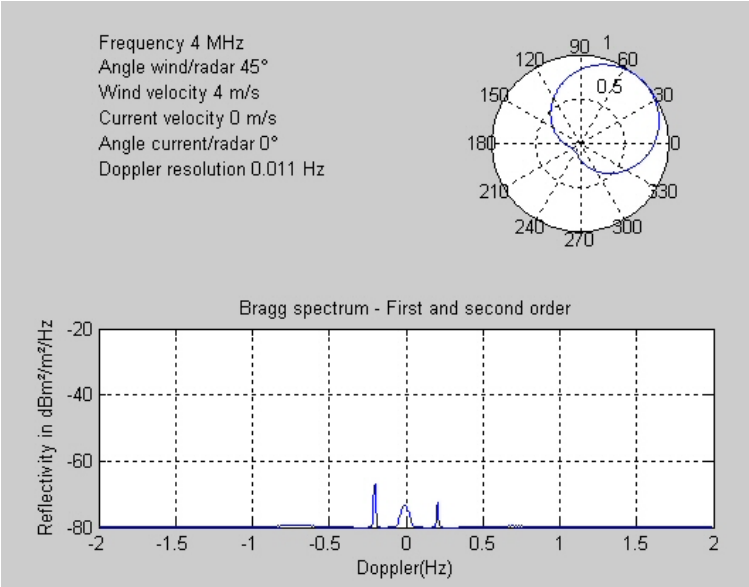

Figure 4.12: Example of a simulated Bragg spectrum at 4 MHz and view of the wind cardioid

For higher frequencies, sea spectrum is different. Refering to figure 4.13 displaying a sea spectrum at 15 MHz for the same wind velocity and orientation, we rapidly notice its higher reflectivity level. It means that higher the frequency is, higher the sea clutter reflectivity will be. It can certainly be explained by the fact that at low frequencies, there are less waves with long wavelength able to interfere with the radar wave. The sea is composed of more wavelets than long swell waves.

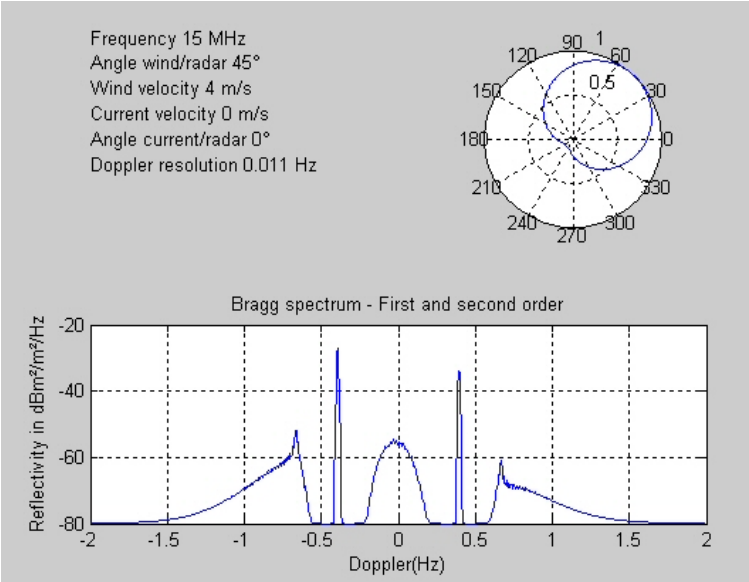

Figure 4.13: Example of a simulated Bragg spectrum at 15 MHz and view of the wind cardioid

4.3 Creation of a simulated sea echoes database

4.3.1 General algorithm used to simulate sea echoes

In this section, the aim is to create an algorithm able to simulate backscattered echoes coming from sea waves.

To better understand sea echoes spectra and to familiarize with them, the best way is to study many samples of them. To do that the idea is to create a database of simulated sea echoes because we do not have enough real sea spectra data. We have to imagine an algorithm able to create the wanted database.

The basis of the algorithm is the sea echo spectrum. The study of precise scattering of the electromagnetic waves on sea surface is difficult to model. Oceanographers established models of sea surface varying with time and it would be very interesting and precise to simulate the interaction between these models and HF waves. Unfortunately, the thesis period is too short to simulate such complex electromagnetic problems that is why we take advantage of the previous studies in the literature where these interactions have already been modeled. And we decide to use a model of sea spectrum, i.e. to simulate the reflectivity of sea waves in function of the Doppler frequency. Consequently, that amounts to saying that the simulated data will be directly available after an imaginary Doppler processing step.

Detailed in the previous section 4.2, the simulated Bragg spectrum depends on the radar frequency, the wind velocity and its orientation compared to the radar's one, the current velocity and its orientation compared to the radar's one and the Doppler resolution. It

means that we have the Doppler dimension but we do not have information about the range where imaginary sea waves and HF waves would have interacted to create this Bragg spectrum. This supplementary dimension has to be created if we want to study simulated Doppler range images and compare them with Doppler range images obtained after the radar processing of real data.

In real Doppler range images, the difference between a Doppler spectrum and its neighboring Doppler spectra at different range cells is the different attenuation of signals due to propagation losses. As a consequence, it is possible to add a range dimension to the simulated spectrum if we apply an attenuation factor corresponding to its fictive position.

Moreover, to be close to reality, it is necessary to add noise in the simulated data. We choose to add a random Gaussian noise to the simulated data.

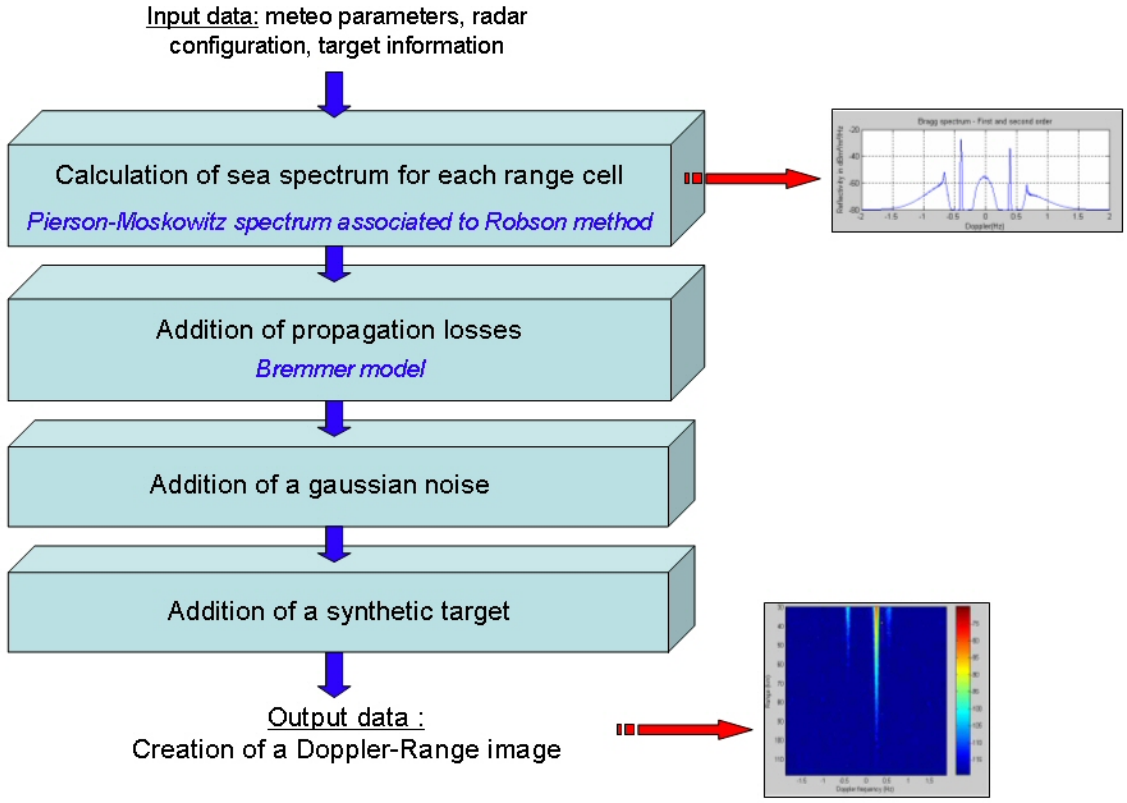

Figure 4.14: Algorithm for the creation of simulated sea echoes

Details of the algorithm are presented afterwards.

4.3.2 Detailed input parameters

The algorithm needs many entering parameters. The first to enter concern radar parameters, the second concern meteorological parameters and thirds concern target parameters:

4.3.2.1 Radar parameters

- **Radar frequency (in Hz) :** This is the carrier frequency transmitted by the radar system. This frequency ranges from 3 to 30 MHz. Here, the default frequency is 10,75 MHz.
- **Transmitted time (in s) :** This is the time duration of the transmitting period. During this period, backscattered echoes cannot be received that is why there is a blind zone. The default transmitted time is fixed at 75 μs, meaning a blind zone about 11 km.
- **Bandwidth (in Hz) :** This is the bandwidth of the transmitted waveform. The default value is 400 kHz, corresponding to a very good range resolution of 375 m.
- **Pulse Repetition Frequency (in Hz) or recurrence duration (in s) :** These two parameters are often confused. In fact, there is an abuse of the language because the PRF is often given in time (inverse of the frequency). This is the repetition time between two transmitting pulses. The default recurrence duration is 500 μs.
- **Coherent integration time :** This is the time during which data are accumulated to improve the frequential resolution of the results. Typically, we use an integration time of a few tens of seconds to obtain a sufficient frequential resolution and to maintain targets and sea parameters unchanged. Preciselly, we use 40.96 s.
- **Transmitted power :** This is the total transmitted power (crest power). The default one is fixed at 200 W.

All these parameters are the most susceptible of changing that is why they can easily be modified by the operator. A dialog window is displayed on the screen at the beginning of the program for this parameters setting. The form fields appear with the default parameters values.

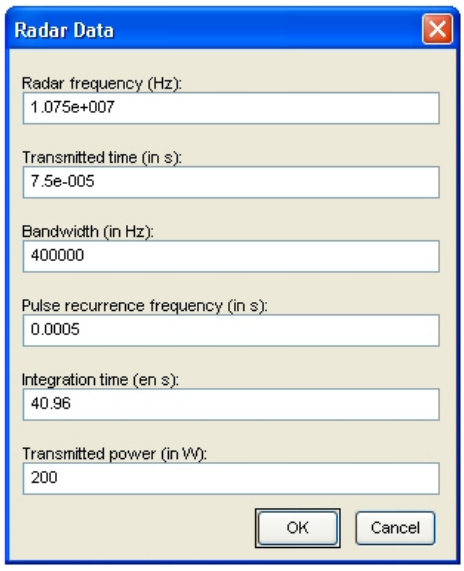

Figure 4.15: Dialog window with default radar parameters

These parameters will be used in the program to create "realistic" simulated results. In fact, thanks to the Radar Equation presented in the chapter 1, we are able to calculate the signal levels as if they were really detected by the radar system.

Other parameters are not available by way of a dialog window but one can modify them directly in the source of the program. They are numerous but rarely changed :

- **Length of the receiving array :** This value is fixed at 90 m, meaning a space between antennas about 6 m (this receiving phased array is sized and optimized for the use of high frequencies). In practice, it would be important to have a system optimized at the carrier frequency to respect the distance $\lambda/2$ between antennas and then avoid or limit mutual coupling in the array. In these simulations, this length is only used to determine the beamwidth dimensions, coupling effects between elements are not taken into account.

- **Number of antennas (transmitting and receiving elements) :** We assume that there are 2 transmitting antennas and 16 receiving elements associated in phased array.

- **Gain of the antennas (transmitting and receiving elements) :** For transmitting, we assume a gain of 3 dB for each antenna. For the receiving elements, a gain of 1 dB is considered.

- **Noise factor :** The noise factor depends on the frequency, the location of the radar on the Earth and day/night period. In the simulation software, the noise factor adapts itself in function of the frequency and day/night period. The following figures have not been measured precisely but they result from experience. At day period, at low frequency, the noise factor is about 40 dB and decreases for higher frequencies where it is about 20 dB. At night period, it is higher and reaches 60 dB at low frequencies up to 20 dB for high frequencies.

- **Frequential extent of the displayed results :** This is the final frequential extent that appears on the Doppler range image. The default value is the display of Doppler frequency shifts between -2 Hz and +2 Hz. For our study where we are interested in sea clutter, this extent is sufficient. In fact, the sea clutter is present between $-0.2\sqrt{f_c}$ and $+0.2\sqrt{f_c}$, which equals to ± 1 Hz for the highest HF frequencies. Taking into account possible violent currents, for example currents with a velocity being 1.5 m/s, it corresponds to a maximum Doppler shifting of 0.3 Hz at 30 MHz. For that reason, we choose a default frequential extent display of ± 2 Hz which is sufficient even in case of strong currents.

4.3.2.2 Meteorological parameters

By meteorological parameters, we mean external conditions such as wind or current. They will be used in the calculation of sea clutter models.

- **Origin of radar direction :** This is the reference direction, generally equals to zero to simplify angles calculation.

- **Wind velocity (in m/s) :** The wind velocity is given between 0 and 30 m/s. A recall of the Beaufort scale is presented in annexe, in table 5.2. For this study, the typical wind velocity values should not be too high because in case of storm, the model used for sea echoes is not valid anymore.

  To simulate a realistic wind, it is possible for the program to increase or decrease the wind velocity from a range cell to another. In fact, we can have, for example, a wind linear acceleration of 20% from the first range cell to the last one. If a the linear law is not sufficient, other wind velocity profiles can be chosen.

- **Wind direction (in degrees) :** This is the angle between the radar direction and the direction of sea waves propagation. This value can span from 0 to 360 degrees (0 degree being generally the origin of the radar direction). For wind direction, it is also possible to have fluctuations from the first to the last range cell.

- **Current velocity (in m/s) :** The velocity is generally given in knot but it is converted here in m/s. It generally ranges from 0 to 1.5 m/s. The current velocity value can also be variable during the simulation. The marine currents are generated by the horizontal displacement of the water particles. They are characterized at a given time t and in a given place by they direction and their velocity. The direction of a current is where it goes, from 0 to 360 degrees (0 degree being the origin of the radar direction). The marine currents are very variable in space and time and their origins are various. Tidal streams can be predicted because they come from the gravitational attraction between the Moon and the Sun. Other currents coming from the wind, the change in sea level, the swell, etc. can aso be predicted and many oceanographers study these phenomena.

- **Current direction (in degrees) :** This is the angle between the radar direction and the direction of the current. This value can span 360 degrees. Same comments as for wind direction, current direction can change all along range cells.

To set meteorological parameters, a dialog window is available as shown on figure 4.16. This is an example of default meteorological values.

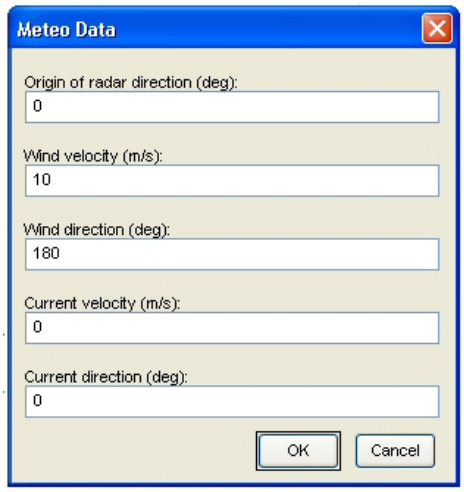

Figure 4.16: Example of meteorological parameters

4.3.2.3 Target parameters

In the algorithm, we defined the possibility of adding synthetic targets in the simulation. To do that, three essential target parameters have to be entered. The program gives the possibility to create several targets.

- **Target velocity (in m/s) :** It corresponds to the radial velocity of an object that would virtually reflect HF waves. Thanks to this velocity, we can calculate the Doppler frequency where the target echo should be after a Doppler range processing step. We have to be realistic in these parameters, for example, a ferry can sail at 8 m/s, or at the same velocity than waves or at 25 m/s for "go fast boats", while a low-flying plane would be about 80 m/s for its landing or takeoff.
- **Target range (in m) :** It corresponds to the distance from the radar to the virtual object. This distance has to be comprised between the distance associated to the end of the blind zone and the maximum range associated to the end of the recurrence duration.
- **Target radar cross section (in m^2) :** this is the RCS of the virtual object. We can simulate echoes coming from various type of targets. These RCS depends on the frequency, the object dimensions, its orientation compared to the radar and its material but in general we consider average RCS. For example, the typical RCS of a small plane is around 1 m^2, while a jumbo jet or a big transport aircraft have 100 m^2 of RCS. For boats, RCS can span a wide range of values from 1 m^2 for really small tourist ship to 100,000 m^2 for a huge oil tanker, a cruise ships or a container ship. A missile has a small RCS around 1 m^2.

The following figure 4.17 is an example of entered target parameters.

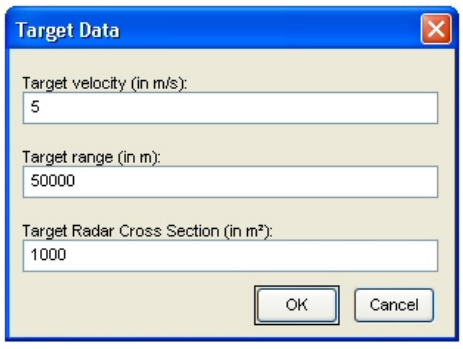

Figure 4.17: Example of target parameters

4.3.3 Calculation of sea spectrum for each range cell

The Pierson-Moskowitz spectrum associated to the Robson method is used to simulate sea echoes. Then, each element of the Radar Equation is taken into account to obtain the theoretical signal level of sea spectra. In this case, we use the transmitted power, the number of antennas and their gains, the range of the simulated spectrum, the wavelength associated to the transmitted frequency, etc.

The sea spectrum reflectivity is proportional to the portion of sea surface illuminated by the radar. Thanks to the entered parameters (bandwidth, array length, frequency), we can calculate the illuminated area and then deduce sea spectra theoretical level. This area differs from a range cell to another. In general, when we want to calculate roughly sea echoes level, we use an average value. In fact, it is assumed that the sea echo reflectivity coefficient is -23 dBm^2/m^2 [21].

The reflectivity level of sea spectra, given by the Robson method, is then normalized by the correction coefficient calculated thanks to the Radar Equation. Thus, the simulated spectra will be really realistic in terms of signal levels. See an example of a Doppler range image 4.18 created by calculating sea spectrum for each range cell. In fact, when the range increases, the sea echoes level decreases because of the term R^4 in the denominator of the Radar Equation. This effect of level reduction is well illustrated on the following figure.

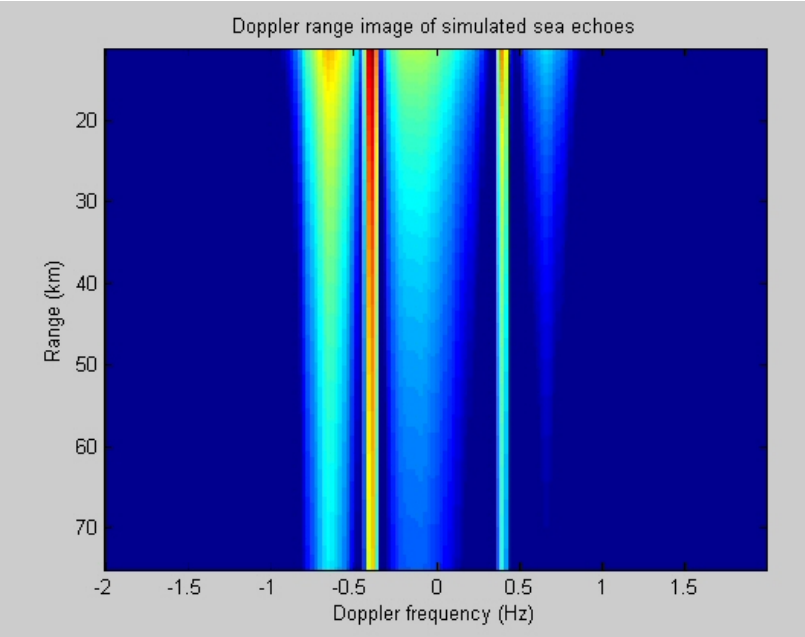

Figure 4.18: Doppler range image of simulated sea echoes

For the moment, propagation losses are not taken into account.

4.3.4 Addition of propagation losses

In the Radar Equation (see chapter 1 for details), a penalizing parameter concerns propagation losses. In fact, the electromagnetic field is diminished during its path above sea surface. As previously shown, the propagation losses are variable in function of the frequency, the distance, the sea state (roughness), the intrinsic conductivity ($\sigma \approx 4$ S/m) and relative permittivity ($\epsilon \approx 80$) of sea water. In our simulation tool, we use a Bremmer model to obtain the propagation losses of HF waves above sea surface for a single trip [3].

For each frequency, we can calculate the losses curve in function of the distance. The Bremmer model calculates propagation losses thanks to the series of Bremmer's remainders but this method can only be used on a smooth and homogeneous sea. Nevertheless, perturbations caused by the sea roughness are very important in the HF band because the electromagnetic wavelengths are the same than mechanical wavelengths (sea waves periodicity).

To take into account sea state in the calculation, a technique based on Barrick's works which dates back to 1970 [22], consists in recalculating the parameters ϵ and σ of the sea considering the scattering resulting from sea roughness. In fact, the conductivity decreases when the sea state deteriorates. The sea conductivity is a function of sea surface temperature and salinity, and as such varies with time. On smaller time-scales, the propagation loss also varies with sea-state ; it increases when the sea state deteriorates. The method proposed by Barrick accounted for the additional loss experienced in rough seas. These additional losses, depending upon the prevailing conditions and operational frequency, can exceed 10 dB.

On figure 4.19, four examples, processed with the crossed method Bremmer/Barrick, are presented for 4 different frequencies (4, 8, 12 and 25 MHz). These curves show that for a frequency of 4 MHz and a distance of an object to detect at 100 km, losses are minimal, in the order of a few dB. For higher frequencies, at 25 MHz for example, losses equal 25 dB for a single trip meaning that the double path losses are very penalizing.

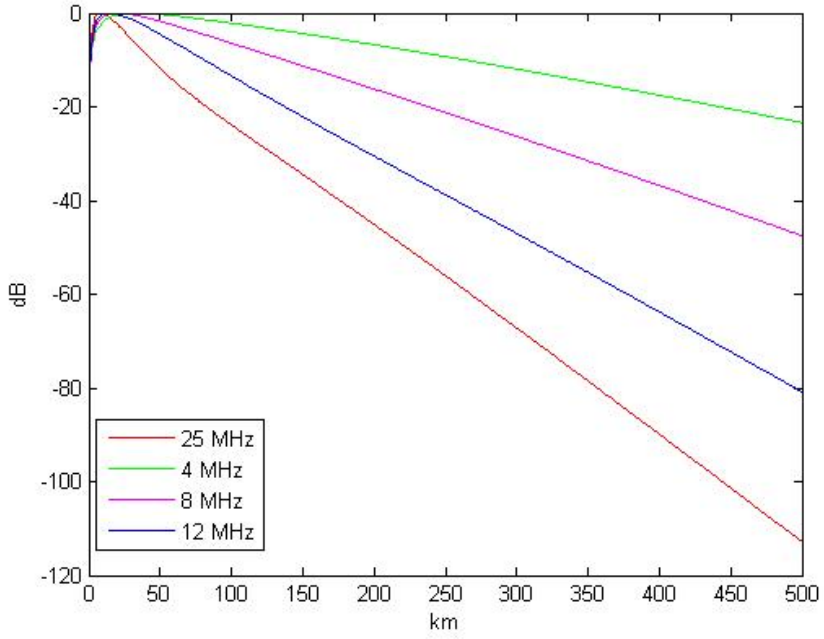

Figure 4.19: Propagation losses in dB above sea surface in function of range (in kilometers) for a single trip

In summary, surface wave attenuation in dB is proportional to carrier frequency. It is possible to take into account added losses due to surface roughness in the losses model. To minimize the attenuation and provide a maximum detection capability, the advice are to operate the radar in the lower end of the HF band.

4.3.5 Addition of a Gaussian noise

A Gaussian noise is added on the whole image, it is a random noise whose level is calculated thanks to the noisy part of the Radar Equation, i.e. $F_b k T_0 \Delta F$ where F_b : external noise factor, k : Boltzmann constant ($= 1.38.10^{-23}$ J.K^{-1}), T_0 : temperature in K and ΔF : frequential resolution.

4.3.6 Addition of a synthetic target

A target echo is created by the backscattering of the transmitted waveform on an object sailing on sea or flying at low altitudes. That is why to obtain a fictive target echo on a Doppler range image, it is quite easy. In our case, by correlation of a transmitted chirp with a pseudo-received chirp (in fact it is a simple chirp autocorrelation), we will have a target echo pattern in the range dimension.

The chirp autocorrelation consists of a principal peak with correlation sidelobes that will be shifted to the range cell corresponding to the input target range. See an example on figure 4.20, where a chirp autocorrelation is generated on 512 points and shifted at the range cell 50 to obtain a location of the fictive echo at the corresponding range. It is then possible to truncate data to keep only the desired number of range cells. In this example, we want to add this false target echo in a Doppler range image comprising 150 range cells and 321 Doppler cells. That is why only 150 points of the shifted echo will be kept.

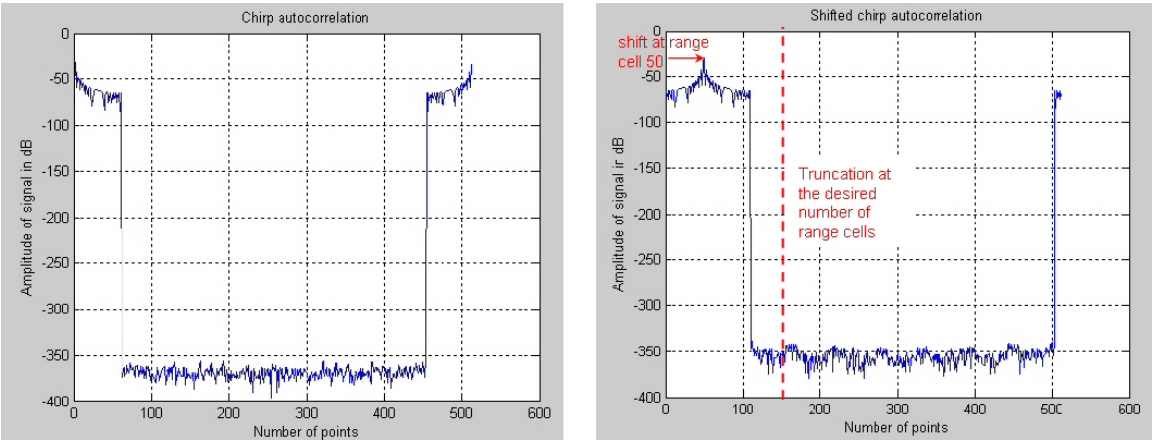

Figure 4.20: Example of a chirp autocorrelation

To create the Doppler dimension, we add Doppler sidelobes to the previous data. To obtain 321 Doppler cells, we create Doppler sidelobes on this precise number of cells. We typically use a cardinal sinus pattern for Doppler sidelobes. Knowing the input target

velocity and the frequential resolution, it is simple to determine the Doppler cell number where the echo should be located in the Doppler dimension. Each point of the range dimension is then multiplied by the Doppler sidelobes pattern.

By the same process than for sea clutter, the theoretical level of the simulated target echo is calculated considering our equipment settings. The signal level is calculated using the transmitted power, the number of antennas and their gain, the wavelength associated to the transmitted frequency, the specified range of the target and its RCS. We also take into account propagation losses in this calculation, corresponding to the target range and the transmitted frequency. This corrective factor is applied on the whole image. In this example, the level of the highest peak corresponding to the target echo is at -127 dB. At the end, a Doppler range image is available as shown on left part of figure 4.21. To limit the plot dynamics and to better distinguish the target echo, a random Gaussian noise is added to the whole image. Final results are displayed on the right part of the figure 4.21.

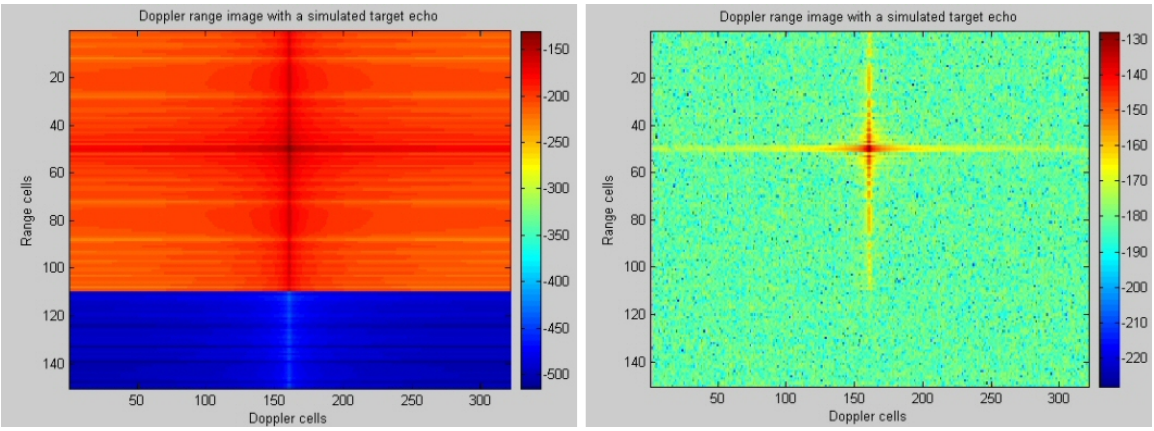

Figure 4.21: Left part : Doppler range image of a simulated target ; Right part : Doppler range image of a simulated target surrounded by a Gaussian noise

It is also possible to create a target and to simulate its processing with a Doppler weighting window. For example, we can use a Blackman window. As we know the pattern of a temporal Blackman window in the frequency domain, we apply it to the shifted chirp autocorrelation to obtain the weighting effect in the simulation result as presented on figure 4.22 where Doppler sidelobes are well reduced.

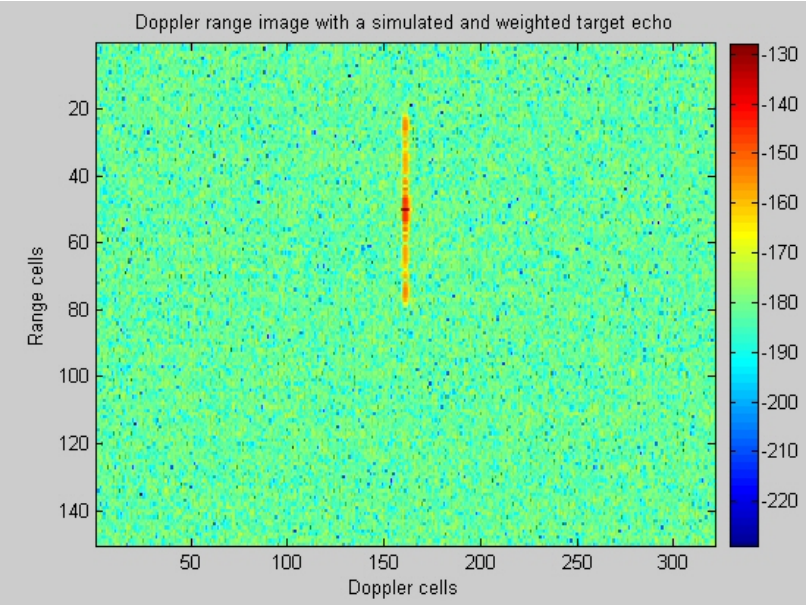

Figure 4.22: Simulated target echo processed with a Doppler weighting window

4.3.7 Effect of radar processing on simulated echoes

In these simulated sea echoes, we directly have a spectrum. With the algorithm, we obtain simulated spectra in function of the range taking into account losses and noise. The problem is that these modeled data differ really from measured data because they do not propagate through the radar equipment and they are not processed through the Doppler range processing step. Thus, simulated spectra are "clean" because they are not affected by the equipment defaults and by the processing effect, meaning they do not have correlation or Doppler sidelobes. If we want to have simulated data resembling to real ones, we propose to add only a fictive processing effect on the simulated data, the disturbing equipment aspect is difficult to model.

4.3.7.1 Effect of range processing

The received sea signal is composed of many echoes, received at successive moments with a delay τ_i. This observation can be written :

$$r(t) = e_1(t - \tau_1) + e_2(t - \tau_2) + \ldots + e_n(t - \tau_n)$$

where $r(t)$ is the total considered received signal and $e_i(t - \tau_i)$ corresponds to the signal portion received after a delay τ_i corresponding to the range cell i.

In range processing, during the correlation step, this received signal is correlated with a replica. Let rep be that replica. This can be written : $r(t) \otimes rep(t)$[1].

The Fourier Transform (FT) of this correlation operation is given by :

[1] $\otimes$ represents a convolution product

$$FT(\textit{Received sea signal}).FT(\textit{Replica})^*$$

The notation $*$ stands for the complex conjugate. Details are given by :

$$\left[E_1(f).e^{-j2\pi\tau_1 f} + E_2(f).e^{-j2\pi\tau_2 f} + \ldots + E_n(f).e^{-j2\pi\tau_n f}\right].REP^*(f)$$

It is assumed that the received signal in this example is a chirp form that can be written:

$$e_1(t) = A_1.e^{-j2\pi f_1 t}.e^{-j\beta t^2}$$

with A_1, amplitude of the signal and β, a constant coefficient.

Its Fourier Transform $E_i(f)$ can be expressed such as : $A_i^{'}.e^{j\varphi_i}.e^{j\alpha f^2}$ with $A_i^{'}$ and α constant coefficients. $\varphi_i = 2\pi f_i t$ is the phase i.

The replica is a chirp and can simply be written : $rep(t) = e^{-j\beta t^2}$. Its Fourier Transform is then $REP(f) = e^{j\alpha f^2}$.

Now, the operation can be expressed :

$$FT(\textit{Received sea signal}).FT(\textit{Replica})^* = E_1(f).e^{-j2\pi\tau_1 f}.REP^*(f) + \ldots + E_n(f).e^{-j2\pi\tau_n f}.REP^*(f)$$

The developed form is :

$$= A_1^{'}.e^{j\varphi_1}.\underbrace{e^{j\alpha f^2}.e^{-j\alpha f^2}}_{REP(f).REP^*(f)}.e^{-j2\pi\tau_1 f} + \ldots + A_n^{'}.e^{j\varphi_n}.\underbrace{e^{j\alpha f^2}.e^{-j\alpha f^2}}_{REP(f).REP^*(f)}.e^{-j2\pi\tau_n f}$$

We can factorize this result by the chirp autocorrelation $REP(f).REP^*(f)$ to obtain :

$$= [REP(f).REP^*(f)]\,.\left[A_1^{'}.e^{j\varphi_1}.e^{-j2\pi\tau_1 f} + \ldots + A_n^{'}.e^{j\varphi_1}.e^{-j2\pi\tau_n f}\right]$$

By an inverse Fourier Transform, we obtain the following temporal signal :

$$= [\textit{Replica autocorrelation}] \otimes \underbrace{\left[A_1^{'}.e^{j\varphi_1}.\delta(t-\tau_1) + \ldots + A_n^{'}.e^{j\varphi_n}.\delta(t-\tau_n)\right]}_{\textit{This is obtained by simulation of sea spectrum for each range cell}}$$

It amounts to apply an inverse Fourier Transform on :

$$[REP(f).REP^*(f)]\,.\,[FT(\textit{Received sea signal})]$$

Nevertheless, by simulation, we have directly the part $FT(\textit{Received sea signal})$ because we model sea spectra. It means that effect caused by range processing can be applied on the simulated sea spectrum by a simple operation (multiplication by $REP(f).REP^*(f)$ and inverse Fourier Transform.

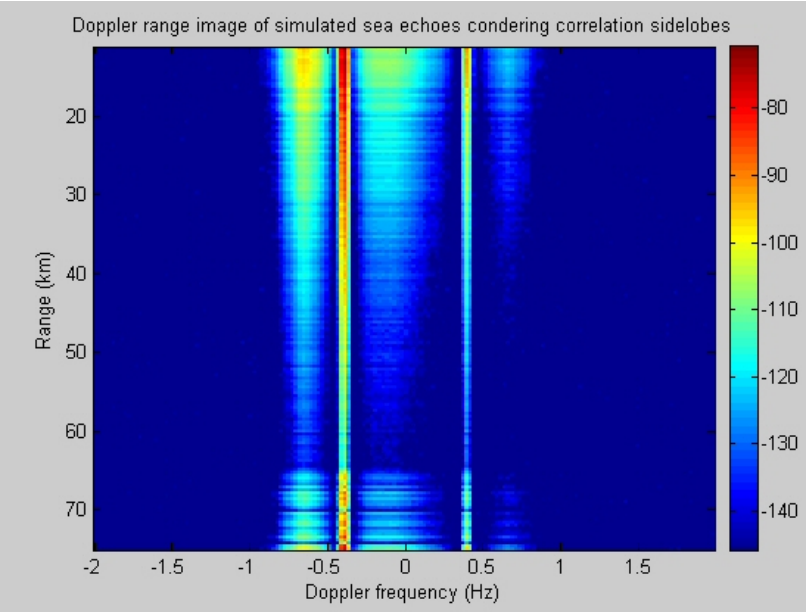

Figure 4.23: Range processing effect applied on simulated sea echoes

The previous figure 4.23 present simulated sea echoes that have been affected by range processing. On this figure, we clearly notice the effects (changes in Bragg lines level and an ascending level in the last range cells).

4.3.7.2 Effect of Doppler processing

For the modeled data to be affected by Doppler processing, it is also possible to taken into account Doppler sidelobes by the same manner that we did for the target simulation (see 4.3.6). A cardinal sinus is the Fourier Transform of a square window, but we can also apply different patterns such as the Fourier Transform of a Blackman window for example.

On the following figure 4.24, this is a final Doppler range image of simulated sea echoes where range and Doppler processing affects are considered.

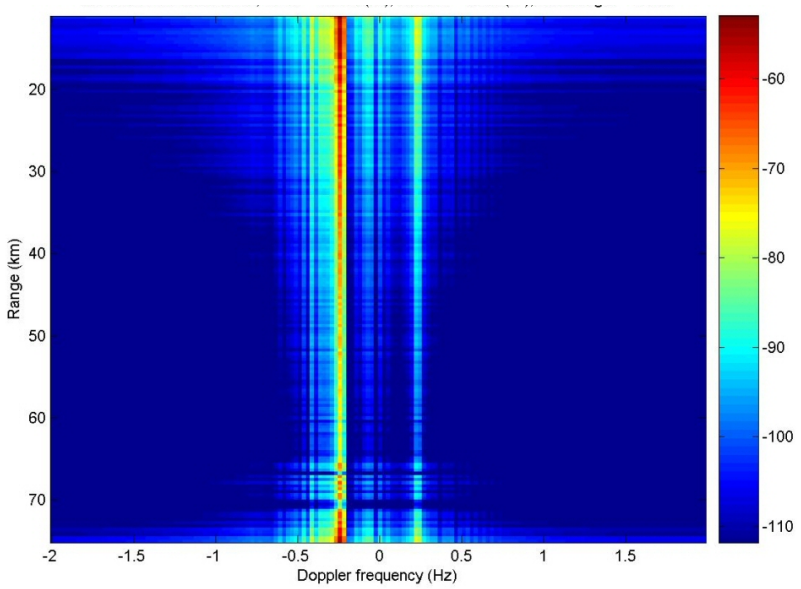

Figure 4.24: f=5.255 MHz, wind 10m/s (0 °), current 0 m/s (0 °)

Afterwards, simulations can use these effects or not.

4.4 Analysis of the simulated sea echoes database

4.4.1 Final result of the simulation process

On the following figures (from 4.25 to 4.28), sea echoes have been simulated for different frequencies, sea states and with various target parameters. Targets have been included in the simulations to see in which case sea clutter is the most disturbing.

On this first simulation (see figure 4.25), sea echoes have been modeled for a low frequency of 4 MHz. At this frequency, propagation losses are weak and sea clutter is present all along the range cells. Targets will only be detected if they have a sufficient RCS and a sufficient velocity to avoid the sea clutter zone.

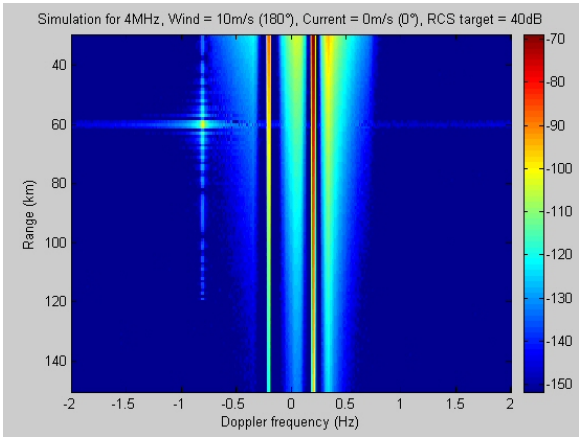

Figure 4.25: Simulated Doppler range image with the following parameters : **Radar :** f_c = 4 MHz, B = 150 kHz, Transmitting time = 200 μs, PRF = 1 ms, Ti = 80 s, Pe = 200 W; **Meteo :** wind velocity = 10 m/s (Force 5), Orientation/radar = 180 °, no current; **Target :** velocity = 30 m/s, range = 60 km, RCS = 40 dB

On this figure 4.26, a target with a strong RCS of 50 dB has been simulated. It has been simulated with a Doppler weighting window to avoid important Doppler sidelobes. Its low velocity locates it at the same Doppler than the negative Bragg line. In spite of its high level, this target will be hidden and its detection will be impossible.

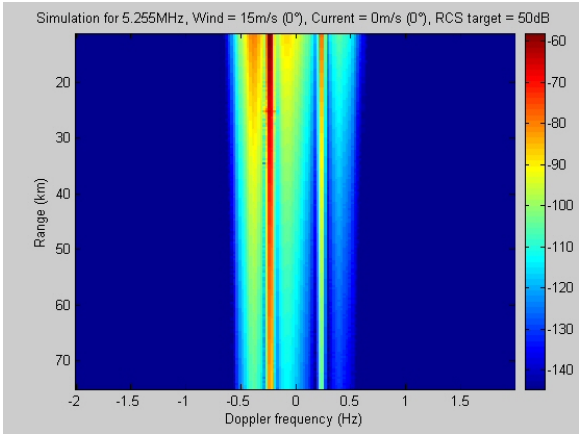

Figure 4.26: Simulated Doppler range image with the following parameters : **Radar :** f_c = 5.255 MHz, B = 400 kHz, Transmitting time = 75 μs, PRF = 500 μs, Ti = 40.96 s, Pe = 2 kW; **Meteo :** wind velocity = 15 m/s (Force 7), no current; **Target :** velocity = 6 m/s, range = 25 km, RCS = 50 dB

On figure 4.27, at 10 MHz, the sea clutter is very disturbing because it is spread on the whole Doppler cells between -1 Hz and + 1 Hz. A target in this Doppler interval could not be detected, except if its level is higher than Bragg lines level thanks to a strong RCS.

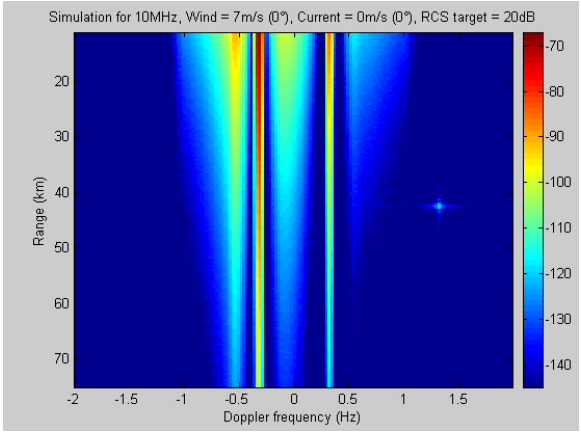

Figure 4.27: Simulated Doppler range image with the following parameters : **Radar :** f_c = 10 MHz, B = 400 kHz, Transmitting time = 75 μs, PRF = 500 μs, Ti = 40.96 s, Pe = 2 kW; **Meteo :** wind velocity = 7 m/s (Force 4), no current; **Target :** velocity = 100 m/s, range = 42.5 km, RCS = 20 dB

On the following image 4.28, we clearly notice that propagation losses are very high at this frequency (25 MHz) because sea clutter is rapidly attenuated and second order Bragg clutter is only present in the first range cells. On this figure, two targets have been simulated (using a Doppler weighting window), the target approaching the radar (at a positive Doppler frequency) has a RCS of 60 dB which is an important value but it is detectable with difficulty because of enormous propagation losses.

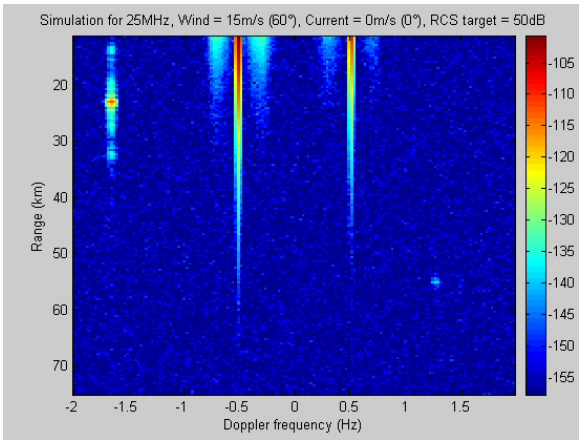

Figure 4.28: Simulated Doppler range image with the following parameters : **Radar :** f_c = 25 MHz, B = 400 kHz, Transmitting time = 75 μs, PRF = 500 μs, Ti = 40.96 s, Pe = 2 kW; **Meteo :** wind velocity = 15 m/s (Force 7), Orientation/radar = 60 °, no current; **Target 1:** velocity = 250 m/s (moving away from the radar), range = 23 km, RCS = 50dB; **Target 2:** velocity = 200 m/s (approaching the radar), range = 55 km, RCS = 60 dB

By simulation, it is very easy to control every parameter and to place targets at a precise location. All these images show the different aspects of received sea clutter in function of

the frequency, the wind force and the radar settings. They underline the disturbing part of sea clutter, mainly for low-velocity or low-RCS targets. These observations justify the need of a filtering tool to provide optimum detection conditions for HF Surface Wave Radars.

4.4.2 Comparison between simulated echoes and real ones

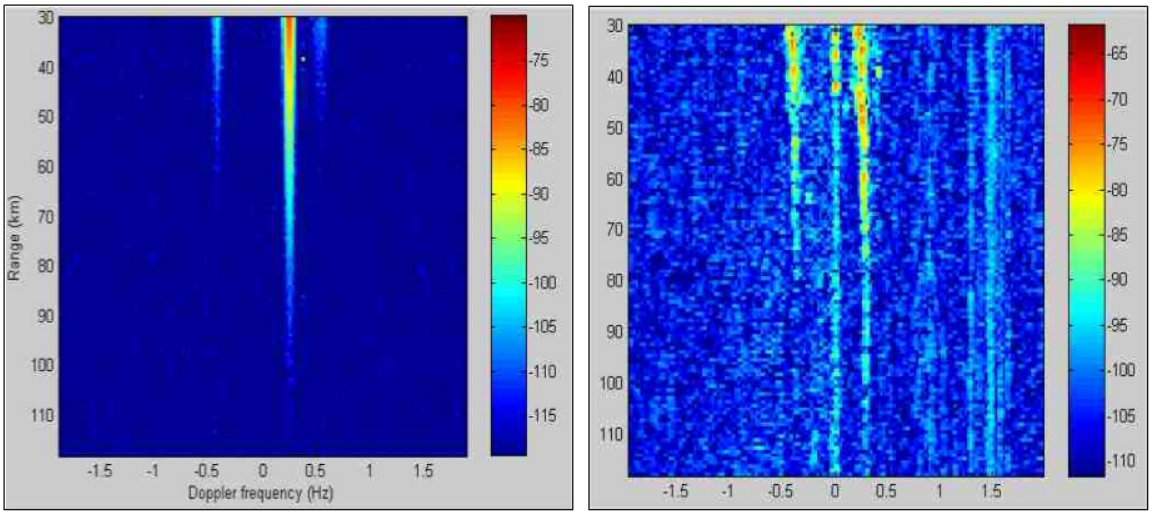

Figure 4.29: Comparison between a simulated Doppler range image and an image obtained with real data after radar processing

It is interesting to compare the simulation results with Doppler range image obtained with real data. Figure 4.29 show a real Doppler range image on the right and the associated Doppler range image on the right, simulated with the same radar settings. Real meteorological data were not available that is why they have been roughly deduced from the real data (observing the Bragg lines orientation and level). The comparison is quite good except the presence of interferences and a central line with real data.

4.5 Interest of the simulated database

The interest of sea echoes modeling are numerous :

4.5.1 Sea clutter knowledge

First, they can help to familiarize with sea clutter, to better understand and visualize the Bragg phenomenon, to see its variation in function of the frequency, the sea state, etc.

4.5.2 Database to test sea clutter reduction algorithm

For the moment, real HF Surface Wave Radar data are still rare. For this thesis, the radar used to obtain real data files is a research radar system, studied in collaboration with Singapore. It is not an operational radar that is why we have only a few data files.

They have been acquired with the same bandwidth (400 kHz), at 3 different frequencies (f_c= 5.255 MHz, 10.750 MHz and 16.050 MHz) but the sea state is not specified, precise meteorological measurements should be organized. Moreover, detected targets are unknown so it is impossible to verify if the associated detected echoes are well located with a right level. Further experiments with cooperative targets will be needed.

The simulated sea echoes database can then be a good intermediate solution to test signal processing algorithms in every condition. Even if they will never replace real data because they do not have exactly the same properties, but we will have an idea about performance of the sea clutter reduction algorithm in function of every parameter.

4.5.3 Predictive tool for optimum radar settings

Before building a radar system, a lot of questions have to be answered in order to size the radar for the best. For example, the transmitted frequency is a sensitive parameter.

- **For the low frequencies of the HF band (4-8 MHz) :** At these frequencies, the advantages are the long reachable ranges and the low level of sea clutter. Nevertheless, Bragg lines can be really disturbing, especially for boats sailing at the same velocity than sea waves. Moreover, the inconvenients are the important receiving array length. Finally, the beamwidth is spread in azimuth.
- **For the high frequencies of the HF band (20-25 MHz) :** On the contrary, at high frequencies, the receiving array length is less deployed, producing as a consequence a thiner radar beam. The inconvenient is that reachable ranges are not important and the sea clutter level is high.

It is difficult to find a compromise about the best frequency to transmit in function of the targets to detect. The simulated sea clutter database could then be an efficient tool to help radar operators for this choice before experiments. In fact, the simulations are realistic because they take into account the precise radar settings. It means that simulated sea echoes are very close to real ones.

The simulated database can then be used to size the radar in function of its applications. In fact, in function of the sea state and the type of targets to detect, simulations can give us an idea of the detection capabilities. With the meteorological and target parameters, we will deduce the best associated radar parameters. Operators will then be able to choose easily the optimum frequency and the power to transmit to obtain a good target detection in simulation.

A model of sea echoes after radar processing is available and provide many information about sea behavior for any event. For many cases, sea echoes are high and disturb target detection. These perturbations have to be reduced and a filtering process is considered in the following chapter.

Chapter 5

Development and validation of a filtering algorithm reducing sea clutter

Contents

The objective of this final chapter is to implement an adaptive filtering method in order to reduce sea echoes. To do that, the first step is to develop and test a filtering algorithm on simulated data and then to validate it on real data.

5.1 How to reduce ocean clutter?

5.1.1 Radar techniques

The sea clutter is proportional to the dimension of the surface illuminated by the receiving array of the HF Surface Wave Radar. That is why the first idea to receive less echoes coming from the sea surface is to reduce dimensions of the radar cell. Three major techniques can be used :

1. **Increase the radar bandwidth**

   The 27 MHz of the HF band are used for marine and aeronautical communications, broadcasting (professional, radio hams, CB), HF radars, ionospheric sounding, radio astronomy experiments, etc. That is why the HF spectrum is very congested. In general, it is difficult to find an important bandwidth of clear channels in this spectrum. The congestion depends on the geographical position of the radar where these external interferences are more or less present. For example, in the French countryside, only a few tens of kHz of bandwidth can be found but rarely more. Moreover, many parts of the spectrum are reserved and you need frequency authorizations to use them for radar experiments. Isolated countries can use a more important bandwidth up to a few hundreds of kHz.

2. **Reduce the beamwidth by increasing the array length**

   The receiving array length is already an inconvenience for HF Surface Wave Radars because they extend over several thousands of square kilometers. As coasts are often preserved, radars are difficult to install (not enough space, protected areas, etc). Increasing the array deployment is possible but it is more a geographical and clearance problem than a feasibility problem. It has to be discussed with coastal authorities.

3. **Use high frequencies to have a smaller wavelength, inducing a narrow beamwidth**

   If we use the higher part of the HF spectrum, it means that the detection capability of the radar will be reduced because of the important propagation losses. Moreover, Bragg clutter is said to be less present in low frequencies. A compromise has to be found.

5.1.2 Signal processing methods

After a study about sea echoes thanks to the simulated database, we now better know the interactions between sea waves and radar signals. In fact, the Bragg scattering is strongly based on a coherence principle because the scattering phenomenon occurs when

radar signals interact with selected sea waves. The important sea clutter contribution is due to the fact that a lot of waves respect the scattering condition at the same time, their crest being in phase all together. It means that there is a spatial regularity of sea waves and this phenomenon is often verified as presented in the following amateur photographs (see figure 5.1).

Figure 5.1: Different views of regular waves of the sea

It means that if this disturbing clutter appears because of a coherence principle, it is possible to reduce it using this property. This observation allows the use of noise mitigation techniques to reduce influence of sea clutter. These techniques are used to detect and filter coherent disturbing signals.

5.1.2.1 Applications of adaptive filtering

In function of interferences or noise to reduce, adaptive filtering will use different domains. The choice of the domain is made by trying to have the best separation between useful and disturbing signals, emerging a coherence between disturbing signals during the estimation.

- SAP filter ("spatio adaptive processing") : an angular filter is created by estimating the covariance matrix on the "fast time" or "slow time".
- STAP filter ("spatio-temporal adaptive processing") : an angular and temporal (slow time) filter is created by estimating the covariance matrix on the "fast time" or "slow time" or ranges.
- Filter to reduce sea clutter : in this thesis, the objective is to create a Doppler filter to reduce Bragg clutter. We can imagine to estimate the covariance matrix on the azimuth dimension or on the range dimension as presented in figure 5.2.

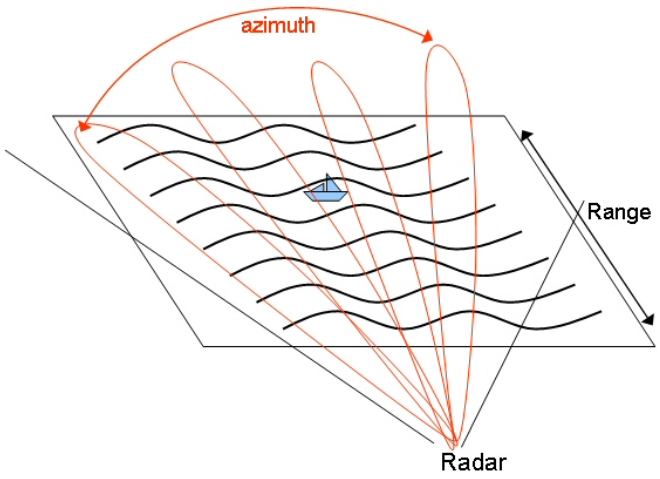

Figure 5.2: Definition of azimuth and range

In both cases, to obtain a good filtering, we need to have enough resolution in range or azimuth. In general, we have more range cells than beams in azimuths, that is why we will prefer to use adaptive filtering by estimating coherence along range cells. We can imagine that sea clutter is not coherent over long distances. The estimation of covariance matrix along ranges has the advantage, for each range, of using only the neighboring ranges where the sea echo is certainly the most stationary.

A method of adaptive filtering seems then to correspond to this problem of reducing coherent signals.

5.2 Choice of a signal processing method to reduce sea echoes: adaptive filtering

5.2.1 Mathematical recalling

5.2.1.1 Matrix calculation

To well understand this theoretical part about adaptive filtering, a recalling about matrix properties is necessary. In fact, in the following section, we will induce to use hermitian matrix.

An hermitian matrix is a square matrix equal to its conjugate transpose.

$$A = A^H = (A^t)^*$$

In this matrix, the diagonal terms are real and the others are complex conjugates.

The eigenvalues and eigenvectors of a matrix A are given by :

$$A.v = \lambda.v$$

where λ is a scalar eigenvalue and v an eigenvector associated to λ.

For an hermitian matrix, all the eigenvalues are real and two eigenvectors associated to two distinct eigenvalues are orthogonal. The set of eigenvectors of an hermitian matrix can then define a new vector space basis.

A quadratic form is a function $Q(X) = X^H.A.X$ with X column vector of the $\mathrm{C^N}$ space (N being the dimension of A). If A is hermitian, Q is real. And if $Q(X) \geq 0$ for all the vectors X, then Q is defined positive and consequently A also is. That means that eigenvalues of A are real and positive.

An hermitian matrix A which is define positive can be expressed in function of its eigenvalues and its eigenvectors :

$$A = V.\Lambda.V^H \tag{5.1}$$

In this formula, Λ is the diagonal matrix containing the eigenvalues of A. V is the matrix of the eigenvectors of A, arranged in column in the same order than the eigenvalues. This is a unit matrix such as $V^{-1} = V^H$.

$$\Lambda = \begin{pmatrix} \lambda_1 & 0 & 0 & 0 & 0 & 0 \\ 0 & \lambda_2 & \ddots & \ddots & 0 & \vdots \\ 0 & \ddots & \ddots & \ddots & \ddots & \vdots \\ \vdots & \ddots & \ddots & \lambda_i & \ddots & 0 \\ \vdots & 0 & \ddots & \ddots & \ddots & 0 \\ 0 & 0 & 0 & 0 & 0 & \lambda_N \end{pmatrix}$$

In fact, the equation 5.1 corresponds to a change of coordinates system, Λ represents the matrix A in the new coordinates system defined by its eigenvalues.

The inverse of an hermitian matrix A can be calculated in function of its eigenvectors :

$$A^{-1} = V.\Lambda^{-1}.V^H$$

Λ^{-1} is a diagonal matrix whose eigenvalues are $1/\lambda$. So, $\mathrm{A^{-1}}$ has eigenvalues being $1/\lambda$ and its eigenvectors are the same than those of A. The matrix A^{-1} is also a positive hermitian matrix.

The rank of a matrix can be defined by different ways, all are equivalent :

- The rank of A is the number of vectors linearly independent that A can generate.
- The rank of A is the number of columns or lines that are linearly independent.
- The rank of A is the maximum dimension of a square matrix extracted from A with a non null determinant.
- The rank of A is the number of eigenvalues of A that are non null.

If A is said to be full rank, it means that its determinant is not null, its eigenvalues are not equal to 0. And in this case, the matrix can be inversed.

5.2.1.2 The covariance matrix and its properties

The notion of intercorrelation is used to measure the degree of similarity between two signals more or less shifted in time. The autocorrelation measures periodic characteristics of a signal. To define this autocorrelation concept, the covariance matrix R is used. If it is calculated on one signal only, we obtain information about characteristics of this signal. The sum of each of its diagonals provide values of the autocorrelation function for different shiftings.

In order to calculate the covariance matrix, two domains must be defined :

- The **reference domain** contains the signals necessary for the calculation of R. It is the domain on which the filter is applied. This application domain can use one or several dimensions simultaneously (this is called multi-dimensional filtering).
- The **integration domain** is the domain on which R will be integrated to obtain the best estimation as possible. It is the same comment than in the previous point, the covariance matrix can be estimated on several dimensions simultaneously.

These two domains can be distinct or merged. It means that the adaptive filtering can be applied on every of the previous dimensions (defined in the paragraph 1.7) and the covariance matrix can be estimated on the same dimension or on another dimension.

The covariance matrix cannot be perfectly known, only an estimation of it is possible :

$$R = E\left[X.X^H\right] = \frac{1}{M_{estimation}} \sum_{i=1}^{M_{estimation}} X_i \cdot X_i^H$$

X is a column vector defined on the reference domain with a dimension of $\mathrm{N_{ref}}$. $\mathrm{X_i}$ is a realization of X in the integration domain. $E[\,]$ is the calculation of the mean on the integration domain. And finally, $\mathrm{M_{estimation}}$ is the dimension of the integration domain, this value has to be high enough for R to be well estimated.

The way R is constructed, it is a positive hermitian matrix and its dimension is ($\mathrm{N_{ref}}$,$\mathrm{N_{ref}}$), $\mathrm{N_{ref}}$ being the number of "sensors". If R is full rank, it is possible to calculate $\mathrm{R^{-1}}$, its eigenvalues λ are not null.

If the "sensors" of the reference domain measure at the same time white noise and signals, R can be written :

$$R = R_S + \sigma^2.I$$

R_S is the covariance matrix of the signals, σ^2 is the white noise variance and I the $\mathrm{N_{ref}}$-dimension identity matrix. Note that the white noise and signals are independent.

If R contains p non correlated signals and if all are independent from white noise, the

eigenvalues are given by :

$$\left(\underbrace{\lambda_1 + \sigma^2, \lambda_2 + \sigma^2, ..., \lambda_p + \sigma^2}_{p\ values}, \underbrace{\sigma^2, \sigma^2, ..., \sigma^2}_{N_{\text{ref}} - p\ values} \right)$$

The λ_i are the different signals powers, which we add the noise variance. The associated eigenvectors correspond to the "directions" of signals contained in R and these "directions" are defined in the reference domain.

The matrix R will only distinguish N_{ref} - 1 signals at the most, one dimension being dedicated to white noise that we find in any system. If the number of signals are superior to N_{ref} - 1, the lowest signals will be merged into the lowest eigenvalue.

If the "sensors" measure interferences independent from other signals,

$$R = R_S + R_B + \sigma^2.I$$

where R_B is the covariance matrix of the interferences. The adaptive filtering will try to reduce these interferences.

The eigenvalues calculation will allow separation of N_{ref} - 1 signals that it is possible to have in R, only if $M_{estim} \geq N_{ref}$. If this condition is not respected , there will be N_{ref} - M_{estim} eigenvalues of R that will be non null and the consequence is that R is not inversible anymore. This is a problem for adaptive filtering because filters are calculated using R^{-1}. Moreover, in literature, Reed and al [23] shown in 1974 that the best estimation of signals contained in R is obtained with the following condition : $M_{estim} \geq 2.N_{ref}$. This inequality will be explained and demonstrate in the following part. If R is not inversible, the adaptive filter will be calculated thanks to other methods. They are based for example on the eigenvalues decomposition ("eigencanceler").

5.2.2 Adaptive filtering principle

Consider Doppler range data. Let X be the column vector of the reference domain (Doppler cells).

$$X = \begin{pmatrix} x1 \\ x2 \\ \vdots \\ x_N \end{pmatrix}$$

For detection, choose between two hypothesis, the noise-only hypothesis H_0(noise is assumed to be a collective reference to background noise, clutter and jammers) and the signal-plus-noise hypothesis H_1. The expected value of X, given H_0 (noise only), is :

$$E(X) = 0$$

and the expected value of X, given H_1 (signal plus noise) is :

$$E(X) = S$$

where S is the column vector

$$S = \begin{pmatrix} s1 \\ s2 \\ \vdots \\ s_N \end{pmatrix}$$

For the hypothesis H_1, the noise is $X - S$.

In order to better detect the presence of a signal S, one designs a filter which is "tuned to" S in such a manner that the effects of noise and interference are minimized. As we shall see, one criterion which accomplishes this is the maximum signal-to-noise principle. Reed et al. [23], shown that if the noise and interference approximate Gaussian processes, then a maximization of the signal-to-noise ratio is equivalent to a maximization of the probability of detection. It is in this sense that the maximum signal-to-noise criterion is an optimal principle. In fact, this is an optimal Neyman-Pearson detector[1] for a known signal vector in colored Gaussian noise with a known covariance matrix is linear, i.e., it consists of a linear combination of the components of the vector.

The filter, needed to detect S, is then a weighted sum of the components of X. If the weight vector is given by :

$$W = \begin{pmatrix} w1 \\ w2 \\ \vdots \\ w_N \end{pmatrix}$$

and the output of the filter is the scalar :

$$y = \sum_{i=1}^{N} \bar{w_i}.x_i = W^H.X$$

where $\bar{w_i}$ denotes complex conjugation and W^H denotes the conjugate transpose of the column matrix W. The first and second order statistics of y, assuming hypothesis H_1, are the mean :

$$E(y) = W^H.S \tag{5.2}$$

[1]The Neyman-Pearson criterion defines the maximum probability of detection while not allowing the probability of false alarm to exceed a certain value α. In other words, the optimal detector according to the Neyman-Pearson criterion is the solution to the following constrained optimization problem : max(Detection probability) such that (False Alarm probability) $\leq \alpha$.

and the variance :

$$Var(y) = E\,|Y|^2 - |Ey|^2 = E(W^H.N.N^H.W) = W^H.R_N.W \tag{5.3}$$

where R_N is the covariance matrix of the noise, given by $R_N = E(N.N^H) = (En_i.\bar{n_j})$ for i, j=1,2,...,N, where the n_j are the noise components of X_j.

In practice, the noise covariance matrix is typically not known. The common approach is to estimate it from a secondary data set that does not contain the signal of interest. In radar, the secondary data may be composed of signals from range cells adjacent to the one under observation.

The output signal-to-noise ratio is the expected signal power out of the filter y divided by the noise power Var(y). Thus, by 5.2 and 5.3,

$$(\frac{S}{N})_{opt} = \frac{|Ey|^2}{Var(y)} = \frac{\left|W^H.S\right|^2}{W^H.R_N.W} \tag{5.4}$$

The "best" or optimum filter W_0 is obtained by maximizing the signal-to-noise ratio given in 5.4. This maximization can be done by various methods. Here we use the following easily proved fact. If X and Y are two N-component column vectors and R_N is a positive definite N $\times$ N hermitian matrix, then :

$$(X, Y) = X^H.R_N.Y$$

is an inner product of the vector space of N-component column vectors. An important property of an inner product is the Schwartz inequality :

$$|(X, Y)|^2 \leq (X, X)(Y, Y). \tag{5.5}$$

If the signal-to-noise ratio 5.4 is re-expressed in terms of the inner product, we have :

$$(\frac{S}{N})_{opt} = \frac{\left|(W, R_N^{-1}.S)\right|^2}{(W, W)} \leq \frac{\left[(W, W)\,(R_N^{-1}.S, R_N^{-1}.S)\right]}{(W, W)}$$

$$= (R_N^{-1}.S, R_N^{-1}.S) = S^H.R_N^{-1}.S \tag{5.6}$$

where the bound on the right follows from the Schwartz inequality 5.5. The bound on the right in 5.6 can be attained if one lets the filter W in 5.4 be given by :

$$W_{opt} = k.R_N^{-1}.S \tag{5.7}$$

with k a complex number.

Thus W_{opt}, is the optimum filter, the optimum set of filter weights, for the detection of S in the presence of noise. This method to find the optimum filter is called the Sample Matrix Inversion (SMI).

5.2.2.1 Optimum number of data samples needed for the estimation of $\mathbf{R_N}$

The weights, i.e. the components of W_{opt}, are adapted to new situations by processing a number of independent samples of received data. The different methods of processing the data to estimate W_{opt} require different numbers of independent samples for the same level of performance. That is, the convergence to achieve a certain signal-to-noise ratio is dependent on the adoption criterion. Let K be this number of independent samples of data. $\hat{R_N}$ is the notation of the noise covariance matrix estimated with K samples (which is called the sample covariance matrix).

If one chooses $\hat{R_N}$ for R_N in the optimum matched filter criterion 5.7, the filter has the form :

$$\hat{W} = k.\hat{R_N}^{-1}.S$$

Let us compute the output signal-to-noise ratio $(S/N|\hat{W})_{opt}$, assuming that the estimated filter $\hat{W}$ is held fixed.

$$(S/N|\hat{W})_{opt} = \frac{(S^H.\hat{R_N}^{-1}.S)^2}{S^H.\hat{R_N}^{-1}.\hat{R_N}.\hat{R_N}^{-1}.S}$$

Denote this normalized signal-to-noise ratio by $\rho(\hat{R_N})$.

$$\rho(\hat{R_N}) = \frac{(S/N|\hat{W})_{opt}}{S^H.R_N^{-1}.S} = \frac{(S^H.\hat{R_N}^{-1}.S)^2}{\left[(S^H.R_N^{-1}.S)(S^H.\hat{R_N}^{-1}.\hat{R_N}.\hat{R_N}^{-1}.S)\right]} \tag{5.8}$$

Evidently, the random variable ρ lies in the interval $0 \leq \rho(\hat{R_N}) \leq 1$. By a simple change of variable, the probability density of the normalized signal-to-noise ratio $\rho(\hat{R_N})$ is likewise a beta function distribution, namely,

$$P(\rho) = K!/[(N-2)!(K+1-N)!] \cdot (1-\rho)^{N-2}\rho^{K+1-N} \tag{5.9}$$

where $0 \leq \rho \leq 1$ and $K \geq N$. The expected value of $\rho(\hat{R_N})$ can be computed, using 5.9, to be

$$E(\rho(\hat{R_N})) = \frac{K+2-N}{K+1}$$

This is the expected loss in power ratio if only K samples of data were used to estimate $\hat{R_N}$. Expressed in decibels, this expected loss in power ratio is :

$$loss = -10.log_{10}(E(\rho(\hat{R_N}))) = -10.log_{10}(\frac{K+2-N}{K+1})$$

If one wishes to maintain an average loss ratio of better than one half (less than 3 dB) by 5.7 and 5.9, at least $K = 2N - 3 \cong 2N$ samples of data are needed.

5.2.2.2 Consequences of the adaptive filtering

- The power of signals is inversed by adaptive filtering. The highest signals become the lowest ones and inversely.
- The adaptive filtering creates a hole in the interferences direction.
- The Fourier transform of signals X can be written as $X_f = T^H \cdot X_t$ with T matrix defining the discrete Fourier transform. T is chosen such as the vectors X_f and X_t have the same dimension. T is a unit matrix ($T^{-1} = T^H$. The adaptive filtering technique can be applied on the signals X or on their Fourier transform. The obtained results will be the same.
- The adaptive filtering will be all the better since the covariance matrix contains only the disturbing signals that we want to reduce (noise reference only) and none of the useful signals (targets). It means that the useful signals must not be present in the matrix R (or if they are, their level have to be very low). To solve this problem, many solutions are possible in function of the targets level:

  1. Use of sensors receiving only disturbing signals
  2. The ideal case (which is valid whatever the targets level) is to use a noise only reference to estimate R, a reference identical to the one surimposed to useful signals.
  3. If useful signals are low and inferior to the unwanted interferences to remove, they can be included in the estimation of R and they will not be so much affected by the adaptive filtering.
  4. If signals have the same level that interferences, it is necessary to protect them by tricks (addition of a white noise or "diagonal loading", blocking matrix, sub-blocks cutting, etc)

5.3 Real data analysis : estimation of coherence

As presented in the previous part about theory of adaptive filtering, characteristics and efficiency of filters are highly dependent on the coherence of processed signals. To size these filters (filter dimension, estimation duration), it is necessary to study if these signals are "stationary" or coherent in the range domain.

The interest of the coherence study is to determine the coherence extent between sea echoes spectra along range cells. The number of coherent consecutive spectra will define the number of points of the integration domain, meaning the number of range cells to take into account in the estimation of the covariance matrix.

The sea coherence depends on many factors :

- **Range resolution :** it is simple to imagine that the smaller the range cells will be, the higher the coherence will be.
- **Sea state :** it is the same for sea state, a calm sea with regular waves will be better than a storm on the ocean.

- **Radar frequency :** in function of the carrier frequency, different sea waves will backscatter the electromagnetic wave to produce sea clutter. If we use low frequencies, they will interact with sea waves having a long wavelength. Details of this phenomenon are available in the chapter 4.
- **Integration time :** the longer the integration time is, the better the frequential resolution will be. But if the integration lasts for too long, sea state may change and may reduce the induced coherence extent.

5.3.1 Method 1 : Estimation of coherence extent by coherence function

What is called coherence is normally the fixed relationship between waves in a beam of an electromagnetic radiation. In fact, two wave trains of this radiation are coherent when they are in phase. That is, they vibrate in unison. In other domains, the term coherence can also be used to describe systems that preserve the phase of the received signal. In this thesis, the coherence is the similarity between consecutive spectra in terms of phase and amplitude.

For example, to study coherence between spectra along range cells on this following real data (see figure 5.3), it is necessary to choose a criteria.

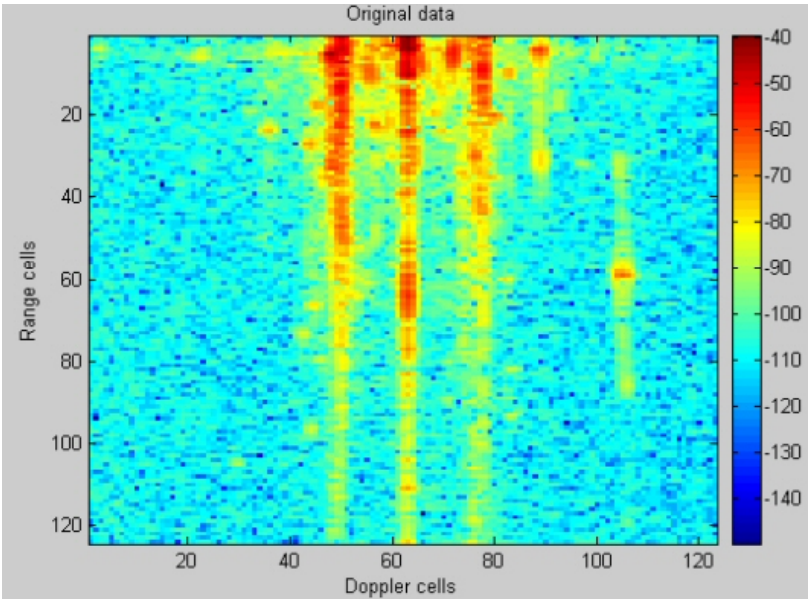

Figure 5.3: Doppler-range image to study

5.3.1.1 Coherence function

The first chosen criteria is the coherence function. In fact, the frequency domain "correlation" between input and output signals of a system can be defined as the ratio of the correlated cross power (i.e. the cross spectrum) to the uncorrelated cross power. The coherence function is an useful tool in helping you validate the quality of a frequency response measurement. Only when the system measuring system is "perfect", you will get a coherence of 1. In addition, errors in your measurement will also result in reduced coherence.

In fact, we consider a spectrum at a given range cell k called $spectrum_k$ (line vector) and the coherence function is determined with the spectrum of its neighboring range cell k+1 called $spectrum_{k+1}$ is :

$$C_{xy} = spectrum_k \cdot spectrum_{k+1}^H$$
$$C_{xx} = spectrum_k \cdot spectrum_k^H$$
$$C_{yy} = spectrum_{k+1} \cdot spectrum_{k+1}^H$$

In this study, the coherence function criteria will be used to quantify the coherence degree between two spectra. Let f be the result of the following calculation :

$$f = \frac{|C_{xy}|}{\sqrt{C_{xx} \cdot C_{yy}}}$$

If f tends towards zero, it means that there is no orthogonality between these two consecutive spectra. If f tends towards one, there is a coherence.

But where is the limit between these two extreme results? We can fix a threshold that determines the coherence limit. If f is comprised between this limit and 1, signals will be considered as coherent. This limit is chosen by the operator. The lower the limit is, the less signals coherent will be. That is why the choice of the coherence threshold is very important because it will influence directly the final adaptive filter efficiency which is based on signals coherence. If incoherent signals are taken into account in the estimation of the covariance matrix, the filter will not be optimum at all. Afterwards, the threshold is fixed at 0,7 because it is a threshold which is not restrictive. This value is generally used in coherence estimation problems.

5.3.1.2 Display of coherence results

Let us take an example. On the considered set of data presented on the image 5.3, we count 124 range cells. If we take, for example, the twentieth spectrum as a reference and if we calculate its coherence function with the spectra of all its neighboring range cells, the result can be display on figure 5.4. First, we clearly notice a peak at the range shifting 20 with a perfect value of 1. It is normal because it characterizes the coherence between the reference spectrum and itself. Moreover, there is a coherence only with spectra in range cells very close to the reference cell. This observation is logical because a spectrum has more chance to be coherent with its direct neighbors rather than with distant spectra.

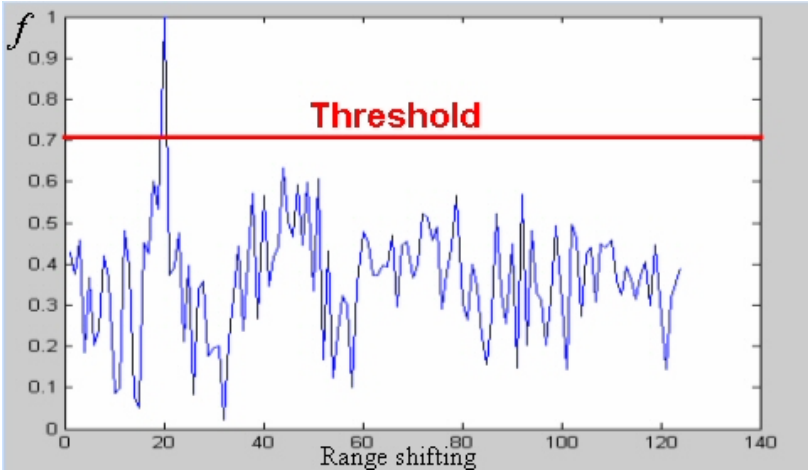

Figure 5.4: Coherence function of the spectrum of the range cell 20 with all other spectra

If the spectrum of the range cell 50 is chosen as a reference, the results of the coherence function calculation with spectra of all range cells will be :

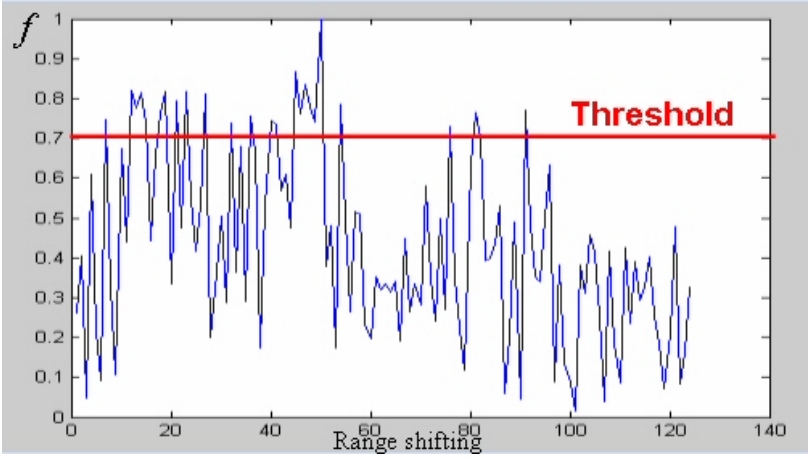

Figure 5.5: Coherence function of the spectrum of the range cell 50 with all other spectra

It is sometimes possible to "feel" the coherence to the naked eyes only in observing the Doppler range image. But it is sometimes more delicate, the coherence peaks of the image 5.5 for example are difficult to anticipate, contrary to the image 5.4.

To display simultaneously these results for every reference range cell, we propose a 3D display (see figure 5.6). The Y abscissa concerns the number of the range cell taken in reference, the X abscissa is the number of the range shifting. The third dimension is the value of the coherence function for the given couples. Note that we display only points above the threshold (here 0,7), other values are colored in blue.

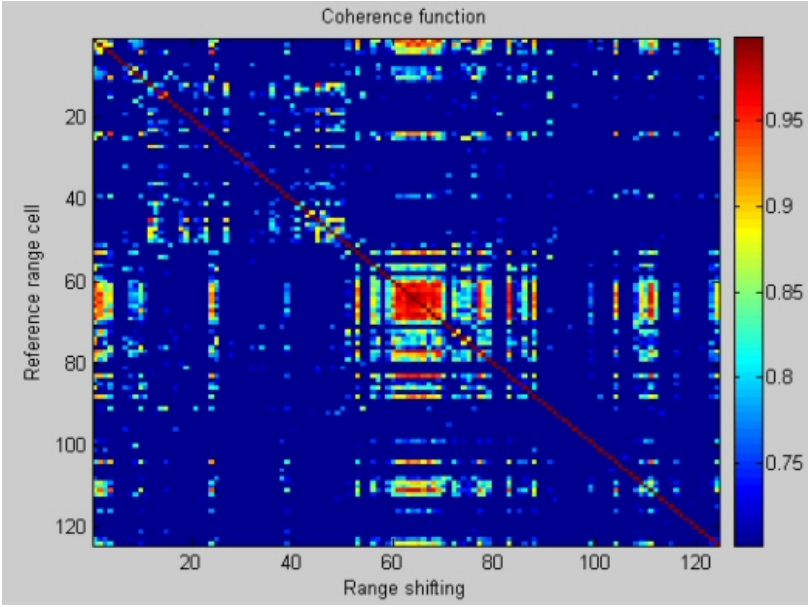

Figure 5.6: 3D coherence function of the image of the whole image

On the previous image, the diagonal red line at a coherence level of 1, is due to the maximum coherence of the spectra with themselves. A strong coherence area is visible between range cells 60 and 70. Referring to the original image to study (cf figure 5.3), this high coherence level is certainly due to the ground echo present at these distances. On this image, the coherence of Bragg line along cells is not obvious. Maybe, data have to be analyzed differently.

5.3.1.3 Selection of data for coherence analysis

On the following figures (5.7 and 5.8), the upper image is the result of coherence study on the whole image. The lower image is a selection of data in the domain $\pm 0.2\sqrt{f_c}$ (where f_c is the transmitted carrier frequency) which is the maximum theoretical extent of the second order Bragg clutter. The coherence result is quite the same. That is understandable because data not considered in the second sample are almost noise.

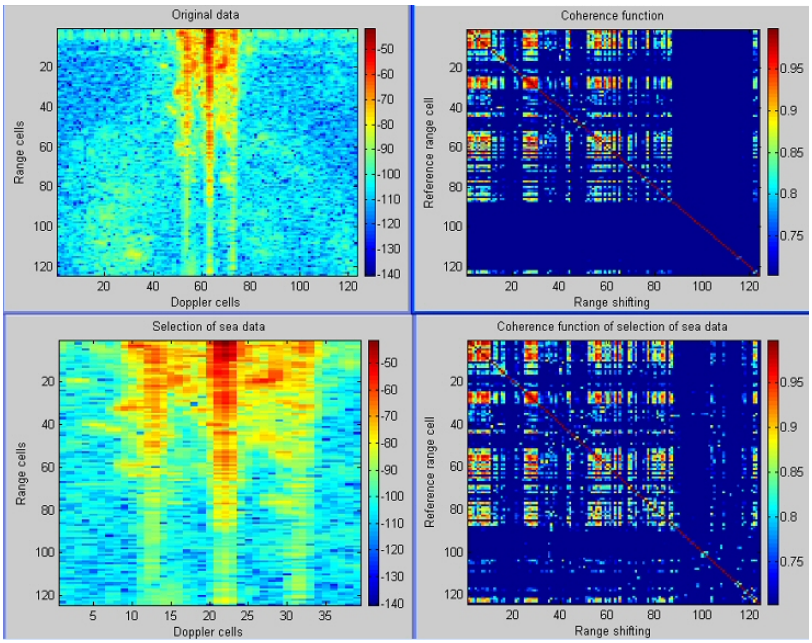

Figure 5.7: Comparison of coherence function with selected data (example 1)

The same example of coherence analysis on another real data set (see figures 5.8).

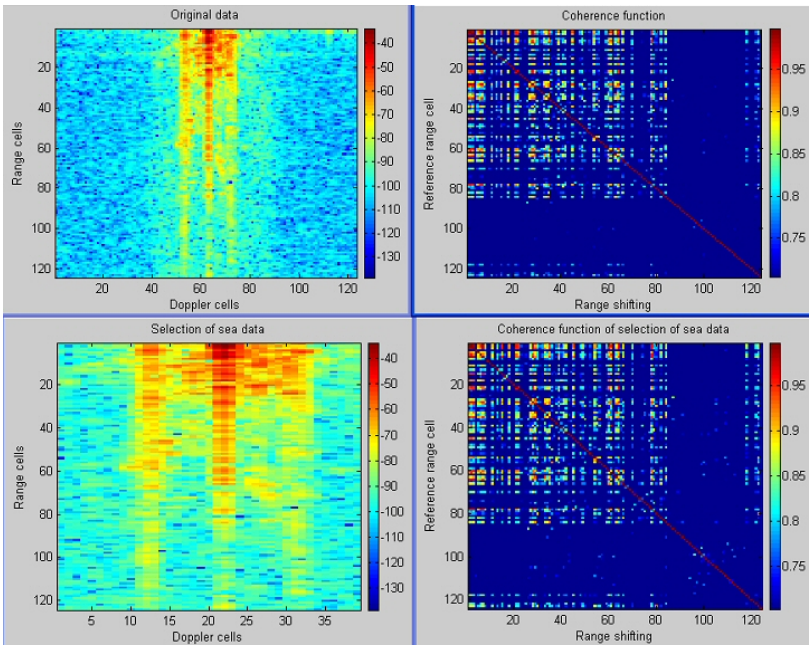

Figure 5.8: Comparison of coherence function with selected data (example 2)

It means that to avoid long computation time, it is better to select only the area to filter where Bragg clutter is present.

5.3.1.4 Coherence of the second order along range cells

To study coherence of the second order Bragg clutter along range cells, first order Bragg line should be ignored in the analysis. The idea is to "suppress" them implementing a kind of CFAR filter. CFAR means Constant False Alarm Rate. It consists in an adaptive thresholding. This CFAR has originally been invented as a detection technique to avoid an enormous number of detection if a unique threshold is fixed. It is a way to have an adaptive detector that uses surrounding cells to calculate a local noise. Figure 5.9 illustrates the CFAR principle that we apply on range cells [24]. In fact, it consists in taking reference cells around the cell under observation, to sum them to obtain a local noise level. Then, a threshold K is defined ; if the level of the considered cell is higher than this limit above the local noise (this is a comparison step representing by the letter C in the figure), the detection equals 1 otherwise 0. This operation is repeated on the next range cell and so on.

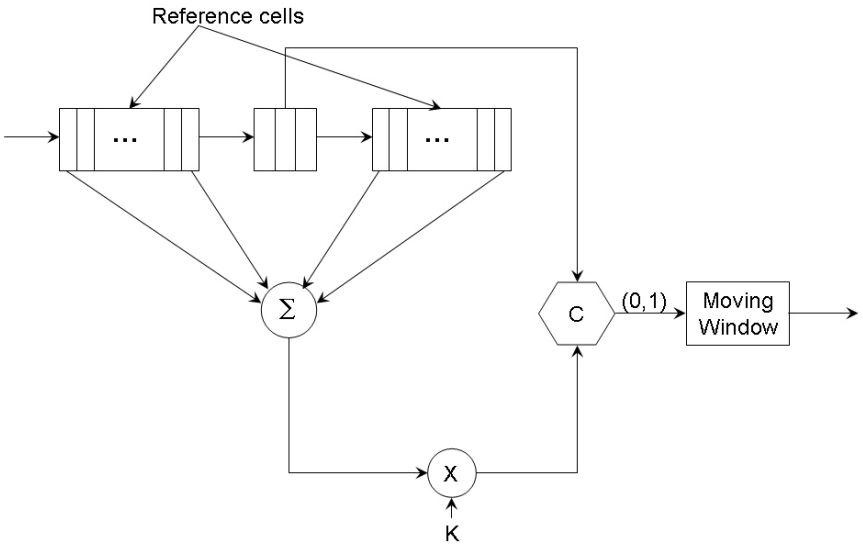

Figure 5.9: CFAR principle

By this way, we are sure that first order Bragg lines and ground clutter will be detected all along range cells, even if they have a decreasing level due to propagation losses. If we represent only non-detected points on a Doppler range image, Bragg lines, ground clutter and strong targets echoes will not be visible (see the left part of figure 5.10). We mainly have data coming from the second order. The coherence analysis can then be applied on these filtered data. Results are presented on the right part of figure 5.10).

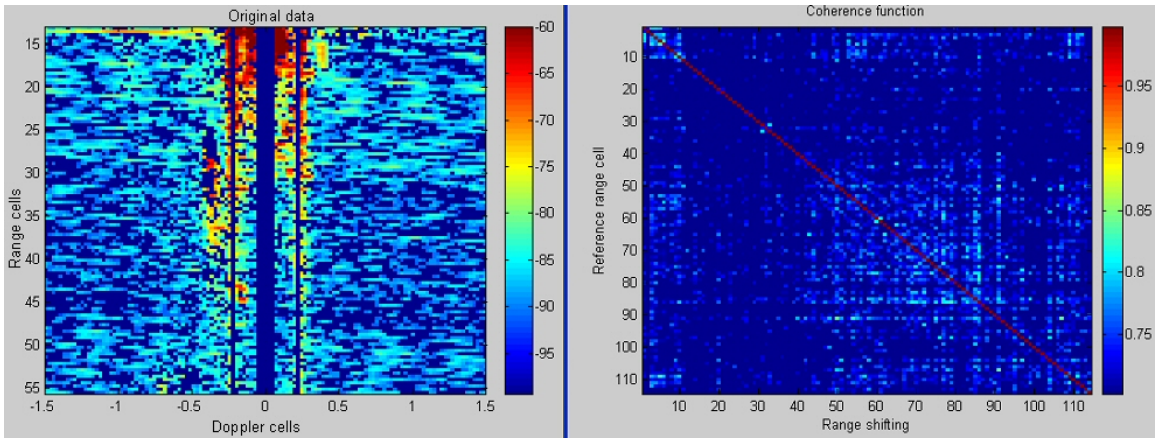

Figure 5.10: Coherence of second order along range cells

We notice that these filtered data are not coherent. Either second order is not coherent, either these filtered data do not represent second order but many target echoes. Maybe there is only second order clutter in the tens first range cells and it is not very visible on the rest of the Doppler range image.

5.3.1.5 Coherence of each line with itself along range cells

Now, if we are only interested in the first order Bragg line, it is possible to extract the Doppler domain where the line is and to apply the coherence analysis only on this sample.

On the first example on figure 5.11, we study coherence of the negative Bragg line. The resulting coherence image is totally red meaning that this Bragg line alone is very coherent all along range cells.

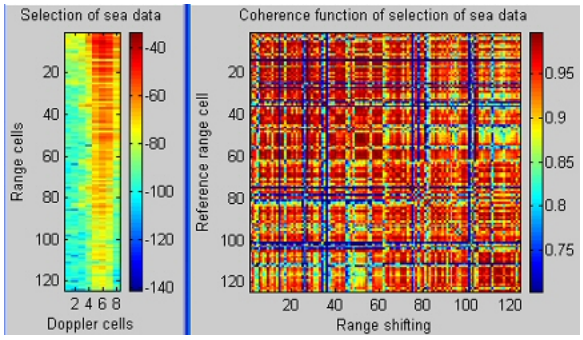

Figure 5.11: Coherence of negative Bragg line alone

Repeating this operation on the positive Bragg line (see figure 5.12), we notice that coherence is high except in the zones where the signal to noise ratio is not sufficient to distinguish Bragg line from noise. Moreover where targets are present, the coherence is bad.

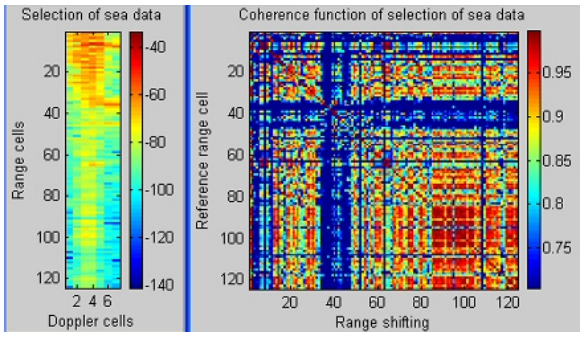

Figure 5.12: Coherence of positive Bragg line alone

It is also very interesting to study coherence of the central line at 0 Hz of Doppler. This line is composed of ground clutter echoes and also sometimes of material interferences. On the following figure 5.13, the central line alone is highly coherent along range cells. The coherence level decreases at the same time than the line level decreases.

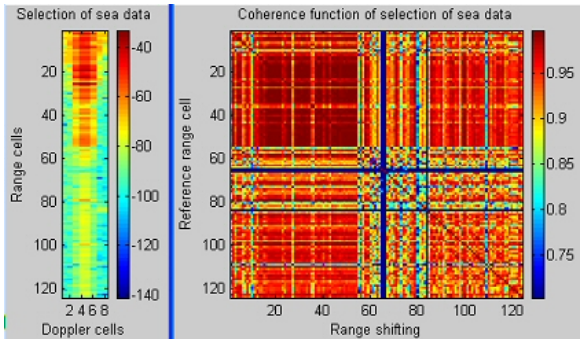

Figure 5.13: Coherence of central line alone

In conclusion, the negative Bragg line is coherent with itself along range cells (while the SNR is sufficient) and it is the same comment for the positive Bragg line. The 0Hz-Doppler line (called central line in the sequel) is also coherent with itself along range cells. But are they coherent if we analyze them all together?

5.3.1.6 Coherence of Bragg lines and central line all together

For this analysis, the idea is to study first the central line and then to increase the number of Doppler cells to see apparition of Bragg lines and their effect on coherence. The influence of the consideration of Bragg in the coherence analysis will then be obvious.

First, the central line is isolated, it is coherent with itself, as shown previously (see figure 5.14).

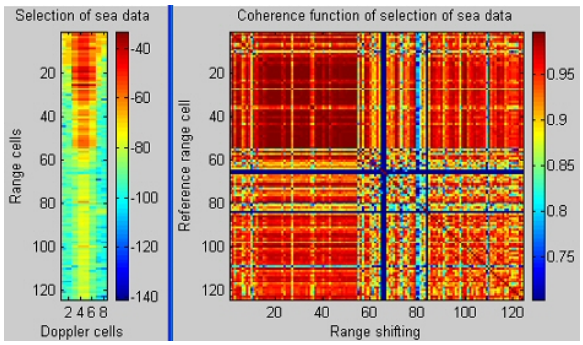

Figure 5.14: Coherence of the central line

Then, we take more data around this central line, we notice that the coherence decreases (see figure 5.15).

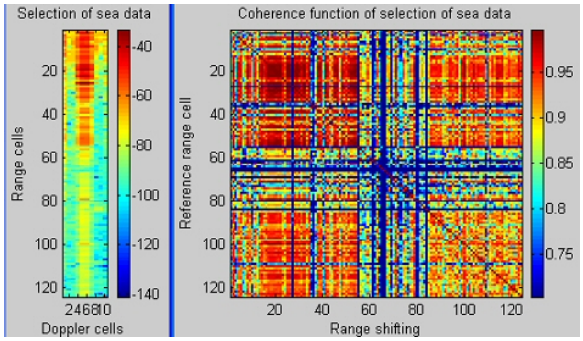

Figure 5.15: Coherence of extended data around central line

When we begin to take into account Bragg lines, the coherence is not good at all as presented on figures 5.16 to 5.18.

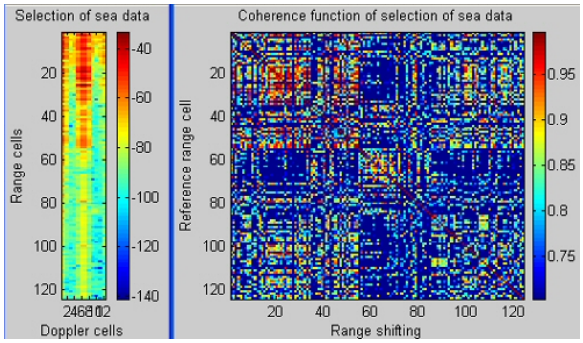

Figure 5.16: Coherence of extended data around central line

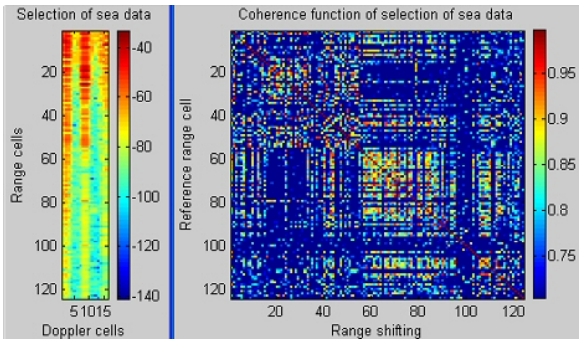

Figure 5.17: Coherence of extended data around central line

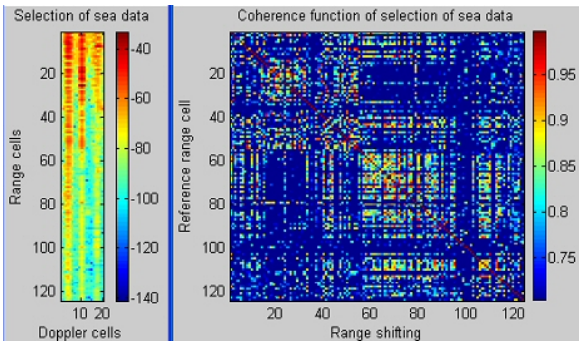

Figure 5.18: Coherence of the three lines

In conclusion, its means that if three coherent lines are analyzed together, they are not necessarily coherent all together. Each line is coherent separately but they do not vary the same way that is why the three lines coherence is different. It can easily be explained by the fact that coherence of three lines together is inferior to the sum of separated coherence.

5.3.1.7 Influence of the integration time on coherence study

The integration time Ti is the time of signal used to process an Doppler range image. To see its influence on the coherence, let us take two examples where the same set of data has been processed with Ti = 20,48 s and Ti = 40,96 s. Results are displayed on figure 5.19 and 5.20. The difference between both coherence results is not flagrant. The coherence is higher for a short Ti (mainly visible on coherence of the whole image) and it is logical because sea state change less during this short time.

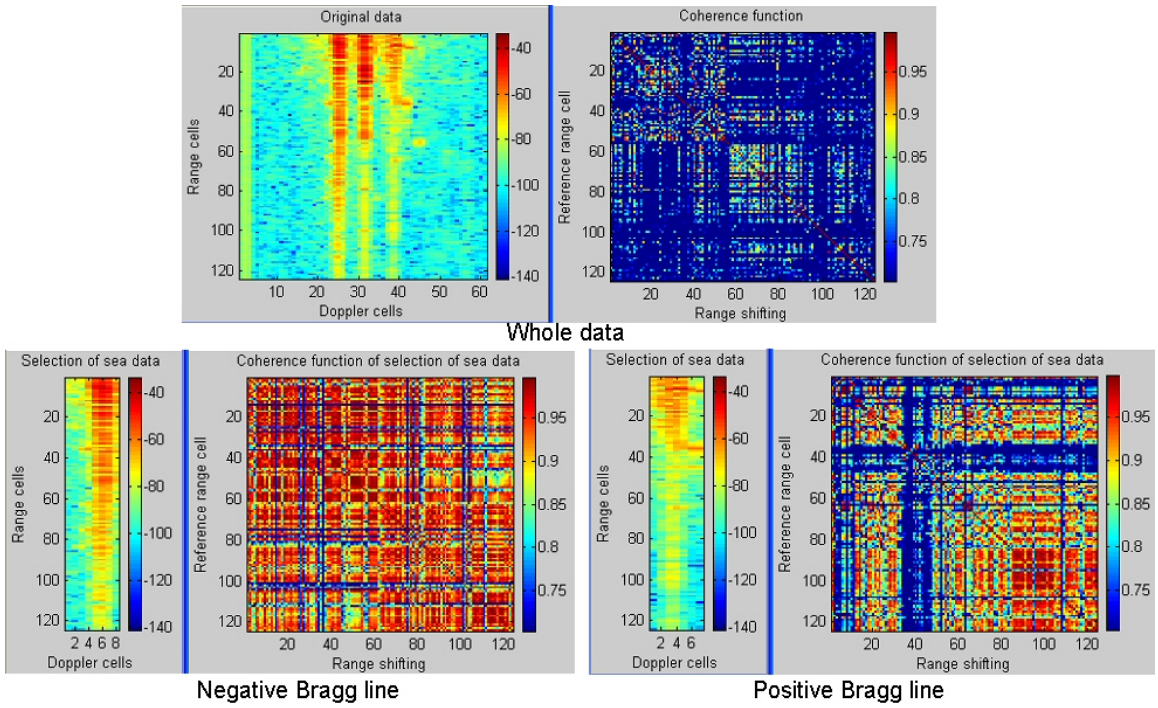

Figure 5.19: Coherence function for data processed with a short integration time of 20.48 s

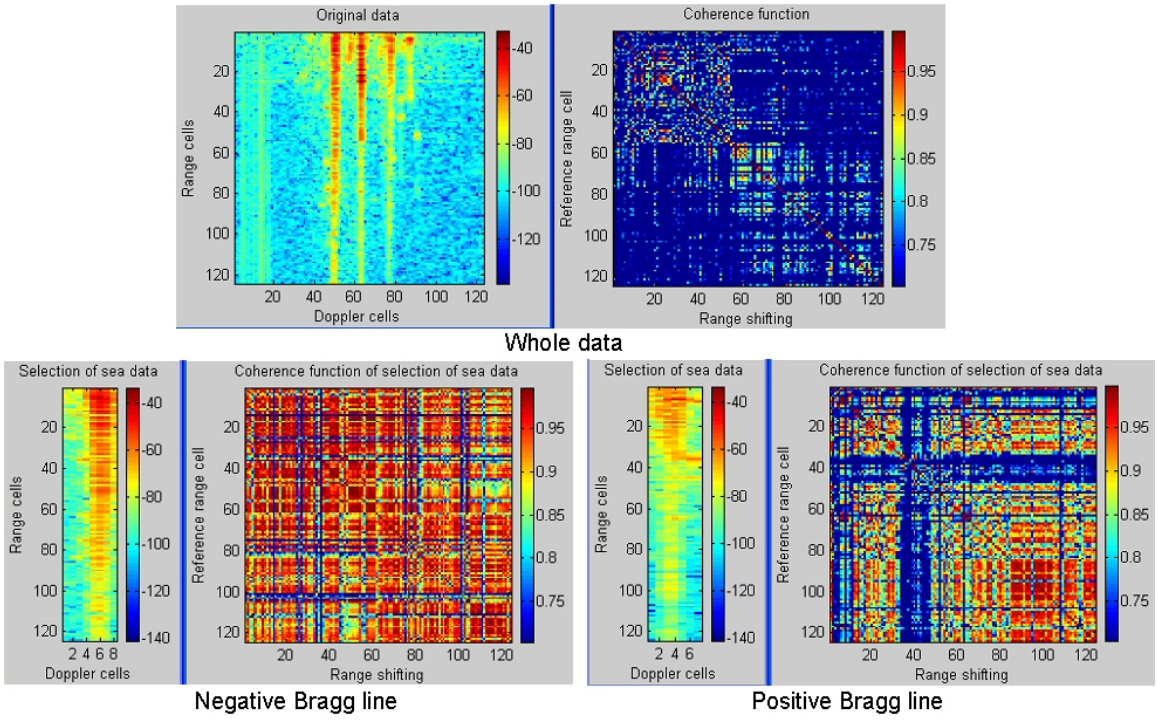

Figure 5.20: Coherence function for data processed with a long integration time of 40.96 s

5.3.1.8 Coherence of simulated data

It is interesting to study coherence of sea echo spectra. By the way they are modeled, they are coherent all along range cells. Let us verify this affirmation.

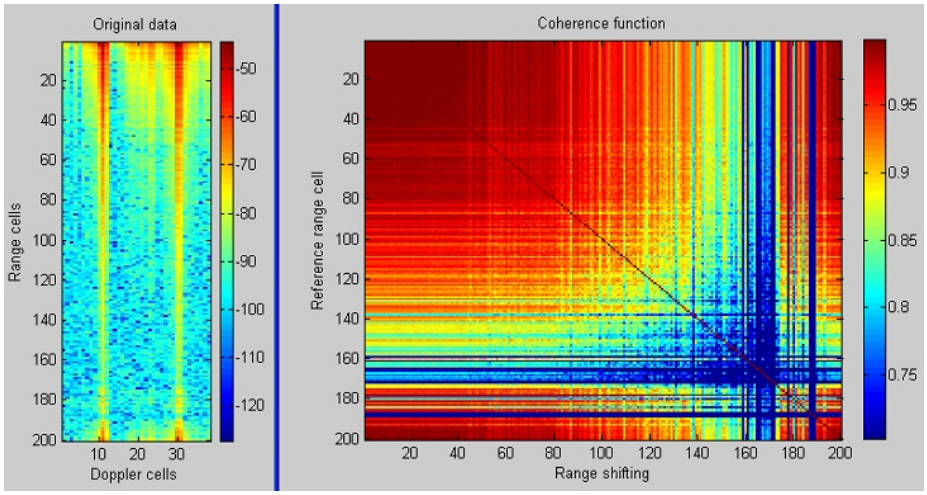

Figure 5.21: Coherence function for simulated Bragg lines

While the SNR is sufficient, simulated data are coherent along range cells.

5.3.1.9 Comparison of coherence between weighting and non-weighting data

The effect of using a weighting window for the Doppler processing reduce the Doppler lobes level and increase the width of principal peak. To see the impact of the weighting on the coherence, the same set of data has been processed with and without weighting window.

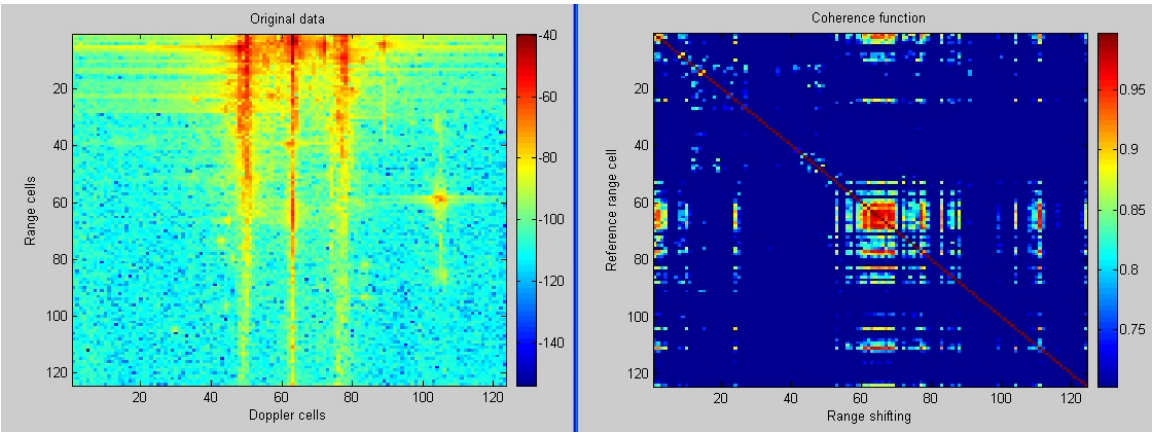

Figure 5.22: Coherence function of non weighting data

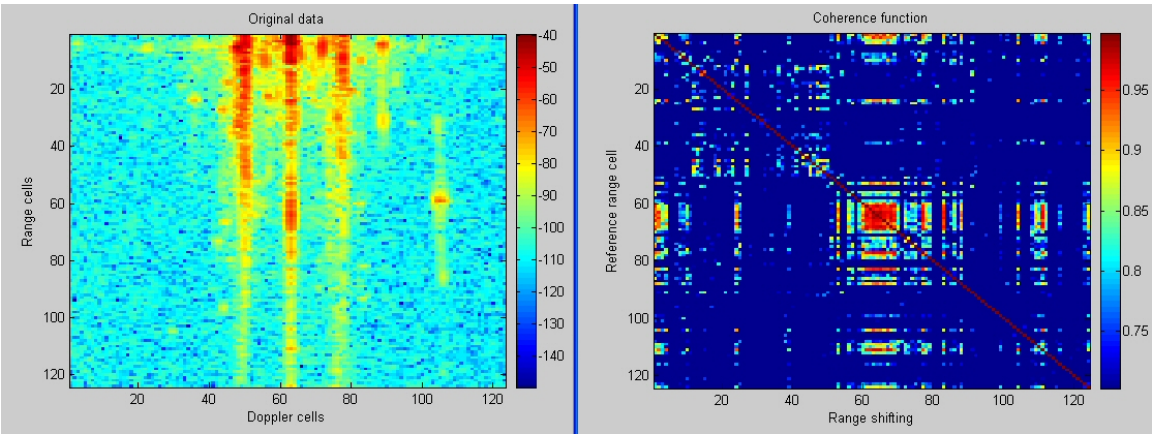

Figure 5.23: Coherence function of weighting data

By comparison between results proposed in figures 5.22 and 5.23, the weighting data seem to be more coherent than non-weighting data.

5.3.1.10 Coherence in Doppler dimension

All the previous results concerned coherence along range cells because this dimension will be used for the estimation of the covariance matrix. Even it is not necessary to study coherence of data along Doppler cells, it can be useful to know, for example, if first and second order Bragg clutter are coherent along Doppler cells or not. The analysis is exactly the same but now range lines are compared instead of spectra.

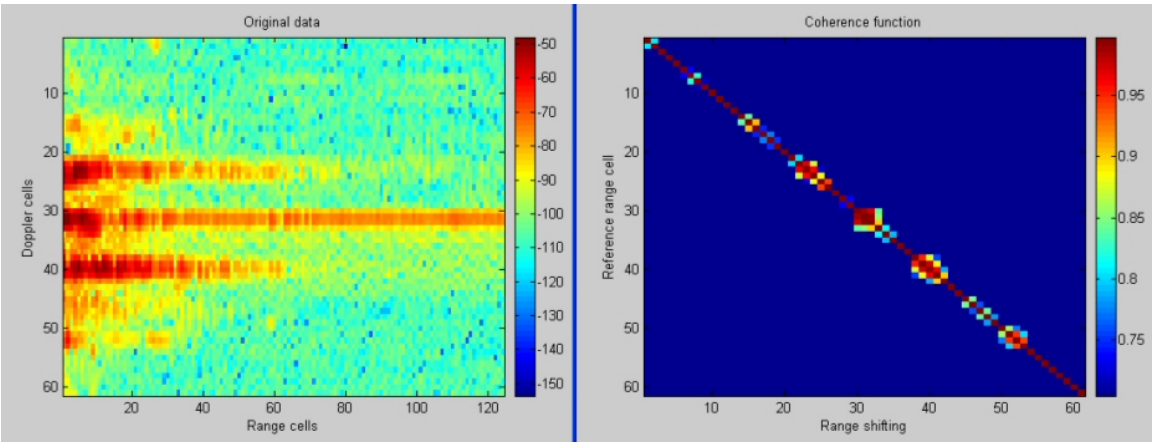

Figure 5.24: Coherence along Doppler cells

The result presented in figure 5.24 shows that coherence along Doppler cells is not good at all. Only a few cells around Bragg lines and central lines can be considered as coherent.

For adaptive filtering along range cells, this non-coherence is not a problem because we use this property on the range dimension.

5.3.1.11 Conclusions about coherence analysis with the coherence function method

- For adaptive filtering, we will only consider data where sea echoes are present, meaning the Doppler domain between $-0.2\sqrt{f_c}$ and $+0.2\sqrt{f_c}$.
- Second order Bragg clutter is not strong enough on our real data to conclude about its coherence.
- First order Bragg lines are coherent along range cells but they have a different coherence from the central line that is why to analyze coherence of Bragg lines, it will be necessary to divide the analysis areas.
- Data are more coherent for a short integration time.
- Simulated or real Bragg lines are coherent while their SNR is sufficient to distinguish them from noise.
- Coherence along Doppler cells is not good at all and that confirms the use of the range dimension to estimate the covariance matrix and the induced adaptive filtering.

In this section, a tool for coherence analysis has been perfected but we do not have enough HF Surface Wave Radar real data to conclude from a statistical point of view, for example about second order coherence (in the available samples, it is not visible enough). Moreover, we do not have information about coherence in function of sea state because sea state is not precised in the data files. It is the same problem for the influence of the transmitted carrier frequency. We have data for various frequencies but they have been acquired on different days, certainly with different sea states, different ships traffic, etc. That is why it is not possible to compare these data, it has no sense. For range resolution also, the study cannot be done because the bandwidth of the transmitted signal in the real data that we have is always 400 KHz (corresponding to a range resolution of 375 m).

5.3.2 Method 2 : Estimation of coherence extent by study of eigenvectors

In this section, another method is used in order to have a better signals separation and to analyze them in a way that is closer to the adaptive filtering. In fact, it analyzes coherence of the covariance matrix eigenvectors of processed signals. This covariance matrix is identical to the one used to calculate the adaptive filter, meaning that this way of analyzing stationarity of signals is really close to the calculation of filter, contrary to the first method based on the coherence function.

5.3.2.1 Presentation of the method

To study signals stationarity, several methods can be conceivable. Every method is based on tools coming from the spectral analysis, such as classical methods that use Fourier transform calculation or digital beam forming. Direction of arrival of signals is determined for different moments but these methods have a resolution limited by the processed signals dimension. A high resolution requires an important duration which is incompatible with the stationarity study.

In reality, to estimate signals stationarity, it is not necessary to determine their direction. The chosen method analyses coherence of the covariance matrix eigenvectors of processed signals. A covariance matrix is said to be well estimated if its estimation domain (M_{estim}) is higher than its dimension (N_{ref}). With the estimation condition : $M_{estim} \geq 2.N_{ref}$, all signals present in the covariance matrix are separated.

The covariance matrix can be decomposed in function of its eigenvalues and eigenvectors.

$$R = V.\Lambda.V^H$$

where V : Eigenvectors matrix and Λ : Diagonal matrix of the eigenvalues arranged in the same order than eigenvectors.

The covariance matrix being hermitian, the eigenvectors are orthogonal in two-two time. So, an eigenvector is only correlated with itself. Used eigenvectors form an orthonormal basis ($v_i^H.v_i = 1$ and $v_i^H.v_k = 0$ if i≠k).

Then, it is possible to write :

$$V^H.V = I$$

with I : Identity matrix.

As a general rule, to every signal present in the covariance matrix corresponds an eigenvector and an eigenvalue. In reality, this rule is only respected if R is well estimated, if the signals are not correlated together and if the measurement sensors are perfectly calibrated (meaning no amplitude, phase or coupling default). For this study, we will admit to respect these conditions.

The algorithms used for eigenelements decomposition arrange the eigenvectors in increasing or decreasing order of the eigenvalues. It means that if a signal fluctuates in level with time, its corresponding eigenvector will change its position in the V matrix, and it is the same for its eigenvalue in the Λ matrix.

The eigenvectors analysis is done on the whole matrix V and not vector by vector. The method analyses all signals whatever their level (sources or noise).

To measure stationarity of the reference eigenvectors, we define the function Q such as:

$$Q(i) = \frac{1}{\sqrt[Nref]{\prod_{k=1}^{Nref} \left| v_{reference}^H(i).v_{current}(k) \right|^2}}$$

where $v_{reference}(i)$: reference eigenvector number i and $v_{current}(k)$: eigenvector (sources and noise) number k. The denominator corresponds to the geometrical mean of the correlations between the reference eigenvector and the different current eigenvectors. If the reference eigenvector is still present in the current covariance matrix, only one correlation is equal to one and all the other are equal to zero. Then, the function Q is high. Otherwise,

all the correlations have a value comprised between 0 and 1 (both excluding) and the Q function is low. The inherent noise of the system disturbs these theoretical results.

To sum up this method, the reference eigenvectors matrix is estimated on a first temporal portion and it is compared to the current eigenvectors matrix at every moment. We then obtain a stationarity map of the reference eigenvectors according to the range cells. The stationarity results are given in $10.log_{10}Q$.

First, it is interesting to analyze simulated signals to familiarize with this method and the display of its results.

5.3.2.2 Analysis of simulated signals

Pure high level signal with white noise The first example is a simulated pure strong signal surrounded by a white noise. A pure signal refers to a mono-directional signal at any given time instant. Moreover, a pure signal has a constant amplitude and direction all through the processed data. The eigenvectors matrix is calculated on a first temporal portion and then compared to the current eigenvectors matrix of the different temporal portions, the first one included.

The left part of figure 5.25 is the considered data. In our case, the abscissa represents Doppler cells and the ordinate represents range cells. The middle part of the figure presents the instantaneous results for the current estimation number 25 of the eigenvectors matrix. The upper graph is the distribution of the eigenvalues of the current covariance matrix (the first eigenvalue is well superior to the others because it is the source and eigenvalues are arranged in decreasing order). The central image represents the correlation of the reference eigenvectors with the current eigenvectors. The lower image is the result of the Q function for the current estimation number 25 of the eigenvectors matrix, so it is the instantaneous stationarity of the reference eigenvectors for this precise estimation. Only the first eigenvector is stationary. Finally, the right part of the figure is the stationarity map with results for all current numbers. We notice that the first eigenvector is stationary all along data. The small variation of the stationarity measurement is due to the presence of the white noise, which disturbs the vector direction.

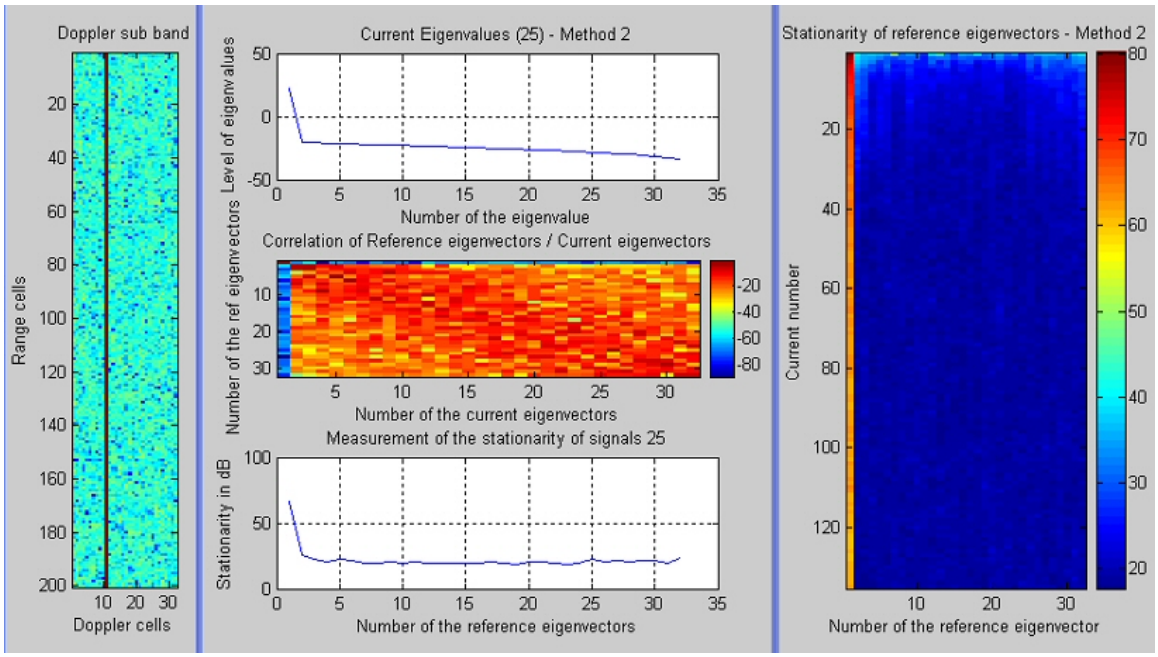

Figure 5.25: Stationarity of a pure signal (high level) with noise

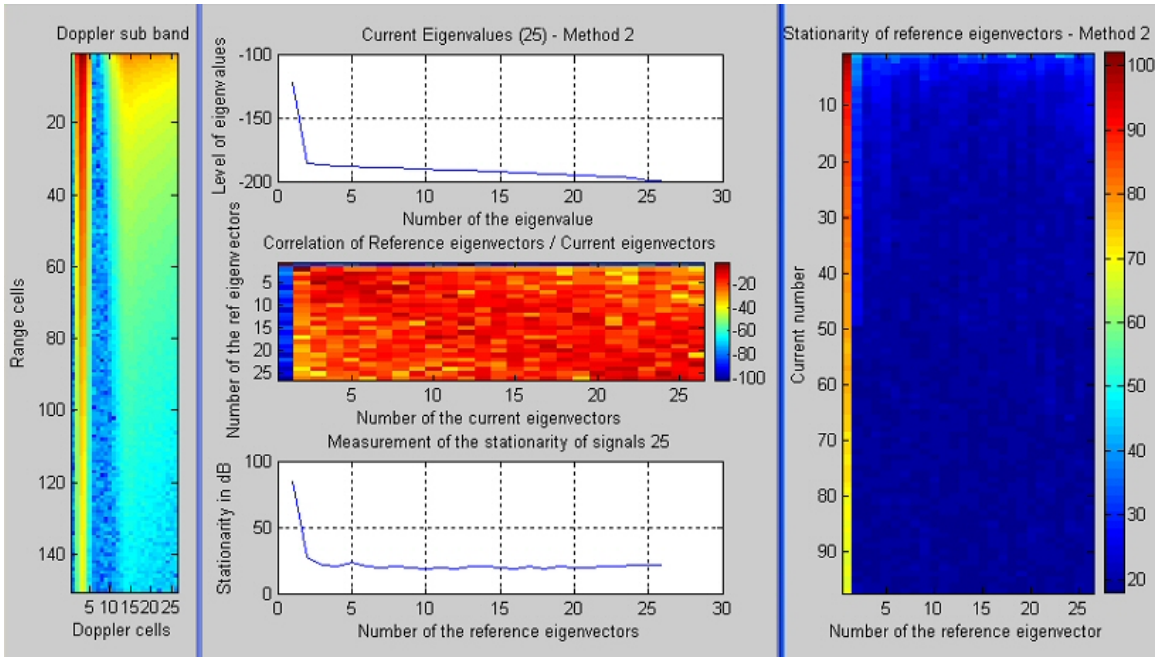

Figure 5.26: Stationarity of simulated sea echoes

Simulated sea echoes It is interesting to study stationarity of simulated sea echoes. The selected data comprise a first order Bragg line and second order continuum. The

reference eigenvectors matrix is estimated on a first portion of signal and then compared to the following estimations.

Stationarity results (displayed on figure 5.26) present only a stationary eigenvector with a decreasing amplitude, that we can assign to the first order Bragg line. The second order is maybe too low and spread in Doppler to be detected as a stationary signal. It may be a continuum of signals that are not separable.

5.3.2.3 Analysis of real data stationarity

For the real data stationarity study, five interesting Doppler sub-bands will be studied as illustrated on figure 5.27 :

- **Zone 1 :** zone with interferences
- **Zone 2 :** zone comprising the negative Bragg line
- **Zone 3 :** zone comprising the central line
- **Zone 4 :** zone comprising the positive Bragg line
- **Zone 5 :** zone with a real target

For each zone, the reference eigenvectors matrix is estimated on the first portion of the considered zone.

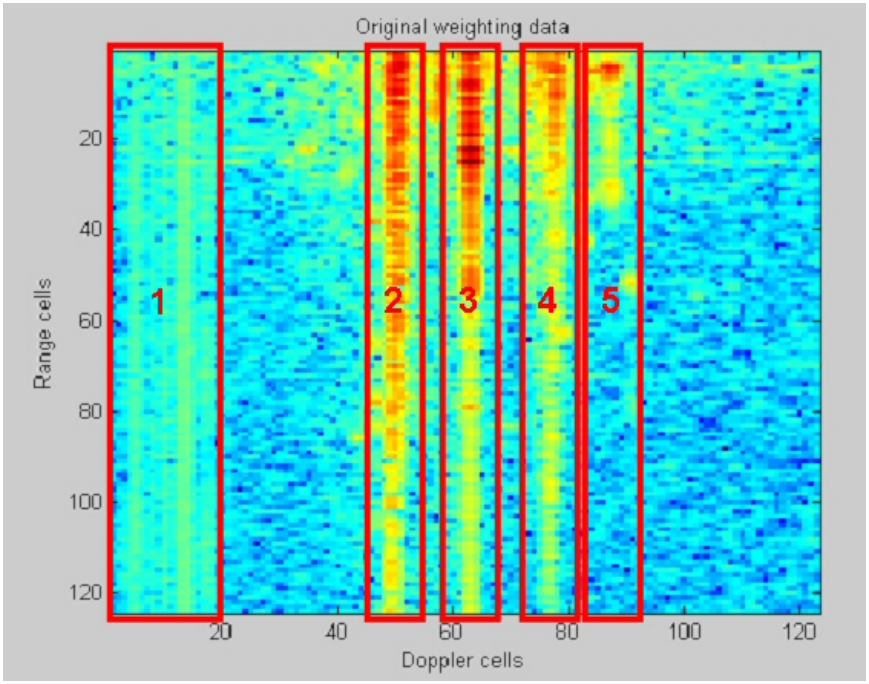

Figure 5.27: Real data to study with definition of the different zones to study

Stationarity of interferences (zone1) The HF spectrum is often congested and we often receive interferences echoes that are disturbing for the radar detection. These real data are a precise example of this problem. Methods such as anti-jamming techniques can be used to reduce their effect. According to this stationarity study (see results on figure 5.28), these interferences can be decomposed in several stationary signals. The first eigenvector and the last ones are stationary. It means that these jammers can be considered as a coherent source in our filtering algorithm and this is a positive point because they will be rejected at the same time than sea clutter.

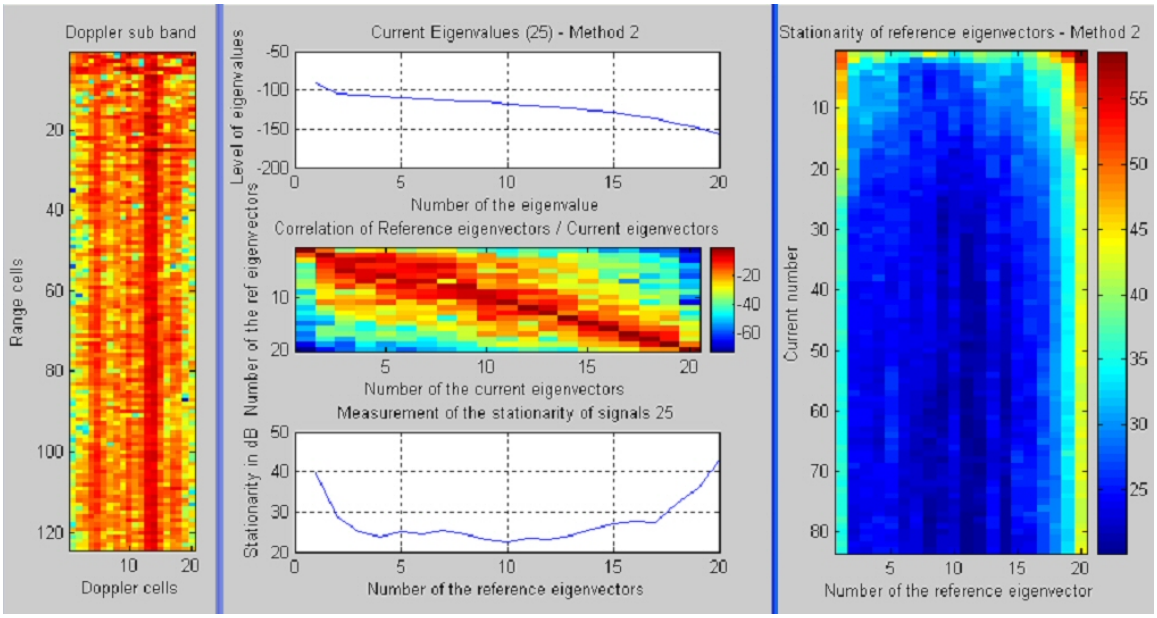

Figure 5.28: Stationarity of interferences

Stationarity of the negative Bragg line (zone 2) In this second zone, the negative Bragg line has been isolated from the other lines to be sure to study its own stationarity. Results on figure 5.29 show that a strong signal is stationary along range cells but there is a weak signal which seems also to be coherent.

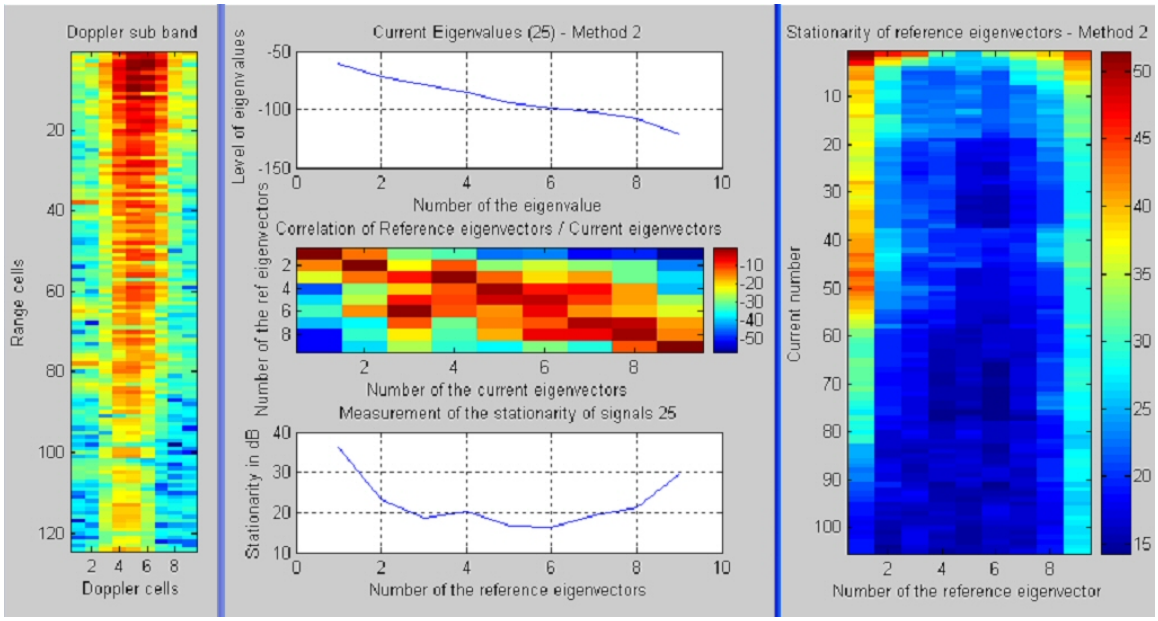

Figure 5.29: Stationarity of the negative Bragg line

Stationarity of the central line (zone 3) The central line is also considered as a stationary signal considering results of figure 5.30. We also notice that a stationary weak signal is detected in this sample.

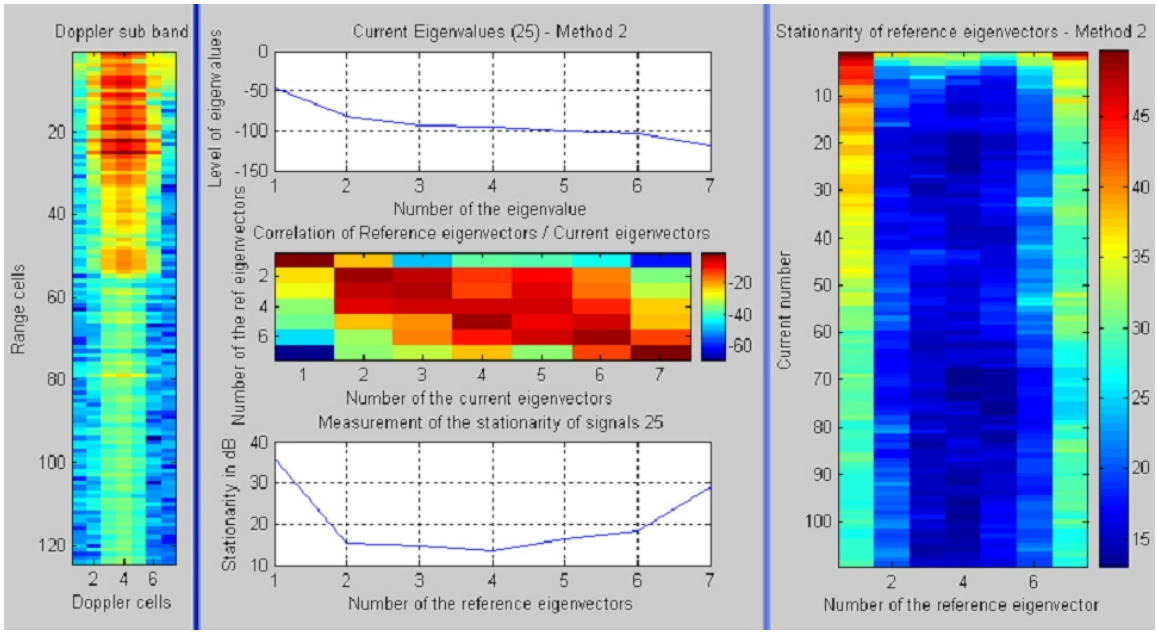

Figure 5.30: Stationarity of the central line

Stationarity of the positive Bragg line (zone 4) Same comments for this fourth zone, the positive Bragg line has been selected and results on figure 5.31 show that a strong signal is stationary along range cells. One more time, there is a weak signal which seems also to be coherent. This phenomenon is strange, it appears on each stationarity study it may be linked to a defect in the material. In fact, there could be a kind of coupling effect in the material that would produce "phantoms".

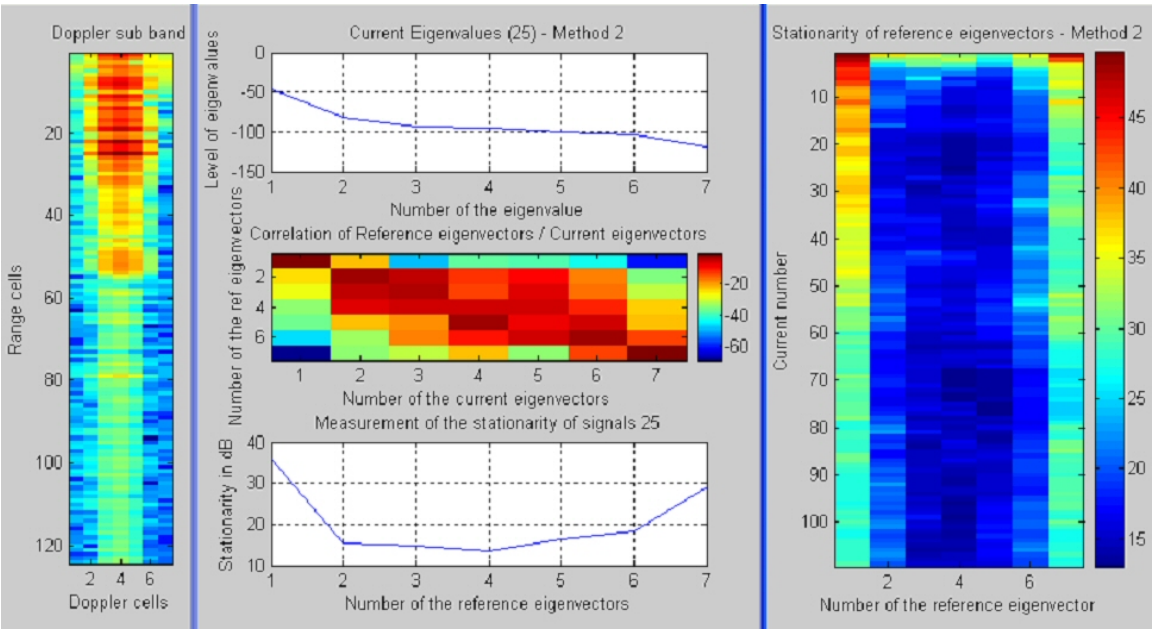

Figure 5.31: Stationarity of the positive Bragg line

Stationarity of a real target (zone 5) What we think to be a target has been isolated and studied. According to results presented on figure 5.32, the target is not so coherent along range cells. Examining precisely this target, we notice that it occupies several Doppler cells and moreover its correlation lobes are not straight along range cells but they are biased along a few Doppler cells. It is certainly because it is a plane flying too fast comparing to the integration time and then it is spread out in Doppler and range because its state changes during the coherent integration time Ti. The coupling effect mentioned previously appears little visible.

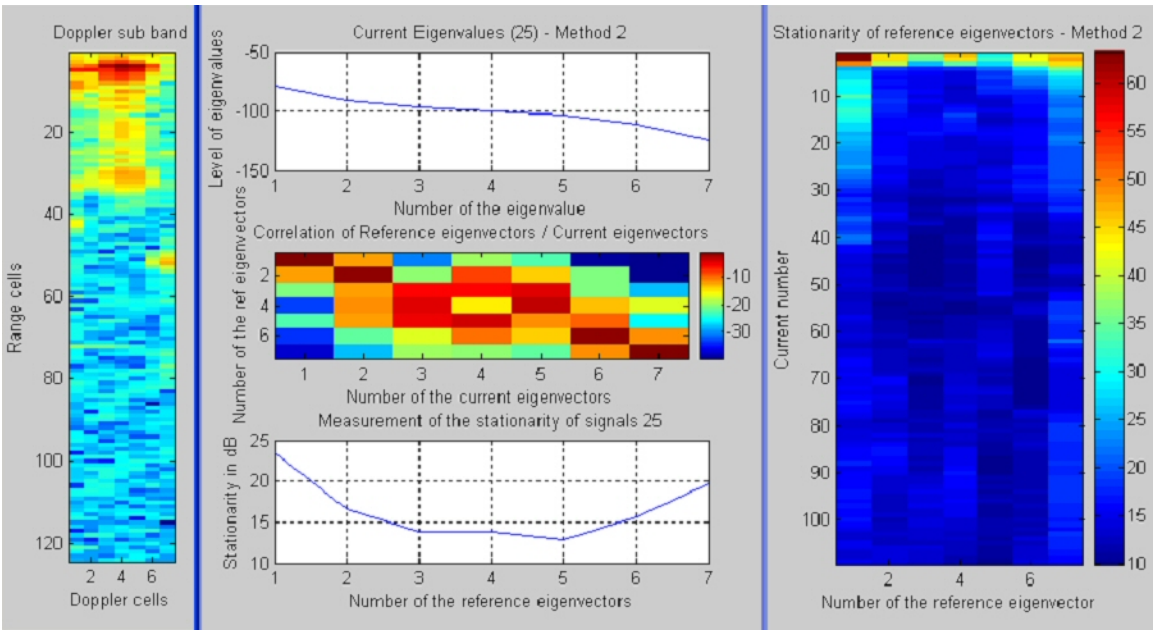

Figure 5.32: Stationarity of a real target

5.4 Application of adaptive filtering to sea echoes reduction

5.4.1 Simple algorithm for sea clutter reduction

Adaptive filtering principle and coherence conclusions are known, so it is possible to imagine how sea clutter can be filtered. Nevertheless, we are not really convinced that there is a coherence in real sea clutter because of the weak number of samples available. That is why it is not sure that it can be efficiently reduced. We can elaborate an algorithm to test that affirmation. The aim of the algorithm to elaborate is to calculate a filter that will be estimated on the range domain in order to reduce sea clutter in the Doppler domain. The range cells will be filtered one by one following the algorithm detailed in figure 5.33.

Let k be the number of the considered range cell that has to be filtered in the Doppler dimension. In fact, the first step is to define the number M_{estim} of coherent range cells that surround the range cell k. This number will be deduced thanks to the results of the coherence study implemented as a function. We assume that sea spectra are coherent in these consecutive range cells. The second step is to use these set of data to estimate the covariance matrix. Finally, the inverse of this covariance matrix is used to calculate the adaptive filter as presented in the SMI (Sample Matrix Inversion) method (see 5.2.2). This Doppler filter is then applied to the original range cell k.

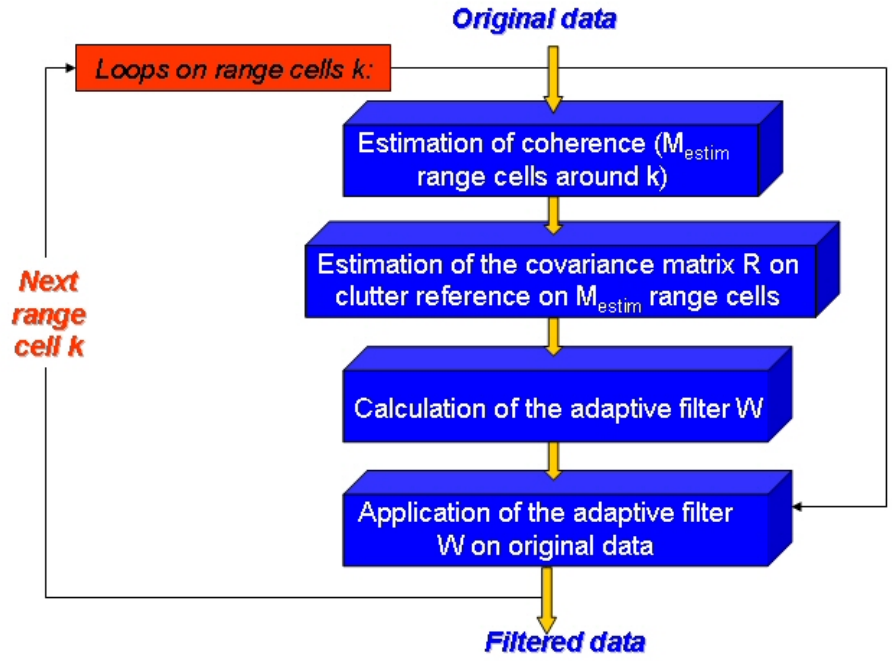

Figure 5.33: Simple sea clutter reduction algorithm

This is a simple algorithm that explains roughly the filtering processing for sea clutter reduction.

5.4.2 Test of the algorithm on simulated data

This algorithm has been implemented with Matlab and it is now an automatic program calling functions. To see if this algorithm is efficient, the first step is to test it on simulated data coming from the database. The advantage is that we control all parameters of these echoes and we can add a target at a specific place, with a known velocity and also a RCS known. It is very easy to hide a target in sea clutter, at an inferior level to see the effect of filtering on the target.

For this example, the following principal parameters have been entered in the sea echoes modeling tool describe in chapter 4 :

- Radar parameters: Frequency : 4 MHz; Bandwidth : 150 kHz (Range resolution : 1 km); Coherent integration time : 80 s (Doppler resolution : 0.0125 Hz).
- Meteorological parameters : Wind velocity : 10 m/s; Angle wind/radar : 180 °; Current velocity : 0 m/s; Angle current/radar : 0 °.
- Target parameters : Velocity : 0,2 m/s; Range : 50 km; RCS : 10 dB.

The other parameters are the same than default ones.

The entered target velocity is very low to be sure that its simulated echo will be hidden in the second order Bragg clutter. In the modeling software it is possible to obtain the final power of the principal peak of the target echo, for this example, the maximum is at -127 dB. On the original image 5.34, the target is not visible, we only know that it should be hidden above second order at the center of the image.

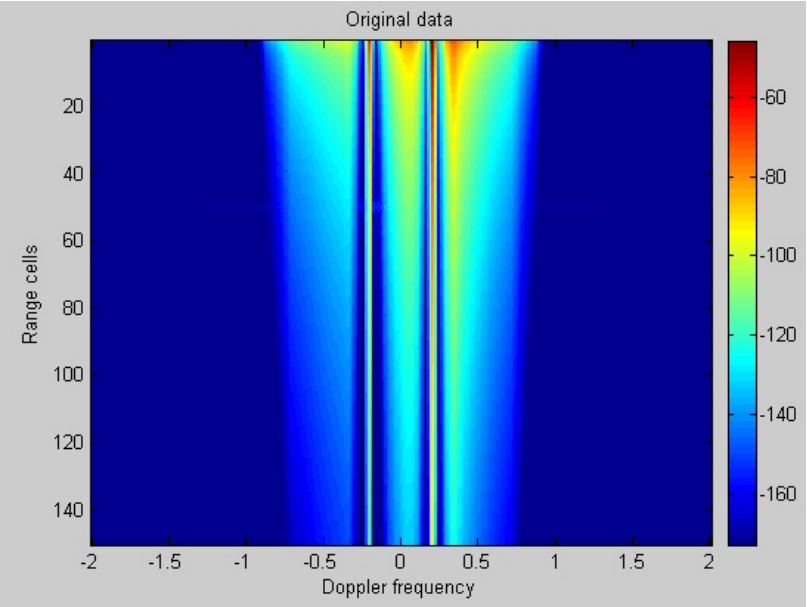

Figure 5.34: Original simulated data before adaptive filtering

After adaptive filtering, the previously hidden target has been detected and all the simulated sea clutter removed as shown on figure 5.35.

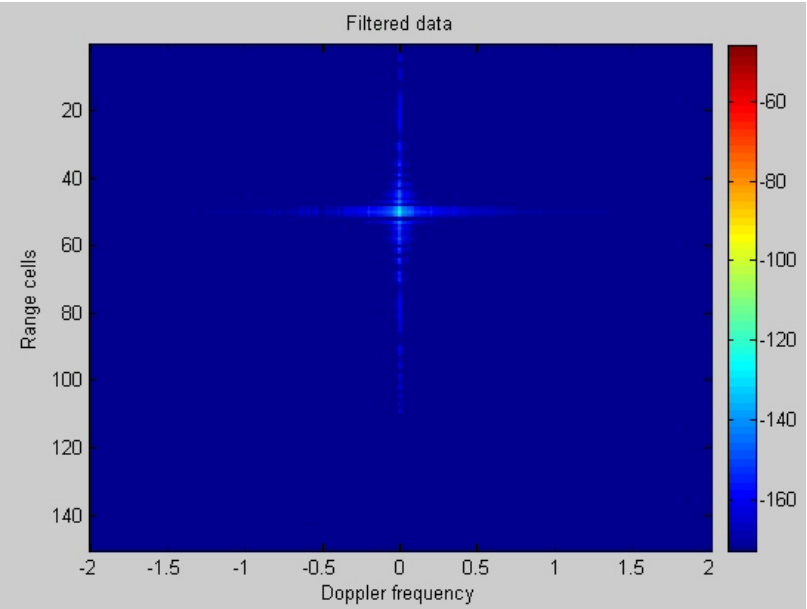

Figure 5.35: Simulated data after adaptive filtering

A precise section at the range cell 50 is more useful to see the filtering effect. On figure 5.36, the rejection level of the first order Bragg lines is comprised between 60 and 80 dB. The second order Bragg clutter is totally removed. The initial target level has not been affected by the filtering, its level is always at -127 dB. This is an encouraging results, showing the efficiency of this kind of methods to reduce sea clutter.

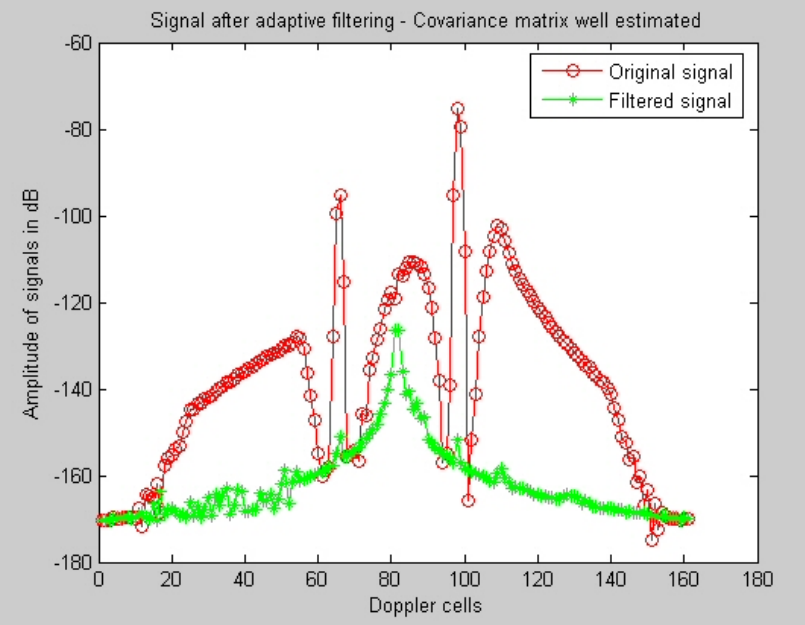

Figure 5.36: View of the filtering adaptive effect at range cell 50

5.4.3 Test of the algorithm on real data

The problem with simulations is that everything is generally okay but in practice, with real data, many problems appear. In fact, if we apply directly the simple algorithm on a sample of real data, the result is not good at all (see figure 5.37 showing the effect of adaptive filtering on real data). We notice that the central line has been reduced but sea clutter has not been affected by the filtering.

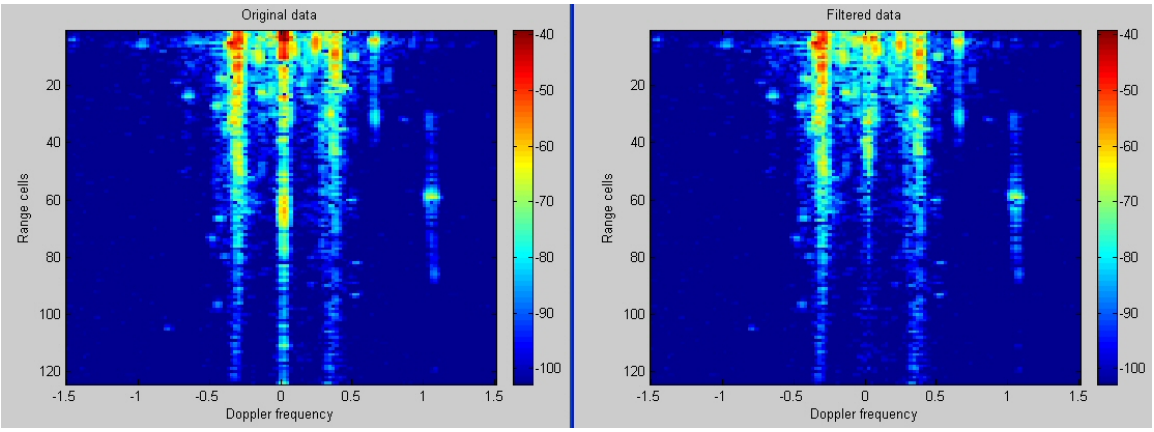

Figure 5.37: View of data before and after adaptive filtering

It means that the algorithm is too simple, it is not adapted to real data properties.

5.5 Optimization of the algorithm on real data

In practice, the sea clutter reduction algorithm has to be more complicated because a lot of parameters have to be taken into account. The following parts describe the new modules that have to be added to the algorithm. They have been developed all along the thesis and are summed up here.

5.5.1 Blocking matrix

Let the primary data be the original data that have to be filtered. As previously shown, the aim of this study is to reduce sea clutter, which is part of the colored noise, from these data. In the theory of adaptive filtering (see 5.2.2), the optimum filter used to optimize the detection of a signal in presence of noise is obtained thanks to the estimation of the noise covariance matrix.

To estimate only a clutter reference covariance matrix, a potential target must not be present in the data because it could be reduced by the adaptive filter while the aim of this thesis is to better detect target echoes in sea clutter. That is why we need to have a secondary data set without useful signals. The first idea is to estimate the covariance matrix on M_{estim}-1 range cells, removing the range cell k. But it is not enough because a simple elimination of the current range cell k is not sufficient. In fact, a target has correlation sidelobes in its neighboring range cells (as shown in chapter 1), so the presence of a potential target could be detected on account of its sidelobes. That is why to whiten the original data from a potential target at the observed range and in its vicinity, a blocking matrix is used. Its principle is based on the same principle than the adaptive filtering, it consists in the calculation of a filter. It will reduce the level of the range cell k and its correlation sidelobes for all the range cells.

The sea clutter reduction algorithm is automatic and processes the same way for each

range cell. In case a target is present at the concerned range cell k, the blocking filter will reduce it and its correlation sidelobes also. The potential target is then well protected before the adaptive filtering step. We obtain a secondary data set. Note that this potential target is not suppressed definitively, original data are preserved all along the processing because the final filter will be applied on them. Moreover, even if there is no target at the range cell k, the filter will reduce influence of this range cell and its surrounding cells in the estimation of the covariance matrix. Indeed, we are sure to estimate the covariance matrix principally on sea clutter .

5.5.1.1 Calculation of the blocking filter

The way the distance of backscattered echoes is obtained is explained in the range processing section 1.7.2, in the first chapter. Due to this processing, echoes appear on a Doppler range map with correlation sidelobes along range cells. The blocking filter consists in using the "inverse" of the correlation pattern induced by range processing.

The first step is to calculate the autocorrelation function of the transmitted chirp to have the exact correlation pattern to eliminate. The autocorrelation amounts to the same thing than correlation between the transmitted chirp and the backscattered one. The autocorrelation function is then shifted in order to have the highest correlation peak at the range cell k.

Then, the blocking filter can be calculated with :

$$W_{block} = \alpha(I - Ac.Ac^H)$$

where α is the blocking filter amplitude, I is the identity matrix (the dimension of this square matrix is the total number of range cells $\times$ the total number of range cells), Ac is the autocorrelation vector of the chirp (the dimension of this vector is the total number of range cells).

This filter can now be applied on the total number of range cells of the image, whatever the number of Doppler cells. To test its efficiency, the first step is to use a really well known target at a precise range cell. The better solution is to use first a simulated target because we can control its position, its velocity and its level.

On the first example, a target has been simulated with a low noise in order to well observe its echo and its lateral correlation sidelobes. Moreover, it is not weighted in Doppler to avoid a large beam. On the simulated target as presented on figure 5.38, we note that the maximum peak is located at the range cell 73 and at the Doppler cell 53. On figure 5.39, the blocking filter is really efficient and we obtain a rejection level of 45-50 dB on the target initial level, that is a very good result. In this case, the filter has been calculated thanks to the autocorrelation function of the transmitted chirp.

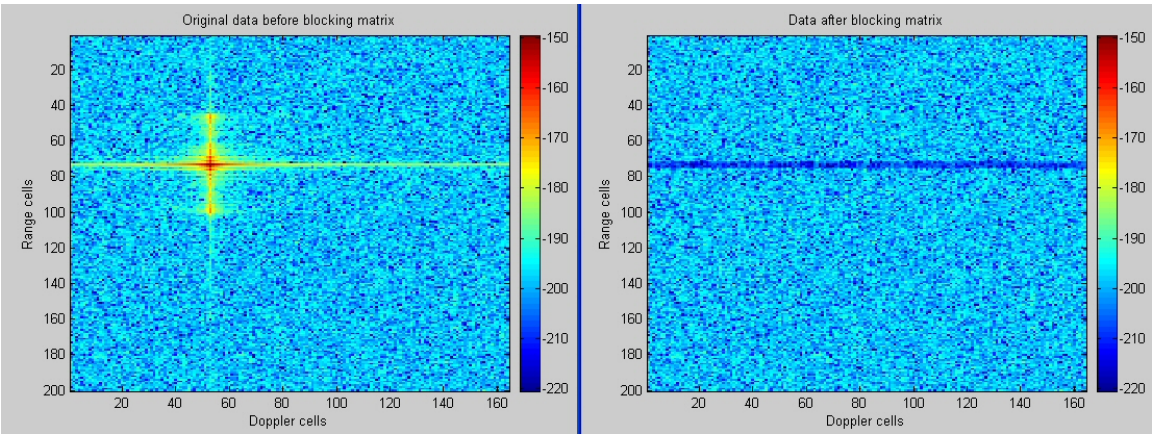

Figure 5.38: Effect of the blocking matrix on a simulated target at the range cell 73

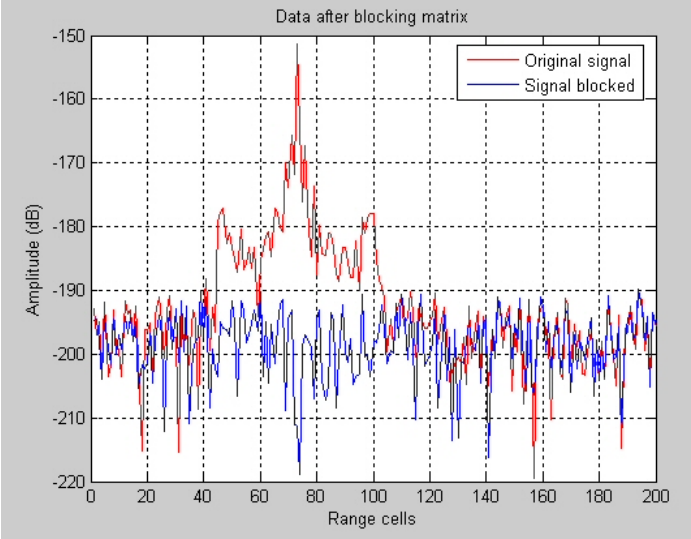

Figure 5.39: View of the blocking effect at the Doppler cell 53

Application of the same blocking filter on real data are not so efficient as shown on the following figures 5.40 and 5.41. In this example, we focus on an eventual target that is present at the intersection on the range cell 13 and the Doppler cell 47. The rejection level on this target after blocking matrix is now about 25 dB.

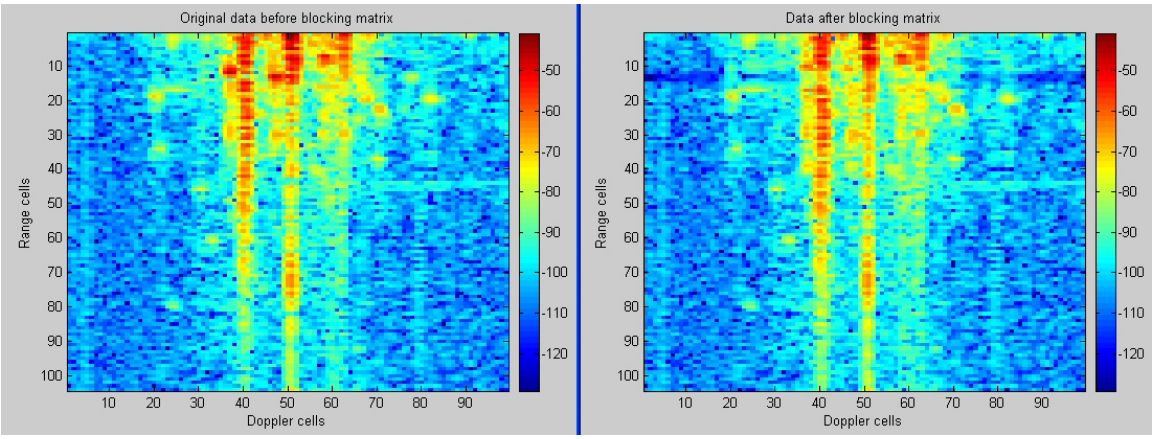

Figure 5.40: Effect of the blocking matrix on real data at the range cell 13

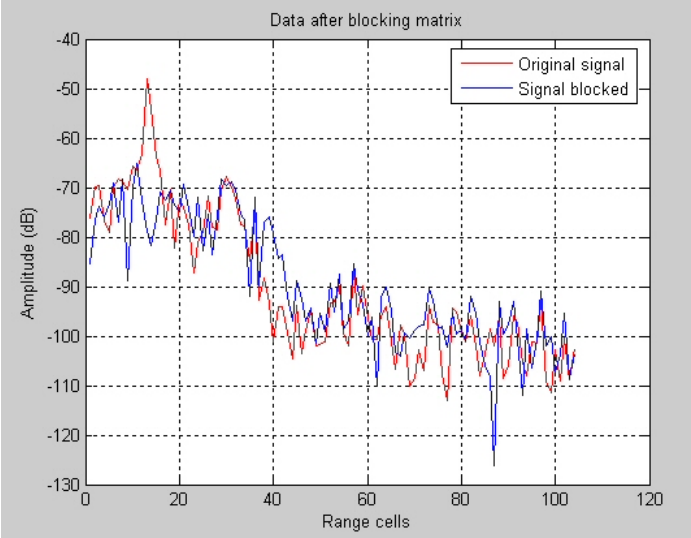

Figure 5.41: View of the blocking effect at the Doppler cell 47

On the image 5.40, we do not really know if the red point on the image (which is certainly a target) has correctly been blocked. There is too much clutter and too many targets around to see clearly the effect. That is why further tests have to be done to be sure of the blocking matrix efficiency.

5.5.1.2 Test of the blocking filter efficiency

We have to insert a target in the Doppler range data to study precisely effects of the blocking matrix. If we use a simulated target to do that, results will be biased because it does not reflect reality. We need to insert a "real target". The problem is that it is impossible to receive only a target echo without noise, ground or sea clutter with the HF Surface Wave Radar system. That is why we decide to create a chirp on a waveform generator and to digitize it directly thanks to a digitizing card installed on a PC with exactly the same

equipment that the one used to acquire real data. On the one hand, the generated chirp will not be distorted through the antenna, backscattered by an object, affected by propagation losses and sent back to the receiving system, but on the other hand it is already a good thing to know effects caused by digital cards used for transmitting and receiving. We will have a reinjected chirp.

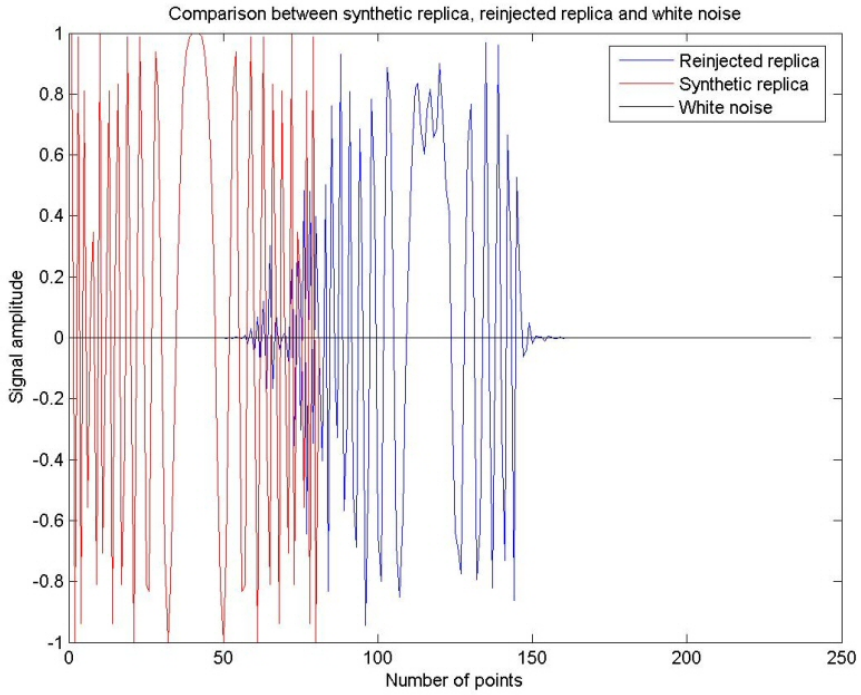

Figure 5.42: Comparison between the real part of a synthetic and a reinjected chirp in function of time

On figure 5.42, the reinjected chirp is clearly distorted compared to the transmitted chirp. This is due to the filters and internal operations of the digitizing card.

It is now possible to create a target with the same tools than for a simulated target but using a reinjected chirp. It means that the autocorrelation function of the reinjected chirp will be calculated and shifted to appear at the right position and at the wanted level on the Doppler range image. It means also that if we want a good rejection of this target, we have to use the autocorrelation function of the reinjected chirp in the blocking filter. The result of the blocking matrix on the target alone is presented on the following figure (cf. figure 5.43).

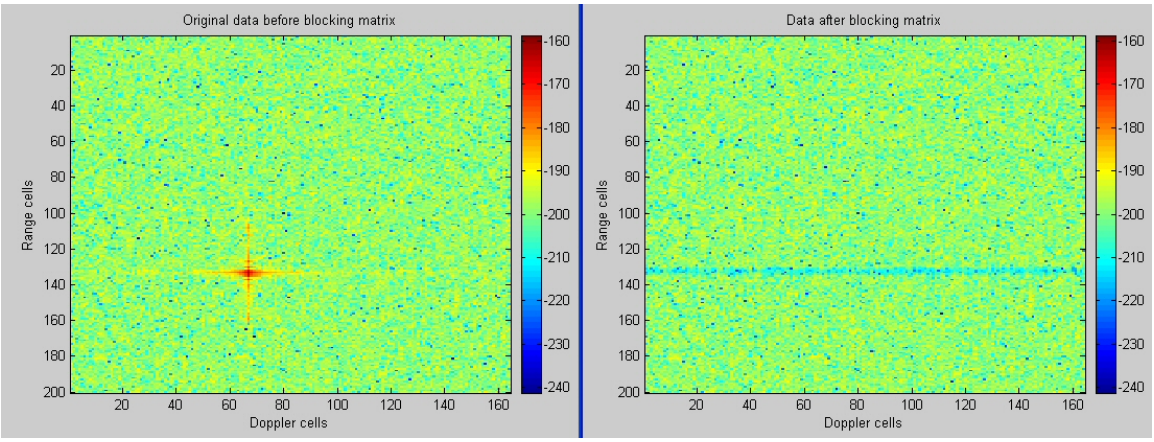

Figure 5.43: Blocking matrix applied at range cell 137 on the target echo created with a digitized chirp

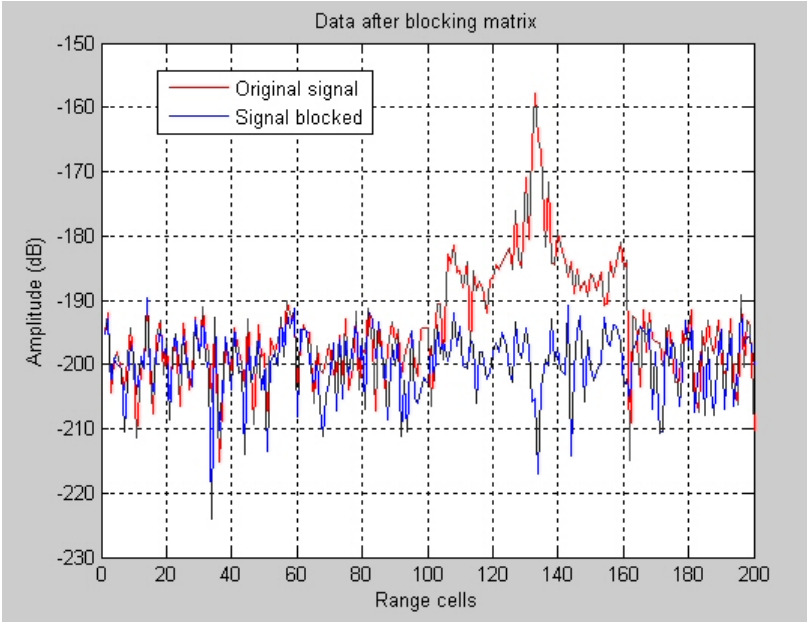

Figure 5.44: View of the blocking effect at Doppler cell 67

With this method, we obtain a rejection level of 35 dB, which is a satisfactory result.

If we insert this reinjected target in real data (as proposed on figure 5.45), its blocking is always good (cf. figure 5.46).

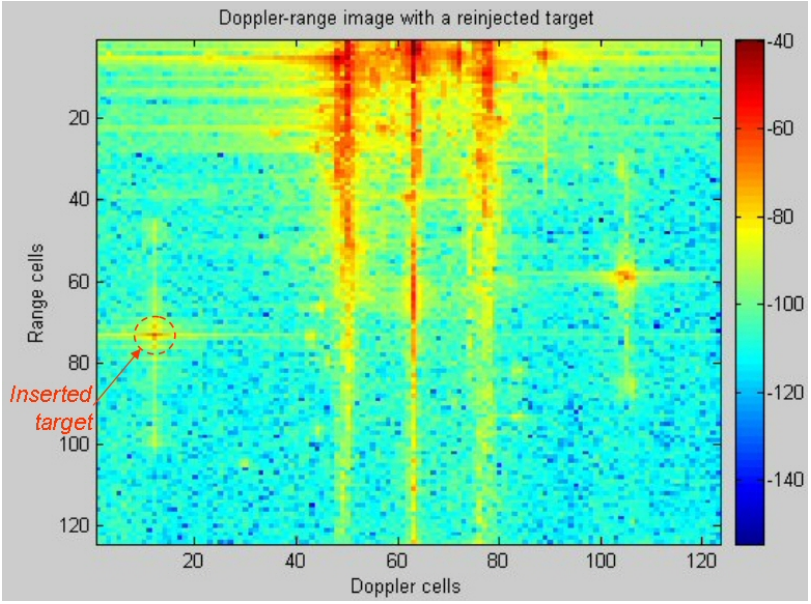

Figure 5.45: Insertion of the created target in real data

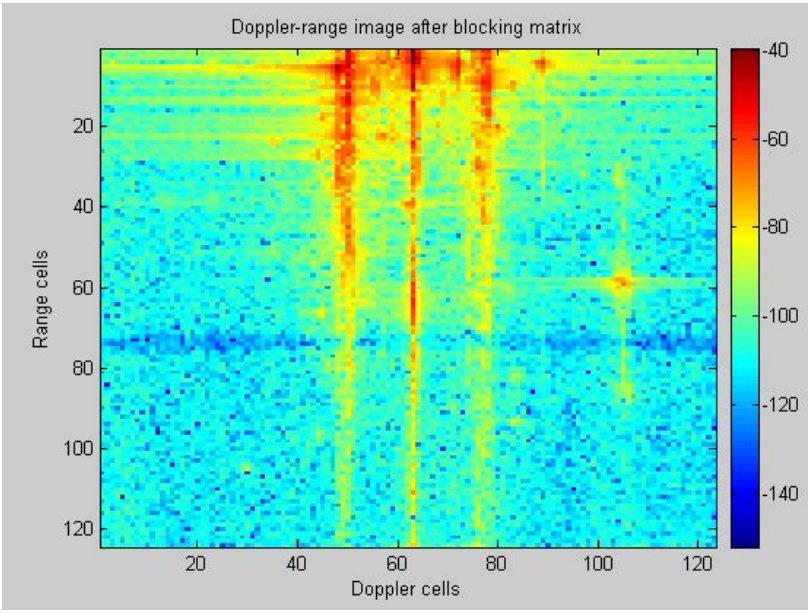

Figure 5.46: Effect of the blocking matrix on the inserted target

The more faithful to reality the blocking filter is, the more efficient it will be. The problem is that the spectrum of a real target echo is obtained by correlation between the transmitted chirp and the received one. It means that the blocking filter must not be calculated with an autocorrelation but with the correlation between the exact transmitted and the exact received chirp. The following figure 5.47 presents a synthetic chirp autocorrelation, a reinjected chirp autocorrelation and finally a crossed correlation between and synthetic and a reinjected chirp. We notice slight differences between the 3 curves but they

can have effects on the blocking efficiency.

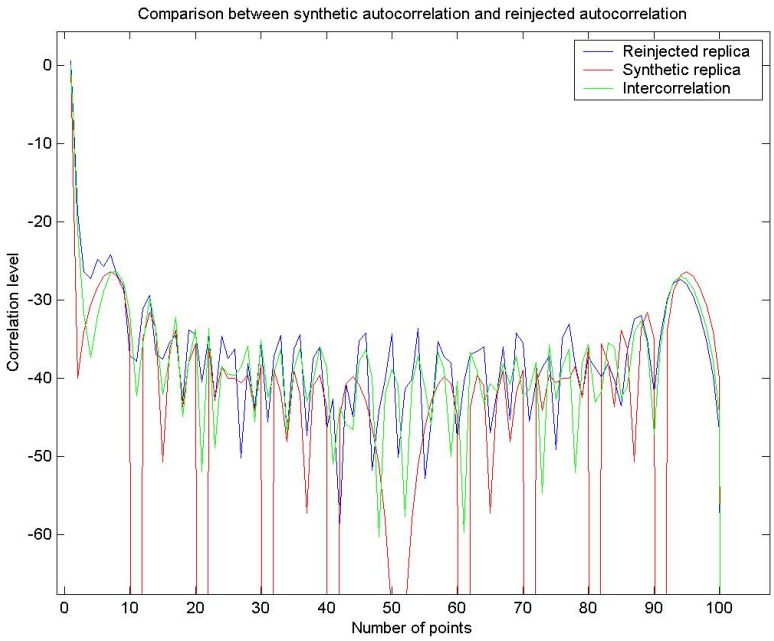

Figure 5.47: Comparison between autocorrelation of the synthetic transmitted chirp, autocorrelation of the reinjected chirp and intercorrelation between both of them

On figure 5.48, you can find the comparison of effects of different blocking filters on a real target. On the left image, the blocking filter has been calculated with the autocorrelation of the reinjected chirp, the central filter with the autocorrelation of the transmitted synthetic chirp and on the left image, the filter results from the correlation between the transmitted synthetic chirp and the reinjected chirp. The best result is obtained for the last one with the filter obtained with the intercorrelation. This solution will be selected to protect potential targets before adaptive filtering.

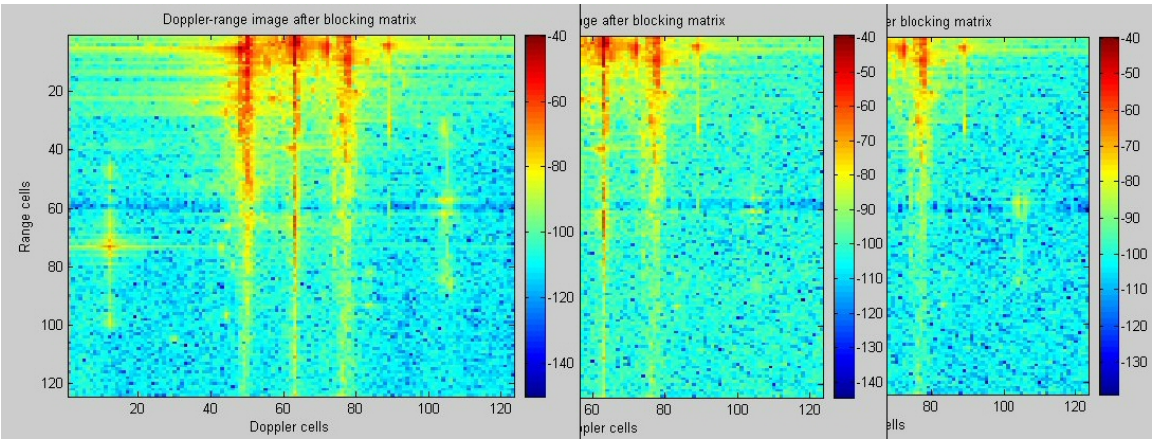

Figure 5.48: Comparison between 3 blocking filters on a real target

In conclusion, to obtain an efficient blocking, we need to digitize the reinjected replica for every kind of transmitted waveform and for each bandwidth and each transmitting time. The idea is to create a database with the most popular waveforms, bandwidths and transmitting times that will be automatically used to block properly potential targets.

5.5.2 Loops on Doppler sub-bands

As explained in the real data analysis part (see 5.3), only data containing sea clutter are selected to be filtered. The induced advantage is the reduction of the number of Doppler cells to filter. Nevertheless this selected Doppler domain contains a great number of points, in general tens of Doppler cells, and it cannot be filtered at one go to respect the condition about the optimum estimation of the covariance matrix. Matrix calculation and inversion would consume too much in terms of calculation power. A sub-bands cutting is absolutely necessary. Moreover, the coherence duration is often different from a Bragg line to another and to the central line. That is why the idea is to separate the selected Doppler cells in 3 sub-bands, each corresponding to an area surrounding a Bragg line or the central line.

A direct division in 3 equal sub-bands is not possible because, as presented in the first chapter about Bragg spectrum, in case of current, Bragg lines are not symmetrical about the central line anymore. They are shifted together from their theoretical position of the value of the Doppler shifting induced by the current velocity. For an automatic division of the Doppler domain, a function has been implemented. It consists in the research of the 3 primary lines of the image. The first step is to average all the range cells to find a mean spectrum and then to avoid confusion between an occasional target (even with a strong echo) and a Bragg or the central line. Then, the 3 Doppler sub-bands can be delimited around these 3 principal peaks.

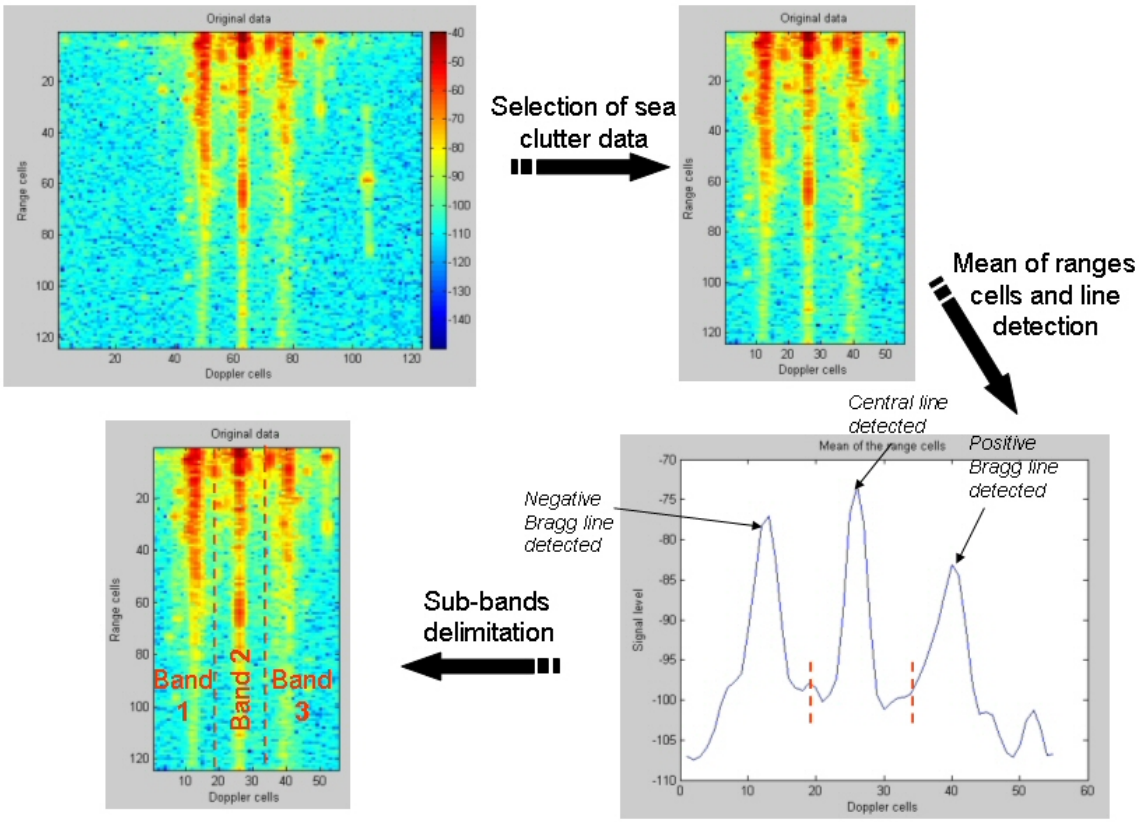

Figure 5.49: Illustration of the Doppler domain division principle

After this Doppler domain division, the number N_{ref} of Doppler cells is fixed. This number is generally different for each of the 3 sub-bands. The number of Doppler cells should not be too small for a an efficient filtering.

5.5.2.1 Study of the minimum size of sub-bands

To determine the minimum size of the reference Doppler domain, a study is necessary. Let an example be a pure signal surrounded by a white noise. After radar processing, the Doppler range image displays a line at a precise Doppler frequency. The aim of this study is to select different size of reference domain (N_{ref} Doppler cells) of the covariance matrix R and then to estimate R on a integration domain having different size (M_{estim} range cells). For all these couples, the adaptive filter will be calculated and applied to reduce the effect of the generated signal. The adaptive filter is not the same in the case of a correctly estimated covariance matrix and in the contrary case (see the different calculation in the following section 5.5.3).

For the first case, the reference domain contains 32 Doppler cells. The adaptive filter is calculated with a covariance matrix estimated on 64, 50 or 16 range cells. Figure 5.50 represents the effects of these different filters in function of the estimation duration. The

rejection level of the signal peak is about 45 dB whatever the number of integration points. This is a good result.

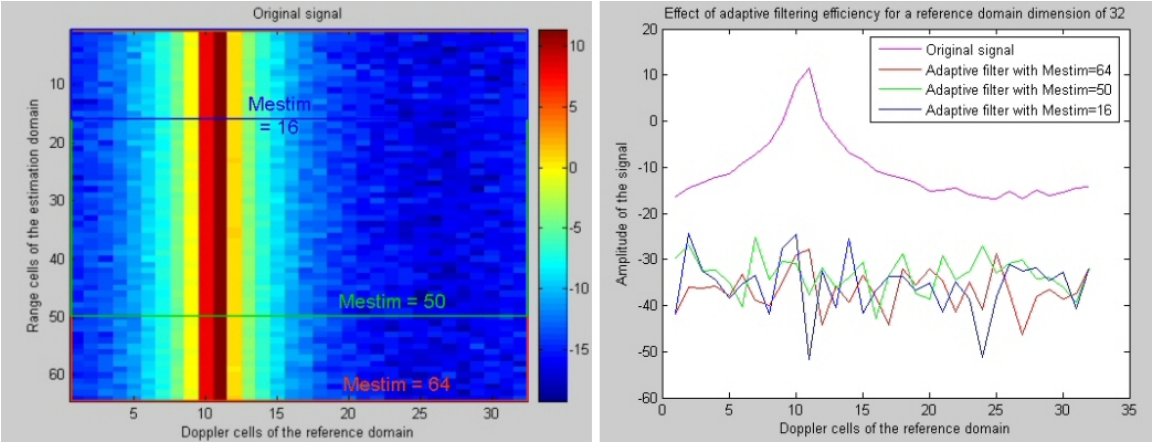

Figure 5.50: Effect of adaptive filter estimated with different numbers of estimation range cells (M_{estim}) in the case where N_{ref}=32

The following figure 5.51 displays results for a reference domain with 16 Doppler cells. In this case, R is estimated on 32, 20 and 8 points. Effects of adaptive filtering is also quite good because the rejection level is about 45 dB.

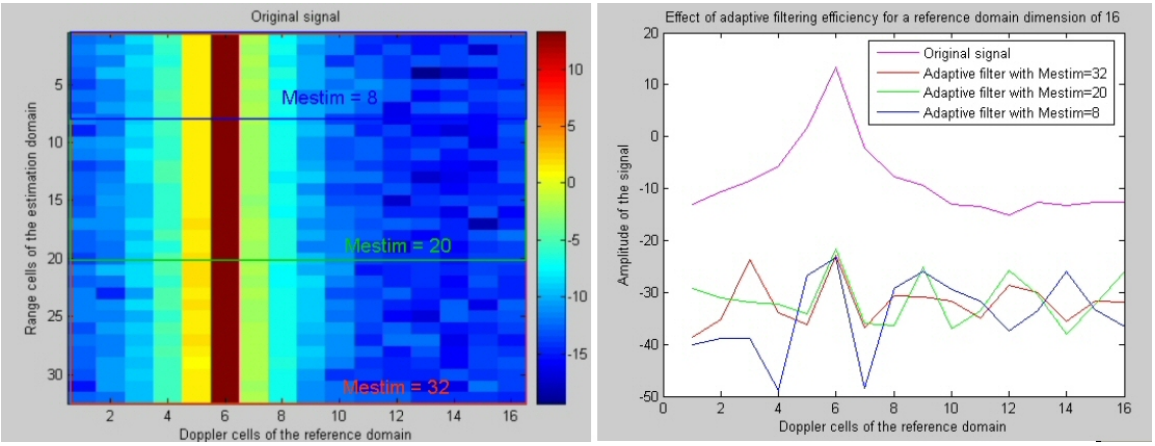

Figure 5.51: Effect of adaptive filter estimated with a different number of estimation range cells (M_{estim}) in the case where N_{ref}=16

The last example is given with a very small reference domain containing 10 Doppler cells. R is estimated on 20, 15 or 5 range cells and in this case, results are really bad (see figure 5.52). Adaptive filter is less efficient than in the previous examples, with a mean rejection level of 5 dB. It means that the filter needs more Doppler cells to provide a good rejection.

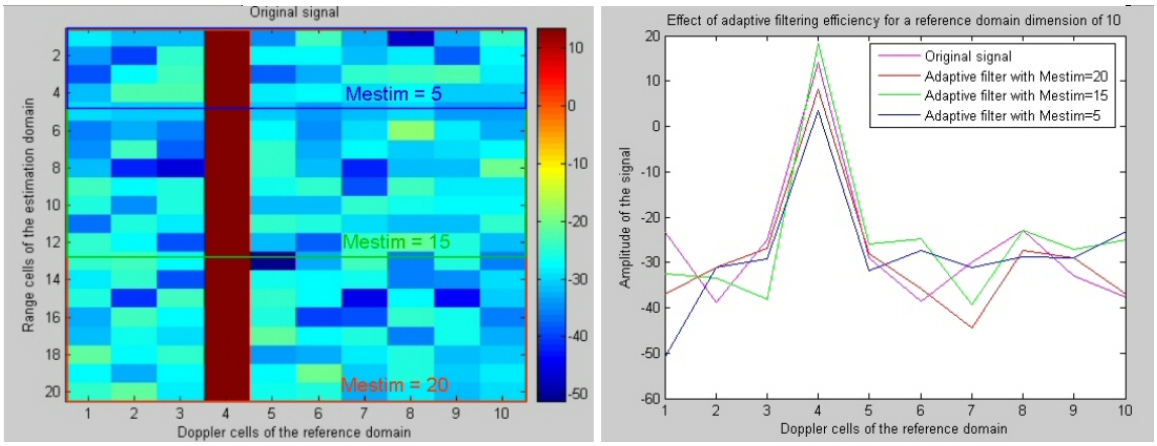

Figure 5.52: Effect of adaptive filter estimated with a different number of estimation range cells (M_{estim}) in the case where N_{ref}=10

Results of these 3 examples can be summarized in a table (see table 5.1). If the reference domain size is smaller than 16 Doppler cells, the adaptive filter has not a very significative impact compared to the level that it can reach with higher values. N_{ref}=16 is the limit from which the rejection is efficient. For higher values of N_{ref}, the adaptive filtering has a better performance. That is why the Doppler sub-bands should respect this minimum size of 16.

N_{ref} Doppler cells	M_{estim} range cells	R correctly estimated ?	Level of peak rejection
32	64	YES	41 dB
32	50	NO	50 dB
32	16	NO	63 dB
16	32	YES	38 dB
16	20	NO	36 dB
16	8	NO	38 dB
10	20	YES	5 dB
10	15	NO	-4 dB
10	5	NO	10 dB

Table 5.1: Results of adaptive filtering in function of the size of the reference and integration domains

In each example, we had a covariance matrix correctly estimated and also poorly estimated. The difference between both is not flagrant on these images. The major difference concerns the difficulty in the calculation of the adaptive filter but not really the filtering performance itself.

5.5.3 Problems about calculation of the adaptive filter

After the step of blocking matrix used to protect potential targets, we obtain a set of secondary data that consist of clutter returns and also other interferences such as jammers. For each sub-band, it is then possible to estimate the secondary data covariance matrix

noted R in the sequel. The inverse of this covariance matrix is used to calculate the adaptive filter as presented in the SMI (Sample Matrix Inversion) method (see 5.2.2). The problem is that R is not always inversible. That is why two cases are possible :

1. **Case 1 :** If $M_{estim} \geq 2.N_{ref}$, R is inversible and correctly estimated, and the filter can easily be calculated with R^{-1}, as suggested in the SMI method.

   The optimum filter is given by :

   $$W_{opt} = k.R^{-1}.S$$

   with k a complex number.

   This is the ideal configuration but the problem is that sometimes N_{ref} is not sufficient to have a good calculation of the filter. The condition is respected but the efficiency can be bad.

2. **Case 2 :** If $M_{estim} < 2.N_{ref}$, R is not correctly estimated and moreover it can be impossible to invert (if $M_{estim} < N_{ref}$). We have to use different methods to calculate the filter. One of them is called the method of the eigencanceler based on the eigenanalysis of the covariance matrix (the theory of eigencanceler is presented in [25]).

   In fact, the decomposition of the covariance matrix can be written:

   $$R = Q_c.\Lambda_c.Q_c^H + \sigma_n^2.Q_n.Q_n^H$$

   where the diagonal of the $n_c \times n_c$ matrix Λ_c consists of the n_c principal eigenvalues of R, the columns of Q_c are the corresponding eigenvectors, σ_v^2 is the variance of the white noise, and the columns of Q_n are the remaining eigenvectors of R. The subspaces spanned by the columns of Q_c and Q_v are referred to as clutter and noise, respectively.

   A determination of the number n_c of coherent signals representing clutter contained in the covariance matrix is then used to separate them from noise. The filter will be calculated using eigenvectors of coherent signals or eigenvectors of noise. The weight vector can be calculated with the following formula proposed in 1997 by Haimovich [26] :

   $$W_{opt} = s\left(I - \left(Q_c.Q_c^H\right)\right) = s(Q_n.Q_n^H)$$

   with s : Scaling factor.

Number-of-source detection method In many problems in signal processing domain, the vector of observations can be modeled as a superposition of a finite number of signals embedded in an additive noise. This is the case for overlapping echoes of the secondary data set, representing clutter and noise. A key issue in these problems is the detection of the number of signals.

One approach to this problem is based on the observation that the number of signals can be determined from the eigenvalues of the covariance matrix of the observation vector. Barlett [27] and Lawley [28] developed a procedure, based on a nested sequence of hypothesis tests, to implement this approach. For each hypothesis, the likelihood ratio statistic is computed and compared to a threshold. The hypothesis accepted is the first one for which the threshold is crossed. The problem with this method is the subjective judgment required for deciding on the threshold levels.

Another approach to the problem is based on the application of the information theoretic criteria for model selection introduced by Akaike in 1974 [29] with the AIC (Akaike's Information Criterion), by Schwartz in 1978 [30] with the BIC (Bayesian Information Criterion) and Rissanen in 1978 [31] with the MDL (Minimum Description Length). The advantage of these approaches is that no subjective judgment is required in the decision process. The number of signals is determined as the value for which the criteria are minimized.

Statistical hypothesis (SH), Akaike's Information Criterion (AIC) and Minimum Description Length (MDL) are the three most popular methods that detect the number of sources based on information theoretic criteria.

For the determination of the number of coherent signals in the clutter that we need to reduce, the MDL is chosen.

$$MDL(k) = -log(\frac{G(\lambda_{k+1}, ..., \lambda_p)}{A(\lambda_{k+1}, ..., \lambda_p)})^{(p-k)N} + \frac{1}{2}k(2p-k)logN$$

where $\lambda_1 \geq \lambda_2 \geq ...\lambda_p$ denote the eigenvalues of R, and G and A denote, respectively, the geometric and the arithmetic mean of their arguments.

$$G(\lambda_{k+1}, ..., \lambda_p) = (\prod_{i=k+1}^{p} \lambda_i)^{(\frac{1}{p-k})}$$

$$A(\lambda_{k+1}, ..., \lambda_p) = (\frac{1}{p-k}) \sum_{i=k+1}^{p} \lambda_i$$

In fact, this criterion detects the point where arithmetic and geometric means are the more distant, it is a kind of detector of the position of the break point on the

eigenvalues curve. The break point represents the separation between signals representing clutter and noise. The number of signals is determined to be the value of $k \in \{0, ..., p-1\}$ for which MDL(k) is minimized.

On the following example (cf. figure 5.53), the MDL criterion is applied on a pure simulated signal surrounded by noise. We assume that the covariance matrix is correctly estimated (64 range cells taken into account for 32 Doppler cells). There a single signal, that we clearly verify with the distribution of the eigenvalues of its covariance matrix. We notice a strong eigenvalue and a flat stage representing the noise eigenvalues. The MDL criterion indicates a minimum at the second position, which means that there is only one detected source (= minimum position (2) - 1).

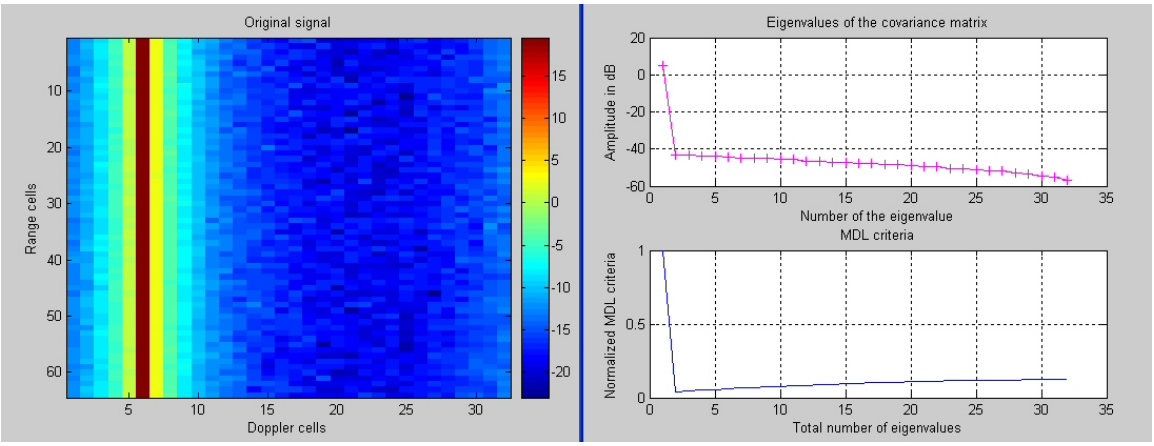

Figure 5.53: View of the MDL criterion applied on a pure signal with white noise

To compare the effect of the weighting on the eigenvalues and consequently on the MDL criterion, a set of data comprising 3 different signals surrounded by noise have been simulated, with and without weighting. First, results for the non-weighted data are presented on figure 5.54, and the MDL criterion detects well 3 signals among the eigenvalues (= minimum position (4) - 1).

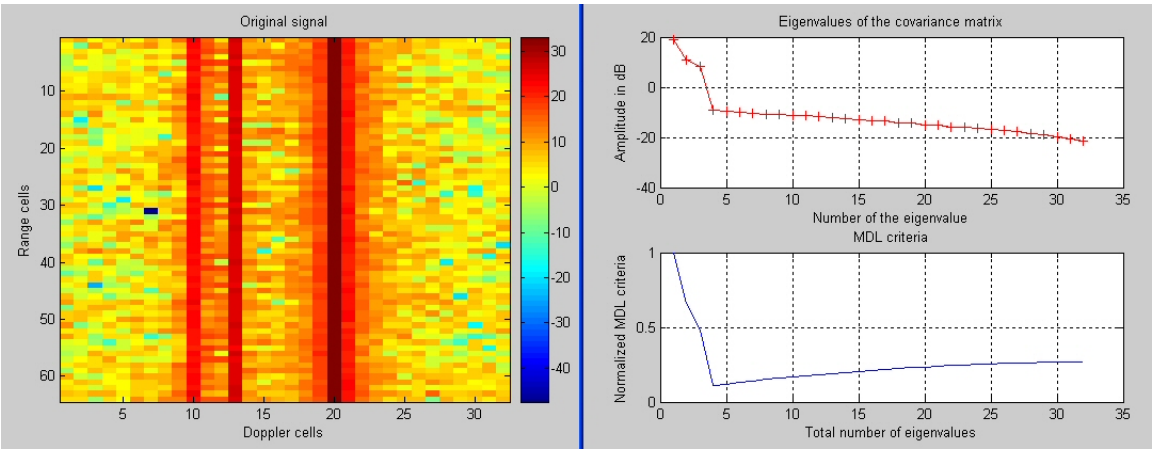

Figure 5.54: View of the MDL criterion applied on data comprising 3 non-weighting simulated signals surrounded by noise

If we compare simulated signals with and without weighting, it is clear that weighting can be a disadvantage because signals can be hidden by the large primary lobe of a stronger signal as shown on figure 5.55. In fact, if two signals are close to each other, the enlargement due to the weighting may confuse both signals. On the contrary, if there is an important difference of level between two signals, it is possible to reduce the secondary lobes by weighting.

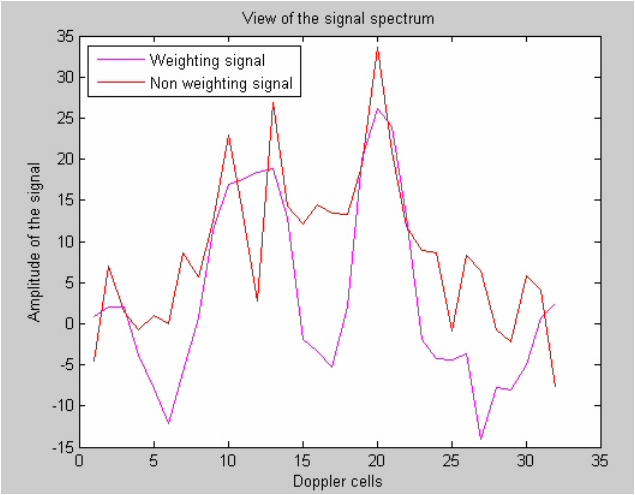

Figure 5.55: Comparison between the simulated spectra with and without weighting

The results of the MDL criterion for the weighted data are presented on figure 5.56. The appearance of the curve is distorted because of the weighting. Lower eigenvalues are modified and present a second flat stage. This is a problem for the detection of source number because the MDL criteria may detect a break point in the eigenvalues curve at the extremity, as shown in the example below where more than 30 sources are detected.

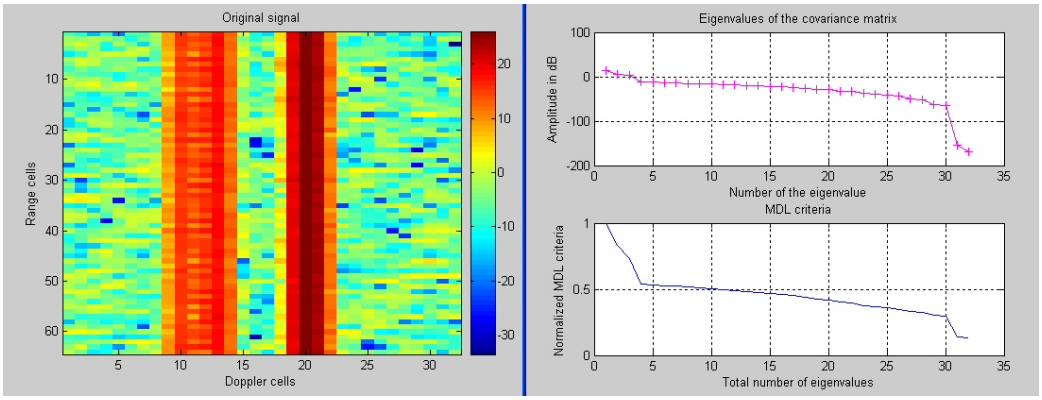

Figure 5.56: View of the MDL criterion applied on 3 weighting simulated signals surrounded by noise

To solve this problem, in case of detection of the source number on weighted data, the MDL criterion can be applied on the partial eigenvalues. In fact, the extremity of the eigenvalues, typically the last quarter (empirical value), is not taken into account in the calculation of the MDL. Moreover, if the covariance matrix is correctly estimated, we know that all its eigenvalues will be significant. If the matrix is not correctly estimated, for example if $M_{estim} = N_{ref}$, we consider that half of the eigenvalues are significant and the MDL criterion will then be applied only on these eigenvalues.

These examples are quite simple to understand and after a few optimization changes, the MDL criterion is validated on simulated data. For real data, it is sometimes difficult to determine the exact number of signals in the covariance matrix. The principal problem is that we totally ignore the exact number of sources that are present in the data samples.

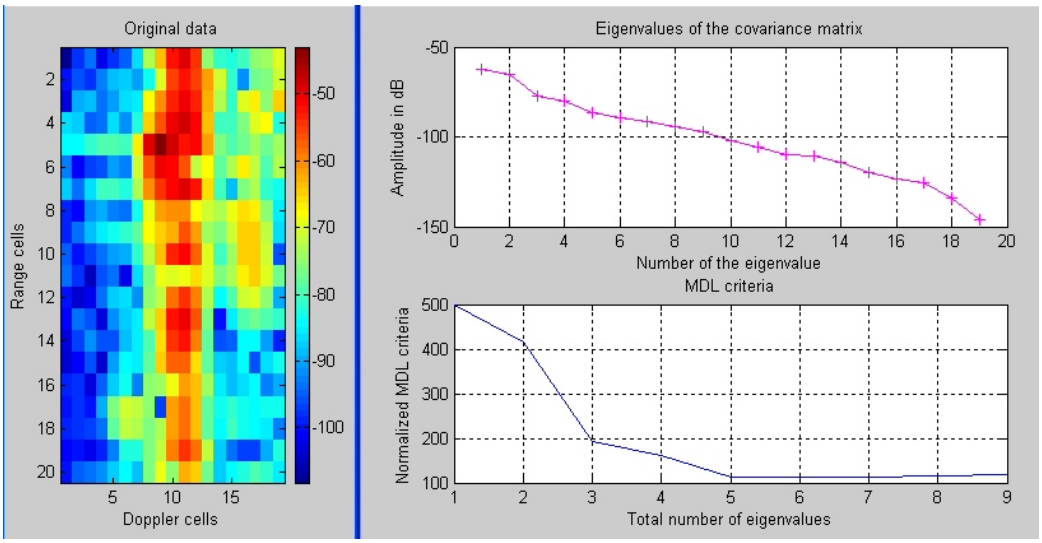

Figure 5.57: View of the MDL criterion applied on real data

5.5.4 Final adopted algorithm

The simple algorithm proposed at the beginning has been improved and optimized to be adapted to sea clutter reduction problem. After the description of all these new modules, it is possible to build a new algorithm as proposed below in figure 5.58.

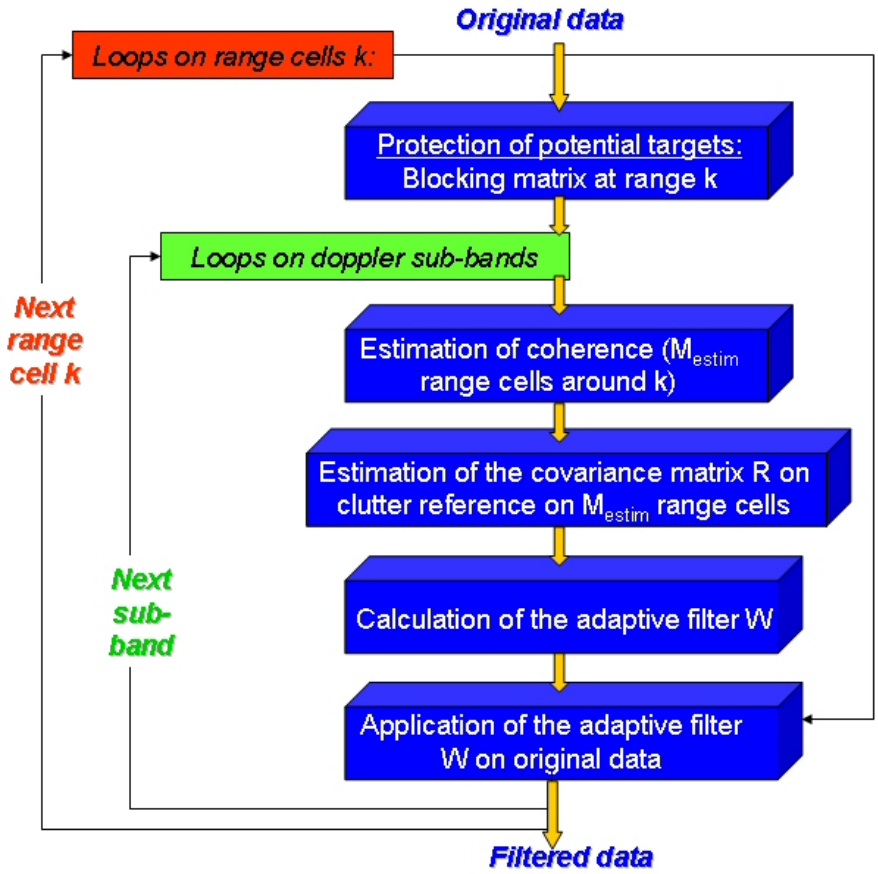

Figure 5.58: Algorithm used to reduce sea clutter

For each range cell k, the filtering occurs as follow :

1. The first step is to protect potential targets from effects of adaptive filtering. The blocking matrix is focused on the range cell k and eliminate this range cell and its neighboring range cells. From the original data, a secondary data set has been obtained with no useful signals around the range cell k.

2. Then the division of the secondary data in sub-bands occurs. After a selection of data containing sea clutter, the Doppler domain is separated in three bands around each of the two Bragg lines and around the central line. The sub-bands consist of N_{ref} Doppler cells, representing the reference domain on which the adaptive filter will be applied.

3. For each sub-band, a coherence study gives the number of consecutive coherent range

cells around k. This number called M_{estim} is the number of range cells of the integration domain. It can be different for each sub-band.

4. The covariance matrix R can be calculated on the reference domain and estimated on the integration domain. This covariance matrix contains only clutter and noise.

5. The optimum filter W_{opt} used to have the best detection of potential targets in presence of clutter can be calculated with two different methods depending on the ratio between the size of the integration and reference domains.

   - For the ideal configuration $M_{estim} \geq 2.N_{ref}$, the SMI method is used based on the direct inversion of the covariance matrix for the calculation of the optimum filter.
   - For other cases where $M_{estim} < 2.N_{ref}$, the eigencanceler method is used for the calculation of the optimum filter. Based on the eigenanalysis of the covariance matrix, the filter is calculated with the eigenvectors of the signals representing the clutter that we want to reduce. A precise determination of the source number of signals coming from sea clutter is necessary to separate them from noise.

6. Finally, the filter is applied on the Doppler cells of the original range cell k of the considered sub-band such as :

$$Filtered\ data = W_{opt}.Original\ data$$

   The output of this process delivers a range cell where all coherent clutter has been filtered. The next step is to make a loop on each Doppler sub-band to have a complete filtering of the range cell k. Then the following range cells can be processed the same way.

5.6 Test and validation of the algorithm with real data

The final algorithm has been created and optimized step by step trying to take into account each problem encountered. The final algorithm has been tested on real data but conclusions are moderate for the moment because the filtering is efficient in half of processed cases.

5.6.1 Problems encountered

Many problems have been encountered by applying the filtering algorithm on real data. In fact, each part of the algorithm has weaknesses. Principal problems are caused by :

- **The MDL criterion has difficulties to detect the source number :** This MDL criterion has been implemented to detect the number of coherent signals that the adaptive filter should reduce. This criterion uses the eigenvalues of the covariance matrix estimated on real data. In the following examples, the same real data sample has been studied, potential targets have been kept to have visible signal marker. In fact, on the left part of figure 5.59, the data sample contains 19 Doppler cells and 124 range cells. In the first time, we estimate the covariance matrix on 9 range cells (half

of the number of Doppler cells) and repeat this estimation on the whole image (124 - 9 = 115 shiftings). For each covariance matrix estimated, the MDL criterion provides a number of coherent signals detected and this number is displayed in the right part of the image 5.59 for each range shifting. For example, in the first estimated covariance matrix, the MDL criterion finds 2 coherent signals while at the 40th estimation, it finds 4 coherent sources. It is impossible to confirm this number because acquisitions of signals have been made blindy. But we can say that these results are plausible considering the image.

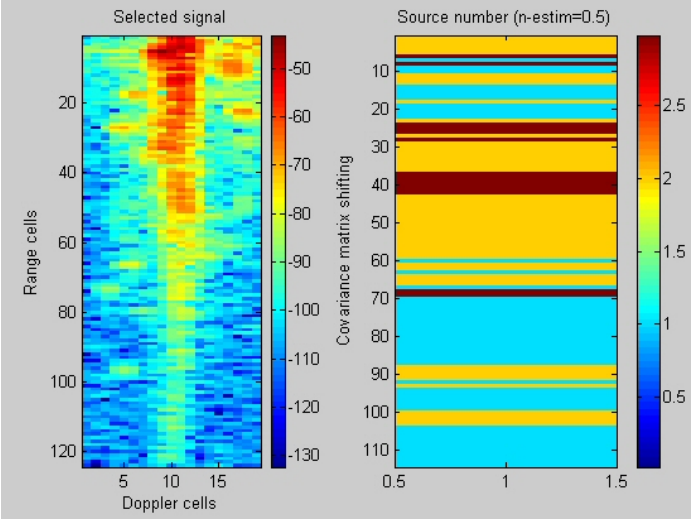

Figure 5.59: View of the Doppler sub-band studied and display of the source number given by the MDL criterion for the different covariance matrix shiftings

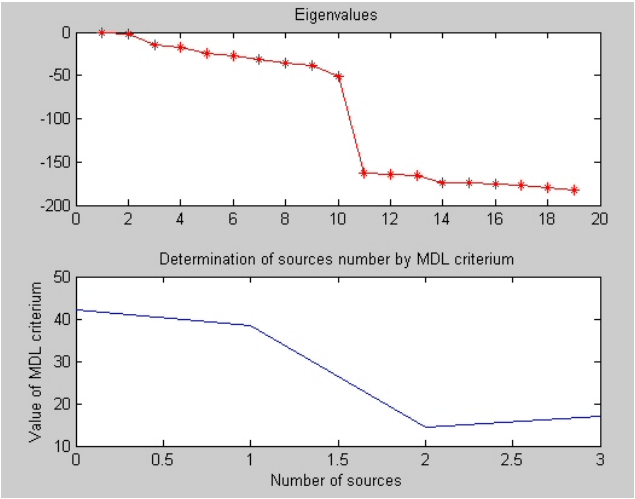

Figure 5.60: Display of eigenvalues of the first covariance matrix and curve of the MDL criterion giving the detected source number

On the previous image 5.60, this is a display of the eigenvalues of the first covariance

matrix and the associated MDL curve. The minimum of the MDL curve indicates the number of detected signals.

Keeping the same real data sample, the covariance matrix is now estimated on 19 range cells (the same number than Doppler cells). It means that the MDL criterion will give a number of detected signals on 105 shiftings (124 - 19). The covariance matrix has the same dimension than previously (19 x 19) but it has been estimated on more range cells, that is why the MDL considers more significant eigenvalues and then it detects more signals while the data are the same (see results on the image 5.61). The detected number of signals decreases along range cells and it can be plausible values.

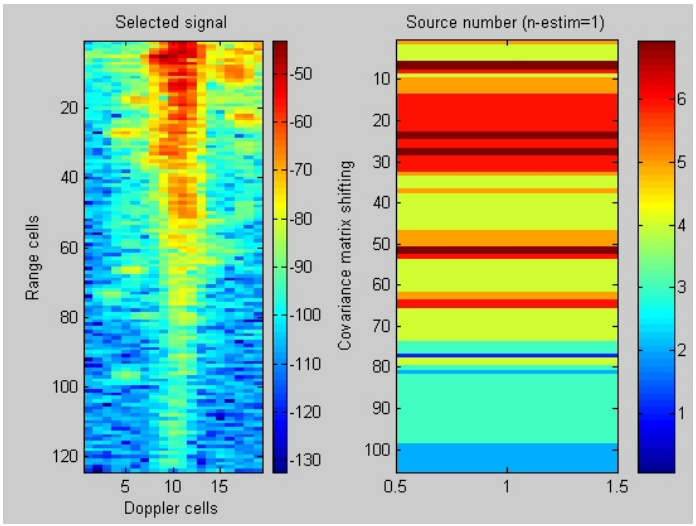

Figure 5.61: View of the Doppler sub-band studied and display of the source number given by the MDL criterion for the different covariance matrix shiftings

On the following image 5.62, the MDL curve is not as curved as in the previous example where the minimum was clearly visible. In this example, the extremity of the curve is flat and we wonder if the number of detected signal means something or not.

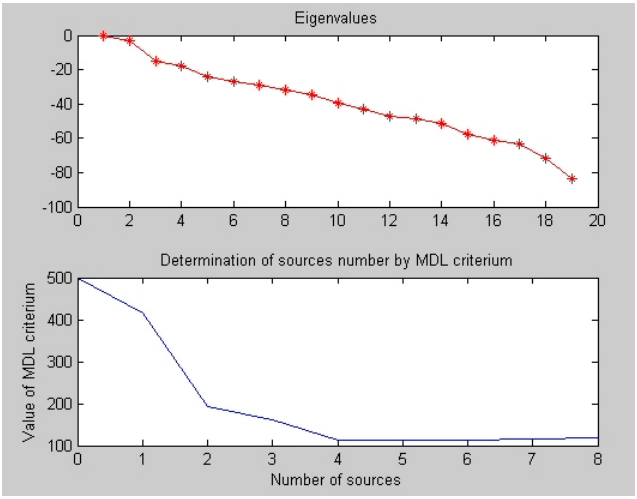

Figure 5.62: Display of eigenvalues of the first covariance matrix and curve of the MDL criterion giving the detected source number

Finally, in the last example, the covariance matrix is correctly estimated meaning that we use 38 range cells to estimate the covariance matrix. In this case all the eigenvalues are significant. But this time, the MDL curve (see figure 5.64) has problem to detect the number of signals because the curve is always decreasing meaning the given value is the maximum number of significant eigenvalues.

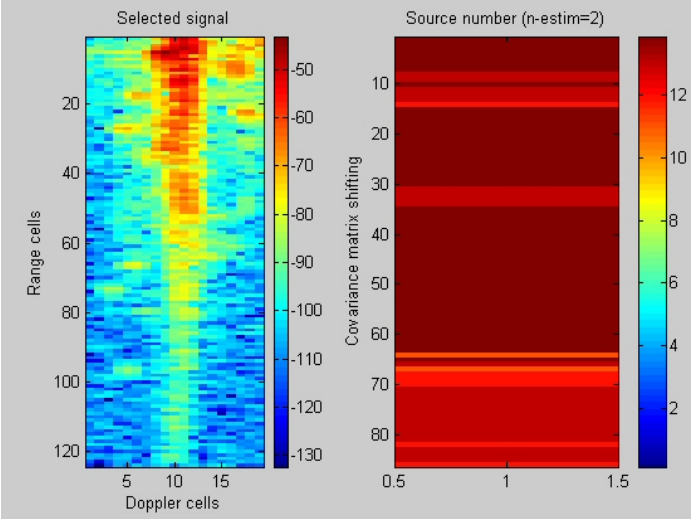

Figure 5.63: View of the Doppler sub-band studied and display of the source number given by the MDL criterion for the different covariance matrix shiftings

The break in the eigenvalues curve is visible to the naked eye but the MDL criterion is wrong and detects too many signals (12 or 14, this is excessive).

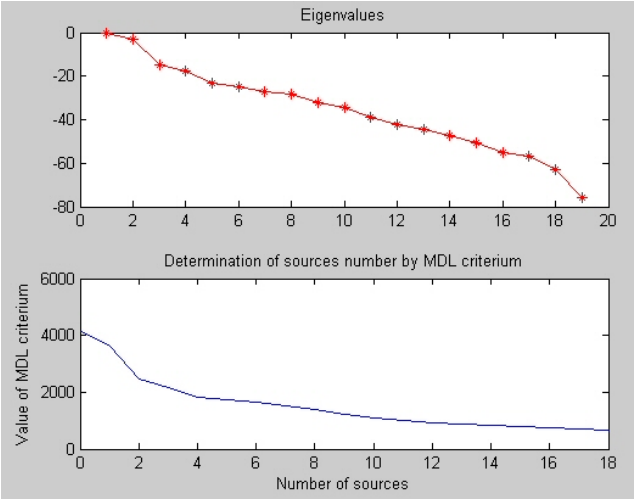

Figure 5.64: Display of eigenvalues of the first covariance matrix and curve of the MDL criterion giving the detected source number

In fact, the MDL criterion has difficulties to detect the exact source number because of the quality of the estimation of the covariance matrix because it influences the decreasing of the eigenvalues of noise signals. To conclude about this problem, another criterion should be found for the determination of source number. That is why a lot of new tests have been made about various manners to detect the break in the eigenvalues curve. For example, there is possibility of calculating an average slope in the curve and to detect the first point that is higher than the average slope, or work with standard deviations to detect an abnormality in the curve, etc. All these methods have been coupled to the MDL criterion to take over from it when it has troubles to find the right source number. But sometimes real data are really difficult to interpret. Even with improvements, the determination of source number is a critical in the filtering process. Moreover, problems are linked to the data themselves because it seems that one signal is considered as several one and that causes many problems for the filtering.

- **Several potential targets are affected by adaptive filtering :** While potential targets are normaly protected before filtering, it seems that some of them are affected by filtering. For example, it happens that targets near Bragg lines that were very visible before filtering disappear after it. It is strange because a blocking matrix has been implemented to protect potential targets.

- **The minimum size of Doppler sub-bands is not always respected after the sub-band division :** Previously, in the paragraph 5.5.2.1, tests have been made to determine the minimum and optimum size of the Doppler sub-band that provides an efficient filtering. We found that 16 Doppler cells was the minimum dimension of the reference domain. The problem is that the automatic sub-band delimitation creates sometimes sub-band of 10 Doppler cells and this is often the central band. If we extend this dimension, we may take into account a Bragg line and due to their different coherence behaviour, it is not possible. This dimension is really small because it reduce the number of potential coherent signals to reduce. Moreover, we do not

know if the process by sub-band is a good solution or not. The problem is that the sub-bands will be processed separately and then a difference between the three bands can be visible when reconstructing the final image. Do we have to envisage a sub-band overlapping or a normalization between bands?

- **Very few real data samples to conclude about coherence :** The demonstrator equipment is not very available to acquire a lot of signals. The real database contains only a few data files and conclusions about the analysis of real data have to be carefully considered because these are only information about trends noticed in a few files. Many other acquisitions are necessary to establish statistics.

- **Potential targets may be taken into account in the estimation of the covariance matrix :** The role of the blocking matrix is to reduce influence of a potential target (and its sidelobes) positioned at the considered range to filter. The problem is that targets being in the environment of the considered range cell will just be a little reduced by the blocking matrix but they will be taken into account in the estimation of the covariance matrix. And then, we do not have sea clutter reference only but targets echoes may be present in the covariance matrix. That could explain filtering results that are not "clean" as in theory.

- **Choice of weighted or non weighted data :** In fact, as previously mentioned in the paragraph, the weighting of data in Doppler can be negative for the filter calculation because weighting have effects on eigenvalues of the covariance matrix and that can disturb the determination of source number. That is why the coherence estimation can be done on the weighting data but it is advisable to calculate the filter on non weighting data to allow a good determination of source number. But if the filter is calculated on non weigthing data, it will be applicated on original non weighting data. Then, if we display results on the whole image (data filtered and non filtered), the non filtered data will be fuzzy because of high level of their secondary Doppler lobes. Moreover, in spite of this logical reasoning, results of filtering are really bad if the adaptive filter is calculated on non weighting data, we have better results with the contrary operation without clear explanations about that.

- **The covariance matrix is not very often correctly estimated :** The coherence duration may be short but we assume a minimum duration of a few range cells to advance in the algorithm and to try to filter signals. It means that the covariance matrix is not very often correctly estimated and then the adaptive filter is more difficult to calculate.

  As a matter of fact, we can say that there are problems at each step of the algorithm and we need time and further studies to solve all these problems.

5.6.2 Final results on real data

In spite of all the previous encountered problems, adaptive filtering is efficient on a few real data files. For example, on the image 5.65 and 5.66, we clearly see the image before and after adaptive filtering. The central line, corresponding to immobile targets or ground clutter, is well filtered while it is not totally the case for Bragg lines. They have been

filtered but a few parts are not very well reduced. Moreover, potential targets that were well visible on the first image are absent on the second one. We do not know if they were real targets or interferences. On this example, the process in three bands is flagrant.

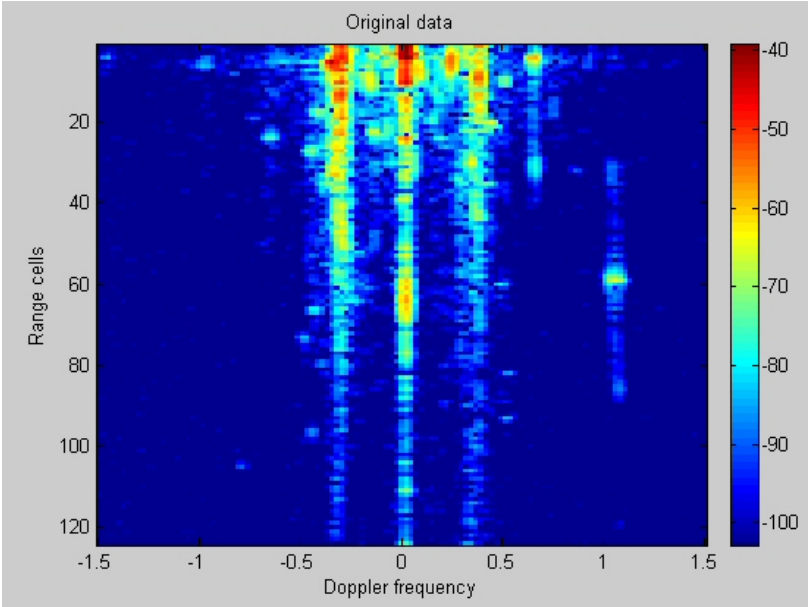

Figure 5.65: Original real data before optimized adaptive filtering

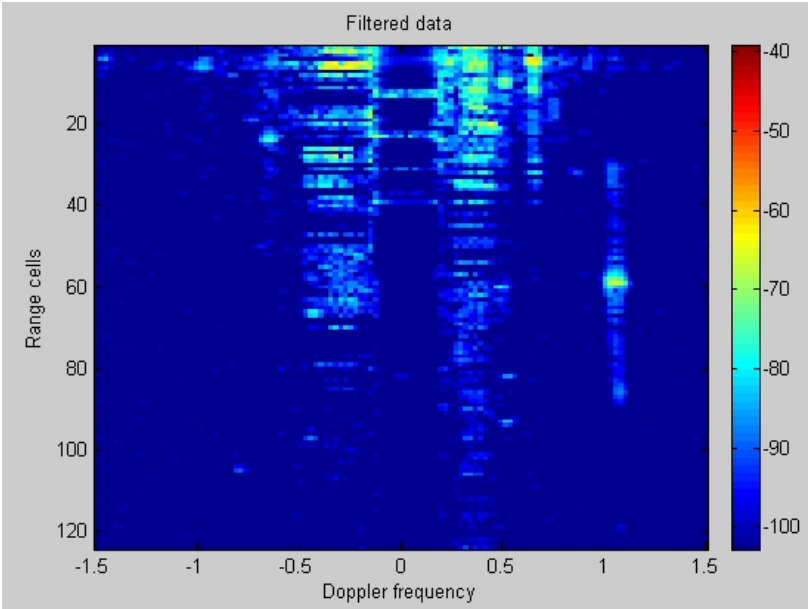

Figure 5.66: Results of the optimized adaptive filtering applied on real data

Conclusion

This report presents a summary of a three-year project dealing with HF Surface Wave Radars. These kinds of radars are recent and not numerous all over the world that is why they are at a study stage in a lot of countries. They use HF frequencies between 3 and 30 MHz and benefit from the sea surface as a conductive plane to propagate surface waves, in vertical polarization, up to great distances. Typically, their range can achieve a few hundreds of kilometers depending on many parameters such as the frequency, the type of targets to detect, the sea state, etc. They are useful instruments for the maritime long ranges surveillance for both military and civil domain. In the civil domain, a surveillance far from coasts allows detection and tracking of potential illegal activities such as drug trafficking, contraband or pirate activities and clandestine immigration. Other applications are the environment and natural resources protection against excessive fishing or pollution. These radars can also provide information about winds and sea states that are useful data for oceanographers and scientists. Military applications of HFSWR include the detection of ocean vessels (ranging from large ships to small boats), low-altitude cruise missiles or low-flying aircrafts. Many countries are interested in these new radars in order to have a complementary system to the usual microwave radars that are limited by the line-of sight of the horizon. But researches have to be lead on the improvements of the performance of these radars because they are not finalized for the moment.

The first problem that has to be solved concerns the too important size of the radiating elements used in the HFSWR. The HF frequencies that correspond to decametric wavelengths imply as a consequence large antennas. Small HF elements do not exist off the shelf and bibliography on the subject is really thin in the HF domain. The problematic is the design of a compact HF antenna. First, usual antennas have been considered to justify the problematic and to underline the bulkiness of these elements mainly for the deployement of HF radars in limited areas such as ships or for a question of furtivity and discretion. Then, we are interested in the characteristics that should have the antenna to create. Compared to the classic HF antennas, the new design should provide an important compactness gain. One of the first specifications to respect for the new design is a maximum height of 1 m, to remain well inferior to usual elements that can measure from 2.5 to 25 m high, depending on the frequency. Another specification concerns the vertical polarization that is required to propagate surface waves efficiently. An impedance of 50 ohms is also needed for an optimum matching between the antenna and the rest of the equipment. Its radiation pattern has to be directive in the sea direction. Moreover, a passive antenna is preferred to an active one to avoid phase jitter and to envisage the use of the antenna for both transmitting and receiving. A difficult objective to achieve is the functioning of the antenna at

several frequencies, typically at a low one around 5 MHz and at a high one around 15 MHz, with a sufficient bandwidth of a few hundreds of kHz. Finally, the antenna should have a simple shape made of common material to allow an easy reproduction in series at a low or reasonable cost.

Among literature and various available studies made in wireless communications domain, a first choice has been made to reduce the size of usual antennas by bending wires like in the meander line antenna technology. This choice was important because all the following design evolution is be based on this primary concept. It has been chosen for its good performance that can be reached in a small volume. By analogy with existing models and simplifying them, a first compact antenna called "generic antenna" has been imagined, made of thin copper wires that are simply bended in meanders. This antenna is considered as an electrically small antenna and its gain, efficiency, impedance, etc can be calculated in a theoretical manner. To determine its precise characteristics, it has been modeled by an electromagnetic code called NEC-2, that is efficient to model wire structures. The antenna perfomance have also been modeled with a private code used by France Telecom that confirms NEC-2 results. At the end of this chapter, a technology has been chosen to reduce usual HF antennas size and a calibration of performance of a first compact design is available. The problem is that its characteristics do not correspond exactly to initial specifications, mainly concerning the impedance and the operational frequency bands that are too high. That implies the continuation of researches to find an optimum geometry responding HFSWR needs.

Then we had a simple objective : find the most compact possible antenna having perfomance of classic HF antennas. To achieve this objective, the first step is a research of geometrical parameters of the "generic antenna" influencing positively its performance. After many series of tests, it appears that the size is the more influent parameter and further design optimizations have to be directed to the increasing of antenna height, maintaining a volumetric size corresponding to specifications. To combine compactness and performance, the idea is to increase the total deployed length of the antenna by adding a second meander structure linked to the first one. The height is the same but the total length has been doubled. This antenna has been modeled and its impedance is well improved. The possible operational band is around 18 MHz but it is still a too high frequency. To verify NEC-2 results, a prototype of this double design has been manufactured and tested in reality. Measurements confirm simulations but efforts have to be made to allow a functioning in the lower part of the HF band.

Instead of doubling the struture, another idea was to add sinusoids on the horizontal branches of the "generic antenna" to increase the deployed length keeping one panel. Results were improved and a prototype of sinusoidal antenna has been manufactured to verify simulation results. In this case, real measurements differ from simulations results and they present an operational frequency band around 13 MHz with a bandwidth of a few hundreds of kHz. With stubs technique, which is a passive matching method, it is possible to match the antenna at various frequencies simultaneously. This result was satisfying but the fragility and stability of the antenna composed of one panel was a critical point that is why a mix antenna has been imagined as a final design. In fact, the antenna, mix between the double and the sinusoidal structure, is small (50 cm high) and stable and its size is 0.50 x 0.85 x 0.5. Due to computation problems, simulations results given by NEC-

2 were inexploitable. A prototype of this final design has been tested in a coastal radar configuration and in a shipboard radar configuration. One the one hand, experimental results prove that the antenna has the same detection capabilities than large antennas with a flagrant compactness gain (in the experiments, the gain was a factor 16). On the other hand, its small size is very penalyzing for transmitting because of a very low radiating gain. This antenna can be matched at many HF frequencies with stubs technique from 5 MHz to 30 MHz. It is made of thin copper wires, with an aluminium ground plane and a fiberglass radome. Its radiation pattern presents a maximum gain in the sea direction, ideal to propagate surface waves, and it has a vertical polarization. The final design responds all the initial specifications and this is a very good conclusion to this part of the study.

With a small passive compact antenna, shipboard HF Surface Wave Radars can now be envisaged and the bulkiness aspect will not be a problem anymore on coasts where this element, even arranged in phased array, is discreet and furtive. Moreover, a small element is an advantage in a phased array to avoid coupling effects between antennas that can disturb received signals. The contract is then fulfiled and this invention can interest many countries involved in HFSWR research. A patent proposal has been written during the thesis but the project fell through because of confidentiality clauses not respected by a third party.

The most important things to remember about this first part concerning antenna design is the intellectual process that leads to the final compact HF antenna and problems posed by simulation codes. Actually, this compact antenna is very difficult, indeed impossible, to simulate correctly, mainly because of the presence of sinusoids. Electromagnetic codes have limitations and the compact HF antenna is out of their validity domain. As a matter of fact, the segment length of sinusoidal parts is very small compared to the decametric wavelength. Due to this tiny length, the meshing condition required by NEC-2 for an optimum computation is not respected. It means that a few hypothesis are not valid anymore and that can explain discrepancies between simulations and reality. Moreover, the electromagnetic code NEC-2 is not dedicated to low frequencies such as the HF band. The original source code does not take certains terms into account in the computation but they become important at low frequencies and cannot be neglected. Other codes such as a powerful ONERA code have been used to try to better reflect reality but without success. It means that this study was very complex because the optimization step was almost impossible without a prototype. Moreover, certain specifications were very difficult to achieve while others were quite easy. To respect all of them, a trade off has to be found. In spite of many simulations of various geometries, due to the lack of efficient codes, a large part of the thesis has been experimental. Whatever the weather, on the top of the offices in ONERA, in Dreux, on grass, on concrete, etc, with various prototypes, with various matching tests, etc. During this project, hundreds of hours were dedicated to experiments and they have been very useful to well understand the complexity of antenna design in HF and the procedure to follow to have exploitable measurements. Many people helped me during all these exciting missions and I am very grateful for that.

In prospect, a modification of the original NEC-2 source code has to be envisaged, but in this case, new practical visualization tools are not available anymore and exploitation of results becomes long and laborious. It would also be interesting to discover and try other electromagnetics codes but they are generally very expensive and represent a large

investment. Concerning the compact HF antenna itself, many ideas can be tested to improve its performance or to reduce once more its size. For example, a dielectric could maybe be added in the free space between the two structures. Moreover, it is possible to imagine the wires plunged in a dielectric that could have a positive effect such as virtually increase their length and then allow natural low resonant frequencies. These ideas have to be simulated with codes able to model dielectric structures.

Finally, another possibility, mentioned previously, is the design of a superdirective array of antennas. Superdirectivity in used to obtain a directive gain greater than ordinary gain obtained with a classical phased array by reducing distance between elements and by feeding them with a non constant phase law. These surperdirective arrays are difficult to implement because phase differences between elements have to be very precise. Moreover, they usually lead to extremely small bandwidths and efficiencies as well as impractical tolerances. Finally, they are very difficult to match.

Another drawback of HF Surface Wave Radars concerns the disturbing role of sea echoes for target detection. Actually, antennas of surface wave radars illuminate sea surface with a HF wave that interacts with sea waves. This interaction is due to their close decametric wavelengths and is known as the coherent Bragg scattering. This phenomenon results in important echoes coming from sea waves in the useful spectrum where target echoes should be detected. Important level of sea clutter can prevent target detection and deteriorate HFSWR performance. The aim of the second part of this thesis was to reduce influence of sea clutter in order to improve detection capabilities of surface wave radars. The disturbing effect of sea echoes were observed during the radar experiments of the final prototype of compact HF antenna. Signals received by the compact antenna are the same than signals received by usual large antennas and, on the resulting Doppler range images, the important presence of sea clutter is very visible. To reduce their influence, it is essential to have a good knowledge of the characteristics of sea echoes. A detailed study about the Bragg phenomenon has been performed and characteristics of sea echoes in order to familiarize with sea spectra. Moreover, literature proposes models of sea spectrum for any event (radar frequencies, wind velocities, sea states, etc), and it is then possible to underline the conditions that imply more or less disturbing sea clutter. To compare modeled sea echoes with real measurements, the idea was to create a database with simulated data displayed as Doppler range images. An algorithm has been developed and optimized to create simulated data faithfull to reality taking into account different propagation losses in function of the distance, effect of radar processing, external noise, radar parameters settings such as the transmitted power for example, etc. The algorithm has also been imagined to simulate the presence of a synthetic target with precise characteristics (RCS, distance, velocity) on the image. Many final examples of the simulated database have been compared to real surface wave images and they resemble each other. Data of HF Surface Wave Radars being still rare, the simulated database appears as a very good intermediate solution to test signal processing methods reducing sea clutter for any event.

To lower level of sea clutter, a simple way is to reduce the sea surface illuminated by the radar by increasing the radar bandwidth and the receiving array length or by using high frequencies. This can limit level of sea clutter but cannot reduce it sufficiently to improve target detection and moreover this is often difficult to put into effect. For an optimum data

"cleaning", a signal processing method seemed to be the best solution.

After a study about sea echoes thanks to the simulated database, interactions between sea waves and radar signals were better grasped. Actually, the Bragg scattering is strongly based on a coherence principle because the scattering phenomenon occurs only when radar signals interact with selected sea waves. The important sea clutter contribution is due to the fact that a lot of waves respect the scattering condition at the same time, their crest being in phase all together. It means that there is a spatial regularity of sea waves and this phenomenon is often verified in reality when you look at the sea. For that reason, we have decided to use physical properties of sea waves to elaborate an efficient reduction method. Simply, we assume the hypothesis that if the disturbing clutter appears because of a coherence principle, it is possible to reduce it using the same property. This observation allows the use of noise mitigation techniques to reduce influence of sea clutter. These techniques are used to detect and filter coherent disturbing signals. For this precise problem, the choice has been directed to an adaptive filtering method. Then, you cannot get away from an analysis of coherence of real sea echoes because this is the base of the filtering method. A first simple algorithm has then been imagined to adapt theory to reduction of sea echoes and it has been tested on simulated data with success. In this case, if target echoes are hidden in first or second order Bragg clutter, they are detected after filtering because level of sea clutter is considerably reduced. Applying this simple algorithm on real data, effects were totally different and not really efficient. That is why a more complicated algorithm has been developed to take into account many aspects of real data. For example, data have to be separated in sub-bands for an optimum process and each part has to be filtered with the coherence properties of its own sub-band.

Moreover, potential targets have to be protected before filtering to avoid being estimated in the covariance matrix and filtered. A blocking filter has been implemented to reduce influence of potential targets and of their correlation sidelobes.

Another algorithm improvement concerns the calculation of the adaptive filtering that is different depending if the covariance matrix is correctly estimated or not. If the covariance matrix is correctly estimated, the adaptive filter will simply be calculated by the matrix inversion. While if it is not correctly estimated, an eigenvalues and eigenvectors decomposition will be needed. A search for the number of coherent signals present in the covariance matrix will be done with the MDL criterion and the adaptive filter will be calculated thanks to eigenvectors of the coherent signals detected. In conclusion, the final adopted algorithm is more complicated than the previous one and is not totally efficient on real data for the moment. In many case, sea clutter and central line are reduced but in other cases, results are disappointing.

In the second part of this thesis, development of an efficient filtering method was difficult for many reasons. First, the poor number of real data samples gives only indications about coherence of sea echoes but we cannot really conclude about that. For example, coherence of the second order Bragg clutter is difficult to assert because it is not very visible on our data files. For this thesis, the radar used to obtain real data files being a research radar system, studied in collaboration with Singapore, it is not operational meaning acquisitions of data are not automatic, missions have to be planned, etc. We only have a few data files that have been acquired with the same bandwidth (400 kHz), at 3 different frequencies (5.255 MHz, 10.750 MHz and 16.050 MHz) but the sea state is not specified, presence or type of

targets are unknown and radar parameters settings are also vague. So it is impossible to verify if the associated detected echoes are well located with a right level. Statistics have to be established with precise measurements of meteorological data (wind velocity, current velocity, orientations, etc). Experiments with cooperative known targets are obligatory to have standard target and to test efficiency of filtering method (analyzis of the performance of adaptive filtering in function of frequency, bandwidth, sea state, etc).

Another point that implies many problems concerns the MDL criterion used to determine the number of coherent signals (that we assume being sea clutter). This criterion is very powerful on simulated data but it is efficient half of the time when applied on real data. This is certainly due to the quality of signals, if data are weighted or not, etc. The MDL criterion is based on the eigenvalues of the covariance matrix. It detects a break in the eigenvalues curve that separates coherent signals from noise and other signals. In real data, the eigenvalues curves are more flat and monotonous than in simulations and then the MDL criterion has problems to detect a break in them. When conditions are optimum, the MDL criterion gives a possible number of coherent signals (but this number cannot be verified with real data) and the final result of adaptive filtering is satisfying. While when the criterion is wrong (it happens really often), filtering can be a disaster, worse than original data.

Moreover, problems can come from the generation and receiving steps that are almost totally digital and that cause signals distorsion and modifications. It was not possible to analyze the digital receiver performance (response in correlation and in Doppler). In fact, the function studying coherence and adaptive filtering should be adjusted with transmitting and receiving signals before filtering data.

Finally, the second part of the thesis has been studied for one year and a half and it is not sufficient to enter the subject, to master adaptive filtering and to solve all encountered problems. Lack of time may explain the moderate final result presented at the end of the document. Nevertheless, I am optimist about the success of this method because of many encouraging results that agree totally. My work was a kind of pre-study to reduction of sea clutter by adaptive filtering and many questions have already been answered.

For all that reasons, it is not possible to conclude clearly this study because many things remain to do before proposing an efficient filetring method.

Many further ideas should be interesting to study in the future. Discussing with colleagues (Michel Menelle and Marc Lesturgie), other methods to reduce sea clutter can be envisaged. For example, a method using a temporal filter such as a LPC filter (Linear Predictive Coefficient) should be able to "predict" the temporal continuity of various coherent signals contained in the received radar signal. Thus, first and second order Bragg clutter should differ from other temporal signals and they should be reduced without reducing target signals. This method has to be verified and studied thouroughly. Another idea would be to study the phase of Bragg clutter along range cells for example. If this phase is stable from a range cell to another, it may be possible to reinject it with a phase difference of 180 $^{\circ}$ in order to reduce it.

To conclude this report, I would like to add a few points. First, this thesis was really a great experiment because of the various subjects tackled. On the one hand, this work needs a good comprehension of the whole radar system, from the antenna, to the equipment, via

software or electronics, signal processing, etc and that makes the subject very interesting. But on the other hand, there is a feeling of frustration because it was a so vast subject that sometimes I only get a general view of certain points. Due to a lack of time, only two points have been chosen for this study but the other drawbacks mentioned in the document were always present, mainly in experiments (congested HF spectrum, ionospheric clutter, electromagnetics compatibility, etc). The two parts of the thesis were totally different and it was sometimes tricky to juggle with both.

A problem is that many countries have research programs on HF Surface Wave Radars but communication between them is still rare that is why there is not a lot of bibliography on the subject and this is regrattable. I hope that this document, in english for a better spreading, will help other people to have a departure point.

On a personal point of view, it was an instructive period. I met many brilliant persons and an international collaboration was also very interesting. The writing of the thesis in english was also necessary to allow foreign teams to share results. I hope the english was good enough for them to understand.

List of Figures

List of Tables

Annexes

5.6.3 ANNEXE 1 : Demonstration of the formula giving the bandwidth Δf in function of the VSWR S and the quality coefficient Q

The VSWR S can be written in function of the reflection coefficient ρ :

$$S = \frac{1 + |\rho|}{1 - |\rho|} \tag{5.10}$$

The antenna can be considered as a resonant circuit in serie, its impedance can then be expressed as :

$$Z = R(1 + j2Q\frac{\omega - \omega_0}{\omega_0})$$

where R is the resistance in ohms.

We know that :

$$|\rho| = \left|\frac{Z - Z_0}{Z + Z_0}\right|$$

Replacing Z by its develop form in the above formula, we obtain :

$$|\rho| = \frac{\sqrt{(R - Z_0)^2 + 4Q^2R^2(\frac{\omega-\omega_0}{\omega_0})^2}}{\sqrt{(R + Z_0)^2 + 4Q^2R^2(\frac{\omega-\omega_0}{\omega_0})^2}}$$

Z_0=50 ohms and $\frac{\omega-\omega_0}{\omega_0} = \frac{\Delta f}{2f_c}$, so we can simplify the expression such as :

$$|\rho| = \frac{\sqrt{(R - 50)^2 + Q^2R^2(\frac{\Delta f}{f_c})^2}}{\sqrt{(R + 50)^2 + Q^2R^2(\frac{\Delta f}{f_c})^2}}$$

We know that S=1 if the antenna is matched, in this case, that means that R=50 ohms.

Reinjecting the reflection coefficient in the VSWR formula 5.10, and factorizing by R^2, we have :

$$S = \frac{\sqrt{4 + Q^2(\frac{\Delta f}{f_c})^2} + (\frac{\Delta f}{f_c})Q}{\sqrt{4 + Q^2(\frac{\Delta f}{f_c})^2} - (\frac{\Delta f}{f_c})Q}$$

$$\sqrt{4 + Q^2(\frac{\Delta f}{f_c})^2} + (\frac{\Delta f}{f_c})Q = S(\sqrt{4 + Q^2(\frac{\Delta f}{f_c})^2} - (\frac{\Delta f}{f_c})Q)$$

$$4 + Q^2(\frac{\Delta f}{f_c})^2 = (\frac{1+S}{1-S})^2 Q(\frac{\Delta f}{f_c})^2$$

$$\frac{\Delta f}{f_c} = \frac{1}{Q}\frac{S-1}{\sqrt{S}}$$

5.6.4 ANNEXE 2 : Final prototype dimensions

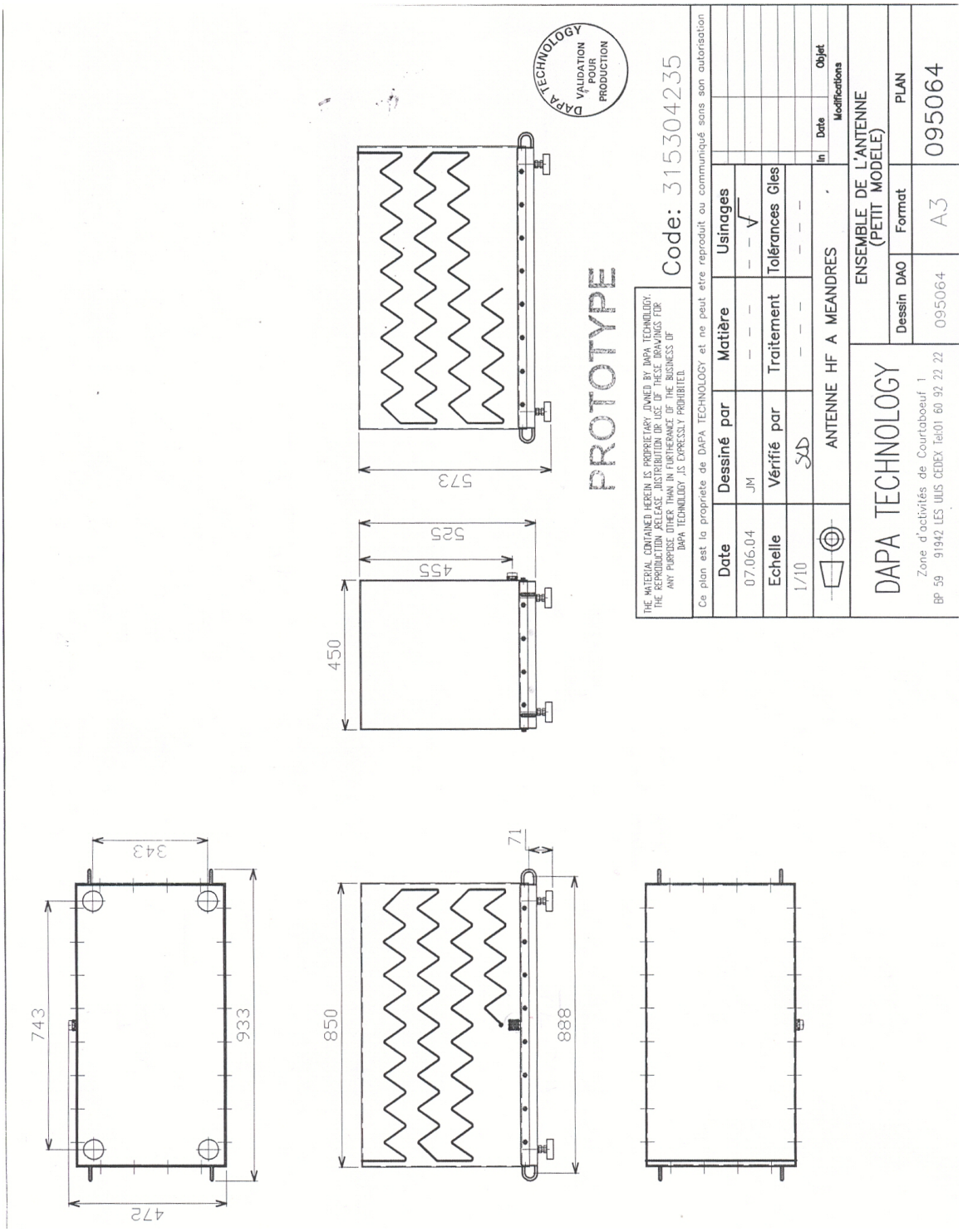

Figure 5.67: Dimensions of the prototype of the final compact HF antenna

5.6.5 ANNEXE 3 : Recall about Beaufort scale

Beaufort scale number (force)	Descriptive term	Units (km/h)	Units (m/s)	Description at Sea
0	Calm	0	0	Sea like a mirror
1-3	Light winds	19 or less	5.2 or less	Small wavelets, ripples formed but do not break : A glassy appearance maintained
4	Moderate winds	20 - 29	5.3 - 8	Small waves longer; fairly frequent - becoming white horses
5	Fresh winds	30 - 39	8.1 - 10.8	Moderate waves, taking a more pronounced long form; many white horses are formed
6	Strong winds	40 - 50	10.9 - 13.9	Large waves begin to form; the white foam crests are more extensive with probably some spray
7	Near gale	51 - 62	14 - 17.2	Sea heaps up and white foam from breaking waves begins to be blown in streaks along direction of wind
8	Gale	63 - 75	17.3 - 20.8	Moderately high waves of greater length; edges of crests begin to break into spindrift; foam is blown in well-marked streaks along the direction of the wind
9	Strong gale	76 - 87	20.9 - 24.1	High waves; dense streaks of foam; crests of waves begin to topple, tumble and roll over; spray may affect visibility
10	Storm	88 - 102	24.2 - 28.3	Very high waves with long overhanging crests; the resulting foam in great patches is blown in dense white streaks; the surface of the sea takes on a white appearance; the tumbling of the sea becomes heavy with visibility affected
11	Violent storm	103 - 117	28.4 - 32.5	Exceptionally high waves; small and medium sized ships occasionally lost from view behind waves; the sea is completely covered with long white patches of foam; the edges of wave crests are blown into froth
12+	Hurricane	118 or more	32.6 or more	Sea completely white with driving spray; visibility seriously affected

Table 5.2: Beaufort scale

Bibliography

[1] Y. Blanchard. *Le Radar 1904-2004 Histoire d'un siècle d'innovations techniques et opérationnelles*. Ellipses, 2004.

[2] H. C. Chan L. Sevgi, A. Ponsford. An integrated maritime surveillance system based on high-frequency surface-wave radars, part I and II. *IEEE antennas and propagation magazine*, 43(4), August 2001.

[3] H. Bremmer. Terrestrial radio waves : Theory of propagation. *New-York*, 7, 1949.

[4] G. Millington. Ground wave propagation over an inhomogeneous smooth Earth. *Proc. IRE*, 96, part III:53–64, January 1949.

[5] F. M. Caimi. Mla antennas - physically small, electrically large.

[6] H.A. Wheeler. Fundamental limits of small antennas. *Proceedings of the I.R.E. (IEEE)*, pages 1479–1484, December 1947.

[7] L.J. Chu. Physical limitations of omni-directional antennas. *Journal of applied physics*, 19:1163–1175, December 1948.

[8] R.F. Harrington. Effect of antenna size on gain, bandwidth and efficiency. *Journal of research of the national bureau of standards, D. radio propagation*, 64D(1):1–12, january-february 1959.

[9] J.S. McLean. A re-examination of the fundamental limitson the radiation q of electrically small antennas. *IEEE Transactions on antennas and propagation*, 44(5):672–675, May 1996.

[10] R. Bancroft. Fundamental dimension limits of antennas ensuring proper antenna dimensions in mobile device design.

[11] S. Satoh T. Endo, Y. Sunahara and T. Katagi. Resonant frequency and radiation efficiency of meander line antennas. *Electronics and communications in Japan*, 83:52–58, November 2000.

[12] T. Yamaguchi Y. Okumura S. Betsudan K. Noguchi, M. Mizusawa. Increasing the bandwidth of a small meander line antenna consisting of two strips. *Electronics and communications in Japan*, 83(10):402–409, 2000.

[13] D.D. Crombie. Doppler spectrum of sea echo at 13.56 Mc/s. *Nature*, 175:681–682, 1955.

[14] D.E. Barrick. First-order theory and analysis of MF/HF/VHF scatter from the sea. *IEEE Transactions on Antennas and Propagation*, 20:2–10, January 1972.

[15] L.R. Meyer T.M. Georges, J.A. Harlan and R.G. Peer. Tracking hurricane claudette with the u.s. air force over the horizon radar. *Journal atmos. and oceanic tech.*, 10:441–451, 1993.

[16] C.T. Carlson J.P. Riley R.M. Jones T.M. Georges, J.W. Maresca and D.E. Westor. Recovering ocean wave-height from hf radar sea echoes distorted by imperfect ionospheric reflection. *Wave propagation lab., Boulder, CO, NOAA tech. memo.*, ERL WPL-73, May 1981.

[17] D.E. Barrick. Accuracy of parameter extraction from sample-averaged sea-echo doppler spectral. *IEEE Trans. ant. prop.*, AP-28:1–11, 1980.

[18] A.E. Long and D.B. Trizna. Mapping of the north atlantic winds by hf radar sea backscattered interpretation. *IEEE Trans. ant. prop.*, AP-21(5):680–685, 1973.

[19] K.-W. Gurgel. Information on HF-Radar, `http://ifmaxp1.ifm.uni-hamburg.de`

[20] D.E. Cartwright M.S. Longuet-Higgins and N.D. Smith. Observations of the directional spectrum of the sea waves using motions of a floating buoy. *Ocean wave spectra Englewood cliffs, NJ: Prentice-Hall*, pages 111–136, 1963.

[21] C. Kerbiriou. *Développement d'un méthode d'étalonnage novatrice d'un radar transhorizon basée sur une analyse fine du fouillis de mer.* PhD thesis, Université de Rennes 1, Février 2002.

[22] E. Barrick. The interaction of hf/vhf radio waves with the sea surface and its applications.

[23] L.E. Brennan I.-S. Reed, J.D. Mallett. Rapid convergence rate in adaptive arrays. *IEEE transactions on aerospace and eletronic systems*, AES-10(6):853–863, November 1974.

[24] M. Skolnik. *Radar Handbook (second edition).* McGraw-Hill publishing company, 1990.

[25] A.M. Haimovich and Y. Bar-Ness. An eigenanalysis interference canceler. *IEEE Transactions on signal processing*, 39(1):76–84, January 1991.

[26] A.M. Haimovich and M. Berin. Eigenanalysis-based space time adaptive radar : performance analysis. *IEEE Transactions on aerospace and electronic systems*, 33(4):1170–1179, October 1997.

[27] M.S. Barlett. A note on the multiplying factors for various χ approximations. *J.Roy. Stat. Soc., ser. B*, 16:296–298, 1954.

[28] D. N. Lawley. Tests of significance of the latent roots of the covariance and correlation matrices. *Biometrica*, 43:128–136, 1956.

[29] H. Akaike. A new look at the statistical model identification. *IEEE Trans. Automat. Contr.*, vol AC-19:716–723, Dec. 1974.

[30] G. Schwartz. Estimating the dimension of a model. *The annals of statistics*, 5(2):461–464, 1978.

[31] J. Rissanen. Modeling by shortest data description. *Automatica*, 14:465–471, March 1978.

[32] E. Bronner and M. Hélier. Meander line antennas for HF radars. In *JINA, International Symposium on Antennas*, pages 446–447. SEE, 2004.

[33] I.S. Reed L.E. Brennan. Theory of adaptive radar. *IEEE Transactions on Aerospace and Electronic Systems*, AES(10):237–252, march 1973.

Publications and articles

- Conferences :

  1. Conference **RADAR 2004** (October 19-21, 2004) in Toulouse, France : "Compact antennas for HF surface wave radars", E. Bronner, M. Hélier, P. Delavictoire.
  2. Conference **JINA 2004** (International Symposium on Antennas, November 8-11, 2004) in Nice, France : "Meander line antennas for HF radars", E. Bronner, M. Hélier.

- Publication : **Revue technique de l'Institut Francais de Navigation** (Navigation, Paris) : "Le radar HF à ondes de surface : un outil bien adapté pour surveiller la zone économique exclusive", E. Bronner, M. Hélier, S. Saillant et G. Auffray, Vol. 53, n°211, July 2005, p. 5-24, ISSN 0028-1530.

Amélioration des performances des radars HF à ondes de surface par étude d'antenne compacte et filtrage adaptatif appliqué à la réduction du fouillis de mer

Les radars HF à ondes de surface (HFSWR) trouvent des applications dans la surveillance maritime, l'océanographie ou la détection de cibles. Ils utilisent des ondes HF (3-30 MHz) qui se propagent sur la surface de la mer jusqu'à quelques centaines de kilomètres. Néanmoins, ils sont récents et encore peu opérationnels à cause de quelques inconvénients. L'objectif de cette thèse est de résoudre deux de ces inconvénients pour améliorer les performances des HFSWR. Tout d'abord, en réduisant la taille des antennes HF usuelles qui sont beaucoup trop grandes. En effet, pour des raisons pratiques et pour envisager des configurations radars embarquées, il est nécessaire de créer une antenne HF compacte pouvant répondre aux cahier des charges du HFSWR. Deuxième préoccupation, les ondes HF et les vagues interagissent et créent des échos de mer élevés qui peuvent masquer des échos de cibles éventuelles. Le second objectif de cette thèse est donc de réduire ces échos marins gênants par une méthode de filtrage adaptatif.

Mots clés: Radar HF à ondes de surface, petites antennes, antenne à méandres, codes électromagnétiques, diffusion de Bragg, spectre de mer, cohérence, filtrage adaptatif, critère MDL.

Improvements of HF surface wave radars perfomance by compact antenna study and adaptive filtering used to reduce sea clutter

HF surface wave radars (HFSWR) find applications in maritime surveillance, oceanography or target detection. They use HF waves (3-30 MHz) that propagate over the sea surface reaching a few hundreds of kilometers. Nevertheless, they are recent and not totally operational for the moment because of several drawbacks. The objective of this thesis is to solve 2 of these drawbacks to improve performance of HFSWR. First, one of the major constraints concerns the important size of the HF antennas. For practical reasons and to envisage a shipboard radar, it is necessary to design a compact HF antenna responding specifications of HFSWR. The first part presents the intellectual process that leads to the final prototype. Secondly, HF waves and sea surface interact and that creates important echoes that can hide echoes of potential targets. The second objective of this thesis is then to reduce the impact of these disturbing sea echoes thanks to an adaptative filtering method.

Key words : HF surface wave radar, small antennas, meander line antenna, electromagnetics codes, Bragg scattering, sea spectrum, coherence, adaptive filtering, MDL criterium.

Intitulé et adresse du laboratoire : Office National d'Etudes et de Recherches Aérospatiales (ONERA), Département Electromagnétisme et Radar, Equipe "Radar Basses Fréquences", Chemin de la Hunière et des Joncherettes, 91761 PALAISEAU CEDEX.